



National Library  
of Canada

Acquisitions and  
Bibliographic Services Branch

395 Wellington Street  
Ottawa, Ontario  
K1A 0N4

Bibliothèque nationale  
du Canada

Direction des acquisitions et  
des services bibliographiques

395, rue Wellington  
Ottawa (Ontario)  
K1A 0N4

*Your file    Votre référence*

*Our file    Notre référence*

## NOTICE

The quality of this microform is heavily dependent upon the quality of the original thesis submitted for microfilming. Every effort has been made to ensure the highest quality of reproduction possible.

If pages are missing, contact the university which granted the degree.

Some pages may have indistinct print especially if the original pages were typed with a poor typewriter ribbon or if the university sent us an inferior photocopy.

Reproduction in full or in part of this microform is governed by the Canadian Copyright Act, R.S.C. 1970, c. C-30, and subsequent amendments.

## AVIS

La qualité de cette microforme dépend grandement de la qualité de la thèse soumise au microfilmage. Nous avons tout fait pour assurer une qualité supérieure de reproduction.

S'il manque des pages, veuillez communiquer avec l'université qui a conféré le grade.

La qualité d'impression de certaines pages peut laisser à désirer, surtout si les pages originales ont été dactylographiées à l'aide d'un ruban usé ou si l'université nous a fait parvenir une photocopie de qualité inférieure.

La reproduction, même partielle, de cette microforme est soumise à la Loi canadienne sur le droit d'auteur, SRC 1970, c. C-30, et ses amendements subséquents.

**Canada**

UNIVERSITY OF ALBERTA

**Quality Local Refinement of Tetrahedral Meshes**

BY

Anwei Liu



A thesis submitted to the Faculty of Graduate Studies and Research in partial fulfillment of the requirements for the degree of Doctor of Philosophy.

DEPARTMENT OF COMPUTING SCIENCE

Edmonton, Alberta  
Fall 1994



National Library  
of Canada

Acquisitions and  
Bibliographic Services Branch

395 Wellington Street  
Ottawa, Ontario  
K1A 0N4

Bibliothèque nationale  
du Canada

Direction des acquisitions et  
des services bibliographiques

395, rue Wellington  
Ottawa (Ontario)  
K1A 0N4

Your file    *Votre référence*

Our file    *Notre référence*

**The author has granted an irrevocable non-exclusive licence allowing the National Library of Canada to reproduce, loan, distribute or sell copies of his/her thesis by any means and in any form or format, making this thesis available to interested persons.**

**L'auteur a accordé une licence irrévocable et non exclusive permettant à la Bibliothèque nationale du Canada de reproduire, prêter, distribuer ou vendre des copies de sa thèse de quelque manière et sous quelque forme que ce soit pour mettre des exemplaires de cette thèse à la disposition des personnes intéressées.**

**The author retains ownership of the copyright in his/her thesis. Neither the thesis nor substantial extracts from it may be printed or otherwise reproduced without his/her permission.**

**L'auteur conserve la propriété du droit d'auteur qui protège sa thèse. Ni la thèse ni des extraits substantiels de celle-ci ne doivent être imprimés ou autrement reproduits sans son autorisation.**

ISBN 0-315-95218-0

**Canada**

UNIVERSITY OF ALBERTA .

RELEASE FORM

NAME OF AUTHOR: Anwei Liu

TITLE OF THESIS: **Quality Local Refinement of Tetrahedral Meshes**

DEGREE: Doctor of Philosophy

YEAR THIS DEGREE GRANTED: 1994

Permission is hereby granted to the University of Alberta Library to reproduce single copies of this thesis and to lend or sell such copies for private, scholarly or scientific research purposes only.

The author reserves all other publication and other rights in association with the copyright in the thesis, and except as hereinbefore provided neither the thesis nor any substantial portion thereof may be printed or otherwise reproduced in any material form whatever without the author's prior written permission.

(Signed) *Anwei Liu* . . . . .  
Anwei Liu

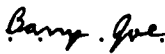
Edmonton, Alberta  
A1B 2C3


Date: *July 27, 1994*

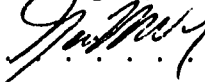
UNIVERSITY OF ALBERTA

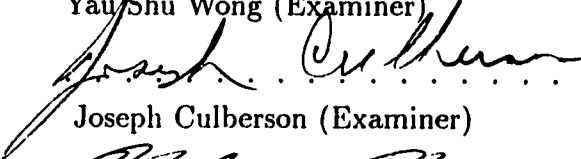
FACULTY OF GRADUATE STUDIES AND RESEARCH


The undersigned certify that they have read, and recommend to the Faculty of Graduate Studies and Research for acceptance, a thesis entitled **Quality Local Refinement of Tetrahedral Meshes** submitted by Anwei Liu in partial fulfillment of the requirements for the degree of Doctor of Philosophy.

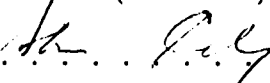
 . . . . .  
Barry Joe (Supervisor)

 . . . . .  
Frank Stenger (External)

 . . . . .  
Yau Shu Wong (Examiner)

 . . . . .  
Joseph Culberson (Examiner)

 . . . . .  
Jim Hoover (Examiner)

 . . . . .  
Stan Cabay (Examiner)

Duane Szafron (Chair)

Date: July 27, 1994

*To my parents*

## Abstract

Mesh refinement is in general a necessary step in the finite element method. To date, few previous results are known for 3-D local mesh refinement of tetrahedral meshes in terms of producing guaranteed-quality refined meshes due to the complexity of the 3-D geometry. The main part of this thesis is focused on developing 3-D local refinement techniques with emphasis on fast algorithm for generating quality refined meshes. Two algorithms, based on a bisection procedure and a regular refinement, have been designed and implemented. In both algorithms, the quality of refined meshes is theoretically ensured. With properly designed data structures, the expected time complexity of the algorithms is linearly related to the number of refined tetrahedra in a refined mesh. Also, local refinement in a refined region can be smoothly extended to its adjacent subregions in a small range of expansion. Implementation details and experimental results of the algorithms are presented.

Another part of the thesis is an analytic study of tetrahedron shape measures. A novel tetrahedron shape measure, the mean ratio, based on an affine transformation from the regular tetrahedron, is introduced, and used in analyzing the quality of meshes produced by our local refinement algorithms. By studying the relationships among three shape measures (radius ratio, minimum solid angle, and mean ratio), we conclude that the three measures in question are “equivalent”, and one can use any of them for reporting and interpreting the quality of tetrahedra in a finite element mesh while being aware of the different distributions of their values.

## Acknowledgements

I am grateful to my supervisor, Professor Barry Joe, for his insightful guidance, unrestricted access to all resources at his disposal, countless reading of thesis drafts, financial assistance, and his unfailing confidence in my motivation and capability. Without all these, this thesis would have been impossible.

I am indebted to Professors Yau Shu Wong, Joe Culberson, Jim Hoover, Stan Cabay, and Frank Stenger for the time spent in reviewing this thesis; and for serving in my examination committee. I would also like to thank Dr. Wenping Wang for many helpful discussions about some problems in this thesis.

A very special thanks goes to my wife who always has an enthusiasm for listening to my “odd” ideas, which are sometimes beyond her knowledge and major, Forest Science; her love and encouragement throughout my research are important.

Finally, I would like to acknowledge the Department of Computing Science at University of Alberta for providing equipment and the financial support during my graduate study.



# Contents

<b>1</b>	<b>Introduction</b>	<b>1</b>
1.1	Review of mesh generation . . . . .	2
1.1.1	Approaches in engineering . . . . .	3
1.1.2	Approaches in theoretical computational geometry . . . . .	4
1.1.3	Approaches in applied computational geometry . . . . .	4
1.2	Review of mesh refinement . . . . .	5
1.2.1	Local refinement . . . . .	5
1.2.2	Remeshing . . . . .	8
1.3	Outline of thesis . . . . .	9
<b>2</b>	<b>Tetrahedron Shape Measures and Their Relationships</b>	<b>11</b>
2.1	Introduction . . . . .	11
2.2	Minimum solid angle $\theta_{min}$ . . . . .	13
2.3	Radius ratio $\rho$ . . . . .	16
2.4	Mean ratio $\eta$ . . . . .	17
2.5	Relationship between $\rho$ and $\eta$ . . . . .	20
2.6	Relationship between $\sigma_{min}$ and $\eta$ . . . . .	23
2.7	Relationship between $\sigma_{min}$ and $\rho$ . . . . .	26

2.8	Discussion of results . . . . .	28
<b>3</b>	<b>On the Shape of Tetrahedra from Bisection</b>	<b>34</b>
3.1	Introduction . . . . .	34
3.2	Bisection procedure based on a canonical tetrahedron . . . . .	36
3.3	Properties of bisection procedure . . . . .	38
3.4	Estimate of constants . . . . .	43
3.5	Further remarks . . . . .	45
<b>4</b>	<b>Quality Local Refinement of Tetrahedral Meshes Based on Bisection</b>	<b>46</b>
4.1	Introduction . . . . .	46
4.2	Bisection of a tetrahedron . . . . .	48
4.3	Local refinement of a conforming mesh . . . . .	52
4.4	Properties of meshes generated by QLRB . . . . .	58
4.5	Data structure and algorithmic details . . . . .	62
4.6	Time complexity . . . . .	71
4.7	Summary . . . . .	72
<b>5</b>	<b>Quality Local Refinement of Tetrahedral Meshes Based on 8-Subtetrahedron Subdivision</b>	<b>73</b>
5.1	Introduction . . . . .	73
5.2	Subdivision of a single tetrahedron . . . . .	75
5.3	Local refinement of a conforming mesh . . . . .	84
5.4	Data structure and algorithmic details . . . . .	91
5.5	Time complexity . . . . .	94
5.6	Summary . . . . .	95

<b>6</b>	<b>Performance of the Algorithms</b>	<b>96</b>
6.1	Test examples . . . . .	97
6.2	Experimental results for QLRB . . . . .	99
6.3	Experimental results for QLRS . . . . .	103
6.4	Summary . . . . .	106
<b>7</b>	<b>Concluding Remarks</b>	<b>115</b>
7.1	Summary . . . . .	115
7.2	Further research problems . . . . .	116
<b>A</b>	<b>Mean Ratio in <math>n</math>-Dimensional Space</b>	<b>118</b>
<b>B</b>	<b>Delaunay Property in SUBDIV</b>	<b>121</b>

## List of Figures

1.1	Illustration for 2-D local refinement based on bisection . . . . .	6
1.2	Illustration for 2-D local refinement based on regular refinement . . . . .	7
2.1	Solid angle $\theta_{min}$ . . . . .	14
2.2	Illustration of incircle, circumcircle, and inscribed ellipse for triangles. . . .	17
2.3	A tetrahedron with $r > 0, t > 0, z > 0$ . . . . .	21
2.4	A comparison among three shape measures for a poorly-shaped tetrahedron without short edges - example 1 . . . . .	30
2.5	A comparison among three shape measures for a poorly-shaped tetrahedron without short edges - example 2 . . . . .	30
2.6	A comparison among three shape measures for a poorly-shaped tetrahedron without short edges - example 3 . . . . .	30
2.7	A comparison among three shape measures for a poorly-shaped tetrahedron with one short edge - example 1 . . . . .	30
2.8	A comparison among three shape measures for a poorly-shaped tetrahedron with one short edge - example 2 . . . . .	31
2.9	A comparison among three shape measures for a poorly-shaped tetrahedron with two short edges . . . . .	31
2.10	A comparison among three shape measures for a poorly-shaped tetrahedron with three short edges - example 1 . . . . .	31

2.11	A comparison among three shape measures for a poorly-shaped tetrahedron with three short edges - example 2 . . . . .	31
2.12	Illustration of 4 types of poor tetrahedra . . . . .	32
3.1	Tetrahedron <b>Q</b> for Lemmas 3.1 and 3.2. . . . .	36
3.2	Canonical tetrahedron <b>P</b> for bisection . . . . .	37
4.1	Four types of tetrahedra according to the number of marked points . . . . .	53
4.2	Tetrahedra produced by 1 to 3 levels of bisection of a tetrahedron of class DD, DSS2, or DSS3 . . . . .	57
4.3	Illustration for the proof of Theorem 4.5 . . . . .	60
4.4	Tetrahedra produced by 1 to 3 levels of bisection of a tetrahedron of class DSS1 . . . . .	66
4.5	Illustration of 2 non-conforming patterns . . . . .	69
4.6	Illustration of the non-conforming patterns produced from a conforming face	69
4.7	Illustration of the non-conforming patterns produced from a non-conforming face . . . . .	70
5.1	Illustration for 2-D local refinement in PLTMG . . . . .	74
5.2	Illustration for the regular refinement $SUB_8$ . . . . .	75
5.3	Rhombic tetrahedron <b>P</b> . . . . .	77
5.4	Illustration for non-regular refinements . . . . .	85
5.5	Illustration for possible split points after $SUB_8$ is applied to <b>T</b> 's parent $T_p(t_0, t_1, t_2, t_3)$ . . . . .	86
6.1	An original mesh of the convex polyhedron. . . . .	98
6.2	An original mesh of the U-shaped object. . . . .	98

6.3	A refined mesh produced by QLRB and IMPR for 4 levels of bisection around a corner of the convex polyhedron. . . . .	109
6.4	A refined mesh produced by QLRB and IMPR for 4 levels of bisection around a corner of the U-shaped object. . . . .	109
6.5	A refined mesh produced by QLRB and IMPR for 4 levels of bisection around the midpoint of an edge of the convex polyhedron. . . . .	110
6.6	A refined mesh produced by QLRB and IMPR for 4 levels of bisection around a point of the U-shaped object. . . . .	110
6.7	A refined mesh produced by QLRB and IMPR for 4 levels of bisection around a line segment of the convex polyhedron. . . . .	111
6.8	A refined mesh produced by QLRB and IMPR for 4 levels of bisection around a line segment of the U-shaped object. . . . .	111
6.9	A refined mesh produced by QLRS and IMPR for 2 levels of subdivision around a corner of the convex polyhedron. . . . .	112
6.10	A refined mesh produced by QLRS and IMPR for 2 levels of subdivision around a corner of the U-shaped object. . . . .	112
6.11	A refined mesh produced by QLRS and IMPR for 2 levels of subdivision around the midpoint of an edge of the convex polyhedron. . . . .	113
6.12	A refined mesh produced by QLRS and IMPR for 2 levels of subdivision around a point of the U-shaped object. . . . .	113
6.13	A refined mesh produced by QLRS and IMPR for 2 levels of subdivision around a line segment of the convex polyhedron. . . . .	114
6.14	A refined mesh produced by QLRS and IMPR for 2 levels of subdivision around a line segment of the U-shaped object. . . . .	114
B.1	Illustration for the proof of Lemma B.1; $t_0t_1t_2t_3$ is a parallelogram. . . . .	122
B.2	Illustration for the proof of Lemmas B.2, B.3, B.4, and B.5 . . . . .	122

B.3	Illustration for the proof of Lemma B.5; $\mathbf{s}_1\mathbf{s}_4\mathbf{s}_2\mathbf{s}_3$ is a parallelogram, and	
	$\mathbf{s}_{ij} = (\mathbf{s}_i + \mathbf{s}_j)/2$ , $i < j$ . . . . .	125

## List of Tables

4.1	Information associated with edges in bisection of $P$ . . . . .	50
6.1	Problems 1 to 4 . . . . .	97
6.2	Bisection results for Problem 1 . . . . .	99
6.3	Bisection results for Problem 2 . . . . .	99
6.4	Bisection results for Problem 3 . . . . .	100
6.5	Bisection results for Problem 4 . . . . .	100
6.6	Improved-quality meshes from QLRB results for Problems 1 and 2 . . . . .	101
6.7	Improved-quality meshes from QLRB results for Problems 3 and 4 . . . . .	101
6.8	QLRB and IMPR results for a convex polyhedron . . . . .	102
6.9	QLRB and IMPR results for a U-shaped object . . . . .	102
6.10	Expansion of refinement and CPU times around a fixed point for QLRB . .	103
6.11	Expansion of refinement and CPU times around a line segment for QLRB .	103
6.12	QLRS results for Problems 1 and 2 . . . . .	104
6.13	QLRS results for Problems 3 and 4 . . . . .	104
6.14	QLRS results for two polyhedral regions . . . . .	104
6.15	Improved-quality meshes from QLRS results for Problems 1 and 2 . . . . .	105
6.16	Improved-quality meshes from QLRS results for Problems 3 and 4 . . . . .	105
6.17	Improved-quality meshes from QLRS results for two polyhedral regions . .	105



6.18	Expansion of refinement and CPU times around a fixed point for QLRS . .	105
6.19	Expansion of refinement and CPU times around a line segment for QLRS .	106
6.20	Statistical results for hash tables . . . . .	107
B.1	Information associated with each interior face of $\mathcal{T}^1$ . . . . .	123

# Chapter 1

## Introduction

In physical simulation, many problems can be formulated as partial differential equations (PDEs), e.g. structural analysis of mechanical parts, semiconductor device simulation, aerodynamics, computational fluid dynamics, etc. A popular method for solving some types of PDEs is the finite element method (FEM), which in general consists of the following steps:

- (a) Mesh generation in the region or domain of interest.
- (b) Solution of linear equations.
- (c) Error estimation.
- (d) Mesh refinement.

Mesh generation is a process of fitting a geometric region with basic elements, such as triangles, quadrilaterals, tetrahedra, or hexahedra. In this thesis, we only consider tetrahedral meshes, because this type of mesh is more suitable for fitting complicated regions. In the error estimation step of FEM, a set of subregions or basic elements (called selected elements) is identified for further refinement due to unacceptable solution accuracy on these elements. Subdivision of the selected elements or subregions into a new set of elements of the same type is referred to as mesh refinement, and the output of the mesh generation step is provided as input to the mesh refinement step.

The FEM starts with an initial mesh, carries out a finite element analysis using the mesh, and then refines the mesh based on error estimates. Several iterations of the adaptive

process cycle (i.e. steps (b), (c), (d), (b), ...) may be applied in order to obtain a prescribed accuracy. Note that the mesh refinement step is usually necessary even if a mesh with elements of good shape is produced in step (a). In practice, mesh refinement techniques have proved to be successful tools for decreasing the size of linear systems in step (b) (compared with the method of remeshing the whole region with smaller elements) and increasing the accuracy of the solution of PDEs. Also, mesh refinement is needed in the multigrid method, in which the solution of a problem is obtained by alternatively solving the problem on several levels of coarse to fine grids.

Most previous existing three dimensional (3-D) tetrahedral mesh refinement approaches are based on ad-hoc strategies, and there has been little previous theoretical analysis on the “quality” of a refined mesh, while some guaranteed-quality mesh refinement techniques do exist for a two dimensional (2-D) triangular mesh. The major part of this thesis will focus on developing 3-D local mesh refinement techniques with emphasis on fast algorithms for producing guaranteed-quality refined meshes. In addition, we will also study the shape of tetrahedra, since producing well-shaped tetrahedra is a major difficult problem in both tetrahedral mesh generation and refinement.

This chapter is organized as follows. In Section 1.1, we briefly review existing approaches for mesh generation with emphasis on the shape of tetrahedra produced by different methods. In Section 1.2, we survey existing mesh refinement techniques. The outline of the thesis is described in Section 1.3.

## 1.1 Review of mesh generation

Most problems in 2-D mesh generation have been solved nicely, and various 2-D mesh generators are available, e.g. [YeS83, Lo85, JoS86, Ban90]. Although the research of 3-D mesh generation started a decade ago, currently, some critical problems in 3-D mesh generation are still in their early stage of research, e.g. how to produce well-shaped elements, how to control varying element sizes [Sab91, Le88, She88], etc. We review the existing approaches for mesh generation from three research areas.

### 1.1.1 Approaches in engineering

Most approaches in this category are described at the “method” level, in which a formal algorithmic description, a correctness/efficiency analysis, and/or a quality analysis of the final mesh is lacking. Among them, the most common approach seems to be based on recursive spatial decompositions or octrees [YeS84, PSK89, ScS90, Bur90, ShG91, JuL93]. The basic idea behind this approach is as follows. The region of interest is covered by a root object, e.g. a square, triangle, cube, or tetrahedron. Then the root object is subdivided into a set of child objects with the same type as the root object. Recursive subdivision of the root objects forms a tree, with smaller objects at lower levels of the tree. The final mesh is generated according to the information represented in the tree. One critical problem in this approach is how to deal with the boundary of the region of interest so that generation of poorly-shaped elements is avoided, and a valid triangulation is ensured. To reach these goals, it often needs to significantly increase the number of levels of subdivision and the number of elements near the boundaries. In practice, this approach does not seem to totally eliminate poor tetrahedra near the boundaries and is also sensitive to the coordinate system used in defining the region.

Another approach is based on the advancing front technique [LoP88, PPF88]. At the start of the process, the front is exactly equal to the collection of triangles on the boundary of the regions (the boundary faces are first triangulated appropriately). The front is updated whenever a new element is constructed. A new element is generated by connecting a mesh point to a triangle of the front. With this approach, it is hard to tell in general whether the different groups of tetrahedra advancing from the different boundaries will join correctly in the interior with no tetrahedra of poor shape. Also, this approach is time-consuming compared to other approaches due to the need to check for a well-shaped element and determine that it does not intersect other elements on the front.

The third approach is based on first generating mesh points on the boundary and in the interior of the 3-D region and then connecting the mesh points into a valid triangulation [CFF85, JaB87, Bak89, FiS91, YTH91]. In general, the Delaunay triangulation (or a variant) is used to connect mesh points into a triangulation. Since the Delaunay triangulation (DT) is defined in the convex hull of the given mesh points, for a complicated nonconvex region, a non-trivial step is needed to extract a valid triangulation from the DT, which is in general not addressed rigorously. Also the 3-D Delaunay triangulation may include some

very poorly-shaped elements, e.g. sliver tetrahedra as reported in [CFF85, Joe91a], where the sliver tetrahedron is one with 4 nearly coplanar vertices.

### 1.1.2 Approaches in theoretical computational geometry

A good survey of this category can be found in [BeE92]. One of main focuses is the DT, since the 2-D Delaunay triangulation simultaneously optimizes several of the quality measures, e.g. it maximizes the minimum interior angle [Law77], minimizes maximum circumcircle [Raj91], etc. However, for the 3-D Delaunay triangulation, none of the above two criteria (with the minimum interior angle and maximum circumcircle corresponding to the minimum solid angle and maximum circumsphere, respectively) is optimized [Joe89, BeE92].

Another approach is based on first decomposing a polyhedron into convex parts, and then triangulating each convex part into a tetrahedral mesh [Dey91, DBS91]. Most of previous results for the first stage, convex decomposition, are of more theoretical interest than of practical use for mesh generation, due to complicated algorithms (with emphasis on optimal time complexity or minimum output size) and omission of discussion of degenerate cases [Cha84, ChP89, Dey91]. Also, the quality of convex parts is in general not considered. A quality triangulation of a convex polyhedron is discussed in [DBS91], in which all types of poor tetrahedra but the sliver are eliminated.

Recently, a quality mesh generation algorithm is proposed in [MiV92]. The algorithm is built on some of the ideas in [BEG90]. A more sophisticated method is first used to construct an octree, and then a complicated set of warping rules is applied to conform the octree to the region boundary so that poorly shaped tetrahedra are avoided. The main result is that the algorithm produces a triangulation having the best possible quality up to a constant, independent of the input polyhedron. It is not clear what the constant is, and there hasn't been any implementation of this algorithm yet.

### 1.1.3 Approaches in applied computational geometry

Approaches here are somewhere in the middle between the previous two categories, and have the merits that algorithmic level procedures are provided, parts of the method may use efficient geometric algorithms, the correctness of the algorithm is ensured, and the

implementation issues are discussed in detail.

Joe [Joe94] develops a 3-D mesh generator by a generalization of his 2-D method [JoS86]. The motivation of his approach is based on the objective of generating well-shaped elements by using the techniques of computational geometry, i.e. efficient and correct geometric algorithms are employed for solving well-defined geometric problems. The output of his method will be the input to our mesh refinement research.

The algorithmic procedure of Joe's method consists of three stages. The first stage is a purely geometric stage in which the given polyhedral region is decomposed into convex parts, with the goal that the creation of small dihedral angles is avoided. In the second stage, a mesh distribution function is automatically generated based on sizes of edges and faces and narrowness of subregions, and is used to further subdivide the convex polyhedron from the first stage into small convex parts, so that the variation of mesh size in each part is limited and a uniform tetrahedron or mesh size can be used in each part. In the third stage, 2-D Delaunay triangulations are first constructed on the boundary faces of the convex polyhedra, and then for each convex part, mesh points are generated on a quasi-uniform grid in the polyhedron and are connected up to form tetrahedra subject to the boundary constraints. Local transformations [Joe89] with respect to a tetrahedron shape measure are used to improve the quality of the tetrahedra in each polyhedron.

The 3-D algorithm is not successful as 2-D in terms of avoiding poorly-shaped convex parts. His recent work based on combinations of local transformations significantly improves the quality of tetrahedra in meshes [Joe93].

## 1.2 Review of mesh refinement

We classify mesh refinement approaches into two categories, *local refinement* and *remeshing*. Local refinement is one in which each selected element is directly refined into a set of subelements of the same type, i.e. each new refined element in a refined mesh of an original mesh  $\mathcal{T}$  is a subelement of an element in  $\mathcal{T}$ . We refer to all other mesh refinement approaches based on reducing the size of elements as remeshing.

### 1.2.1 Local refinement

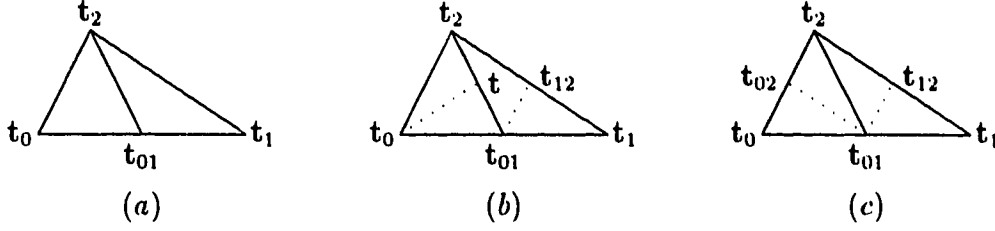


Figure 1.1: Illustration for 2-D local refinement based on bisection;  $t_{ij} = (t_i + t_j)/2$ ,  $i < j$ .

We restrict most of our survey for this category in 2-D, since little previous work exists in 3-D. One of the local refinement approaches is bisection, in which a triangle is refined by connecting a vertex to the midpoint of its opposite edge (see Figure 1.1a). One choice is to divide the longest edge of a triangle, called longest edge bisection. Longest edge bisection can be applied to a triangle or its subsequent subtriangles to produce a sequence of triangular meshes. The properties of refined meshes based on longest edge bisection are well studied [RoS75, Sty80, Adl83, Kea78]. It has been proved that there are only a finite number of similar triangles produced in any refined mesh, independent of the number of refinement levels, and the minimum interior angle over any refined mesh is at least half as good as the minimum interior angle of the original triangle. The above properties demonstrate that longest edge bisection of a single triangle does not produce subtriangles of arbitrarily poor shape. Consequently, several 2-D local refinement techniques based on these properties have been designed [Riv84, Riv87, Riv89]. In [Riv84], each selected triangle is first bisected by longest edge. Then iteratively bisecting the non-conforming triangles by longest edge bisection produces a conforming mesh in a finite number of steps, where a non-conforming triangle means that at least one of the edges of the triangle is subdivided (see triangle  $t_{01}t_{12}t_2$  in Figure 1.1b). Since the conforming process may introduce a large number of intermediate triangles, a modified version is given in [Riv87], where a refined triangle  $T$  is first subdivided into two subtriangles  $T_1$  and  $T_2$  by the longest edge bisection, and then  $T_i$ ,  $i = 1, 2$ , is bisected into two subtriangles by the bisection of the common edge of  $T$  and  $T_i$ ,  $i = 1, 2$  (see Figure 1.1c).

In [RiL92], the method of [Riv84] is extended to 3-D, but there hasn't been any theoretical analysis on the shape of tetrahedra produced in a refined mesh, and experimental results are reported only on some initial meshes of a single tetrahedron. In Chapters 3 and 4, we will present a 3-D local refinement algorithm based on a bisection procedure in which

guaranteed-quality refined meshes are produced.

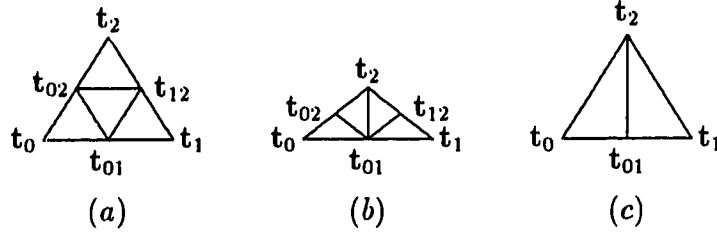


Figure 1.2: Illustration for 2-D local refinement based on regular refinement;  $t_{ij} = (t_i + t_j)/2$ ,  $i < j$ . (a) Refinement with no interior angles greater than  $\pi/2$ . (b) Refinement with one interior angle greater than  $\pi/2$ . (c) Irregular refinement.

The second local refinement approach is regular refinement, in which the midpoints of the edges of a triangle are connected to each other to subdivide the triangle into four similar ones having the same shape as the original triangle [LM85, BaS81] (see Figure 1.2a). When only selected triangles are subdivided by regular refinement in a conforming mesh, non-conforming triangles may arise. To fix the non-conformity, regular refinement is repeatedly applied to any triangle in which at least two edges of the triangle have been subdivided due to the subdivision of its adjacent triangles until each non-conforming triangle has a unique subdivided edge, and then any non-conforming triangle is bisected by its subdivided edge (see Figure 1.2c). The bisection step cleans up the non-conformity at the boundary of regularly refined regions. At the next refinement, if any triangle, produced in the cleaning-up step of the last refinement, needs refinement, its parent is subdivided by regular refinement. Obviously, the shape of any refined triangle is bounded below, since the triangle created in a cleaning-up step is never further refined. In [Ban90], the regular refinement is extended to contain two cases. If no interior angle of a triangle  $T$  is greater than  $\pi/2$ , the regular refinement on  $T$  is the one mentioned above (i.e. Figure 1.2a); otherwise,  $T$  is first refined by bisecting its longest edge, and then each subtriangle is bisected by the common edge of the subtriangle and  $T$  (see Figure 1.2b). It is proved that this refinement produces two triangles with the same shape as the original, and two triangles of better shape in terms of the minimum interior angle of a triangle.

Similar to bisection, the regular refinement technique has been used in the 3-D case with no systematic analysis on the quality of refined tetrahedra, where a 3-D regular refinement



means that each face of a tetrahedron is first refined by the regular refinement of Figure 1.2a, and then the midpoints of a pair of opposite edges are connected to subdivide the inner octahedron into four tetrahedra. It is pointed out in [CSW88] that repeated subdivision of a tetrahedron by regular refinement will yield elements that become arbitrarily slender, which is not always correct because the shape of refined tetrahedra strongly depends on how the inner octahedron is triangulated. In Chapter 5, we will extend the 2-D regular refinement to 3-D, and prove that guaranteed-quality meshes are produced.

In [Mit89], a comparison of adaptive mesh refinement, based on bisection, regular refinement, and some variants of the two methods, is made for some elliptic PDE's problems in 2-D. The main conclusion is that all of the methods considered are efficient and satisfactory for general purpose PDEs solvers with adaptive refinement. This indicates that the extension of bisection and regular refinement to 3-D with guaranteed-quality refined meshes will most likely yield similar results as in 2-D. This is one of the motivations for our thesis.

One main concern of local refinement approaches is how to make them work for a subregion near a curved surface boundary, since the approaches perform refinement directly on each selected element of an existing mesh without considering the boundary information of the original region. A possible solution to this problem is to pull some points on planar boundary faces to the corresponding curved surface boundary of the original region.

### 1.2.2 Remeshing

One remeshing approach uses a similar technique as in a method of mesh generation that is based on recursive spatial decompositions (quadtree/octree) [BaS89, SYB86]. Since tree-based structures are the most common data structure adopted in this mesh generation approach, refinement of selected elements means that a set of leaf-nodes of the tree need a few more levels of subdivision. It seems very simple to perform mesh refinement based on recursive spatial decompositions. However, the refinement also inherits the drawbacks of the corresponding mesh generator.

The second approach for remeshing is based on Delaunay triangulation methods. A set of new mesh points is first added, and then an incremental technique (e.g. [Wat81, Fie86]) is used to construct a new Delaunay triangulation. In [NeF91], the new mesh points are added at the midpoints of edges incident on selected points, which are given by a posteriori error

indicator. In [Fre87], a new mesh point is added somewhere between the circumcentre and centroid of each selected triangle. Note that in this approach, considerable checking may be needed to preserve a valid boundary of a resulting mesh. Also, the Delaunay triangulation in 3-D may contain many “sliver” tetrahedra, which are poorly-shaped.

The third approach is based on an edge “flip” procedure [CSS83]. Each selected triangle is subdivided into three subtriangles by connecting the centroid of the triangle to its three vertices, and then local edge “flip” procedure based on the Delaunay criterion (i.e. empty circumcircle) is used to obtain a global Delaunay triangulation. The extension of this method to 3-D might not be very promising because of the reasons that local face flip (i.e. local transformations) based on the Delaunay criterion (or any valid tetrahedron shape measure) may not produce a global Delaunay (or optimal) triangulation, and that Delaunay triangulation is not necessary a good-quality triangulation.

In this thesis, we are only concerned with local mesh refinement techniques, which are independent of mesh generators.

### 1.3 Outline of thesis

The purpose of this thesis is to study local mesh refinement techniques in 3-D. We choose our research topics based on extensions of 2-D local refinement techniques (e.g. bisection, regular refinement, etc.), since the corresponding 2-D approaches have proved to be successful in practice, but little previous work has been done in 3-D. The extensions are not trivial just as in extending a 2-D mesh generator to 3-D, substantial difficulties may exist.

In Chapter 2, we give an analytic study of tetrahedron shape measures. Formulae for two commonly used shape measures (radius ratio and minimum solid angle) are derived. A novel shape measure based on a mapping from the regular tetrahedron is introduced. The new measure is used in analyzing the quality of meshes generated by our algorithms in later chapters. We conclude that all valid tetrahedron shape measures in question are “equivalent”.

In Chapter 3, we design a bisection procedure for repeated bisection of a single tetrahedron. Some theoretical properties of the procedure are established. In particular, we prove that the bisection procedure produces only a finite number of similar tetrahedra in a

refined mesh, and the shape of any refined tetrahedron is bounded below, independent of the number of refinement levels, in terms of the new tetrahedron shape measure. In Chapter 4, a 3-D local refinement algorithm for a conforming mesh based mainly on the bisection procedure in Chapter 3 is presented. The algorithm not only inherits the main properties from the bisection procedure, but also has the properties that the refinement on some local subregions can be smoothly extended to their adjacent regions, and that the expected time complexity of the algorithm is linearly related to the number of refined tetrahedra in a refined mesh.

In Chapter 5, we present a 3-D local refinement algorithm for a conforming mesh based mainly on a regular refinement. Very similar results to Chapter 4 are obtained, i.e., the algorithm yields guaranteed-quality meshes. In Chapter 6, experimental results from an implementation of the algorithms in Chapters 4 and 5 are provided in terms of the quality of refined meshes as well as the locality of the algorithms. Concluding remarks and some further research problems are discussed in Chapter 7.

Some parts of the thesis will be published, or have been submitted for publication. In particular, a version of Chapter 2 except Section 2.4 will appear in *BIT*, June, 1994 [LiJ94b]. A version of Chapter 3 plus Section 2.4 will be published in *Mathematics of Computation*, July, 1994 [LiJ94a]. Chapters 4, 5, and 6 have been reorganized into two papers submitted for publication [LiJ94c, LiJ94d].

## Chapter 2

# Tetrahedron Shape Measures and Their Relationships

Tetrahedron shape measures are used for evaluating the quality of tetrahedra in finite element meshes. Researchers have used various quantities for measuring the shape or quality of tetrahedra. In this chapter, we first study two commonly used tetrahedron shape measures, and then a novel tetrahedron shape measure is introduced. We compare these three tetrahedron shape measures, and conclude that the three shape measures are “equivalent”.

### 2.1 Introduction

In 2-D triangular mesh generation, the minimum interior angle of a triangle is a commonly used triangle shape measure, and the Delaunay triangulation, which satisfies a max-min angle criterion [Law77], is often used. A natural extension of the minimum interior angle to three dimensions is the *minimum solid angle*  $\theta_{min}$  of a tetrahedron. For finite element meshes, the 3-D Delaunay triangulation may have poorly-shaped tetrahedra [CFF85, Joe91a], and it does not in general satisfy any max-min solid angle criterion [Joe89]. Therefore  $\theta_{min}$  is used in [Joe91a] to improve the quality of 3-D Delaunay triangulations by local transformations.

The *radius ratio*  $\rho$ , which is the ratio of inradius to circumradius of a tetrahedron, scaled by 3, is another shape measure used for tetrahedral meshes [CFF85, Fie86, Joe94]. The radius ratio is also called the *aspect ratio* (e.g. in [Fie86]), but we use the former term, since

the latter is also used for other tetrahedron shape measures (e.g. in [BEG90]). We define a novel shape measure, the *mean ratio*  $\eta$ , based on a mapping from the regular tetrahedron, and use it for analyzing the quality of meshes generated by a bisection procedure in Chapter 3. Some variations of  $\eta$ , such as  $\eta^{3/2}$  [Lo91b] and the analogue of  $\eta$  in 2-D [Lo91a, Ban90], are used in mesh generation, but no theoretical basis is given in these latter references.

In addition to  $\theta_{min}$ ,  $\rho$ , and  $\eta$ , other tetrahedron shape measures have been defined, e.g. see [BEG90, RiL92]. We naturally hope that all of them are “equivalent” in that larger values of the measure represent good quality tetrahedra (i.e. close to a regular tetrahedron) and smaller values represent poor quality tetrahedra (i.e. close to a degenerate tetrahedron). In [Joe94], experimental results show that local transformations based on the  $\theta_{min}$  and  $\rho$  measures produce similar triangulations. Let  $\mu$  and  $\nu$  denote two shape measures (with values  $\leq 1$ ) of a tetrahedron. From experiments,  $\mu$  and  $\nu$  do not seem to possess a linear relationship, similar to that for different vector norms. We shall look for a relationship between  $\mu$  and  $\nu$  of the form  $c_0\mu^{e_0} \leq \nu \leq c_1\mu^{e_1}$  where  $c_0$ ,  $c_1$ ,  $e_0$ , and  $e_1$  are positive constants. This means that if one measure approaches zero, so does the other. If  $e_0$  ( $e_1$ ) is the minimum (maximum) possible exponent, then we say that the lower (upper) bound is *optimal*. If  $c_0$  ( $c_1$ ) is the maximum (minimum) possible constant, then we say that the lower (upper) bound is *tight*.

Throughout this chapter, we will use the following notation. Let  $\mathbf{T}(\mathbf{t}_0, \mathbf{t}_1, \mathbf{t}_2, \mathbf{t}_3)$  stand for a nondegenerate tetrahedron  $\mathbf{T}$  with vertices  $\mathbf{t}_0$ ,  $\mathbf{t}_1$ ,  $\mathbf{t}_2$ , and  $\mathbf{t}_3$ ; sometimes  $\mathbf{t}_i$  denotes the column vector of the coordinates of the vertex. Let  $v$  denote the volume of  $\mathbf{T}$ ,  $s_0 = \text{area}(\Delta \mathbf{t}_1 \mathbf{t}_2 \mathbf{t}_3)$ ,  $s_1 = \text{area}(\Delta \mathbf{t}_0 \mathbf{t}_2 \mathbf{t}_3)$ ,  $s_2 = \text{area}(\Delta \mathbf{t}_0 \mathbf{t}_1 \mathbf{t}_3)$ ,  $s_3 = \text{area}(\Delta \mathbf{t}_0 \mathbf{t}_1 \mathbf{t}_2)$ , and  $l_{ij} = |\mathbf{t}_j - \mathbf{t}_i|$ ,  $0 \leq i < j \leq 3$ , denote the edge lengths of  $\mathbf{T}$ .

This chapter is organized as follows. In Section 2.2, we derive a new formula for the computation of the minimum solid angle  $\theta_{min}$ . An expression for the radius ratio  $\rho$  is given in Section 2.3. The novel measure, mean ratio  $\eta$ , is introduced in Section 2.4. In Sections 2.5, 2.6 and 2.7, the relationships among the three shape measures are established (to avoid the use of trigonometric functions,  $\sigma_{min} = \sin(\theta_{min}/2)$  is actually used instead of  $\theta_{min}$ ). In Section 2.8, we provide a discussion of our results.

## 2.2 Minimum solid angle $\theta_{min}$

The solid angle  $\theta_i$  at vertex  $\mathbf{t}_i$  of tetrahedron  $\mathbf{T}(\mathbf{t}_0, \mathbf{t}_1, \mathbf{t}_2, \mathbf{t}_3)$  is defined to be the surface area formed by projecting each point on the face not containing  $\mathbf{t}_i$  to the unit sphere centered at  $\mathbf{t}_i$  (see Figure 2.1b). The minimum solid angle  $\theta_{min}$  is defined to be the minimum of  $\theta_i$ ,  $i = 0, 1, 2, 3$ . It is shown in [Gad52] that  $0 \leq \sum_{i=0}^3 \theta_i \leq 2\pi$ . Therefore, a very large solid angle (near  $2\pi$ ) for  $\mathbf{T}$  implies that  $\mathbf{T}$  has some small solid angles. That is the reason we only consider the minimum solid angle.

For tetrahedron  $\mathbf{T}$ , let  $\alpha_1 = \angle \mathbf{t}_2 \mathbf{t}_0 \mathbf{t}_3$ ,  $\alpha_2 = \angle \mathbf{t}_1 \mathbf{t}_0 \mathbf{t}_3$ ,  $\alpha_3 = \angle \mathbf{t}_1 \mathbf{t}_0 \mathbf{t}_2$ ,  $\tau = (\alpha_1 + \alpha_2 + \alpha_3)/2$ ,  $\delta_1, \delta_2$ , and  $\delta_3$  be the dihedral angles at edges  $\mathbf{t}_0 \mathbf{t}_1$ ,  $\mathbf{t}_0 \mathbf{t}_2$ , and  $\mathbf{t}_0 \mathbf{t}_3$ , respectively, and  $\mathbf{t}'_1, \mathbf{t}'_2$ , and  $\mathbf{t}'_3$  be the points on the half-lines  $\overrightarrow{\mathbf{t}_0 \mathbf{t}_1}$ ,  $\overrightarrow{\mathbf{t}_0 \mathbf{t}_2}$ , and  $\overrightarrow{\mathbf{t}_0 \mathbf{t}_3}$  such that  $|\mathbf{t}_0 \mathbf{t}'_1| = |\mathbf{t}_0 \mathbf{t}'_2| = |\mathbf{t}_0 \mathbf{t}'_3| = 1$  (see Figure 2.1a). A formula for  $\theta_0$  is  $\theta_0 = \delta_1 + \delta_2 + \delta_3 - \pi$  [Bey81, p. 146]. This formula involves the computation of three dihedral angles, which requires *arccosines*. It is also not easy to use this formula to analyze the relationship between different shape measures. After the following lemma, a simpler formula for the computation of a solid angle is given in Theorem 2.1, and an upper bound for  $\theta_{min}$  is given in Theorem 2.2.

**Lemma 2.1** *The volume  $v'$  of tetrahedron  $\mathbf{T}'(\mathbf{t}_0, \mathbf{t}'_1, \mathbf{t}'_2, \mathbf{t}'_3)$  is*

$$v' = \sqrt{\sin(\tau) \sin(\tau - \alpha_1) \sin(\tau - \alpha_2) \sin(\tau - \alpha_3)} / 3. \quad (2.2.1)$$

**Proof.** It is well known that

$$v' = \sqrt{1 - \cos^2(\alpha_1) - \cos^2(\alpha_2) - \cos^2(\alpha_3) + 2 \cos(\alpha_1) \cos(\alpha_2) \cos(\alpha_3)} / 6,$$

e.g. see [Eri90]. Equations (16) and (17) in [ToL49, p. 28] state that

$$n^2 = \sin(\tau) \sin(\tau - \alpha_1) \sin(\tau - \alpha_2) \sin(\tau - \alpha_3),$$

$$4n^2 = 1 - \cos^2(\alpha_1) - \cos^2(\alpha_2) - \cos^2(\alpha_3) + 2 \cos(\alpha_1) \cos(\alpha_2) \cos(\alpha_3),$$

where  $n$  is called the *norm of the sides* of a spherical triangle. Combining the above three equations yields (2.2.1).  $\square$

**Theorem 2.1** *For any tetrahedron  $\mathbf{T}$ ,*

$$\sin(\theta_0/2) = \frac{12v}{\sqrt{\prod_{1 \leq i < j \leq 3} (l_{0i} + l_{0j} + l_{ij})(l_{0i} + l_{0j} - l_{ij})}}, \quad (2.2.2)$$

where  $v$  is the volume of  $\mathbf{T}$  and the  $l_{ij}$  are the edge lengths of  $\mathbf{T}$ .

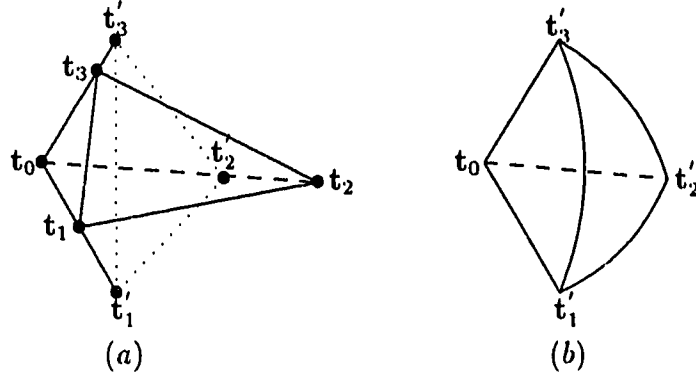


Figure 2.1: (a) Tetrahedron  $t_0 t_1 t_2 t_3$ ;  $|t_0 t'_1| = |t_0 t'_2| = |t_0 t'_3| = 1$ . (b) Solid angle  $\theta_0$  at  $t_0$  is area of spherical triangle  $t'_1 t'_2 t'_3$ .

**Proof.** From Cagnoli's theorem [ToL49, p. 99], we have

$$\sin(\theta_0/2) = \frac{\sqrt{\sin(\tau) \sin(\tau - \alpha_1) \sin(\tau - \alpha_2) \sin(\tau - \alpha_3)}}{2 \cos(\alpha_1/2) \cos(\alpha_2/2) \cos(\alpha_3/2)}. \quad (2.2.3)$$

Let  $v'$  be the volume of tetrahedron  $\mathbf{T}'(t_0, t'_1, t'_2, t'_3)$ . Combining (2.2.3) and (2.2.1) yields

$$\sin(\theta_0/2) = \frac{3v'}{2 \cos(\alpha_1/2) \cos(\alpha_2/2) \cos(\alpha_3/2)}. \quad (2.2.4)$$

Let  $h$  and  $h'$  be the distances from  $t_3$  and  $t'_3$  to the plane containing face  $t_0 t_1 t_2$ , respectively. Then from similar triangles,  $h/h' = |t_0 t_3|/|t_0 t'_3| = l_{03}$ . Also,

$$\text{area}(\Delta t_0 t_1 t_2) / \text{area}(\Delta t_0 t'_1 t'_2) = l_{01} l_{02}.$$

Therefore,

$$\frac{v}{v'} = \frac{h \times \text{area}(\Delta t_0 t_1 t_2)}{h' \times \text{area}(\Delta t_0 t'_1 t'_2)} = l_{01} l_{02} l_{03}. \quad (2.2.5)$$

Since  $\cos(\alpha_1) = (l_{02}^2 + l_{03}^2 - l_{23}^2) / (2l_{02}l_{03})$ , it follows that

$$\cos(\alpha_1/2) = \sqrt{(1 + \cos(\alpha_1))/2} = \frac{1}{2} \sqrt{\frac{(l_{02} + l_{03} + l_{23})(l_{02} + l_{03} - l_{23})}{l_{02}l_{03}}}.$$

Similar formulae can be derived for  $\cos(\alpha_2/2)$  and  $\cos(\alpha_3/2)$ . Substituting these formulae into (2.2.4), and using (2.2.5) yields (2.2.2).  $\square$

**Theorem 2.2** *Let  $\Omega$  be the solid angle of the regular tetrahedron. For any tetrahedron  $\mathbf{T}$ ,*

$$\theta_{\min} \leq \Omega = 3 \arccos(1/3) - \pi, \quad (2.2.6)$$

*where the equality holds iff the tetrahedron is regular.*

**Proof.** Referring to Figure 2.1,  $\alpha_1$ ,  $\alpha_2$ , and  $\alpha_3$  are the arclengths of the three sides of the spherical triangle  $\mathbf{t}'_1\mathbf{t}'_2\mathbf{t}'_3$  on the unit sphere centered at  $\mathbf{t}_0$ . By equation (11) in [ToL49, p. 28],

$$\sin(\delta_1/2) = \sqrt{\frac{\sin(\tau - \alpha_2) \sin(\tau - \alpha_3)}{\sin(\alpha_2) \sin(\alpha_3)}}.$$

Note that  $0 < (\pi + \theta_0)/6 \leq \pi/2$ . When  $\alpha_1 = \alpha_2 = \alpha_3$ , using the above equation,  $0 < \sin((\pi + \theta_0)/6) = \sin((\delta_1 + \delta_2 + \delta_3)/6) = \sin(\delta_1/2) = \sin(\tau/3)/\sin(2\tau/3) = 1/(2\cos(\tau/3))$ . From the well known fact that the area of any spherical triangle does not exceed the area of the equilateral spherical triangle with the same perimeter, and since the area of the spherical triangle  $\mathbf{t}'_1\mathbf{t}'_2\mathbf{t}'_3$  is  $\theta_0$ , we have

$$\sin\left(\frac{\pi + \theta_0}{6}\right) \leq \frac{1}{2\cos(\tau/3)}, \quad (2.2.7)$$

where equality holds iff  $\alpha_1 = \alpha_2 = \alpha_3$ . For  $0 < \tau \leq \pi/2$ ,  $\cos(\tau/3) \geq \sqrt{3}/2$  implies that

$$\sin\left(\frac{\pi + \theta_0}{6}\right) \leq \sqrt{3}/3. \quad (2.2.8)$$

By (2.2.7), the equality (2.2.8) holds iff  $\alpha_1 = \alpha_2 = \alpha_3 = \pi/3$ . Since the sum of all face angles is  $4\pi$ , there exists a vertex, say  $\mathbf{t}_0$ , at which the sum of face angles around it is at most  $\pi$  (i.e.  $\tau \leq \pi/2$ ). Since  $0 \leq \theta_i \leq 2\pi$  and  $\theta_{\min} \leq \theta_i$ ,  $i = 0, 1, 2, 3$ , it follows that

$$\sin\left(\frac{\pi + \theta_{\min}}{6}\right) \leq \sin\left(\frac{\pi + \theta_0}{6}\right). \quad (2.2.9)$$

Combining (2.2.8) and (2.2.9) yields

$$\theta_{\min} \leq \theta_0 \leq 6 \arcsin(\sqrt{3}/3) - \pi = 3 \arccos(1/3) - \pi, \quad (2.2.10)$$

where the last equality follows from elementary trigonometry.

If the tetrahedron is regular, all face angles are  $\pi/3$  and all solid angles are the same. Thus (2.2.8), (2.2.10), and (2.2.6) hold with equality. On the other hand, suppose  $\theta_{\min} = 6 \arcsin(\sqrt{3}/3) - \pi$ . We need to prove that the tetrahedron is regular. Since there exists a vertex at which the sum of its face angles is  $\leq \pi$ , using (2.2.9) and (2.2.8) with equality, we obtain that all of the face angles at the vertex must be  $\pi/3$ . Therefore, there exists at least one of the other three vertices at which the sum of its face angles is  $\leq \pi$ . By a similar argument, the value of its face angles can only be  $\pi/3$ . Continuing this argument shows that the tetrahedron is regular.  $\square$



We have not seen the solid angle formula (2.2.2) in the literature. In [Eri90], a formula is given in terms of  $\tan(\theta_0/2)$ . That is,

$$\tan(\theta_0/2) = \frac{6v'}{1 + \mathbf{u}_1 \cdot \mathbf{u}_2 + \mathbf{u}_1 \cdot \mathbf{u}_3 + \mathbf{u}_2 \cdot \mathbf{u}_3}, \quad (2.2.11)$$

where  $\mathbf{u}_i = \mathbf{t}_i' - \mathbf{t}_0$ ,  $i = 1, 2, 3$ . Formula (2.2.2) is as simple as (2.2.11), but has the advantage that  $\sin(\theta_0/2)$  is bounded whereas  $\tan(\theta_0/2)$  is unbounded. However, the formula (2.2.11) is better if  $\theta_0$  must be computed since  $\sin(\theta_0/2) = \sin(\pi - \theta_0/2)$ ; the sign of the denominator of (2.2.11) can be used to determine whether  $\theta_0$  is closer to 0 or  $2\pi$ .

Since the right hand side of (2.2.2) has no trigonometric functions, a better shape measure for computation is  $\sigma_{\min} = \min(\sigma_0, \sigma_1, \sigma_2, \sigma_3)$  where  $\sigma_i = \sin(\theta_i/2)$ . Suppose  $\theta_{\min} = \theta_0 \leq \theta_1 \leq \theta_2 \leq \theta_3$ . Since  $0 \leq \sum_{i=0}^3 \theta_i \leq 2\pi$ , only  $\theta_3$  may be larger than  $\pi$ , so  $\sigma_0 \leq \sigma_1 \leq \sigma_2$ . Since  $\theta_2 \leq \theta_3 \leq 2\pi - \theta_2$ , we have  $\sigma_2 \leq \sigma_3$ . Hence

$$\sigma_{\min} = \sin(\theta_{\min}/2) \leq \sin(\Omega/2) = \sqrt{6}/9,$$

with equality holding only for the regular tetrahedron, where the last equality is obtained using (2.2.3). To 4 decimal places,  $\theta_{\min} = 0.5513$  and  $\sigma_{\min} = 0.2722$  for the regular tetrahedron.

### 2.3 Radius ratio $\rho$

The *radius ratio* of a tetrahedron  $\mathbf{T}$  is defined to be  $\rho = 3r_{\text{in}}/r_{\text{circ}}$ , where  $r_{\text{in}}$  and  $r_{\text{circ}}$  are the inradius and circumradius, respectively, of  $\mathbf{T}$  (see Figures 2.2a and 2.2b for an illustration in the 2-D case). The following theorem gives a formula for computing  $\rho$ .

**Theorem 2.3** *For any tetrahedron  $\mathbf{T}$ ,*

$$\rho = \frac{216v^2}{\sum_{i=0}^3 s_i \sqrt{(a+b+c)(a+b-c)(a+c-b)(b+c-a)}}, \quad (2.3.1)$$

where  $v$  is the volume of  $\mathbf{T}$ , the  $s_i$  are the areas of the four faces of  $\mathbf{T}$ , and  $a, b, c$  are the products of the lengths of opposite edges of  $\mathbf{T}$ .

**Proof.** From [MPV89, pp. 463, 555]

$$r_{\text{in}} = 3v / \sum_{i=0}^3 s_i, \quad (2.3.2)$$

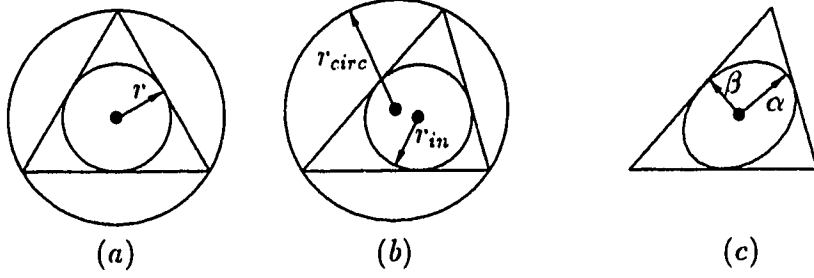


Figure 2.2: Illustration of incircle, circumcircle, and inscribed ellipse for triangles. (a) Equilateral triangle with  $r_{in} = r$ ,  $r_{circ} = 2r$ . (b) For a triangle,  $\rho = 2r_{in}/r_{circ}$ . (c) Triangle and inscribed ellipse are formed by applying affine transformation to equilateral triangle and incircle of (a);  $\eta = 2\sqrt{\lambda_1\lambda_2}/(\lambda_1 + \lambda_2)$  where  $\lambda_1 = \alpha^2/r^2$ ,  $\lambda_2 = \beta^2/r^2$ .

$$r_{circ} = \frac{\sqrt{(a+b+c)(a+b-c)(a+c-b)(b+c-a)}}{24v}, \quad (2.3.3)$$

where the latter 3 factors in the numerator are all positive. Combining (2.3.2) and (2.3.3) yields (2.3.1).  $\square$

It is known that  $\rho \leq 1$  for any tetrahedron, and the equality holds iff the tetrahedron is regular [MPV89, p. 553].

## 2.4 Mean ratio $\eta$

In this section, we introduce a novel shape measure  $\eta$ , and derive a simple expression for its computation. The basic idea is as follows. The regular tetrahedron, in which all edges have the same length, is considered well-shaped. For any tetrahedron  $\mathbf{T}$ , we compare the shape of  $\mathbf{T}$  with the regular tetrahedron via a transformation matrix from the regular tetrahedron to  $\mathbf{T}$ . More details about the application of  $\eta$  in local refinement algorithms will be addressed in Chapters 3, 4, and 5.

**Definition 2.1** For any (nondegenerate) tetrahedron  $\mathbf{T}(\mathbf{t}_0, \mathbf{t}_1, \mathbf{t}_2, \mathbf{t}_3)$ , define the 3 by 3 non-singular matrix  $T = [\mathbf{t}_1 - \mathbf{t}_0, \mathbf{t}_2 - \mathbf{t}_0, \mathbf{t}_3 - \mathbf{t}_0]$ . Note that the matrix has the same name as the tetrahedron but italic font is used instead of bold font, and  $T$  depends on the ordering of vertices of  $\mathbf{T}$ . For any two tetrahedra  $\mathbf{S}(\mathbf{s}_0, \mathbf{s}_1, \mathbf{s}_2, \mathbf{s}_3)$  and  $\mathbf{T}(\mathbf{t}_0, \mathbf{t}_1, \mathbf{t}_2, \mathbf{t}_3)$ , define the 3 by 3 matrices  $M(\mathbf{S}, \mathbf{T}) = TS^{-1}$  and  $A(\mathbf{S}, \mathbf{T}) = M^T(\mathbf{S}, \mathbf{T})M(\mathbf{S}, \mathbf{T})$ . Note that  $M$  and  $A$  also depend on the ordering of tetrahedron vertices, and  $M$  is the matrix involved in the affine transformation from points of  $\mathbf{S}$  to points of  $\mathbf{T}$  such that  $\mathbf{t}_i = M(\mathbf{S}, \mathbf{T})\mathbf{s}_i + \mathbf{b}$ ,  $0 \leq i \leq 3$ , where  $\mathbf{b} = \mathbf{t}_0 - M(\mathbf{S}, \mathbf{T})\mathbf{s}_0$ .

**Definition 2.2** Let  $\mathbf{T}(\mathbf{t}_0, \mathbf{t}_1, \mathbf{t}_2, \mathbf{t}_3)$  be any tetrahedron, and  $\mathbf{R}(\mathbf{r}_0, \mathbf{r}_1, \mathbf{r}_2, \mathbf{r}_3)$  be a regular tetrahedron with the same volume as  $\mathbf{T}$ . Define the tetrahedron shape measure  $\eta(\mathbf{T}) = 3\sqrt[3]{\lambda_1\lambda_2\lambda_3}/(\lambda_1 + \lambda_2 + \lambda_3)$ , where  $\lambda_1, \lambda_2$ , and  $\lambda_3$  are the eigenvalues of the matrix  $A(\mathbf{R}, \mathbf{T})$ . Note that the 3 eigenvalues are positive since  $A$  is positive definite, and  $0 < \eta(\mathbf{T}) \leq 1$  with  $\eta(\mathbf{T}) = 1$  iff  $\lambda_1 = \lambda_2 = \lambda_3$ .

**Theorem 2.4** For any tetrahedron  $\mathbf{T}(\mathbf{t}_0, \mathbf{t}_1, \mathbf{t}_2, \mathbf{t}_3)$ ,

$$\eta(\mathbf{T}) = 12(3v)^{2/3} / \sum_{0 \leq i < j \leq 3} l_{ij}^2 \quad (2.4.1)$$

where  $v$  is the volume of  $\mathbf{T}$  and the  $l_{ij}$  are the lengths of the edges of  $\mathbf{T}$ . Furthermore  $\eta(\mathbf{T})$  is independent of the ordering of vertices of  $\mathbf{T}$ ,  $\mathbf{R}$  and  $\mathbf{o}_i$  the vertex coordinates of  $\mathbf{R}$ .

**Proof.** We first let  $\mathbf{R}(\mathbf{r}_0, \mathbf{r}_1, \mathbf{r}_2, \mathbf{r}_3)$  be the regular tetrahedron with the same volume as  $\mathbf{T}(\mathbf{t}_0, \mathbf{t}_1, \mathbf{t}_2, \mathbf{t}_3)$ , whose vertex coordinates are  $\mathbf{r}_0 = (-\sqrt{3}a/2, 0, 0)^T$ ,  $\mathbf{r}_1 = (0, -a/2, 0)^T$ ,  $\mathbf{r}_2 = (0, a/2, 0)^T$ , and  $\mathbf{r}_3 = (-\sqrt{3}a/6, 0, \sqrt{6}a/3)^T$ , where  $a = (6\sqrt{2}v)^{1/3}$  and  $v$  is the volume of  $\mathbf{T}$ . Let  $T = [\mathbf{t}_1 - \mathbf{t}_0, \mathbf{t}_2 - \mathbf{t}_0, \mathbf{t}_3 - \mathbf{t}_0]$  and  $R = [\mathbf{r}_1 - \mathbf{r}_0, \mathbf{r}_2 - \mathbf{r}_0, \mathbf{r}_3 - \mathbf{r}_0]$ . Then

$$R = a \begin{bmatrix} \sqrt{3}/2 & \sqrt{3}/2 & \sqrt{3}/3 \\ -1/2 & 1/2 & 0 \\ 0 & 0 & \sqrt{6}/3 \end{bmatrix}, \quad R^{-1} = \frac{1}{a} \begin{bmatrix} 1/\sqrt{3} & -1 & -1/\sqrt{6} \\ 1/\sqrt{3} & 1 & -1/\sqrt{6} \\ 0 & 0 & 3/\sqrt{6} \end{bmatrix}. \quad (2.4.2)$$

Let  $d_{ij} = (\mathbf{t}_j - \mathbf{t}_i)^T(\mathbf{t}_j - \mathbf{t}_i)$ ,  $0 \leq i < j \leq 3$ . Then

$$T^T T = \begin{bmatrix} d_{01} & (d_{01} + d_{02} - d_{12})/2 & (d_{01} + d_{03} - d_{13})/2 \\ (d_{01} + d_{02} - d_{12})/2 & d_{02} & (d_{02} + d_{03} - d_{23})/2 \\ (d_{01} + d_{03} - d_{13})/2 & (d_{02} + d_{03} - d_{23})/2 & d_{03} \end{bmatrix}. \quad (2.4.3)$$

From (2.4.2), (2.4.3), and  $A(\mathbf{R}, \mathbf{T}) = M^T(\mathbf{R}, \mathbf{T})M(\mathbf{R}, \mathbf{T}) = (R^{-1})^T T^T T R^{-1}$ , we obtain

$$A(\mathbf{R}, \mathbf{T}) = \frac{1}{a^2} \begin{bmatrix} (2d_{01} + 2d_{02} - d_{12})/3 & \# & \# \\ \# & d_{12} & \# \\ \# & \# & (3d_{03} + 3d_{13} + 3d_{23} - d_{01} - d_{02} - d_{12})/6 \end{bmatrix} \quad (2.4.4)$$

where # denotes a value which is irrelevant. Then

$$\lambda_1 + \lambda_2 + \lambda_3 = \text{trace}(A(\mathbf{R}, \mathbf{T})) = (d_{01} + d_{02} + d_{03} + d_{12} + d_{13} + d_{23})/(2a^2). \quad (2.4.5)$$

Since  $\mathbf{R}$  and  $\mathbf{T}$  have the same volume,  $\det(M(\mathbf{R}, \mathbf{T})) = \pm 1$ . So

$$\lambda_1 \lambda_2 \lambda_3 = \det(A(\mathbf{R}, \mathbf{T})) = 1. \quad (2.4.6)$$

From (2.4.5), (2.4.6), and Definition 2.2,

$$\eta(\mathbf{T}) = \frac{3\sqrt[3]{\det(A(\mathbf{R}, \mathbf{T}))}}{\text{trace}(A(\mathbf{R}, \mathbf{T}))} = \frac{12(3v)^{2/3}}{\sum_{0 \leq i < j \leq 3} l_{ij}^2} \quad (2.4.7)$$

where the  $l_{ij}$  are the lengths of the edges of  $\mathbf{T}$ .

Now we allow the vertices of  $\mathbf{T}$  and  $\mathbf{R}$  to be permuted and different vertex coordinates for  $\mathbf{R}$ . Let  $\bar{T}$ ,  $\bar{R}$ ,  $\bar{M}(\mathbf{R}, \mathbf{T})$ , and  $\bar{A}(\mathbf{R}, \mathbf{T})$  be the resulting matrices. Then  $\bar{T} = TP_1L_1P_2$  and  $\bar{R} = QRP_3L_2P_4$ , where  $Q$  is an orthogonal matrix, the  $P_i$  are permutation matrices, and each  $L_i$  is either the identity matrix  $I$  or

$$L = \begin{bmatrix} 1 & 0 & 0 \\ 0 & 1 & 0 \\ -1 & -1 & -1 \end{bmatrix},$$

because  $[t_1 - t_3, t_2 - t_3, t_0 - t_3] = [t_1 - t_0, t_2 - t_0, t_3 - t_0]L = TL$ . Since  $L^{-1} = L$ ,

$$\bar{A}(\mathbf{R}, \mathbf{T}) = (\bar{R}^{-1})^T \bar{T}^T \bar{T} \bar{R}^{-1} = Q(R^{-1})^T P_3 L_2^T P_4 P_2^T L_1^T P_1^T T^T T P_1 L_1 P_2 P_4^T L_2 P_3^T R^{-1} Q^T.$$

Let  $\hat{A}(\mathbf{R}, \mathbf{T}) = Q^T \bar{A}(\mathbf{R}, \mathbf{T}) Q$ . If  $P$  is a permutation matrix, then  $P^T T^T T P$  just applies a symmetric permutation to the matrix of (2.4.3). Similarly,

$$L^T T^T T L = \begin{bmatrix} d_{13} & (d_{13} + d_{23} - d_{12})/2 & (d_{03} + d_{13} - d_{01})/2 \\ (d_{13} + d_{23} - d_{12})/2 & d_{23} & (d_{03} + d_{23} - d_{02})/2 \\ (d_{03} + d_{13} - d_{01})/2 & (d_{03} + d_{23} - d_{02})/2 & d_{03} \end{bmatrix}.$$

Therefore  $\hat{A}(\mathbf{R}, \mathbf{T})$  has the same form as (2.4.4), with the  $d_{ij}$  permuted, and (2.4.5), (2.4.6), and (2.4.7) are unchanged if  $A$  is replaced with  $\hat{A}$ . Finally, the eigenvalues  $\lambda_i$  of  $\hat{A}(\mathbf{R}, \mathbf{T})$  and

$\bar{A}(\mathbf{R}, \mathbf{T}) = Q \hat{A}(\mathbf{R}, \mathbf{T}) Q^T$  are identical, so  $\eta(\mathbf{T}) = 12(3v)^{2/3} / \sum_{0 \leq i < j \leq 3} l_{ij}^2$  is independent of the ordering of vertices of  $\mathbf{T}$ ,  $\mathbf{R}$  and of the vertex coordinates of  $\mathbf{R}$ .  $\square$

Now we give a geometric explanation of  $\eta(\mathbf{T})$ . Let  $O$  be the inscribed sphere in the regular tetrahedron  $\mathbf{R}$  and  $r$  be its radius. The affine transformation  $\mathbf{y} = M(\mathbf{R}, \mathbf{T})\mathbf{x} + \mathbf{b}$ , which transforms the points of  $\mathbf{R}$  into the points of  $\mathbf{T}$ , transforms the sphere  $O$  into an inscribed ellipsoid  $E$  in  $\mathbf{T}$ . Let the equation of  $O$  be

$$(\mathbf{x} + \mathbf{b}_0)^T(\mathbf{x} + \mathbf{b}_0) = r^2.$$

Then the equation of  $E$  is

$$(\mathbf{y} + \mathbf{b}_1)^T(M^{-1}(\mathbf{R}, \mathbf{T}))^T M^{-1}(\mathbf{R}, \mathbf{T})(\mathbf{y} + \mathbf{b}_1) = r^2.$$

Let  $\alpha, \beta, \gamma$  be the half-lengths of the three principal axes inside the ellipsoid, and  $\lambda_1, \lambda_2$ , and  $\lambda_3$  be the eigenvalues of  $M^T(\mathbf{R}, \mathbf{T})M(\mathbf{R}, \mathbf{T})$ . After a translation and a rotation, the equation of the ellipsoid becomes

$$\frac{x_1^2}{\lambda_1} + \frac{x_2^2}{\lambda_2} + \frac{x_3^2}{\lambda_3} = r^2,$$

where  $(x_1, x_2, x_3)$  is any point on the ellipsoid. So  $\alpha^2 = \lambda_1 r^2$ ,  $\beta^2 = \lambda_2 r^2$ , and  $\gamma^2 = \lambda_3 r^2$ . Since  $\lambda_1 \lambda_2 \lambda_3 = 1$ ,  $r^2 = \sqrt[3]{\alpha^2 \beta^2 \gamma^2}$ . From Definition 2.2,

$$\eta(\mathbf{T}) = \frac{3\sqrt[3]{\lambda_1 \lambda_2 \lambda_3}}{\lambda_1 + \lambda_2 + \lambda_3} = \frac{3\sqrt[3]{\alpha^2 \beta^2 \gamma^2}}{\alpha^2 + \beta^2 + \gamma^2}.$$

So  $\eta(\mathbf{T})$  is the ratio of the geometric mean to the arithmetic mean of  $\alpha^2, \beta^2$ , and  $\gamma^2$  (see Figure 2.2c for an illustration in the 2-D case). In some sense we can say that  $\eta(\mathbf{T})$  reflects the shape of the inscribed ellipsoid  $E$  and hence the shape of  $\mathbf{T}$ .

From Definition 2.2, Theorem 2.4, and the above explanation, it follows that  $\eta(\mathbf{T}) = 1$  iff  $\mathbf{T}$  is a regular tetrahedron, and  $\eta(\mathbf{T})$  approaches zero for poorly-shaped tetrahedra.

Since our research is focused on 3-D tetrahedral meshes, the definition of  $\eta$  is given in 3-D. In fact, we can define  $\eta$  for any  $n$ -dimensional simplex  $\mathbf{T}$ . This is given in Appendix A.

## 2.5 Relationship between $\rho$ and $\eta$

In the remainder of this chapter, we will use the fact that for any tetrahedron  $\mathbf{T}$ , there is a coordinate system such that the vertices of  $\mathbf{T}$  have the coordinates shown in Figure 2.3.

Sometimes, we will also assume that  $t_0t_1$  has the maximum length among the edges. Note that if  $r = l_{01}$  is the maximum length then  $0 < s < r$ ,  $0 < t < r$ ,  $0 < x < r$ ,  $-r < y < r$ , and  $0 < z < r$ . Also we will frequently use the inequality:

$$\sqrt[n]{\prod_{i=1}^n x_i} \leq \frac{\sum_{i=1}^n x_i}{n} \leq \sqrt{\sum_{i=1}^n x_i^2/n}, \quad (2.5.1)$$

where  $x_i \geq 0$ ,  $i = 1, \dots, n$ . The left inequality states that the arithmetic mean is not less than the geometric mean [Kaz61, p. 20]. The right inequality can be obtained by expanding  $(\sum_{i=1}^n x_i)^2$  and using  $2x_i x_j \leq x_i^2 + x_j^2$ .

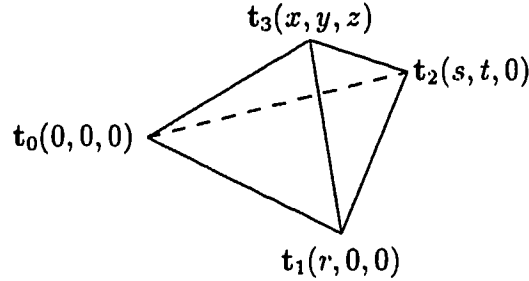


Figure 2.3: A tetrahedron with  $r > 0$ ,  $t > 0$ ,  $z > 0$ .

The following lemma is needed to establish the relationship between  $\rho$  and  $\eta$ .

**Lemma 2.2** *For any tetrahedron  $\mathbf{T}$ ,*

$$\sum_{i=0}^3 s_i \geq 3\sqrt[3]{3} \sqrt{v \max_{0 \leq i < j \leq 3} l_{ij}}, \quad (2.5.2)$$

where the lower bound is tight.

**Proof.** Without loss of generality, suppose the coordinate system is chosen so that  $\mathbf{T}$  has the coordinates shown in Figure 2.3 and  $r = \max_{0 \leq i < j \leq 3} l_{ij}$ . Then  $v = rtz/6$ . Using Heron's triangle area formula [Kaz61, p. 35],

$$s_0 = \sqrt{(tz)^2 + (rz - sz)^2 + (tx - sy + ry - rt)^2}/2, \quad s_3 = rt/2,$$

$$s_1 = \sqrt{(tz)^2 + (sz)^2 + (tx - sy)^2}/2, \quad s_2 = r\sqrt{y^2 + z^2}/2.$$

From [Kaz61, pp. 106, 27],  $\sqrt{x_1^2 + y_1^2} + \sqrt{x_2^2 + y_2^2} \geq \sqrt{(x_1 + x_2)^2 + (y_1 + y_2)^2}$  for  $x_i \geq 0$  and  $y_i \geq 0$ ,  $i = 1, 2$ , and  $|x_1 \pm x_2| + |y_1| \geq |x_2|$ , so it follows that

$$2(s_0 + s_1) \geq \sqrt{(rz - sz)^2 + (tx - sy + ry - rt)^2} + \sqrt{(sz)^2 + (tx - sy)^2}$$

$$\begin{aligned}
&\geq \sqrt{(rz)^2 + (|tx - sy + ry - rt| + |tx - sy|)^2} \geq \sqrt{(rz)^2 + r^2(y - t)^2} = r\sqrt{z^2 + (y - t)^2}, \\
2(s_0 + s_1 + s_2) &\geq r(\sqrt{z^2 + (y - t)^2} + \sqrt{z^2 + y^2}) \geq r\sqrt{4z^2 + (|y - t| + |y|)^2} \geq r\sqrt{4z^2 + t^2}, \\
2 \sum_{i=0}^3 s_i / \sqrt{vr} &\geq (rt + r\sqrt{4z^2 + t^2}) / \sqrt{r^2 tz / 6} = \sqrt{6} (t + \sqrt{4z^2 + t^2}) / \sqrt{tz}.
\end{aligned}$$

Since  $f(z) = (t + \sqrt{t^2 + 4z^2}) / \sqrt{tz}$  achieves the minimum value of  $3\sqrt{2}/\sqrt[4]{3}$  at  $z = \sqrt{3}t/2$ ,  $\sum_{i=0}^3 s_i / \sqrt{vr} \geq \sqrt{6} f(\sqrt{3}t/2) / 2 = 3\sqrt[4]{3}$ , which is (2.5.2).

We now prove that the lower bound is tight. Using the coordinate system of Figure 2.3, let  $s = r/2$ ,  $t = \sqrt{3}r/2$ ,  $x = r/2$ ,  $y = \sqrt{3}r/6$ , and  $z = 1$  (i.e.  $\Delta t_0 t_1 t_2$  is an equilateral triangle and  $t_3$  is above the centroid of  $\Delta t_0 t_1 t_2$ ). Then  $\sum_{i=0}^3 s_i = \sqrt{3}r^2/4 + 3r\sqrt{1 + r^2/12}/2$  and  $\sqrt{v \max_{0 \leq i < j \leq 3} l_{ij}} = \sqrt[4]{3} r \sqrt[4]{1 + r^2/3} / \sqrt{12}$  if  $r$  is sufficiently small. So  $\sum_{i=0}^3 s_i / \sqrt{v \max_{0 \leq i < j \leq 3} l_{ij}}$  approaches  $3\sqrt[4]{3}$  when  $r$  approaches zero.  $\square$

**Theorem 2.5** *For any tetrahedron  $T$ ,*

$$\eta^3 \leq \rho \leq (2/\sqrt[4]{6}) \eta^{3/4}. \quad (2.5.3)$$

*Furthermore, the lower bound is optimal and tight, and the upper bound is optimal.*

**Proof.** We first prove the left inequality. From the well known fact that the area of any triangle does not exceed the area of the equilateral triangle with the same perimeter, we have

$$s_0 \leq (\sqrt{3}/36)(l_{12} + l_{13} + l_{23})^2, \quad (2.5.4)$$

where the right side is the area of an equilateral triangle with edge length  $(l_{12} + l_{13} + l_{23})/3$ .

We can obtain similar inequalities for  $s_1$ ,  $s_2$ , and  $s_3$ , so

$$\sum_{i=0}^3 s_i \leq (\sqrt{3}/36) \sum_{0 \leq i < j < k \leq 3} (l_{ij} + l_{ik} + l_{jk})^2. \quad (2.5.5)$$

Let  $a = l_{01}l_{23}$ ,  $b = l_{02}l_{13}$ , and  $c = l_{03}l_{12}$ . From the left inequality of (2.5.1),

$$\begin{aligned}
&\sqrt{(a + b + c)(a + b - c)(a + c - b)(b + c - a)} \leq (\sqrt{3}/9)(a + b + c)^2 \\
&= (\sqrt{3}/9)(l_{01}l_{23} + l_{02}l_{13} + l_{03}l_{12})^2 \leq (\sqrt{3}/36) \left( \sum_{0 \leq i < j \leq 3} l_{ij}^2 \right)^2,
\end{aligned} \quad (2.5.6)$$

where the last inequality is from  $(l_{01} - l_{23})^2 + (l_{02} - l_{13})^2 + (l_{03} - l_{12})^2 \geq 0$ . Combining (2.3.1), (2.5.5), and (2.5.6), we have

$$\rho \geq \frac{216 \cdot 36 \cdot 12v^2}{(\sum_{0 \leq i < j \leq 3} l_{ij}^2)^2 \sum_{0 \leq i < j < k \leq 3} (l_{ij} + l_{ik} + l_{jk})^2}.$$

From (2.4.1), it follows that

$$\frac{\rho}{\eta^3} \geq \frac{6 \sum_{0 \leq i < j \leq 3} l_{ij}^2}{\sum_{0 \leq i < j < k \leq 3} (l_{ij} + l_{ik} + l_{jk})^2}.$$

Expanding the denominator of the above equation and using  $2xy \leq x^2 + y^2$ , we have  $\rho/\eta^3 \geq 1$ . For the regular tetrahedron,  $\rho = \eta = 1$ , so the lower bound is tight.

We now prove the right inequality in (2.5.3). Since  $\rho$  and  $\eta$  are invariant under uniform scaling (i.e. when the scaling factors along the three axes are the same), without loss of generality, assume the circumradius of  $\mathbf{T}$  is 1. Then  $\rho = 9v/\sum_{i=0}^3 s_i$  by (2.3.2). So combining (2.4.1) and (2.5.2), it follows that

$$\rho/\eta^{3/4} = (3^{3/4} \sqrt{2}/4)v^{1/2} \left( \sum_{0 \leq i < j \leq 3} l_{ij}^2 \right)^{3/4} / \sum_{i=0}^3 s_i \leq (\sqrt{6}/12) \left( \sum_{0 \leq i < j \leq 3} l_{ij}^2 \right)^{3/4} / \sqrt{\max_{0 \leq i < j \leq 3} l_{ij}}.$$

Since  $(\sum_{0 \leq i < j \leq 3} l_{ij}^2)^{1/4} \leq \sqrt[4]{6} \sqrt{\max_{0 \leq i < j \leq 3} l_{ij}}$  and  $\sum_{0 \leq i < j \leq 3} l_{ij}^2 \leq 16$  from [MPV89, p. 558], it follows that

$$\rho/\eta^{3/4} \leq (6^{3/4}/12) \left( \sum_{0 \leq i < j \leq 3} l_{ij}^2 \right)^{1/2} \leq 2/\sqrt[4]{6}.$$

Finally we show that both bounds in (2.5.3) are optimal, i.e. if there exist constants  $c_0, c_1, e_0$ , and  $e_1$  such that  $c_0 \eta^{e_0} \leq \rho$  and  $c_1 \eta^{e_1} \geq \rho$ , then  $e_0 \geq 3$  and  $e_1 \leq 3/4$ . Using the coordinate system of Figure 2.3, let  $r = 1, s = 1/2, t = \sqrt{3}/2, x = 1/2$ , and  $y = \sqrt{3}/6$ . If  $z$  approaches 0, it is easily verified that  $\rho = O(z^2)$  and  $\eta = O(z^{2/3})$  by using the formulae (2.3.1) and (2.4.1). Therefore, it is impossible that  $c_0 \eta^{e_0} \leq \rho$  for  $e_0 < 3$ , when  $z$  approaches zero. If  $z$  approaches  $\infty$ , we obtain  $\rho = O(1/z)$  and  $\eta = O(1/z^{4/3})$ . By a similar argument,  $e_1$  must be less than or equal to  $3/4$ .  $\square$

## 2.6 Relationship between $\sigma_{min}$ and $\eta$

Let

$$\begin{aligned} d_0^2 = & (l_{01} + l_{02} + l_{12})(l_{01} + l_{02} - l_{12})(l_{01} + l_{03} + l_{13})(l_{01} + l_{03} - l_{13}) \\ & \cdot (l_{02} + l_{03} + l_{23})(l_{02} + l_{03} - l_{23}), \end{aligned} \quad (2.6.1)$$

$$\begin{aligned} d_1^2 = & (l_{01} + l_{02} + l_{12})(l_{01} + l_{12} - l_{02})(l_{01} + l_{03} + l_{13})(l_{01} + l_{13} - l_{03}) \\ & \cdot (l_{12} + l_{13} + l_{23})(l_{12} + l_{13} - l_{23}). \end{aligned} \quad (2.6.2)$$

The following lemma is needed to establish the relationship between  $\sigma_{min} = \sin(\theta_{min}/2)$  and  $\eta$ .



**Lemma 2.3** Suppose  $l_{01}$  is the maximum edge length and  $l_{02} \geq l_{12}$ . If  $l_{03} \geq l_{13}$ ,

$$\max(d_0, d_1) \geq 2l_{01}^{5/2} \sqrt{l_{02} + l_{03} - l_{23}}. \quad (2.6.3)$$

If  $l_{03} < l_{13}$ ,

$$\max(d_0, d_1) \geq l_{01}^2 \sqrt{l_{03} l_{12}}. \quad (2.6.4)$$

**Proof.** Since  $l_{01} + l_{02} + l_{12} > 2l_{01}$  and  $l_{01} + l_{03} + l_{13} > 2l_{01}$ , from (2.6.1) and (2.6.2), we have

$$d_0^2 \geq 4l_{01}^2(l_{01} + l_{02} - l_{12})(l_{01} + l_{03} - l_{13})(l_{02} + l_{03} - l_{23})(l_{02} + l_{03} + l_{23}), \quad (2.6.5)$$

$$d_1^2 \geq 4l_{01}^2(l_{01} + l_{12} - l_{02})(l_{01} + l_{13} - l_{03})(l_{12} + l_{13} - l_{23})(l_{12} + l_{13} + l_{23}). \quad (2.6.6)$$

Case 1:  $l_{03} \geq l_{13}$ . By (2.6.5), we obtain

$$d_0^2 \geq 4l_{01}^2 \cdot l_{01} \cdot l_{01} \cdot (l_{02} + l_{03} - l_{23}) \cdot (l_{02} + l_{03}) \geq 4l_{01}^5(l_{02} + l_{03} - l_{23}),$$

since  $l_{02} \geq l_{01}/2$  and  $l_{03} \geq l_{01}/2$ . Thus,  $\max(d_0, d_1) \geq d_0 \geq 2l_{01}^{5/2} \sqrt{l_{02} + l_{03} - l_{23}}$ , which is (2.6.3).

Case 2:  $l_{03} < l_{13}$ . From (2.6.5), (2.6.6),  $l_{02} + l_{03} + l_{23} \geq 2l_{02} \geq l_{01}$ , and  $l_{12} + l_{13} + l_{23} \geq 2l_{13} \geq l_{01}$ , it follows that

$$d_0^2 \geq 4l_{01}^4(l_{01} + l_{03} - l_{13})(l_{02} + l_{03} - l_{23}) \geq 4l_{01}^4 l_{03}(l_{02} + l_{03} - l_{23}), \quad (2.6.7)$$

$$d_1^2 \geq 4l_{01}^4(l_{01} + l_{12} - l_{02})(l_{12} + l_{13} - l_{23}) \geq 4l_{01}^4 l_{12}(l_{12} + l_{13} - l_{23}). \quad (2.6.8)$$

If  $l_{03} \geq 3l_{01}/4$ , then from (2.6.7),

$$\max(d_0^2, d_1^2) \geq d_0^2 \geq 4l_{01}^4 l_{03}(l_{01}/2 + 3l_{01}/4 - l_{23}) \geq l_{01}^4 l_{03} l_{12},$$

which is equivalent to (2.6.4). Similarly, if  $l_{12} \geq 3l_{01}/4$ ,  $\max(d_0^2, d_1^2) \geq l_{01}^4 l_{03} l_{12}$  by using (2.6.8). The final subcase is  $l_{03} < 3l_{01}/4$  and  $l_{12} < 3l_{01}/4$ . From [MPV89, p. 549],  $l_{23} < l_{02}l_{13}/l_{01} + l_{03}l_{12}/l_{01}$ . Thus, from (2.6.7),

$$d_0^2 \geq 4l_{01}^4 l_{03}(l_{02} + l_{03} - l_{02}l_{13}/l_{01} - l_{03}l_{12}/l_{01}) \geq 4l_{01}^4 l_{03}^2(1 - l_{12}/l_{01}) \geq l_{01}^4 l_{03}^2.$$

Likewise, from (2.6.8), we have  $d_1^2 \geq l_{01}^4 l_{12}^2$ . Therefore,

$$\max(d_0^2, d_1^2) \geq (d_0^2 + d_1^2)/2 \geq l_{01}^4(l_{12}^2 + l_{03}^2)/2 \geq l_{01}^4 l_{03} l_{12}. \quad \square$$

**Theorem 2.6** *For any tetrahedron  $\mathbf{T}$ ,*

$$\eta^{3/2}/16 \leq \sigma_{\min} \leq \sqrt[4]{8} \eta^{3/4}. \quad (2.6.9)$$

*Furthermore, the lower bound is optimal and tight, and the upper bound is optimal.*

**Proof.** We first prove the left inequality. Without loss of generality, assume  $\sigma_{\min} = \sin(\theta_0/2)$ . By (2.5.1), we have

$$\prod_{0 \leq i < j \leq 3} (l_{0i} + l_{0j} + l_{ij}) \leq \left[ \sum_{0 \leq i < j \leq 3} (l_{0i} + l_{0j} + l_{ij})/3 \right]^3 = [2(l_{01} + l_{02} + l_{03})/3 + (l_{12} + l_{13} + l_{23})/3]^3, \quad (2.6.10)$$

$$\prod_{0 \leq i < j \leq 3} (l_{0i} + l_{0j} - l_{ij}) \leq \left[ \sum_{0 \leq i < j \leq 3} (l_{0i} + l_{0j} - l_{ij})/3 \right]^3 = [2(l_{01} + l_{02} + l_{03})/3 - (l_{12} + l_{13} + l_{23})/3]^3. \quad (2.6.11)$$

Combining (2.6.10) and (2.6.11) yields

$$\begin{aligned} \prod_{0 \leq i < j \leq 3} (l_{0i} + l_{0j} + l_{ij})(l_{0i} + l_{0j} - l_{ij}) &\leq [4(l_{01} + l_{02} + l_{03})^2 - (l_{12} + l_{13} + l_{23})^2]^3 / 3^6 \\ &\leq 4^3 (l_{01} + l_{02} + l_{03})^6 / 3^6. \end{aligned} \quad (2.6.12)$$

By (2.2.2) and (2.6.12), it follows that

$$\sigma_{\min} \geq (3^4/2)v/(l_{01} + l_{02} + l_{03})^3. \quad (2.6.13)$$

From (2.4.1) and (2.6.13), we obtain

$$\begin{aligned} \sigma_{\min}/\eta^{3/2} &\geq (3\sqrt{3}/16) \left( \sum_{0 \leq i < j \leq 3} l_{ij}^2 \right)^{3/2} / (l_{01} + l_{02} + l_{03})^3 \\ &\geq (3\sqrt{3}/16) (l_{01}^2 + l_{02}^2 + l_{03}^2)^{3/2} / (l_{01} + l_{02} + l_{03})^3 \geq 1/16, \end{aligned}$$

since  $\sqrt{l_{01}^2 + l_{02}^2 + l_{03}^2} \geq (l_{01} + l_{02} + l_{03})/\sqrt{3}$  by (2.5.1).

We now prove the right inequality in (2.6.9). Without loss of generality, suppose  $\mathbf{T}$  has the coordinates shown in Figure 2.3,  $l_{01}$  is the maximum edge length, and  $l_{02} \geq l_{12}$ , i.e.  $s \geq r/2$ . From the Cauchy-Schwartz inequality,  $\sqrt{s^2 + t^2} \sqrt{x^2 + y^2 + z^2} \geq sz - ty$ . When  $l_{03} \geq l_{13}$ ,

$$\begin{aligned} &(\sqrt{s^2 + t^2} + \sqrt{x^2 + y^2 + z^2})^2 - (z/2 + \sqrt{(s-x)^2 + (t-y)^2 + z^2})^2 \\ &= 2\sqrt{s^2 + t^2} \sqrt{x^2 + y^2 + z^2} + 2sx + 2ty - z^2/4 - z\sqrt{(s-x)^2 + (t-y)^2 + z^2} \end{aligned}$$

$$\geq 2sx + 2sz - z^2/4 - z\sqrt{(s-x)^2 + (t-y)^2 + z^2} \geq 2sx + 2sz - z^2/4 - rz \geq z^2/2 - z^2/4 \geq 0,$$

since  $s \geq r/2$  and  $x \geq r/2$ . Thus

$$l_{02} + l_{03} - l_{23} = \sqrt{s^2 + t^2} + \sqrt{x^2 + y^2 + z^2} - \sqrt{(s-x)^2 + (t-y)^2 + z^2} \geq z/2,$$

and by (2.6.3),

$$\max(d_0, d_1) \geq \sqrt{2}r^{3/2}\sqrt{r^2z} \geq 2\sqrt{3} \max_{0 \leq i < j \leq 3} l_{ij}^{3/2} \sqrt{v}, \quad (2.6.14)$$

since  $v = rtz/6$ . When  $l_{03} < l_{13}$ , by (2.6.4), since  $l_{03}l_{12} = \sqrt{x^2 + y^2 + z^2}\sqrt{(r-s)^2 + t^2} \geq tz$ ,

$$\max(d_0, d_1) \geq r^{3/2}\sqrt{rtz} = \sqrt{6} \max_{0 \leq i < j \leq 3} l_{ij}^{3/2} \sqrt{v}. \quad (2.6.15)$$

From (2.2.2), it is obvious that  $\sigma_{\min} \leq 12v/\max(d_0, d_1)$ . Therefore, from (2.4.1), (2.6.14) and (2.6.15), it follows that

$$\sigma_{\min}/\eta^{3/4} \leq (2\sqrt{2}/12^{3/4}) \left( \sum_{0 \leq i < j \leq 3} l_{ij}^2 \right)^{3/4} / \max_{0 \leq i < j \leq 3} l_{ij}^{3/2} \leq \sqrt[4]{8},$$

since  $\sum_{0 \leq i < j \leq 3} l_{ij}^2 \leq 6 \max_{0 \leq i < j \leq 3} l_{ij}^2$ .

Finally we show that the lower bound in (2.6.9) is optimal and tight, and the upper bound is optimal. Using the coordinate system of Figure 2.3, let  $s = r/2$ ,  $t = \sqrt{3}r/2$ ,  $x = r/2$ ,  $y = \sqrt{3}r/6$ , and  $z = 1$ . Using (2.2.2) and (2.4.1), we have  $\sigma_{\min} = \sigma_3 = \sqrt{3}r^2/(r^2/3 + 4)^{3/2}$  when  $r$  is sufficiently small, and  $\eta^{3/2} = 18r^2/(4r^2 + 3)^{3/2}$ . When  $r$  approaches 0,  $\sigma_{\min} = O(r^2)$ ,  $\eta^{3/2} = O(r^2)$ , and  $\sigma_{\min}/\eta^{3/2} \rightarrow 1/16$ . Therefore the constant  $1/16$  and the power  $3/2$  in the left inequality of (2.6.9) cannot be improved. If  $r = 1$ ,  $s = 1$ ,  $t = z$ ,  $x = 0$ , and  $y = 0$ , then when  $z$  approaches 0,  $\sigma_{\min} = O(z)$  and  $\eta = O(z^{4/3})$ . Thus the upper bound is optimal.  $\square$

## 2.7 Relationship between $\sigma_{\min}$ and $\rho$

**Theorem 2.7** *For any tetrahedron  $\mathbf{T}$ ,*

$$\sqrt{3}/24 \rho^2 \leq \sigma_{\min} \leq (2/\sqrt[4]{3}) \rho^{1/2}. \quad (2.7.1)$$

*Furthermore, the lower bound is optimal and tight, and the upper bound is optimal.*

**Proof.** Without loss of generality, suppose  $l_{01}$  is the maximum edge length,  $l_{02} \geq l_{12}$ , and the circumradius of  $\mathbf{T}$  is 1. We first prove the left inequality. From (2.3.2) and (2.5.2),

$$\rho = 3r_{in}/r_{circ} = 9v/\sum_{i=0}^3 s_i \leq 3/\sqrt[4]{3} \sqrt{v/l_{01}}. \quad (2.7.2)$$

If  $\sigma_{min} = \sin(\theta_0/2)$  then (2.6.13) holds. If  $\sigma_{min} = \sin(\theta_k/2)$ ,  $k > 0$ , then a similar inequality holds. In all cases,  $\sigma_{min} \geq (3^4/2)v/(3l_{01})^3$ . By (2.7.2), we obtain

$$\sigma_{min}/\rho^2 \geq \sqrt{3}/(6l_{01}^2).$$

By considering the triangle with vertices  $\mathbf{t}_0$ ,  $\mathbf{t}_1$ , and circumcenter of  $\mathbf{T}$ , it follows that  $l_{01} \leq 2r_{circ} = 2$ . So  $\sigma_{min}/\rho^2 \geq \sqrt{3}/24$ .

We now prove the right inequality in (2.7.1). From [MPV89, p. 551],

$$\sum_{i=0}^3 s_i \leq (\sqrt{3}/6) \sum_{0 \leq i < j \leq 3} l_{ij}^2 \leq \sqrt{3} \max_{0 \leq i < j \leq 3} l_{ij}^2. \quad (2.7.3)$$

Let  $a = l_{01}l_{23}$ ,  $b = l_{02}l_{13}$ , and  $c = l_{03}l_{12}$ . Then combining (2.3.1) and (2.7.3) produces

$$\sqrt{\rho} \geq 6\sqrt{2}\sqrt[4]{3}v/[\max_{0 \leq i < j \leq 3} l_{ij} \sqrt{(a+b+c)(a+b-c)(a+c-b)(b+c-a)}]. \quad (2.7.4)$$

It is obvious that  $\sigma_{min} \leq 12v/\max(d_0, d_1)$ , by (2.2.2), (2.6.1), and (2.6.2). Thus, from (2.7.4),

$$\sigma_{min}/\sqrt{\rho} \leq (\sqrt{2}/\sqrt[4]{3}) \max_{0 \leq i < j \leq 3} l_{ij} \sqrt{(a+b+c)(a+b-c)(a+c-b)(b+c-a)}/\max(d_0, d_1). \quad (2.7.5)$$

Case 1:  $l_{03} \geq l_{13}$ . We first prove that

$$b+c-a \leq (l_{02}+l_{03}-l_{23})^2. \quad (2.7.6)$$

Since  $b+c-a = l_{02}l_{13}+l_{03}l_{12}-l_{01}l_{23} \leq l_{02}l_{03}+l_{03}l_{02}-l_{23}^2 = 2l_{02}l_{03}-l_{23}^2$ ,

$$(l_{02}+l_{03}-l_{23})^2 - b - c + a \geq (l_{02}+l_{03}-l_{23})^2 - 2l_{02}l_{03} + l_{23}^2 = (l_{02}-l_{23})^2 + (l_{03}-l_{23})^2 \geq 0.$$

Therefore, the inequality (2.7.6) holds. We also have

$$(a+b-c)(a+c-b) = a^2 - (b-c)^2 \leq a^2 = l_{01}^2 l_{23}^2 \leq l_{01}^4. \quad (2.7.7)$$

Since  $a+b+c = l_{01}l_{23}+l_{02}l_{13}+l_{03}l_{12} \leq 3l_{01}^2$ , combining (2.7.5), (2.7.6), (2.7.7) and (2.6.3) yields

$$\sigma_{min}/\sqrt{\rho} \leq \frac{\sqrt{2}l_{01}^{5/2}\sqrt{l_{02}+l_{03}-l_{23}}}{2l_{01}^{5/2}\sqrt{l_{02}+l_{03}-l_{23}}} = \sqrt{2}/2. \quad (2.7.8)$$

Case 2:  $l_{03} < l_{13}$ . Since  $(a + c - b)(b + c - a) = l_{03}^2 l_{12}^2 - (l_{02} l_{13} - l_{01} l_{23})^2 \leq l_{03}^2 l_{12}^2$  and  $(a + b + c)(a + b - c) = (a + b)^2 - c^2 < (a + b)^2 = (l_{01} l_{23} + l_{02} l_{13})^2 \leq 4l_{01}^4$ ,

$$(a + b + c)(a + b - c)(a + c - b)(b + c - a) \leq 4l_{01}^4 l_{03}^2 l_{12}^2. \quad (2.7.9)$$

By (2.7.5), (2.7.9) and (2.6.4), we have

$$\sigma_{\min}/\sqrt{\rho} \leq \frac{2l_{01}^2 \sqrt{l_{03} l_{12}}}{\sqrt[4]{3} l_{01}^2 \sqrt{l_{03} l_{12}}} \leq 2/\sqrt[4]{3}. \quad (2.7.10)$$

Inequalities (2.7.8) and (2.7.10) establish the right inequality in (2.7.1). Finally we show that the lower bound is optimal and tight, and the upper bound is optimal. Using the coordinate system of Figure 2.3, let  $s = r/2$ ,  $t = \sqrt{3}r/2$ ,  $x = r/2$ ,  $y = \sqrt{3}r/6$ , and  $z = 1$ . Then  $\sigma_3 = \sqrt{3}r^2/(r^2/3 + 4)^{3/2}$  and  $\rho = 3\sqrt{3}r/[(\sqrt{3}r/2 + 3\sqrt{1 + r^2/12})(1 + r^2/3)]$ . When  $r$  approaches zero,  $\sigma_{\min} = \sigma_3 = O(r^2)$ ,  $\rho^2 = O(r^2)$ , and  $\sigma_{\min}/\rho^2 \rightarrow \sqrt{3}/24$ . Therefore the lower bound is optimal and tight. If  $r = 1$ ,  $s = 1/2$ ,  $t = \sqrt{3}/2$ ,  $x = 1/2$ , and  $y = \sqrt{3}/6$ , then when  $z$  approaches zero,  $\rho^{1/2} = O(z)$  and  $\sigma_{\min} = O(z)$ . Hence the upper bound is optimal.  $\square$

## 2.8 Discussion of results

Each of the three measures  $\sigma_{\min}$ ,  $\rho$ , and  $\eta$  is invariant under translation, rotation, reflection, and uniform scaling of tetrahedra. Since each measure attains a maximum value only for the regular tetrahedron, and the formulae (2.2.2), (2.3.1), and (2.4.1) can each be expressed as continuous functions of the coordinates  $r, s, t, x, y, z$  shown in Figure 2.3, it follows that a larger measure value for a tetrahedron means that the tetrahedron is well-shaped, i.e. close to the regular tetrahedron. At the other end, the inequalities (2.5.3), (2.6.9), and (2.7.1) imply that if one of the shape measures approaches zero, which indicates a poorly-shaped tetrahedron, then so do the others. If any shape measure is zero, then the tetrahedron is degenerate, i.e. it has zero volume.

The relationship  $c_0 \mu^{e_0} \leq \nu \leq c_1 \mu^{e_1}$  for different shape measures  $\mu$  and  $\nu$  means that the bounds  $a \leq \nu \leq b$  transform into the bounds  $a' \leq \mu \leq b'$ , where  $a, b, a' = (a/c_1)^{1/e_1}$ , and  $b' = (b/c_0)^{1/e_0}$  are positive constants. However, the bounds  $a \leq \nu(\mathbf{S})/\nu(\mathbf{T}) \leq b$ , where  $\nu(\mathbf{S})$  and  $\nu(\mathbf{T})$  are the measures of different tetrahedra  $\mathbf{S}$  and  $\mathbf{T}$ , do not transform into bounds  $a' \leq \mu(\mathbf{S})/\mu(\mathbf{T}) \leq b'$  when  $e_0 > e_1$  (which is the case in (2.5.3), (2.6.9), and (2.7.1)). These

properties mean that the three shape measures  $\sigma_{\min}$ ,  $\rho$ , and  $\eta$  are “equivalent” in a weak sense. This “equivalence” is not as strong as that in the equivalence of different vector norms [Atk78, p. 414], where the exponents are 1 so that bounds of the latter form do transform between different norms.

Other tetrahedron shape measures may be defined, such as in [BEG90, RiL92]. From the above observations, we may define a valid shape measure as one which is invariant under translation, rotation, reflection, and uniform scaling, attains a maximum value only for the regular tetrahedron, and approaches zero if and only if  $\sigma_{\min}$ ,  $\rho$ , or  $\eta$  approaches zero. An example of an invalid shape measure is the ratio of minimum edge length to maximum edge length, since it is possible for a poorly-shaped tetrahedron to have no short edges (see Figure 2.12a below). We conjecture that if two valid shape measures  $\mu$  and  $\nu$  can each be expressed algebraically in terms of the volume, face areas, and edge lengths of a tetrahedron, then they have a relationship of the form  $c_0\mu^{e_0} \leq \nu \leq c_1\mu^{e_1}$ .

In (2.5.3), (2.6.9), and (2.7.1), different classes of poorly-shaped tetrahedra (see below) were analyzed to guess at the exponents of the optimal bounds before obtaining the precise proof. This technique may also be useful if similar relationships are sought for other pairs of shape measures. Although we were able to obtain tight lower bounds in all three cases, we were not able to obtain tight upper bounds. From looking at the regular tetrahedron and different classes of poorly-shaped tetrahedra, we conjecture that the constants for a tight upper bound in (2.5.3), (2.6.9), and (2.7.1) are 1,  $\sqrt[4]{12}/6$ , and  $\sqrt{6}/9$ , respectively. These tight upper bounds occur for the regular tetrahedron in the first and third cases, and for a tetrahedron with opposite edges approaching zero length in the second case.

Let  $\sigma = 3\sqrt{6}\sigma_{\min}/2$  be the scaled version of  $\sigma_{\min}$  so that  $\sigma = 1$  for the regular tetrahedron. Using the conjectured constants for the tight upper bounds and expressing constants to 4 decimal places, the relationships between  $\sigma$ ,  $\rho$ , and  $\eta$  are:

$$\eta^3 \leq \rho \leq \eta^{3/4}, \quad \rho^{4/3} \leq \eta \leq \rho^{1/3}, \quad (2.8.1)$$

$$0.2296 \eta^{3/2} \leq \sigma \leq 1.1398 \eta^{3/4}, \quad 0.8399 \sigma^{4/3} \leq \eta \leq 2.6667 \sigma^{2/3}, \quad (2.8.2)$$

$$0.2651 \rho^2 \leq \sigma \leq \rho^{1/2}, \quad \sigma^2 \leq \rho \leq 1.9420 \sigma^{1/2} \quad (2.8.3)$$

Although  $\sigma$ ,  $\rho$ , and  $\eta$  are “equivalent” shape measures, they don’t approach 0 or 1 at the same rate for different tetrahedra. Figures 2.4 to 2.11 contain graphs illustrating

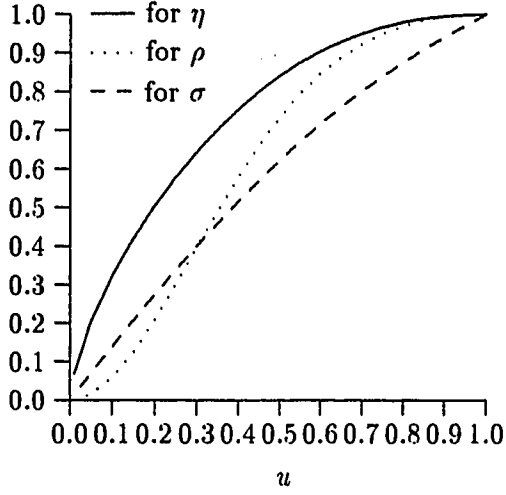


Figure 2.4: No short edges when  $u \rightarrow 0$ ;  
 $\mathbf{t}_0 = (0, 0, 0)$ ,  $\mathbf{t}_1 = (1, 0, 0)$ ,  
 $\mathbf{t}_2 = (1/2, \sqrt{3}/2, 0)$ ,  $\mathbf{t}_3 = (1/2, \sqrt{3}/6, \sqrt{6}u/3)$ .

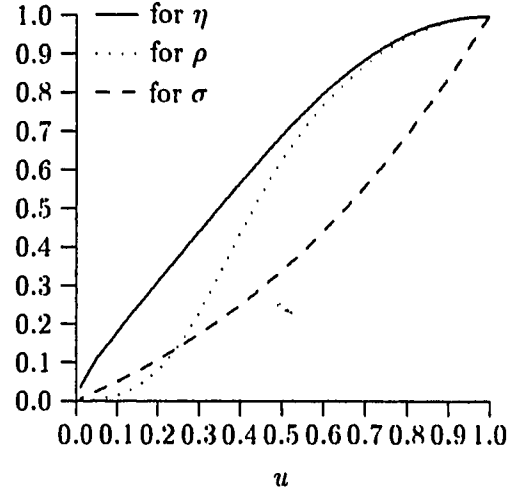


Figure 2.5: No short edges when  $u \rightarrow 0$ ;  
 $\mathbf{t}_0 = (0, 0, 0)$ ,  $\mathbf{t}_1 = (1, 0, 0)$ ,  $\mathbf{t}_2 = (1/2, \sqrt{3}/2, 0)$ ,  
 $\mathbf{t}_3 = (1/2, -\sqrt{3}/2 + 2\sqrt{3}u/3, \sqrt{6}u/3)$ .

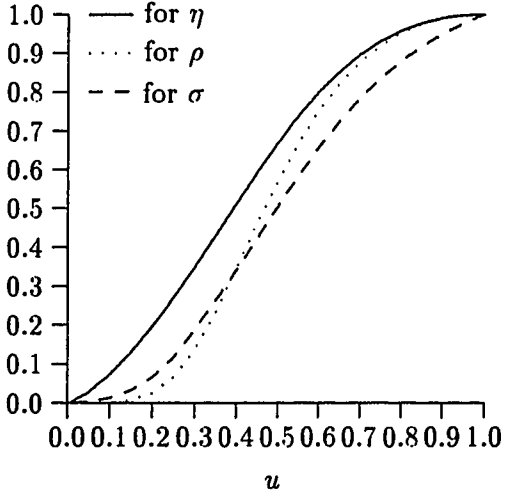


Figure 2.6: No short edges when  $u \rightarrow 0$ ;  
 $\mathbf{t}_0 = (0, 0, 0)$ ,  $\mathbf{t}_1 = (1, 0, 0)$ ,  
 $\mathbf{t}_2 = (1/2, \sqrt{3}u/2, 0)$ ,  
 $\mathbf{t}_3 = (1/2, -\sqrt{3}/2 + 2\sqrt{3}u/3, \sqrt{6}u/3)$ .

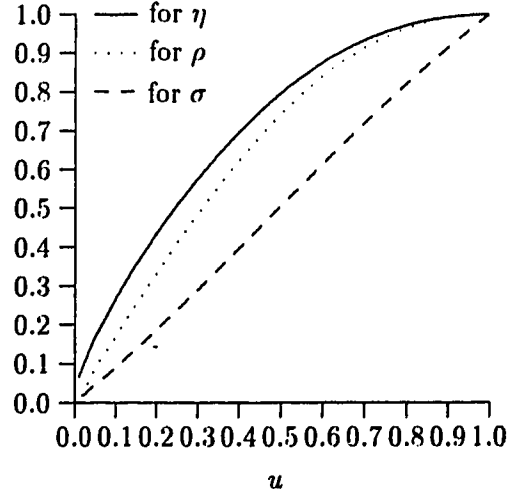


Figure 2.7: One short edge when  $u \rightarrow 0$ ;  
 $\mathbf{t}_0 = (0, 0, 0)$ ,  $\mathbf{t}_1 = (1, 0, 0)$ ,  $\mathbf{t}_2 = (1/2, \sqrt{3}/2, 0)$ ,  
 $\mathbf{t}_3 = (1/2, \sqrt{3}/6, \sqrt{6}/3)u$ .

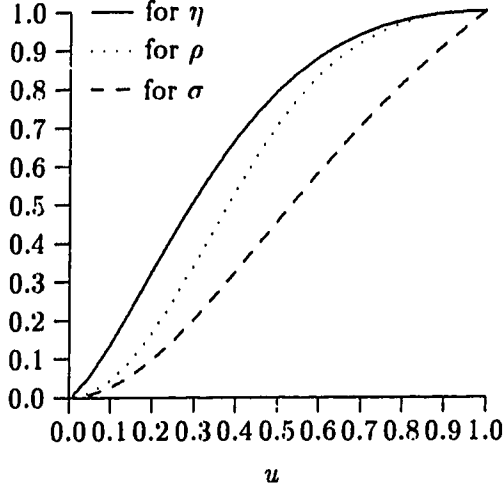


Figure 2.8: One short edge when  $u \rightarrow 0$ ;  
 $t_0 = (0, 0, 0)$ ,  $t_1 = (1, 0, 0)$ ,  
 $t_2 = (1/2, \sqrt{3}u/2, 0)$ ,  
 $t_3 = (1/2, \sqrt{3}u/6, \sqrt{6}u/3)$ .

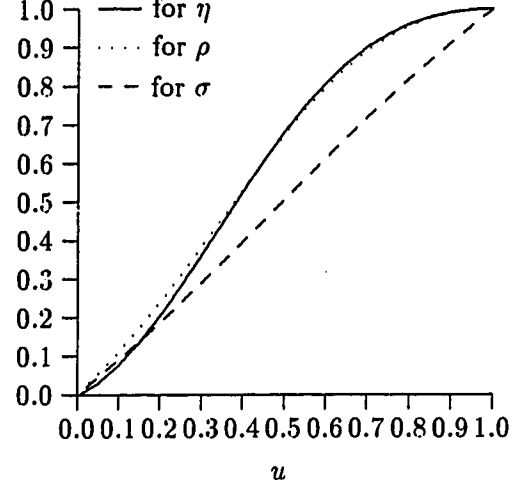


Figure 2.9: Two short edges when  $u \rightarrow 0$ ;  
 $t_0 = (0, 0, 0)$ ,  $t_1 = (1, 0, 0)$ ,  
 $t_2 = (1 - u/2, \sqrt{3}u/2, 0)$ ,  
 $t_3 = (1/2, \sqrt{3}/6, \sqrt{6}/3)u$ .

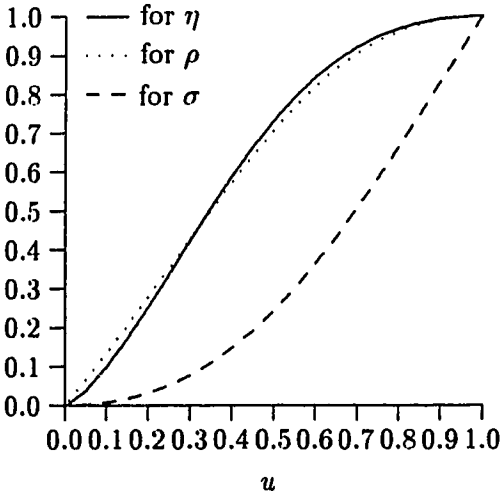


Figure 2.10: Three short edges when  $u \rightarrow 0$ ;  
 $t_0 = (0, 0, 0)$ ,  $t_1 = (u, 0, 0)$ ,  
 $t_2 = (u/2, \sqrt{3}u/2, 0)$ ,  $t_3 = (1/2, \sqrt{3}/6, \sqrt{6}/3)$ .

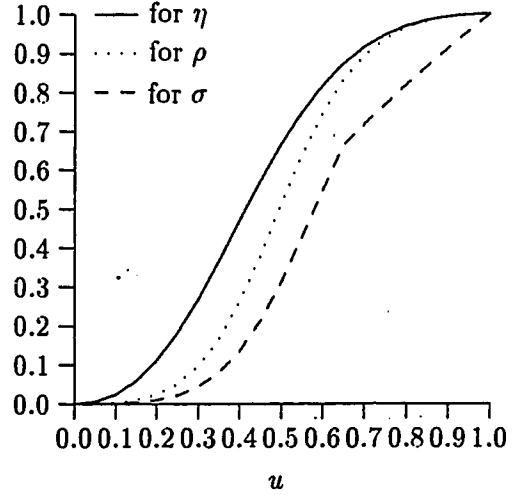


Figure 2.11: Three short edges when  $u \rightarrow 0$ ;  
 $t_0 = (0, 0, 0)$ ,  $t_1 = (u, 0, 0)$ ,  $t_2 = (u/2, \sqrt{3}u/2, 0)$ ,  
 $t_3 = (1/2, -\sqrt{3}/2 + 2\sqrt{3}u/3, \sqrt{6}u/3)$ .



these different behaviors for 8 different families of tetrahedra parameterized by a variable  $u$ ,  $0 < u \leq 1$ , where  $u = 1$  occurs for the regular tetrahedron and  $u \rightarrow 0$  for poorly-shaped tetrahedra. The classification of poorly-shaped tetrahedra used in these figures is based on the following. For a tetrahedron, we can always assume that the sum of squares of its edge lengths is not small when compared with its volume raised to the power  $2/3$ , since the ratio of these two quantities is invariant under uniform scaling. So, from (2.4.1), we can classify poorly-shaped tetrahedra (with shape measures approaching zero) according to the number of “short” edges, namely, no short edges, one short edge, two opposite short edges, and three short edges on the same face (see Figure 2.12). Note that these are the only classes since two short edges from the same face implies the third edge of the face is also short.

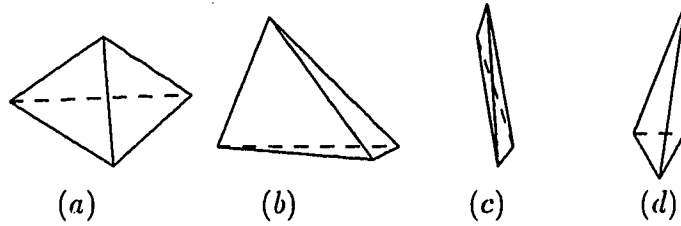


Figure 2.12: Illustration of 4 types of poor tetrahedra; (a) no short edges, and 4 vertices are nearly coplanar, i.e. “sliver” tetrahedron; (b) 1 short edge; (c) 2 opposite short edges; (d) 3 short edges on the same face.

The inequalities in (2.8.1), (2.8.2), and (2.8.3) demonstrate that any shape measure can approach zero faster than the others for poorly-shaped tetrahedra. This is illustrated in Figure 2.4 ( $\rho$  approaches zero faster than  $\eta$  and  $\sigma$ ), Figure 2.9 ( $\eta$  approaches zero faster than  $\rho$  and  $\sigma$ ), and Figure 2.10 ( $\sigma$  approaches zero faster than  $\eta$  and  $\rho$ ). Also, the inequalities demonstrate that for a particular tetrahedron, the ranking of the three measures from highest to lowest values may take on any of the 6 permutations. In the figures, 4 of the 6 permutations can be seen; the exceptions are the two with  $\sigma$  having the unique highest value. For well-shaped tetrahedra, when the three measures are close to 1, the figures indicate a  $\eta > \rho > \sigma$  ordering. This ordering is reflected in some sense by (2.8.1), (2.8.2), and (2.8.3) as follows. If  $\eta \geq 0.9$ , then  $\rho \geq 0.729$  and  $\sigma \geq 0.1960$ . If  $\rho \geq 0.9$ , then  $\eta \geq 0.8689$  and  $\sigma \geq 0.2147$ . If  $\sigma \geq 0.9$ , then  $\eta \geq 0.7298$  and  $\rho \geq 0.81$ . Also, this  $\eta > \rho > \sigma$  ordering is evident in the tetrahedral meshes generated by the method described in [Joe91a, Joe94].

Finally, we would like to mention that the results of this chapter have helped us in the interpretation of results and statistics on the quality of tetrahedra using different shape

measures, and they should also be helpful to others. For example, in the next chapter, we obtain a positive lower bound for  $\eta(\mathbf{S})/\eta(\mathbf{T})$  where  $\mathbf{S}$  is any tetrahedron obtained by applying a certain repeated bisection procedure to a tetrahedron  $\mathbf{T}$ . The weak equivalence between the shape measures means that this result is not directly extendable to  $\sigma$  or  $\rho$ . Also, in [Joe94], Joe describes an approach which uses local transformations to improve the quality of tetrahedral meshes with respect to a tetrahedron shape measure; it is found that similar triangulations are produced using  $\sigma$ ,  $\rho$ , and  $\eta$ , due to their “equivalence”. The  $\eta > \rho > \sigma$  ordering mentioned above means that  $\rho$  tends to distribute measure values more uniformly in the middle of the interval  $[0, 1]$ , so this might indicate a preference for reporting statistical results using  $\rho$ . Anyways, one must be aware of the different distributions when reporting and interpreting statistics using different shape measures.

## Chapter 3

# On the Shape of Tetrahedra from Bisection

In this chapter, we present a procedure for bisecting a tetrahedron successively into an infinite sequence of tetrahedral meshes. We will mainly consider the shape of tetrahedra from the bisection procedure, which will be used for local refinement in the next chapter, and demonstrate how the novel shape measure  $\eta$  is used in analyzing the quality of meshes generated.

### 3.1 Introduction

Let  $T(t_0, t_1, t_2, t_3)$  be a tetrahedron with vertices  $t_0, t_1, t_2, t_3$ . Using the midpoint  $t$  of one of the edges,  $t_1 t_2$  say, and the face  $t_0 t_3 t$ ,  $T$  can be bisected into two subtetrahedra  $T_1^1(t_0, t_1, t, t_3)$  and  $T_2^1(t_0, t, t_2, t_3)$ . Next, these two tetrahedra can be bisected, producing four subtetrahedra. This process can be repeated iteratively to produce an infinite sequence of tetrahedral meshes  $T^0, T^1, T^2, \dots$ , where  $T^n$  contains  $2^n$  tetrahedra.

In the bisection method of [Kea78], which works for simplices of any dimension, the longest edge is always chosen to be bisected. Let  $\delta(S)$  denote the diameter (length of longest edge) of a simplex  $S$ . [Kea78] derives a bound on how fast the diameters of the simplices in the sequence of meshes converge to zero. In the tetrahedron case, this bound is  $\delta(T_i^n) \leq (\sqrt{3}/2)^{\lfloor n/3 \rfloor} \delta(T)$  where  $T_i^n$  is a tetrahedron in  $T^n$ . In the two-dimensional or triangle case, [RoS75, Sty80, Adl83] discuss results on the bisection method in which the

longest edge of each triangle is bisected. [Sty80] and [Adl83] give diameter bounds which improve on the bound of [Kea78] (in the 2-D case).

In this chapter, we present a bisection procedure for tetrahedra which does not always bisect the longest edge; instead a mapping to a canonical tetrahedron is used to choose the bisected edge. We show that this procedure has the following properties:

- (1) Each mesh  $\mathcal{T}^n$  is conforming, where a *conforming* mesh is one in which the intersection of any two tetrahedra  $\mathbf{T}_1, \mathbf{T}_2$  of the mesh is either a common face of  $\mathbf{T}_1$  and  $\mathbf{T}_2$ , or a common edge, or a common vertex, or empty.
- (2) There are a finite number of classes of similar tetrahedra in all the  $\mathcal{T}^n, n \geq 0$ .
- (3)  $\eta(\mathbf{T}_i^n) \geq c_1 \eta(\mathbf{T})$  where  $\eta$  is the tetrahedron shape measure defined in Section 2.4, and  $c_1$  is a positive constant independent of  $\mathbf{T}$ .
- (4)  $\delta(\mathbf{T}_i^n) \leq c_2 (1/2)^{n/3} \delta(\mathbf{T})$  where  $c_2$  is a positive constant independent of  $\mathbf{T}$ .

Property (1) is not generally satisfied if the longest edge is always bisected and each subtetrahedron is bisected to the same level. Property (2) generalizes a similar result for the 2-D case, given in [Sty80] and [Adl83]. The diameter bound in property (4) is better than that given in [Kea78]. Property (3) is important for the local refinement of tetrahedral finite element meshes in which it is desired that poorly-shaped tetrahedra be avoided (to get better approximations and to avoid ill-conditioned matrices in the finite element method). In two dimensions, it is shown in [RoS75] that  $\theta \geq \alpha/2$  where  $\alpha$  is the minimum interior angle in the original triangle and  $\theta$  is any interior angle in a refined triangle. So property (3) extends this result to three dimensions (using a different shape measure and a smaller constant). There has been no previous result on the shape of the refined tetrahedra.

These properties are useful in designing a local refinement algorithm for tetrahedral meshes in the next chapter, which is a generalization of Rivara's algorithms for triangular meshes [Riv84, Riv87]. After describing our bisection procedure based on a canonical tetrahedron in Section 3.2, we establish the properties in Section 3.3. Estimates of the constants  $c_1$  and  $c_2$  are provided in Section 3.4. Some further remarks are given in Section 3.5.

### 3.2 Bisection procedure based on a canonical tetrahedron

When a tetrahedron is bisected, the two resulting subtetrahedra are generally not similar to each other or the original tetrahedron. So we try to design a bisection procedure that creates a finite number of classes of similar tetrahedra. To this end, we need the canonical tetrahedron  $\mathbf{P}$  shown in Figure 3.2 below. Let  $|\mathbf{q}_i\mathbf{q}_j|$  denote the length of edge  $\mathbf{q}_i\mathbf{q}_j$ . The following two lemmas, which are proved in [Sen81], are needed for Theorem 3.1 below.

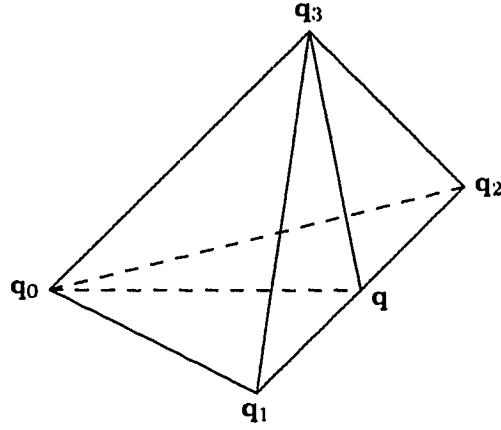


Figure 3.1: Tetrahedron  $\mathbf{Q}$  for Lemmas 3.1 and 3.2.

**Lemma 3.1** *Let  $\mathbf{Q}(\mathbf{q}_0, \mathbf{q}_1, \mathbf{q}_2, \mathbf{q}_3)$  be a tetrahedron with  $|\mathbf{q}_0\mathbf{q}_1| = |\mathbf{q}_0\mathbf{q}_2|$  and  $|\mathbf{q}_1\mathbf{q}_3| = |\mathbf{q}_2\mathbf{q}_3|$ , and let  $\mathbf{q}$  be the midpoint of  $\mathbf{q}_1\mathbf{q}_2$  (see Figure 3.1). Then  $\mathbf{Q}_1(\mathbf{q}_0, \mathbf{q}_1, \mathbf{q}, \mathbf{q}_3)$  is similar to  $\mathbf{Q}_2(\mathbf{q}_0, \mathbf{q}, \mathbf{q}_2, \mathbf{q}_3)$ .*

**Lemma 3.2** *Let  $\mathbf{Q}(\mathbf{q}_0, \mathbf{q}_1, \mathbf{q}_2, \mathbf{q}_3)$  be a tetrahedron with  $|\mathbf{q}_0\mathbf{q}_1| = |\mathbf{q}_2\mathbf{q}_3|$  and  $|\mathbf{q}_0\mathbf{q}_2| = |\mathbf{q}_1\mathbf{q}_3|$ , and let  $\mathbf{q}$  be the midpoint of  $\mathbf{q}_1\mathbf{q}_2$  (see Figure 3.1). Then  $\mathbf{Q}_1(\mathbf{q}_0, \mathbf{q}_1, \mathbf{q}, \mathbf{q}_3)$  is similar to  $\mathbf{Q}_2(\mathbf{q}_0, \mathbf{q}, \mathbf{q}_2, \mathbf{q}_3)$ .*

**Theorem 3.1** *In the first three levels of longest edge bisection applied to the canonical tetrahedron  $\mathbf{P}$ , the subtetrahedra at the same level are similar to each other, and the subtetrahedra at the third level are all similar to  $\mathbf{P}$  (see Figure 3.2).*

**Proof.** Let  $\mathbf{p}_{ij} = (\mathbf{p}_i + \mathbf{p}_j)/2$ ,  $i < j$ . The longest edge of  $\mathbf{P}(\mathbf{p}_0, \mathbf{p}_1, \mathbf{p}_2, \mathbf{p}_3)$  is  $\mathbf{p}_1\mathbf{p}_2$  with  $|\mathbf{p}_1\mathbf{p}_2| = 2a$ . First,  $\mathbf{P}$  is bisected into two subtetrahedra  $\mathbf{P}_1^1(\mathbf{p}_0, \mathbf{p}_1, \mathbf{p}_3, \mathbf{p}_{12})$  and  $\mathbf{P}_2^1(\mathbf{p}_0, \mathbf{p}_2, \mathbf{p}_3, \mathbf{p}_{12})$ . Since  $|\mathbf{p}_0\mathbf{p}_1| = |\mathbf{p}_0\mathbf{p}_2| = \sqrt{6}a/2$  and  $|\mathbf{p}_1\mathbf{p}_3| = |\mathbf{p}_2\mathbf{p}_3| = \sqrt{2}a$ , these two subtetrahedra are similar to each other by Lemma 3.1. Next, we only need to consider

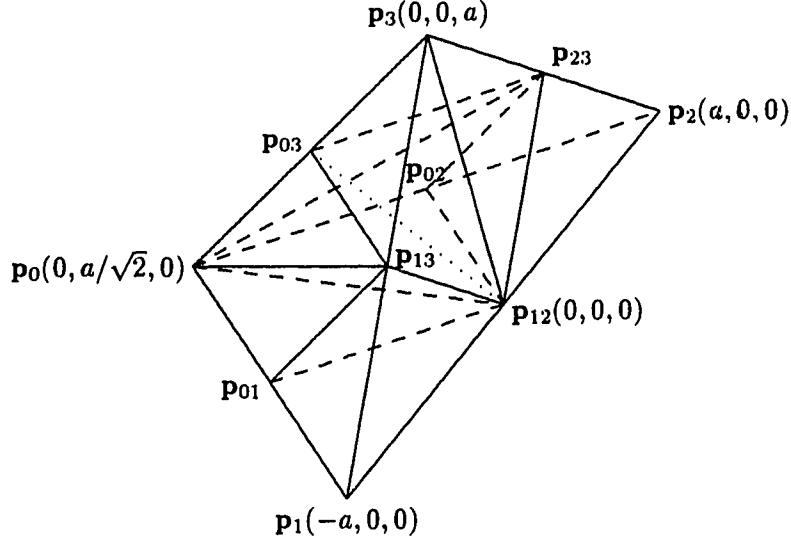


Figure 3.2: Canonical tetrahedron  $\mathbf{P}$ ; other coordinates are  $\mathbf{p}_{01}(-a/2, \sqrt{2}a/4, 0)$ ,  $\mathbf{p}_{02}(a/2, \sqrt{2}a/4, 0)$ ,  $\mathbf{p}_{03}(0, \sqrt{2}a/4, a/2)$ ,  $\mathbf{p}_{13}(-a/2, 0, a/2)$ ,  $\mathbf{p}_{23}(a/2, 0, a/2)$ .

the subtetrahedron  $\mathbf{P}_1^1(\mathbf{p}_0, \mathbf{p}_1, \mathbf{p}_3, \mathbf{p}_{12})$ , whose longest edge is  $\mathbf{p}_1\mathbf{p}_3$  with  $|\mathbf{p}_1\mathbf{p}_3| = \sqrt{2}a$ . It is bisected into two subtetrahedra  $\mathbf{P}_1^2(\mathbf{p}_0, \mathbf{p}_1, \mathbf{p}_{12}, \mathbf{p}_{13})$  and  $\mathbf{P}_2^2(\mathbf{p}_0, \mathbf{p}_3, \mathbf{p}_{12}, \mathbf{p}_{13})$ . Since  $|\mathbf{p}_0\mathbf{p}_1| = |\mathbf{p}_0\mathbf{p}_3| = \sqrt{6}a/2$  and  $|\mathbf{p}_1\mathbf{p}_{12}| = |\mathbf{p}_3\mathbf{p}_{12}| = a$ , these two subtetrahedra are similar to each other by Lemma 3.1. Finally, we only need to consider the subtetrahedron  $\mathbf{P}_1^2(\mathbf{p}_0, \mathbf{p}_1, \mathbf{p}_{12}, \mathbf{p}_{13})$ , whose longest edge is  $\mathbf{p}_0\mathbf{p}_1$  with  $|\mathbf{p}_0\mathbf{p}_1| = \sqrt{6}a/2$ . It is bisected into two subtetrahedra  $\mathbf{P}_1^3(\mathbf{p}_0, \mathbf{p}_{12}, \mathbf{p}_{13}, \mathbf{p}_{01})$  and  $\mathbf{P}_2^3(\mathbf{p}_1, \mathbf{p}_{12}, \mathbf{p}_{13}, \mathbf{p}_{01})$ . Since  $|\mathbf{p}_0\mathbf{p}_{12}| = |\mathbf{p}_1\mathbf{p}_{13}| = a/\sqrt{2}$  and  $|\mathbf{p}_0\mathbf{p}_{13}| = |\mathbf{p}_1\mathbf{p}_{12}| = a$ , these two subtetrahedra are similar to each other by Lemma 3.2.

Since  $\mathbf{P}_2^3(\mathbf{p}_1, \mathbf{p}_{12}, \mathbf{p}_{13}, \mathbf{p}_{01})$  is similar to  $\mathbf{P}$ , it follows that after three levels of bisections, the 8 subtetrahedra  $\mathbf{P}_1^3, \mathbf{P}_2^3, \mathbf{P}_3^3(\mathbf{p}_0, \mathbf{p}_{12}, \mathbf{p}_{13}, \mathbf{p}_{03}), \mathbf{P}_4^3(\mathbf{p}_3, \mathbf{p}_{12}, \mathbf{p}_{13}, \mathbf{p}_{03}), \mathbf{P}_5^3(\mathbf{p}_0, \mathbf{p}_{12}, \mathbf{p}_{23}, \mathbf{p}_{02}), \mathbf{P}_6^3(\mathbf{p}_2, \mathbf{p}_{12}, \mathbf{p}_{23}, \mathbf{p}_{02}), \mathbf{P}_7^3(\mathbf{p}_0, \mathbf{p}_{12}, \mathbf{p}_{23}, \mathbf{p}_{03}), \mathbf{P}_8^3(\mathbf{p}_3, \mathbf{p}_{12}, \mathbf{p}_{23}, \mathbf{p}_{03})$  are all similar to the original tetrahedron  $\mathbf{P}$ .  $\square$

It follows from Theorem 3.1 that if  $\mathbf{P}$  is iteratively bisected by the longest edge to an arbitrary number of levels, any subtetrahedron at level  $3k, 3k+1$ , or  $3k+2$  is similar to  $\mathbf{P}(\mathbf{p}_0, \mathbf{p}_1, \mathbf{p}_2, \mathbf{p}_3)$ ,  $\mathbf{P}_1^1(\mathbf{p}_0, \mathbf{p}_1, \mathbf{p}_3, \mathbf{p}_{12})$ , or  $\mathbf{P}_1^2(\mathbf{p}_0, \mathbf{p}_1, \mathbf{p}_{12}, \mathbf{p}_{13})$ , respectively, for  $k = 0, 1, \dots$ . Hence we define a subtetrahedron at level  $3k, 3k+1$ , or  $3k+2$  to be a tetrahedron of type  $\mathbf{P}^0, \mathbf{P}^1$ , or  $\mathbf{P}^2$ , respectively.

We now present a bisection procedure for iteratively bisecting any tetrahedron  $\mathbf{T}$  to  $n$  levels. Let  $\mathbf{P}$  be the canonical tetrahedron of Figure 3.2 such that  $\mathbf{T}$  and  $\mathbf{P}$  have the same volume. By using the notation in Definition 2.1, the procedure is as follows.

- (a) Transform  $\mathbf{T}$  to  $\mathbf{P}$  by the affine transformation  $\mathbf{y} = M^{-1}(\mathbf{P}, \mathbf{T})\mathbf{x} + \mathbf{b}_0$ .
- (b) Iteratively bisect  $\mathbf{P}$  to  $n$  levels by always bisecting the longest edge.
- (c) Transform all subtetrahedra  $\mathbf{P}_i^n$  of  $\mathbf{P}$  back to subtetrahedra  $\mathbf{T}_i^n$  of  $\mathbf{T}$  using the inverse affine transformation  $\mathbf{y} = M(\mathbf{P}, \mathbf{T})\mathbf{x} + \mathbf{b}_1$ .

Note that in the subtetrahedra of  $\mathbf{T}$ , the longest edge may not be the one bisected.

### 3.3 Properties of bisection procedure

In this section, we prove the four properties of the bisection procedure stated in Section 3.1. Let  $\mathcal{T}^n$  and  $\mathcal{P}^n$  be the meshes of  $2^n$  subtetrahedra of  $\mathbf{T}$  and  $\mathbf{P}$  produced by  $n$  levels of bisection, respectively. Let  $\mathbf{R}$  be the regular tetrahedron such that  $\mathbf{T}$ ,  $\mathbf{P}$ , and  $\mathbf{R}$  have the same volume.

**Theorem 3.2** *The mesh  $\mathcal{T}^n$  is conforming.*

**Proof.** Due to the affine transformation used in the bisection procedure, it suffices to prove that the mesh  $\mathcal{P}^n$  of subtetrahedra in  $\mathbf{P}$  is conforming. By considering the first three levels of bisection of  $\mathbf{P}$ , it is easily seen that at any level, each subtetrahedron of  $\mathbf{P}$  has only one longest edge and all of the longest edges of the subtetrahedra have the same length (e.g. after the first level, the two subtetrahedra have longest edges  $\mathbf{p}_1\mathbf{p}_3$  and  $\mathbf{p}_2\mathbf{p}_3$ , respectively, and  $|\mathbf{p}_1\mathbf{p}_3| = |\mathbf{p}_2\mathbf{p}_3| = \sqrt{2}a$ , etc.). So the midpoint of any longest edge  $e$  is also a bisecting point of any other subtetrahedra incident on  $e$ . Hence  $\mathcal{P}^n$  is a conforming mesh.  $\square$

In the above proof, we have assumed that each subtetrahedron is bisected to the same level. This is not necessary in order to get a conforming mesh. For example, after  $\mathbf{P}$  is bisected, if only  $\mathbf{P}_1^1(\mathbf{p}_0, \mathbf{p}_1, \mathbf{p}_3, \mathbf{p}_{12})$  is bisected at the first level, and the same for  $\mathbf{P}_1^2(\mathbf{p}_0, \mathbf{p}_1, \mathbf{p}_{12}, \mathbf{p}_{13})$  at the second level, then the resulting mesh is still conforming. This property can be used to smoothly extend local refinements to adjacent tetrahedra. For the

case when the bisection starts with more than one tetrahedron, it is not easy to guarantee the conformity of the resulting mesh by using the above procedure alone. In the next chapter, we will present a local refinement algorithm which uses this procedure plus some pre-processing to ensure conformity.

**Theorem 3.3** *There are a finite number of classes of similar tetrahedra in all the  $T^n$ ,  $n \geq 0$ .*

**Proof.** We define two tetrahedra to be in the same equivalence class if one can be transformed into the other by translation and uniform scaling (i.e. the scale factors for the three coordinate axes are the same). So any two tetrahedra in the same equivalence class are similar to each other after any affine transformation. In order to prove the theorem, it suffices to prove that all subtetrahedra  $P_i^n$ ,  $n \geq 0$ , generated by the bisection procedure are only in a finite number of equivalence classes. First we prove that the tetrahedra of type  $P^0$  are only in a finite number of equivalence classes.

After three levels of bisection, by Theorem 3.1, all 8 subtetrahedra  $P_i^3$  are similar to  $P$ . Let these tetrahedra be labeled  $P_1^3(p_{01}, p_1, p_{12}, p_{13})$ ,  $P_2^3(p_{02}, p_{12}, p_2, p_{23})$ ,  $P_3^3(p_{01}, p_0, p_{13}, p_{12})$ ,  $P_4^3(p_{03}, p_{13}, p_0, p_{12})$ ,  $P_5^3(p_{03}, p_3, p_{12}, p_{13})$ ,  $P_6^3(p_{02}, p_0, p_{23}, p_{12})$ ,  $P_7^3(p_{03}, p_3, p_{12}, p_{23})$ , and  $P_8^3(p_{03}, p_{23}, p_0, p_{12})$ . Let  $M_i = M(P, P_i^3)$ ,  $1 \leq i \leq 8$ . From the coordinates of Figure 3.2, we obtain  $M_1 = M_2 = 1/2 I$ , where  $I$  is the identity matrix, and

$$M_3 = \frac{1}{4} \begin{bmatrix} -1 & -\sqrt{2} & 1 \\ -\sqrt{2} & 0 & -\sqrt{2} \\ 1 & -\sqrt{2} & -1 \end{bmatrix}, \quad M_4 = \frac{1}{4} \begin{bmatrix} 1 & \sqrt{2} & 1 \\ \sqrt{2} & 0 & -\sqrt{2} \\ -1 & \sqrt{2} & -1 \end{bmatrix},$$

$$M_5 = \frac{1}{2} \begin{bmatrix} 0 & 0 & -1 \\ 0 & 1 & 0 \\ -1 & 0 & 0 \end{bmatrix}, \quad M_6 = \frac{1}{4} \begin{bmatrix} 1 & \sqrt{2} & -1 \\ -\sqrt{2} & 0 & -\sqrt{2} \\ 1 & -\sqrt{2} & -1 \end{bmatrix},$$

$$M_7 = \frac{1}{2} \begin{bmatrix} 0 & 0 & 1 \\ 0 & 1 & 0 \\ -1 & 0 & 0 \end{bmatrix}, \quad M_8 = \frac{1}{4} \begin{bmatrix} -1 & -\sqrt{2} & -1 \\ \sqrt{2} & 0 & -\sqrt{2} \\ -1 & \sqrt{2} & -1 \end{bmatrix}.$$

Note that the vertices of the  $P_i^3$  are ordered so that  $M_i = 1/2 Q_i$  where  $Q_i$  is an orthogonal matrix.



Let

$$\text{diag}(a_1, a_2, a_3) = \begin{bmatrix} a_1 & 0 & 0 \\ 0 & a_2 & 0 \\ 0 & 0 & a_3 \end{bmatrix}, \quad \text{skew}(a_1, a_2, a_3) = \begin{bmatrix} 0 & 0 & a_1 \\ 0 & a_2 & 0 \\ a_3 & 0 & 0 \end{bmatrix}.$$

The following equations can be obtained by straightforward computation.

$$\begin{aligned} M_6 &= \text{diag}(-1, 1, 1)M_3, \quad M_8 = \text{diag}(-1, 1, 1)M_4, \\ M_3^2 &= 1/4 I, \quad M_3M_4 = 1/4 \text{diag}(-1, -1, 1), \quad M_4M_3 = 1/2 \text{diag}(-1, -1, 1)M_4, \\ M_3M_5 &= 1/2 \text{diag}(1, -1, 1)M_3, \quad M_5M_3 = 1/2 \text{skew}(-1, 1, -1)M_3, \\ M_3M_6 &= 1/2 \text{skew}(-1, -1, 1)M_4, \quad M_6M_3 = 1/4 \text{diag}(-1, 1, 1), \\ M_3M_7 &= 1/2 \text{diag}(-1, 1, -1)M_4, \quad M_7M_3 = 1/2 \text{skew}(1, 1, -1)M_3, \\ M_3M_8 &= 1/2 \text{skew}(-1, -1, 1)M_3, \quad M_8M_3 = 1/2 \text{diag}(1, -1, 1)M_4, \\ M_4^2 &= 1/2 \text{diag}(-1, -1, 1)M_3, \quad M_4M_5 = 1/2 \text{skew}(1, 1, 1)M_4, \\ M_5M_4 &= 1/2 \text{skew}(-1, 1, -1)M_4, \quad M_4M_6 = 1/4 \text{skew}(-1, 1, -1), \\ M_6M_4 &= 1/4 \text{diag}(1, -1, 1), \quad M_4M_7 = 1/2 \text{skew}(-1, -1, -1)M_3, \\ M_7M_4 &= 1/2 \text{skew}(1, 1, -1)M_4, \quad M_4M_8 = 1/4 \text{skew}(-1, -1, 1), \\ M_8M_4 &= 1/2 \text{diag}(1, -1, 1)M_3, \quad M_5^2 = 1/4 I, \quad M_5M_6 = 1/2 \text{skew}(-1, 1, 1)M_3, \\ M_6M_5 &= 1/2 \text{diag}(-1, -1, 1)M_3, \quad M_5M_7 = 1/4 \text{diag}(1, 1, -1), \\ M_7M_5 &= 1/4 \text{diag}(-1, 1, 1), \quad M_5M_8 = 1/2 \text{skew}(-1, 1, 1)M_4, \\ M_8M_5 &= 1/2 \text{skew}(-1, 1, 1)M_4, \quad M_6^2 = 1/2 \text{skew}(1, -1, 1)M_4, \\ M_6M_7 &= 1/2 \text{diag}(1, 1, -1)M_4, \quad M_7M_6 = 1/2 \text{skew}(1, 1, 1)M_3, \\ M_6M_8 &= 1/2 \text{skew}(1, -1, 1)M_3, \quad M_8M_6 = 1/4 \text{skew}(1, 1, -1), \\ M_7^2 &= 1/4 \text{diag}(-1, 1, -1), \quad M_7M_8 = 1/2 \text{skew}(1, 1, 1)M_4, \\ M_8M_7 &= 1/2 \text{skew}(1, -1, -1)M_3, \quad M_8^2 = 1/4 \text{skew}(1, -1, 1). \end{aligned}$$

After 6 levels of bisection,  $M(\mathbf{P}, \mathbf{P}_i^6) = M(\mathbf{P}_j^3, \mathbf{P}_i^6)M(\mathbf{P}, \mathbf{P}_j^3)$  where  $\mathbf{P}_i^6$  is a subtetrahedron of  $\mathbf{P}_j^3$ . With a suitable ordering of vertices of  $\mathbf{P}_i^6$ , it follows that  $P_i^6 = M_j P_l^3$  for some  $l$ . So

$$M(\mathbf{P}, \mathbf{P}_i^6) = P_i^6 P^{-1} = M_j P_l^3 P^{-1} = M_j M_l,$$

since  $P_l^3 = M_l P$ . By induction, after  $3k$  levels of bisection, for each subtetrahedron  $\mathbf{P}_i^{3k}$  with a suitable ordering of vertices  $\mathbf{p}_{ij}^{3k}$ , we have

$$\mathbf{p}_{ij}^{3k} = M_{l_1} M_{l_2} \cdots M_{l_k} \mathbf{p}_j + \mathbf{b}_i^{3k}, \quad 0 \leq j \leq 3,$$

where each  $M_{lm}$ ,  $1 \leq m \leq k$ , is one of the  $M_i$ ,  $1 \leq i \leq 8$ . Let  $\mathcal{S}$  be the set of all diagonal and skew diagonal matrices with elements 1 or  $-1$ . Obviously,  $\mathcal{S}$  is closed under matrix multiplication, and  $|\mathcal{S}| = 2^3 + 2^3 = 16$ . So, by the above equations,  $M_{l_1}M_{l_2} \cdots M_{l_k} = fDM$ , where  $f$  is a scale factor,  $D$  is an element of  $\mathcal{S}$ , and  $M$  is either  $I$ ,  $M_3$ , or  $M_4$ . Note that  $D$  and  $-D$  can be considered to be the same matrix of  $\mathcal{S}$  due to the factor  $f$ . Therefore the number of different equivalence classes of tetrahedra of type  $\mathbf{P}^0$  in  $\mathcal{P}^n$ ,  $n \geq 0$ , is  $\leq 3 \times 8 = 24$ . Note that a type  $\mathbf{P}^1$  tetrahedron is generated by bisecting the longest edge of a type  $\mathbf{P}^0$  tetrahedron. Since the longest edge of a tetrahedron is still the longest edge under translation and uniform scaling, each one of the 24 possible equivalence classes of tetrahedra of type  $\mathbf{P}^0$  creates two equivalence classes of tetrahedra of type  $\mathbf{P}^1$ . So the number of different equivalence classes of tetrahedra of type  $\mathbf{P}^1$  is  $\leq 2 \times 24 = 48$ . Using a similar argument, the number of different equivalence classes of tetrahedra of type  $\mathbf{P}^2$  is  $\leq 2 \times 48 = 96$ . Hence the total number of classes of similar tetrahedra in all the  $\mathcal{T}^n$ ,  $n \geq 0$ , is finite and bounded above by 168.  $\square$

Although there are a large number of subtetrahedra produced with the increase of the levels of bisection, Theorem 3.3 implies that most subtetrahedra are geometrically similar to each other. Also, from Theorem 3.3, it follows that  $\eta(\mathbf{T}_i^n) \geq c_1 \eta(\mathbf{T})$  for some constant  $c_1$  that may depend on  $\mathbf{T}$ . The following theorem establishes that  $c_1$  is independent of  $\mathbf{T}$ .

**Theorem 3.4** *For any tetrahedron  $\mathbf{T}_i^n$  in  $\mathcal{T}^n$ ,*

$$\eta(\mathbf{T}_i^n) \geq c_1 \eta(\mathbf{T}) \quad (3.3.1)$$

*where  $c_1$  is a positive constant independent of  $\mathbf{T}$ .*

**Proof.** Let  $M(\mathbf{P}, \mathbf{T})$  and  $M(\mathbf{R}, \mathbf{P})$  be the two matrices involved in the affine transformations from  $\mathbf{P}$  to  $\mathbf{T}$  and  $\mathbf{R}$  to  $\mathbf{P}$ , respectively. Using the notation in Definition 2.1,

$$\mathbf{T} = M(\mathbf{P}, \mathbf{T})\mathbf{P} = M(\mathbf{P}, \mathbf{T})M(\mathbf{R}, \mathbf{P})\mathbf{R}.$$

From step (c) of the bisection procedure, the tetrahedron  $\mathbf{T}_i^n$  is transformed from  $\mathbf{P}_i^n$  using  $M(\mathbf{P}, \mathbf{T})$ , so

$$\mathbf{T}_i^n = M(\mathbf{P}, \mathbf{T})\mathbf{P}_i^n.$$

If  $\mathbf{P}_i^n$  is a tetrahedron of type  $\mathbf{P}^0$ , then with a suitable ordering of vertices of  $\mathbf{P}_i^n$ ,  $\mathbf{P}_i^n = \alpha Q \mathbf{P}$  where  $\alpha$  is a positive constant and  $Q$  is an orthogonal matrix, since  $\mathbf{P}_i^n$  is similar to  $\mathbf{P}$ . If  $\mathbf{P}_i^n$  is a tetrahedron of type  $\mathbf{P}^1$ , then  $\mathbf{P}_i^n = \alpha Q M(\mathbf{P}, \mathbf{P}_k^1) \mathbf{P}$  where  $\alpha$  is a positive constant,  $Q$

is an orthogonal matrix, and  $\mathbf{P}_k^1$  is any of the two tetrahedra in  $\mathcal{P}^1$ . If  $\mathbf{P}_i^n$  is a tetrahedron of type  $\mathbf{P}^2$ , then  $P_i^n = \alpha Q M(\mathbf{P}, \mathbf{P}_k^2) P$  where  $\alpha$  is a positive constant,  $Q$  is an orthogonal matrix, and  $\mathbf{P}_k^2$  is any of the four tetrahedra in  $\mathcal{P}^2$ .

Let  $\mathbf{R}^n$  be the regular tetrahedron having the same volume as  $\mathbf{T}_i^n$ . Then

$$T_i^n = M(\mathbf{P}, \mathbf{T}) C' M(\mathbf{R}, \mathbf{P}) R^n$$

where  $C'$  is one of  $Q$ ,  $\sqrt[3]{2} Q M(\mathbf{P}, \mathbf{P}_k^1)$ , or  $\sqrt[3]{4} Q M(\mathbf{P}, \mathbf{P}_k^2)$  depending on the type of  $\mathbf{P}_i^n$ . Due to uniqueness,  $M(\mathbf{P}, \mathbf{T}) C' M(\mathbf{R}, \mathbf{P}) = M(\mathbf{R}^n, \mathbf{T}_i^n)$ . Since  $\mathbf{R}$  and  $\mathbf{R}^n$  have the same volume as  $\mathbf{T}$  and  $\mathbf{T}_i^n$ , respectively,  $\det(A(\mathbf{R}, \mathbf{T})) = 1$ , and  $\det(A(\mathbf{R}^n, \mathbf{T}_i^n)) = 1$ . So, from the formula for the computation of  $\eta$  (Eqn. (2.4.7)), it follows that

$$\eta(\mathbf{T}) = \frac{3}{\text{trace}(A(\mathbf{R}, \mathbf{T}))} = \frac{3}{\text{trace}((M(\mathbf{P}, \mathbf{T}) M(\mathbf{R}, \mathbf{P}))^T M(\mathbf{P}, \mathbf{T}) M(\mathbf{R}, \mathbf{P}))}, \quad (3.3.2)$$

$$\eta(\mathbf{T}_i^n) = \frac{3}{\text{trace}(A(\mathbf{R}^n, \mathbf{T}_i^n))} = \frac{3}{\text{trace}((M(\mathbf{P}, \mathbf{T}) C' M(\mathbf{R}, \mathbf{P}))^T M(\mathbf{P}, \mathbf{T}) C' M(\mathbf{R}, \mathbf{P}))}. \quad (3.3.3)$$

Let  $\|B\|_F$  denote the Frobenius norm of matrix  $B$  [GoV89], i.e.  $\|B\|_F = (\text{trace}(B^T B))^{1/2}$  is the square root of the sum of squares of the elements of  $B$ . From (3.3.2) and (3.3.3),

$$\frac{\eta(\mathbf{T}_i^n)}{\eta(\mathbf{T})} = \frac{\|M(\mathbf{P}, \mathbf{T}) M(\mathbf{R}, \mathbf{P})\|_F^2}{\|M(\mathbf{P}, \mathbf{T}) C' M(\mathbf{R}, \mathbf{P})\|_F^2}. \quad (3.3.4)$$

Since  $\|Q\|_F^2 = 3$  for  $3 \times 3$  orthogonal matrix  $Q$  and  $\|AB\|_F \leq \|A\|_F \|B\|_F$  for any  $3 \times 3$  matrices  $A$  and  $B$ ,

$$\begin{aligned} \|M(\mathbf{P}, \mathbf{T}) C' M(\mathbf{R}, \mathbf{P})\|_F^2 &\leq \|M(\mathbf{P}, \mathbf{T}) M(\mathbf{R}, \mathbf{P})\|_F^2 \|M^{-1}(\mathbf{R}, \mathbf{P}) C' M(\mathbf{R}, \mathbf{P})\|_F^2 \\ &\leq 3 \|M(\mathbf{P}, \mathbf{T}) M(\mathbf{R}, \mathbf{P})\|_F^2 \|M^{-1}(\mathbf{R}, \mathbf{P})\|_F^2 \|M(\mathbf{R}, \mathbf{P})\|_F^2 \max(1, s_1, s_2), \end{aligned} \quad (3.3.5)$$

where  $s_1 = 2^{2/3} \max_{1 \leq k \leq 2} (\|M(\mathbf{P}, \mathbf{P}_k^1)\|_F^2)$  and  $s_2 = 2^{4/3} \max_{1 \leq k \leq 4} (\|M(\mathbf{P}, \mathbf{P}_k^2)\|_F^2)$ . From (3.3.4) and (3.3.5),  $\eta(\mathbf{T}_i^n)/\eta(\mathbf{T}) \geq c_1$  where

$$c_1 = 1 / [3 \|M^{-1}(\mathbf{R}, \mathbf{P})\|_F^2 \|M(\mathbf{R}, \mathbf{P})\|_F^2 \max(1, s_1, s_2)]. \square$$

**Theorem 3.5** For any tetrahedron  $\mathbf{T}_i^n$  in  $\mathcal{T}^n$ ,

$$\delta(\mathbf{T}_i^n) \leq c_2 (1/2)^{n/3} \delta(\mathbf{T})$$

where  $c_2$  is a positive constant independent of  $\mathbf{T}$ .

**Proof.** By Theorem 2.4,

$$\eta(\mathbf{T}) = \frac{12(3v)^{2/3}}{\sum_{i=1}^6 l_{i,0}^2}, \quad (3.3.6)$$

where  $v$  is the volume of  $\mathbf{T}$  and the  $l_{i,0}$  are the lengths of the edges of  $\mathbf{T}$ . At each level of bisection, the volume of a subtetrahedron is decreased by a factor of 2, so after  $n$  levels of bisection,

$$\eta(\mathbf{T}_i^n) = \frac{12(1/2)^{2n/3}(3v)^{2/3}}{\sum_{i=1}^6 l_{i,n}^2}, \quad (3.3.7)$$

where the  $l_{i,n}$  are the lengths of the edges of  $\mathbf{T}_i^n$ . Substituting (3.3.6) and (3.3.7) in (3.3.1) yields

$$\sum_{i=1}^6 l_{i,n}^2 \leq (1/c_1)(1/2)^{2n/3} \sum_{i=1}^6 l_{i,0}^2,$$

where  $c_1$  is a positive constant independent of  $\mathbf{T}$ . So

$$\delta(\mathbf{T}_i^n)^2 \leq \sum_{i=1}^6 l_{i,n}^2 \leq (1/c_1)(1/2)^{2n/3} \sum_{i=1}^6 l_{i,0}^2 \leq (1/c_1)(1/2)^{2n/3} 6\delta(\mathbf{T})^2.$$

That is,  $\delta(\mathbf{T}_i^n) \leq c_2(1/2)^{n/3}\delta(\mathbf{T})$  where  $c_2 = \sqrt{6/c_1}$ .  $\square$

### 3.4 Estimate of constants

In this section, we obtain an estimate of the constant  $c_1$  in Theorem 3.4, which then provides an estimate of the constant  $c_2$  in Theorem 3.5. Our derivation of the estimate of  $c_1$  starts from (3.3.4) in the proof of Theorem 3.4, since (3.3.5) provides an estimate that is too small. At the first two levels of bisection, we use the tetrahedra  $\mathbf{P}_1^1(\mathbf{p}_{12}, \mathbf{p}_1, \mathbf{p}_3, \mathbf{p}_0)$  and  $\mathbf{P}_1^2(\mathbf{p}_{12}, \mathbf{p}_0, \mathbf{p}_1, \mathbf{p}_{13})$ .

By the singular value decomposition [GoV89],  $M(\mathbf{P}, \mathbf{T}) = Q_1 \text{diag}(\sqrt{\lambda_1}, \sqrt{\lambda_2}, \sqrt{\lambda_3}) Q_2$  where  $Q_1, Q_2$  are orthogonal matrices and  $\lambda_1, \lambda_2, \lambda_3$  are the eigenvalues of  $A(\mathbf{P}, \mathbf{T})$  ( $\sqrt{\lambda_1}, \sqrt{\lambda_2}, \sqrt{\lambda_3}$  are the singular values of  $M(\mathbf{P}, \mathbf{T})$ ). Similarly,

$$M(\mathbf{R}, \mathbf{P}) = Q_3 \text{diag}(\sqrt{\mu_{11}}, \sqrt{\mu_{12}}, \sqrt{\mu_{13}}) Q_4,$$

$$\sqrt[3]{2} M(\mathbf{P}, \mathbf{P}_1^1) M(\mathbf{R}, \mathbf{P}) = Q_5 \text{diag}(\sqrt{\mu_{21}}, \sqrt{\mu_{22}}, \sqrt{\mu_{23}}) Q_6,$$

$$\sqrt[3]{4} M(\mathbf{P}, \mathbf{P}_1^2) M(\mathbf{R}, \mathbf{P}) = Q_7 \text{diag}(\sqrt{\mu_{31}}, \sqrt{\mu_{32}}, \sqrt{\mu_{33}}) Q_8,$$

where the  $Q_i$  are orthogonal matrices and the  $\mu_{ij}$  are eigenvalues. It follows that

$$\|M(\mathbf{P}, \mathbf{T}) M(\mathbf{R}, \mathbf{P})\|_F^2 = \|\text{diag}(\sqrt{\lambda_1}, \sqrt{\lambda_2}, \sqrt{\lambda_3}) Q_2 Q_3 \text{diag}(\sqrt{\mu_{11}}, \sqrt{\mu_{12}}, \sqrt{\mu_{13}})\|_F^2, \quad (3.4.1)$$

$$\|M(\mathbf{P}, \mathbf{T})C M(\mathbf{R}, \mathbf{P})\|_F^2 = \|\text{diag}(\sqrt{\lambda_1}, \sqrt{\lambda_2}, \sqrt{\lambda_3})Q_9\text{diag}(\sqrt{\mu_{i1}}, \sqrt{\mu_{i2}}, \sqrt{\mu_{i3}})\|_F^2, \quad (3.4.2)$$

where  $Q_9$  is an orthogonal matrix and  $i$  is 1, 2, or 3. For any orthogonal matrix  $Q$ , let  $S = \text{diag}(\sqrt{\lambda_1}, \sqrt{\lambda_2}, \sqrt{\lambda_3})Q\text{diag}(\sqrt{\mu_{i1}}, \sqrt{\mu_{i2}}, \sqrt{\mu_{i3}})$ . By carrying out the two matrix multiplications, it is easy to see that

$$\min(\mu_{i1}, \mu_{i2}, \mu_{i3})(\lambda_1 + \lambda_2 + \lambda_3) \leq \|S\|_F^2 \leq \max(\mu_{i1}, \mu_{i2}, \mu_{i3})(\lambda_1 + \lambda_2 + \lambda_3). \quad (3.4.3)$$

From (3.4.1), (3.4.2), and (3.4.3), it follows that

$$\|M(\mathbf{P}, \mathbf{T})M(\mathbf{R}, \mathbf{P})\|_F^2 \geq (\lambda_1 + \lambda_2 + \lambda_3) \min_{1 \leq j \leq 3}(\mu_{1j}), \quad (3.4.4)$$

$$\|M(\mathbf{P}, \mathbf{T})C M(\mathbf{R}, \mathbf{P})\|_F^2 \leq (\lambda_1 + \lambda_2 + \lambda_3) \max_{1 \leq i, j \leq 3}(\mu_{ij}). \quad (3.4.5)$$

Substituting (3.4.4) and (3.4.5) into (3.3.4) yields

$$\frac{\eta(\mathbf{T}_i^n)}{\eta(\mathbf{T})} \geq \frac{\min_{1 \leq j \leq 3}(\mu_{1j})}{\max_{1 \leq i, j \leq 3}(\mu_{ij})}. \quad (3.4.6)$$

We now compute the eigenvalues  $\mu_{ij}$ . Suppose the vertex coordinates of the regular tetrahedra  $\mathbf{R}$  are  $\mathbf{r}_0 = (-\sqrt{3}a'/2, 0, 0)^T$ ,  $\mathbf{r}_1 = (0, -a'/2, 0)^T$ ,  $\mathbf{r}_2 = (0, a'/2, 0)^T$ , and  $\mathbf{r}_3 = (-\sqrt{3}a'/6, 0, \sqrt{6}a'/3)^T$ , where  $a' = \sqrt[3]{2}a$  since  $\mathbf{R}$  and  $\mathbf{P}$  have the same volume (see Figure 3.2). Using the coordinates of Figure 3.2 with  $\mathbf{r}_i$  being transformed to  $\mathbf{p}_i$ , we obtain

$$M(\mathbf{R}, \mathbf{P}) = PR^{-1} = \frac{1}{\sqrt[3]{2}} \begin{bmatrix} 0 & 2 & 0 \\ -\sqrt{6}/3 & 0 & -\sqrt{3}/6 \\ 0 & 0 & \sqrt{6}/2 \end{bmatrix}.$$

So in decreasing order,  $\mu_{11} = 4/\sqrt[3]{4}$ ,  $\mu_{12} = (9 + \sqrt{17})/(8\sqrt[3]{4})$ , and  $\mu_{13} = (9 - \sqrt{17})/(8\sqrt[3]{4})$ . From

$$\sqrt[3]{2} M(\mathbf{P}, \mathbf{P}_1^1)M(\mathbf{R}, \mathbf{P}) = \begin{bmatrix} -\sqrt{3}/3 & 1 & -\sqrt{6}/6 \\ 0 & 0 & \sqrt{3}/2 \\ \sqrt{3}/3 & 1 & -\sqrt{6}/6 \end{bmatrix},$$

$\mu_{21} = 2$ ,  $\mu_{22} = (7 + \sqrt{17})/8$ , and  $\mu_{23} = (7 - \sqrt{17})/8$  in decreasing order. From

$$\sqrt[3]{4} M(\mathbf{P}, \mathbf{P}_1^2) M(\mathbf{R}, \mathbf{P}) = \sqrt[3]{2} \begin{bmatrix} -\sqrt{3}/3 & -1 & -\sqrt{6}/12 \\ \sqrt{6}/6 & -\sqrt{2}/2 & -\sqrt{3}/6 \\ 0 & 0 & \sqrt{6}/4 \end{bmatrix},$$

$\mu_{31} = \sqrt[3]{4} (2 + \sqrt{2})/2$ ,  $\mu_{32} = \sqrt[3]{4}/2$ , and  $\mu_{33} = \sqrt[3]{4} (2 - \sqrt{2})/2$  in decreasing order.

From (3.4.6),  $\eta(\mathbf{T}_i^n)/\eta(\mathbf{T}) \geq c_1 = \mu_{13}/\mu_{31} = \sqrt[3]{4} (9 - \sqrt{17})(2 - \sqrt{2})/32 = 0.1417$ . Then it follows from  $c_2 = \sqrt{6/c_1}$  that  $c_2 = 6.5068$ . By using a different approach, it may be possible to obtain better estimates of  $c_1$  and  $c_2$ , but we believe that our current estimates can be improved by at most a small factor (unless a better  $\mathbf{P}$  tetrahedron can be found).

### 3.5 Further remarks

It has been conjectured that the shape of any subtetrahedron  $\mathbf{T}_i^n$  produced by repeated longest edge bisection of a tetrahedron  $\mathbf{T}$  is bounded below by a function of the shape of  $\mathbf{T}$  [RiL92], and that the diameter bound on  $\mathbf{T}_i^n$  is  $\delta(\mathbf{T}_i^n) = O(2^{-n/3})$  [Adl83], where  $n$  is the number of levels of bisection applied to  $\mathbf{T}$ . As far as we know, these two problems are still open. By formula (2.4.1) and an argument similar to the proof of Theorem 3.5, it follows that

$$\frac{1}{6} [(1/2)^{n/3} \frac{\delta(\mathbf{T})}{\delta(\mathbf{T}_i^n)}]^2 \leq \frac{\eta(\mathbf{T}_i^n)}{\eta(\mathbf{T})} \leq 6 [(1/2)^{n/3} \frac{\delta(\mathbf{T})}{\delta(\mathbf{T}_i^n)}]^2.$$

The above equation establishes the relationship between the two open problems mentioned above. That is, the  $1/\sqrt[3]{2}$  convergence rate of the diameter of refined subtetrahedra for sufficiently large  $n$  (i.e. the diameter decreases by a factor of 2 in every three levels of bisection) precisely reflects the degeneration on the shape of subtetrahedra produced by repeated longest edge bisection (this is also true for any bisection procedure as long as each bisection decreases the volume of subtetrahedra by a factor of 2). Due to the “equivalence” among tetrahedron shape measures (see Chapter 2), we conclude that the two open problems are equivalent.

## Chapter 4

# Quality Local Refinement of Tetrahedral Meshes Based on Bisection

In this chapter, we present a 3-D local refinement algorithm for tetrahedral meshes based mainly on the bisection procedure described in the previous chapter. The quality of refined meshes is discussed, and implementation details are provided. Experimental results from the algorithm are given in Chapter 6.

### 4.1 Introduction

As mentioned in Chapter 1, mesh generation is a time-consuming step, and remeshing the whole region is in general not recommended. A more efficient mesh refinement scheme, local refinement, is a popular method in current finite element analysis. It is desirable that the adaptive mesh refinement produce refined elements of good shape using a fast refining process. These are the goals of our 3-D local refinement algorithm.

We consider a local refinement process that includes two major steps. First, a set  $S$  of basic elements is chosen from an existing mesh  $\mathcal{T}$  according to numerical results and error estimates from previous computations. Next, each element in  $S$  is refined, and then a procedure is needed to keep the final mesh conforming. Recall that a *conforming* mesh is one in which the intersection of any two tetrahedra  $\mathbf{T}_1, \mathbf{T}_2$  of the mesh is either a common face of  $\mathbf{T}_1$  and  $\mathbf{T}_2$ , or a common edge, or a common vertex, or empty.

One popular refinement technique uses bisection. Let  $\mathbf{T}(\mathbf{t}_0, \mathbf{t}_1, \mathbf{t}_2, \mathbf{t}_3)$  be a tetrahedron

with vertices  $t_0, t_1, t_2, t_3$ . One step of bisection of a tetrahedron  $T$  is as follows. Using the midpoint  $t$  of one of the edges (called *bisected edge*),  $t_1t_2$  say, and the face  $t_0t_3t$ ,  $T$  can be bisected into two subtetrahedra  $T_1(t_0, t_1, t, t_3)$  and  $T_2(t_0, t, t_2, t_3)$ . Rivara and Levin [RiL92] present a 3-D local refinement algorithm based on longest edge bisection. Let  $S$  be a set of tetrahedra chosen from a conforming mesh  $\mathcal{T}$ . If tetrahedra in  $S$  are bisected by longest edge bisection, some non-conforming edges may be produced, where a *non-conforming* edge is one that is bisected due to the bisections of some tetrahedra incident on this edge, but at least one tetrahedron incident on the edge is not bisected using this edge. It is proved in [RiL92] that iteratively bisecting tetrahedra with a non-conforming edge by the longest edge produces a conforming mesh in a finite number of steps. They also conjecture that the shape of refined tetrahedra do not degenerate when the process based on longest edge bisection proceeds indefinitely, but no theoretical basis is given. By experiments, we found that their algorithm may bisect many tetrahedra with a non-conforming edge and introduce a large number of vertices in order to obtain a conforming mesh. This increases not only the time spent on refinement, but also the time in finite element analysis.

In this chapter, instead of longest edge bisection, we present a local refinement algorithm based on the bisection procedure described in the previous chapter, which has the following properties.

- (1) For an initial mesh  $\mathcal{T}$ , there are only a finite number, which depends on the number of tetrahedra in  $\mathcal{T}$ , of classes of similar tetrahedra in all refined tetrahedra.
- (2)  $\eta(T_i^n) \geq c \eta(T)$  where  $T_i^n$  is any refined tetrahedron of  $T$  and  $c$  is a positive constant independent of  $\mathcal{T}$ .
- (3) For any interior face in a refined mesh, the absolute value of the difference of the bisection levels of the two adjacent tetrahedra incident on the face is  $\leq 2$ .
- (4) The expected time complexity of the algorithm is  $O(N)$  where  $N$  is the number of refined tetrahedra in a refined mesh.

The superscript  $n$  of  $T_i^n$  indicates that  $T_i^n$  is created after  $n$  levels of bisection. Properties (1) and (2) demonstrate that the shape of refined tetrahedra do not get substantially worse. Property (3) indicates that local refinements on tetrahedra can be smoothly extended to their neighbors.



This chapter is organized as follows. In Section 4.2, we describe a procedure for the bisection of a tetrahedron. The bisection of tetrahedra in a conforming mesh is given in Section 4.3. In Section 4.4, the properties of our local refinement algorithm are established. Data structure and algorithmic details are discussed in Section 4.5. Time complexity analysis is given in Section 4.6. In Section 4.7, we provide a brief summary.

## 4.2 Bisection of a tetrahedron

In the previous chapter, we presented a method for repeated bisection of a tetrahedron  $\mathbf{T}$ . The basic idea is that  $\mathbf{T}$  is first mapped to the canonical tetrahedron  $\mathbf{P}$  (see Figure 3.2) with the same volume as  $\mathbf{T}$ , and then the bisection is controlled by longest edge bisection on  $\mathbf{P}$ . We first recall the procedure for iterative bisection of  $\mathbf{T}$  from the end of Section 3.2, which is called TRANBIS.

### Algorithm TRANBIS

- (a) Transform  $\mathbf{T}$  to  $\mathbf{P}$  by the affine transformation  $\mathbf{y} = M^{-1}(\mathbf{P}, \mathbf{T})\mathbf{x} + \mathbf{b}_0$ .
- (b) Iteratively bisect  $\mathbf{P}$  to  $n$  levels by longest edge bisection.
- (c) Transform all subtetrahedra  $\mathbf{P}_i^n$  of  $\mathbf{P}$  back to subtetrahedra  $\mathbf{T}_i^n$  of  $\mathbf{T}$  using the inverse affine transformation  $\mathbf{y} = M(\mathbf{P}, \mathbf{T})\mathbf{x} + \mathbf{b}_1$ .

The above procedure provides an intrinsic view of our bisection procedure, i.e., the utilization of canonical tetrahedron  $\mathbf{P}$ . However, the use of affine transformations costs extra computation time. In fact, procedure TRANBIS can be viewed as bisecting  $\mathbf{T}$  and its subsequent subtetrahedra in a fixed order so that canonical tetrahedron  $\mathbf{P}$  and the affine transformation are not involved. So, the goal of this section is to design a scheme to carry out the bisection on  $\mathbf{T}$  and its subtetrahedra directly, and the same set of tetrahedra is produced as in TRANBIS.

To decide the bisection order on  $\mathbf{T}$ , we first study the bisection order on  $\mathbf{P}$ . Instead of using longest edge, which is not invariant under an affine transformation, we try to describe step (b) in TRANBIS by another equivalent method such that it can be used on  $\mathbf{T}$  directly. The most important property of canonical tetrahedron  $\mathbf{P}$  is stated in Theorem 3.1. That is, in the first three levels of longest edge bisection applied to the canonical tetrahedron  $\mathbf{P}$ ,

the subtetrahedra at the same level are similar to each other, and the subtetrahedra at the third level are all similar to  $\mathbf{P}$ .

Notice that  $\mathbf{P}$  has three types of edges in terms of the lengths of edges (see Figure 3.2), the longest edge ( $\mathbf{p}_1\mathbf{p}_2$ ), the second longest edges ( $\mathbf{p}_1\mathbf{p}_3$  and  $\mathbf{p}_2\mathbf{p}_3$ ), and the shortest edges ( $\mathbf{p}_0\mathbf{p}_1$ ,  $\mathbf{p}_0\mathbf{p}_2$ , and  $\mathbf{p}_0\mathbf{p}_3$ ). We assign a type to each edge to indicate the three different lengths. Namely, the longest edge  $\mathbf{p}_1\mathbf{p}_2$  has type 1; the second longest edges  $\mathbf{p}_1\mathbf{p}_3$  and  $\mathbf{p}_2\mathbf{p}_3$  have type 2; the shortest edges  $\mathbf{p}_0\mathbf{p}_1$ ,  $\mathbf{p}_0\mathbf{p}_2$ , and  $\mathbf{p}_0\mathbf{p}_3$  have type 3. In the first level of bisection on  $\mathbf{P}$ , the edge  $\mathbf{p}_1\mathbf{p}_2$  with type 1 is bisected. Next, the edges with type 2 are bisected at the second level of bisection. Finally, all edges with type 3 are bisected at the third level of bisection. By Theorem 3.1, all eight subtetrahedra  $\mathbf{P}_i^3$ ,  $1 \leq i \leq 8$ , are geometrically similar to  $\mathbf{P}$ . We assign a type to each edge of  $\mathbf{P}_i^3$  in the same way as to  $\mathbf{P}$  (i.e., assigning 1 to the longest edge, 2 to the second longest edges, 3 to the shortest edges). Then the bisected edge in each  $\mathbf{P}_i^3$  is the one with type 1. If the levels of bisection are continued, the types of bisected edges form a cycle like 1, 2, 3, 1, 2, 3, ...

The types of the edges formed at each level of bisection on  $\mathbf{P}$  can be obtained as follows. Let  $\tau(e)$  stand for the type of edge  $e$ ,  $e_B$  for a bisected edge, and  $[a, b, \tau(e_B)]$  indicate a configuration associated with a face where  $a, b$ , and  $\tau(e_B)$  are the types of the three edges in the face. Let  $\tau([a, b, \tau(e_B)])$  denote the type of the new edge added in the interior of a face, and

$$\mathcal{F} = \{[2, 2, 1], [1, 1, 2], [3, 3, 2], [3, 3, 1], [1, 2, 3], [2, 1, 3], [2, 2, 3]\}. \quad (4.2.1)$$

The first 6 configurations of  $\mathcal{F}$  occur in the first three levels of bisection on  $\mathbf{P}$ , and  $[2, 2, 3]$  is not used until the next section. In each bisection, the types of new edges are assigned as follows.

Rule NEWTYPE (for the types of new edges in each bisection):

- (a) The edge  $e_B$  is divided into two new edges;  
each of them is given the same type as  $e_B$ .
- (b) The types of the other two new edges added in the interior of the two faces sharing  $e_B$  are assigned by the following rule:  
 $\tau([a, b, c]) = c$  if  $[a, b, c] \in \mathcal{F}$  and  $[a, b, c] \neq [3, 3, d], d = 1, 2$ ;  
 $\tau([3, 3, d]) = 3 - d, d = 1, 2$ .

Table 4.1 illustrates the lengths and types of new edges created in the first three levels of

Description	Edge	Length	Type	Level created	Level bisected
Original edges of $\mathbf{P}$	$\mathbf{P}_1\mathbf{P}_2$	$2a$	1	0	1
	$\mathbf{P}_1\mathbf{P}_3$	$\sqrt{2}a$	2	0	2
	$\mathbf{P}_2\mathbf{P}_3$	$\sqrt{2}a$	2	0	2
	$\mathbf{P}_0\mathbf{P}_1$	$\sqrt{6}a/2$	3	0	3
	$\mathbf{P}_0\mathbf{P}_2$	$\sqrt{6}a/2$	3	0	3
	$\mathbf{P}_0\mathbf{P}_3$	$\sqrt{6}a/2$	3	0	3
New edges from bisection of $\mathbf{P}(\mathbf{p}_0, \mathbf{p}_1, \mathbf{p}_2, \mathbf{p}_3)$ using $e_B = \mathbf{P}_1\mathbf{P}_2$	$\mathbf{P}_1\mathbf{P}_{12}$	$a$	1	1	4
	$\mathbf{P}_2\mathbf{P}_{12}$	$a$	1	1	4
	$\mathbf{P}_3\mathbf{P}_{12}$	$a$	$\tau([2, 2, 1]) = 1$	1	4
	$\mathbf{P}_0\mathbf{P}_{12}$	$\sqrt{2}a/2$	$\tau([3, 3, 1]) = 2$	1	5
New edges from bisection of $\mathbf{P}_1^1(\mathbf{p}_0, \mathbf{p}_1, \mathbf{p}_{12}, \mathbf{p}_3)$ using $e_B = \mathbf{P}_1\mathbf{P}_3$	$\mathbf{P}_1\mathbf{P}_{13}$	$\sqrt{2}a/2$	2	2	5
	$\mathbf{P}_3\mathbf{P}_{13}$	$\sqrt{2}a/2$	2	2	5
	$\mathbf{P}_0\mathbf{P}_{13}$	$a$	$\tau([3, 3, 2]) = 1$	2	4
	$\mathbf{P}_{12}\mathbf{P}_{13}$	$\sqrt{2}a/2$	$\tau([1, 1, 2]) = 2$	2	5
New edges from bisection of $\mathbf{P}_1^2(\mathbf{p}_0, \mathbf{p}_1, \mathbf{p}_{12}, \mathbf{p}_{13})$ using $e_B = \mathbf{p}_0\mathbf{p}_1$	$\mathbf{P}_0\mathbf{P}_{01}$	$\sqrt{6}a/4$	3	3	6
	$\mathbf{P}_1\mathbf{P}_{01}$	$\sqrt{6}a/4$	3	3	6
	$\mathbf{P}_{12}\mathbf{P}_{01}$	$\sqrt{6}a/4$	$\tau([1, 2, 3]) = 3$	3	6
	$\mathbf{P}_{13}\mathbf{P}_{01}$	$\sqrt{6}a/4$	$\tau([1, 2, 3]) = 3$	3	6

Table 4.1: Information associated with edges in bisection of  $\mathbf{P}$ 

bisection on  $\mathbf{P}$ ; only one subtetrahedron is shown bisected at the second and third levels, since the others are similar by Theorem 3.1. It is easy to verify that the types of edges of subtetrahedra at the third level derived by rule NEWTYPE are 1 for the longest edge, 2 for the second longest edges, and 3 for the shortest edges.

When repeated bisection is performed on  $\mathbf{P}$ , the bisected edge  $e_B$  of a subtetrahedron is determined as follows. In the  $i$ th level of bisection, where  $i \equiv 1$  or  $3 \pmod{3}$ ,  $e_B$  is the unique edge with type 1 or 3, respectively. For example, at the first level,  $e_B = \mathbf{P}_1\mathbf{P}_2$  is the unique edge of  $\mathbf{P}$  with type 1, and at the third level  $e_B = \mathbf{p}_0\mathbf{p}_1$  is the unique edge of  $\mathbf{P}_1^2(\mathbf{p}_0, \mathbf{p}_1, \mathbf{p}_{12}, \mathbf{p}_{13})$  with type 3. In the  $i$ th level of bisection, where  $i \equiv 2 \pmod{3}$ ,  $e_B$  is the older of the two edges with type 2. For example, at the second level,  $e_B = \mathbf{P}_1\mathbf{P}_3$  and  $\mathbf{p}_0\mathbf{p}_{12}$  are the edges of  $\mathbf{P}_1^1(\mathbf{p}_0, \mathbf{p}_1, \mathbf{p}_{12}, \mathbf{p}_3)$  with type 2, and  $\mathbf{P}_1\mathbf{P}_3$  existed before  $\mathbf{p}_0\mathbf{p}_{12}$ .

The above description of repeated bisection of  $\mathbf{P}$  is equivalent to longest edge bisection in step (b) of TRANBIS, and it can be easily generalized for bisection of any tetrahedron. Let  $\mathbf{T}(\mathbf{t}_0, \mathbf{t}_1, \mathbf{t}_2, \mathbf{t}_3)$  be a tetrahedron with vertices  $\mathbf{t}_0, \mathbf{t}_1, \mathbf{t}_2, \mathbf{t}_3$ , with labels chosen so that  $\mathbf{p}_i$  is mapped to  $\mathbf{t}_i$ ,  $0 \leq i \leq 3$ , by an affine transformation. Suppose the bisected edge  $e_B$  of  $\mathbf{T}$  is  $\mathbf{t}_1\mathbf{t}_2$ . The initial set-up for the types of edges of  $\mathbf{T}$  can be set as follows. Set  $\tau(\mathbf{t}_1\mathbf{t}_2) = 1$ ,  $\tau(\mathbf{t}_1\mathbf{t}_3) = 2$ ,  $\tau(\mathbf{t}_2\mathbf{t}_3) = 2$ , and the types of the three longest edges to 3. The following

procedure BISECT1 describes one step of bisection on  $\mathbf{T}$  or one of its refined subtetrahedra  $\mathbf{S}$ .

```

Procedure BISECT1( $\mathbf{S}$ )
  if  $\mathbf{S}$  is the original tetrahedron  $\mathbf{T}$  then
    Set initial types of edges and  $e_B$  for  $\mathbf{T}$ 
    Mark all edges to be old
  endif
  Bisect  $\mathbf{S}$  using  $e_B$  and set types of new edges by rule NEWTYPE
  Mark new edges to be new
  if no old edges in a subtetrahedron then
    Mark all its edges to be old
  endif
  Set the bisected edge of each subtetrahedron to be the edge
  whose type is  $\tau(e_B) \bmod 3 + 1$  among the edges marked old

```

To ensure the validity of the above procedure, we need to prove that any configuration of a face, which is created by performing BISECT1 to an individual tetrahedron repeatedly, is in  $\mathcal{F}$ , and there is a unique bisected edge when a subtetrahedron is bisected. To do this, we need the lemma below. We say that two tetrahedra are *type similar* to each other if there is a one to one mapping in which all corresponding edges have the same types, and the bisected edges are mapped to each other.

**Lemma 4.1** *For any tetrahedron  $\mathbf{T}(t_0, t_1, t_2, t_3)$ , set  $e_B = t_1 t_2$ ,  $\tau(t_1 t_2) = 1$ ,  $\tau(t_1 t_3) = 2$ ,  $\tau(t_2 t_3) = 2$ , and the types of the three remaining edges to 3. Then after three levels of bisection by performing BISECT1 to  $\mathbf{T}$  and its subtetrahedra, all eight subtetrahedra of  $\mathbf{T}$  are type similar to  $\mathbf{T}$ .*

**Proof.** Note that  $\mathbf{T}$  is type similar to  $\mathbf{P}$  if  $t_i$  is mapped to  $p_i$ ,  $0 \leq i \leq 3$ . By the above discussion on the bisection of  $\mathbf{P}$ , the lemma is established.  $\square$

We can also verify that, in the first three levels of bisection, each subtetrahedron has a unique bisected edge, and the configuration of any face is in  $\mathcal{F}$ . By Lemma 4.1 and Theorem 3.1, these are also true to any level of bisection.

We now give the relationship between procedure TRANBIS and the procedure in which BISECT1 is iteratively performed to  $\mathbf{T}$  under the initial set-up given in Lemma 4.1.

**Theorem 4.1** *In procedure TRANBIS, let  $\mathbf{T}$  be transformed to  $\mathbf{P}$  such that  $t_i$  is mapped to  $p_i$ ,  $0 \leq i \leq 3$ . If  $\mathbf{T}$  and  $\mathbf{P}$  are bisected to the same level, then iterative bisection on  $\mathbf{T}$  by*

performing BISECT1 under the initial set-up given in Lemma 4.1 produces the same set of tetrahedra as TRANBIS does.

**Proof.** Since under affine transformation the midpoint of a line segment is still the midpoint of the corresponding line segment, this lemma can be verified in the first three levels of bisection. By Lemma 4.1, after three levels of bisection, in terms of the types of edges and the bisected edge, all eight subtetrahedra of  $\mathbf{T}$  are type similar to  $\mathbf{T}$ ; and all eight subtetrahedra of  $\mathbf{P}$  are geometrically similar (and also type similar) to  $\mathbf{P}$  by Theorem 3.1. Thus the theorem is established by induction.  $\square$

Note that BISECT1 does not need to be applied to all subtetrahedra of a tetrahedron as long as a conforming mesh can be guaranteed. We will use this freedom to design a local refinement algorithm producing meshes with varying element sizes in the next section.

### 4.3 Local refinement of a conforming mesh

The basic idea of local refinement of a conforming mesh  $\mathcal{T}$  is that, whenever a tetrahedron needs to be refined, we want to use BISECT1 because the shape of refined tetrahedra produced by repeatedly performing BISECT1 are bounded according to the discussion in Chapter 3. Simply performing BISECT1 to tetrahedra in  $\mathcal{T}$  may produce non-conforming edges. Therefore, for each tetrahedron in  $\mathcal{T}$ , we set up initial types of edges and its bisected edge such that a conforming mesh is ensured when BISECT1 is performed to each individual tetrahedron. To this end, we first classify tetrahedra in  $\mathcal{T}$ .

Let  $\mathcal{V} = \{v_1, v_2, \dots, v_n\}$  be a set of vertices of tetrahedra in  $\mathcal{T}$ . We say the label of edge  $v_i v_j$  is greater than the label of edge  $v_k v_l$  if  $\max(i, j) > \max(k, l)$  or  $\max(i, j) = \max(k, l)$  and  $\min(i, j) > \min(k, l)$ . For each face of  $\mathcal{T}$ , a *marked point* is defined to be the midpoint of its longest edge. If the longest edge of a face is unique, then the marked point associated with the face is uniquely determined; otherwise, the marked point is chosen to be the midpoint of the edge that has the largest label among the edges with maximum edge length. If two faces of a tetrahedron share the same marked point, the marked point is called a *doubly marked point* of the tetrahedron; otherwise, it is called a *singly marked point*. It is obvious that the midpoint of the longest edge (with largest label if there is a tie) of a tetrahedron must be a doubly marked point. Therefore, according to the number of marked points and their layouts, a tetrahedron  $\mathbf{T} \in \mathcal{T}$  can be classified into four different classes as follows.

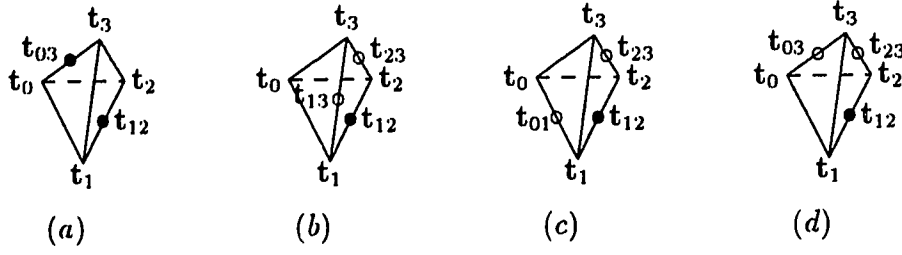


Figure 4.1: Four types of tetrahedra according to the number of marked points; (a) two doubly marked points on a pair of opposite edges; (b) three marked points on the same face; (c) three marked points, two singly marked points on a pair of opposite edges; (d) three marked points, one singly ( $t_{03}$ ) and one doubly marked point ( $t_{12}$ ) on a pair of opposite edges.

- DD: Tetrahedron  $\mathbf{T}$  has two doubly marked points on a pair of opposite edges, as illustrated in Figure 4.1a.
- DSS1: Tetrahedron  $\mathbf{T}$  has one doubly marked point and two singly marked points; all marked points are on the same face, as illustrated in Figure 4.1b.
- DSS2: Tetrahedron  $\mathbf{T}$  has one doubly marked point and two singly marked points; two singly marked points are on a pair of opposite edges, as illustrated in Figure 4.1c.
- DSS3: Tetrahedron  $\mathbf{T}$  has one doubly marked point and two singly marked points; one singly marked point and the doubly marked point are on a pair of opposite edges, as illustrated in Figure 4.1d.

Note that the tetrahedron  $\mathbf{T}$  discussed in the last section is assumed to be a tetrahedron of class DSS1. Since we want to extend BISECT1 to work for all classes of tetrahedra, we need the initial set-up for a tetrahedron of class DD, DSS2, or DSS3. The motivation for the initial set-up is as follows. We still use rule NEWTYPE for the types of new edges, and hope that refined subtetrahedra of a tetrahedron of class DD, DSS2, or DSS3 can be type similar to a tetrahedron of class DSS1 as soon as possible, since DSS1 is well studied. The initial set-up, which is specially designed, for a tetrahedron of class DD, DSS1, DSS2, or DSS3 is as follows.

- DD: Referring to Figure 4.1a, suppose  $t_1t_2$  is the longest edge. Set  $\tau(t_1t_2) = 3$ ,  $\tau(t_0t_3) = 1$ , and the types of remaining edges to 2. Set the bisected edge  $e_B$  to  $t_1t_2$ .

- DSS1: Referring to Figure 4.1b, set the type of the edge with doubly marked point to 1 ( $\tau(t_1t_2) = 1$ ), the types of two edges with singly marked point to 2 ( $\tau(t_1t_3) = 2$  and  $\tau(t_2t_3) = 2$ ), and the types of remaining edges to 3. Set the bisected edge  $e_B$  to  $t_1t_2$ .
- DSS2: Referring to Figure 4.1c, set the type of the edge with doubly marked point to 3 ( $\tau(t_1t_2) = 3$ ), the types of two edges with singly marked point to 1 ( $\tau(t_0t_1) = 1$  and  $\tau(t_2t_3) = 1$ ), and the types of remaining edges to 2. Set the bisected edge  $e_B$  to  $t_1t_2$ .
- DSS3: Referring to Figure 4.1d, set the type of the edge with doubly marked point to 3 ( $\tau(t_1t_2) = 3$ ), the types of two edges with singly marked point to 1 ( $\tau(t_0t_3) = 1$  and  $\tau(t_2t_3) = 1$ ), and the types of remaining edges to 2. Set the bisected edge  $e_B$  to  $t_1t_2$ .

Note that for a tetrahedron of class DSS3, after one step of bisection, there are two edges ( $t_0t_3$  and  $t_2t_3$ ) whose types are 1 in subtetrahedron  $T_1(t_0, t_{12}, t_2, t_3)$ . We change the type of edge  $t_0t_3$  to 2 in this subtetrahedron. So the configurations of face  $t_0t_{12}t_3$  are  $[3, 3, 2]$  and  $[3, 3, 1]$  in subtetrahedra  $T_1(t_0, t_{12}, t_2, t_3)$  and  $T_2(t_0, t_1, t_{12}, t_3)$ , respectively. This does not cause any conflict on face  $t_0t_{12}t_3$  because the midpoint of  $t_0t_3$  can be thought as the unique marked point on face  $t_0t_{12}t_3$ , and the marked point uniquely determines the bisection on a face. That is, the edge with marked point is bisected first; then other two edges are bisected if necessary. The last configuration  $[2, 2, 3]$  in  $\mathcal{F}$  (see (4.2.1)), e.g., face  $t_0t_1t_2$  in Figure 4.1a, is the only one that is not in the collection of face configurations in the first three levels of bisection on the canonical tetrahedron  $P$ .

In summary, for any tetrahedron  $T$  in the initial mesh  $\mathcal{T}$ , based on the above initial set-up and the rule NEWTYPE for types of new edges, iterative bisection of  $T$  is uniquely determined. The extension of BISECT1 for any tetrahedron of class DD, DSS1, DSS2, or DSS3 is as follows.

**Procedure BISECT2(S)**

```

if S is a tetrahedron in the original mesh  $\mathcal{T}$  then
  Classify S as DD, DSS1, DSS2, or DSS3
  Set initial types of edges and  $e_B$  for S according to its class
  Mark all edges to be old
endif
```

```

Bisect  $S$  using  $c_B$  and set types of new edges by rule NEWTYPE
Mark new edges to be new
if  $S$  is an original tetrahedron of class DSS3 in  $\mathcal{T}$  then
    Change the type of the edge opposite to the edge with doubly marked
    point to be 2 in the subtetrahedron with two edges of type 1
endif
if no old edges in a subtetrahedron then
    Mark all its edges to be old
endif
Set the bisected edge of each subtetrahedron to be the edge
whose type is  $\tau(\cdot) \bmod 3 + 1$  among the edges marked old

```

The validity of BISECT2 is guaranteed by Lemma 4.1 and the following lemma.

**Lemma 4.2** *If  $T$  is a tetrahedron of class DD, DSS2, or DSS3, after one level of bisection by performing BISECT2 to  $T$ , each subtetrahedron of  $T$  is type similar to a tetrahedron of class DSS1.*

**Proof.** We first suppose that  $T$  is a tetrahedron of class DD. Referring to Figure 4.1a, after one level of bisection by procedure BISECT2, according to rule NEWTYPE,  $T$  is bisected into two subtetrahedra having the same configuration as a tetrahedron of class DSS1 in terms of the types of edges and the bisected edge, e.g., in subtetrahedron  $T(t_0, t_1, t_{12}, t_3)$ ,  $\tau(t_0 t_3) = 1$ ,  $\tau(t_0 t_1) = 2$ ,  $\tau(t_1 t_3) = 2$ , the types of remaining edges are 3, and the bisected edge  $c_B$  is  $t_0 t_3$ . So  $T(t_0, t_1, t_{12}, t_3)$  is type similar to a tetrahedron of class DSS1. Similarly, the result can also be verified for a tetrahedron of class DSS2 or DSS3.  $\square$

By Lemmas 4.1 and 4.2, the configuration of any face created by applying BISECT2 to  $T$  and its subtetrahedra is in  $\mathcal{F}$ , and bisected edges can be uniquely determined during the bisection.

To explain BISECT2 further, suppose  $T$  is a tetrahedron of class DSS1 in the original mesh. Looking at the first three levels of bisection by performing BISECT2 to  $T$  and its subtetrahedra, we notice that the longest edge of  $T$  is bisected in the first bisection; in each of the two subtetrahedra of  $T$ , the bisected edge is chosen to be the longest edge among the edges of  $T$ ; in the third bisection, the three remaining edges of  $T$  are bisected. We do not want any edge of  $T$  to be bisected more than once in three levels of bisection, and at the same time try to bisect longer edges as soon as possible (at least in the first three levels of bisection). An intuitive idea is that if the first three levels of bisection do not generate



very poorly-shaped tetrahedra, then we keep the same order of bisection (this is carried out by “type similar”). Hopefully, there are no arbitrarily poor tetrahedra generated while the bisection procedure goes on.

So far, we have described how to set up initial types of edges and the bisected edge, and how to repeatedly bisect a tetrahedron of class DD, DSS1, DSS2, or DSS3. A local refinement algorithm, called QLRB (quality local refinement based on bisection), is presented here. A more detailed pseudocode is provided after we discuss the data structure in a later section.

### Algorithm QLRB

- (1) Set  $\mathcal{T}^0 := \mathcal{T}$ ,  $m := 0$ .
- (2) Select a set  $S_m$  of tetrahedra needed to be refined from  $\mathcal{T}^m$ ; perform procedure BISECT2 to each tetrahedron of  $S_m$ . The refined mesh is labeled  $\overline{\mathcal{T}}^{m+1}$ .
- (3) If  $\overline{\mathcal{T}}^{m+1}$  is non-conforming, i.e., there exist non-conforming edges, then perform procedure BISECT2 to any tetrahedron with non-conforming edges; repeat this process until there is no non-conforming edge. The conforming refined mesh is labeled  $\mathcal{T}^{m+1}$ .
- (4)  $m := m + 1$ ; go to (2) if necessary or terminate.

The superscript  $m$  of  $\mathcal{T}^m$  indicates that mesh  $\mathcal{T}^m$  is created after  $m$  levels of refinement on  $\mathcal{T}^0$ . Note that in step (3), the order of processing non-conforming edges does not affect the final conforming mesh because the order of repeated bisection of a tetrahedron in  $\mathcal{T}^0$  is uniquely determined by the class of the tetrahedron. That is, the bisection of a tetrahedron, which may be incident on more than one non-conforming edge, is determined by its bisected edge no matter which non-conforming edge is processed first. If a tetrahedron  $\mathbf{T}$  has a non-conforming edge  $e$ , it is not necessary that the bisected edge  $e_B$  of  $\mathbf{T}$  is  $e$ .  $\mathbf{T}$  is bisected according to  $e_B$  rather than  $e$ . For instance, if  $\mathbf{T}$  is the case in Figure 4.1b, current bisected edge  $e_B = t_1t_2$ , and  $e$  is  $t_0t_1$ , then  $e$  will be bisected after two levels of bisection on  $\mathbf{T}$ . So, in step (3), bisecting a tetrahedron with non-conforming edges may introduce more non-conforming edges. In the initial mesh  $\mathcal{T}$ , each face has a unique marked point. The edge with marked point will be bisected first when the face is bisected, the other two edges of the face will be bisected edges when the two subfaces are bisected. Thus the marked point associated with a face uniquely determines the bisected edges of the face and its

subsequent subfaces, and the interior of two distinct subfaces do not intersect. Therefore edge conformity is sufficient to guarantee the conformity of the refined mesh.

Obviously, we need to prove that step (3) will terminate after a finite number of conforming checks. To do this, we need Lemma 4.3 below. The *bisection level* of a subtetrahedron of  $\mathbf{T}$  is defined to be the number of times that BISECT2 is performed to  $\mathbf{T}$  to obtain this subtetrahedron.

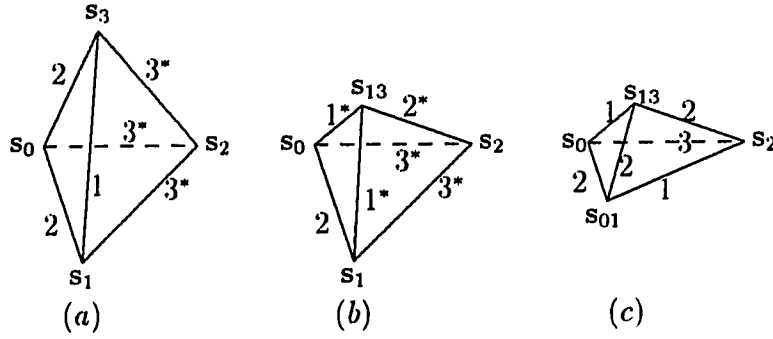


Figure 4.2: Tetrahedra produced by 1 to 3 levels of bisection of a tetrahedron of class DD, DSS2, or DSS3. (a) After 1 level. (b) After 2 levels. (c) After 3 levels; the tetrahedron is type similar to a tetrahedron of class DSS2.

**Lemma 4.3** *If every tetrahedron in  $\mathcal{T}^0$  is bisected to level  $3r$ ,  $r > 0$ , for some  $r$ , then the refined mesh is conforming.*

**Proof.** From Lemma 4.1, after three levels of bisection on a tetrahedron of class DSS1, all its edges are bisected, and the subtetrahedra are type similar to a tetrahedron of class DSS1. By a straightforward verification, after one level of bisection on a tetrahedron of class DD, DSS2, or DSS3, the two subtetrahedra have the same configuration as in Figure 4.2a, where the numbers stand for types of edges, and a star superscript denotes an edge marked *new* in BISECT2. One level of bisection on a tetrahedron with configuration shown in Figure 4.2a produces two subtetrahedra with the same configuration as shown in Figure 4.2b. Likewise, the tetrahedron in Figure 4.2c, which is type similar to a tetrahedron of class DSS2, is obtained by one level of bisection on the tetrahedron shown in Figure 4.2b. Therefore, after three levels of bisection on a tetrahedron of class DD, DSS2, or DSS3, all its edges are bisected, and all subtetrahedra are type similar to a tetrahedron of class DSS2. It is obvious that the mesh at level 3 is conforming since all original edges are bisected exactly once and no new edges are bisected. By induction, the lemma is established.  $\square$

**Theorem 4.2** *Step (3) in QLRB will terminate in a finite number of conforming checks, and the bisection level of any refined tetrahedron in mesh  $T^m$  is at most  $3m$ ,  $m \geq 0$ , where  $m$  is the number of refinements on  $T^0$ .*

**Proof.** We prove the theorem by induction. The theorem is obvious for the basis step  $m = 0$ . Suppose the theorem is true for  $m = k, k \geq 0$ , i.e., in  $T^k$ , the bisection level of any refined tetrahedron is  $\leq 3k$ . After step (2) in QLRB, let  $r$  be the maximum number of bisection levels in  $\bar{T}^{k+1}$ . Then  $r \leq 3k + 1$ . Therefore, step (3) in QLRB will terminate in the worst case that all tetrahedra in  $\bar{T}^{k+1}$  are bisected to level  $3(k + 1)$ , since any edge of a tetrahedron with bisection level  $3(k + 1)$  can only be bisected as a bisected edge of some tetrahedron with bisection level no less than  $3(k + 1)$  by Lemma 4.3. By induction, the theorem is established.  $\square$

In our experiments, instead of the worst case behavior, the conforming step in general converges much faster.

## 4.4 Properties of meshes generated by QLRB

We establish some theoretical results on the quality of meshes produced by QLRB in this section.

**Theorem 4.3** *For any initial mesh  $T$ , there are only a finite number, which depends on the number of tetrahedra in  $T$ , of classes of similar tetrahedra in all refined tetrahedra generated by QLRB.*

**Proof.** By Lemma 4.2, it suffices to prove that each tetrahedron  $T$  of class DSS1 produces only a finite number of classes of similar tetrahedra. Note that in QLRB, repeated use of BISECT2 to  $T$  is actually a modified version of TRANBIS (not all subtetrahedra are bisected to the same level), since Theorem 4.1 demonstrates that any subtetrahedron produced by iteratively performing BISECT2 (BISECT2( $S$ ) is the same as BISECT1( $S$ ) when  $S$  is a tetrahedron of class DSS1) to  $T$  must also be a subtetrahedron created by performing TRANBIS to  $T$  if  $T$  is transformed to  $P$  such that the edge with doubly marked point in  $T$  corresponds to the longest edge of  $P$  and the edges with singly marked points in  $T$  correspond to the second longest edges of  $P$  (see Figure 4.1b). Therefore, by Theorem 3.3 in Chapter 3, which states that there are a finite number of classes of similar tetrahedra in all refined tetrahedra produced by TRANBIS, the theorem is established.  $\square$

The above theorem implies that the shape of refined tetrahedra do not decrease arbitrarily with the process of refinement. Theorem 4.4 below, which needs Lemma 4.4, provides a more detailed analysis in terms of the tetrahedron shape measure  $\eta$ . Recall the formula for computing  $\eta$  (i.e. Eqn. (2.4.1)),

$$\eta(\mathbf{T}) = 12(3v)^{2/3} / \sum_{0 \leq i < j \leq 3} l_{ij}^2, \quad (4.4.1)$$

where  $v$  is the volume of  $\mathbf{T}$  and the  $l_{ij}$  are the lengths of the edges of  $\mathbf{T}$ .

**Lemma 4.4** *If  $\mathbf{T}$  is a tetrahedron of class DD, DSS2, or DSS3, and  $\mathbf{T}_i$ ,  $i = 1, 2$ , are subtetrahedra produced by performing BISECT2 to  $\mathbf{T}$ , then*

$$\eta(\mathbf{T}_i) \geq 6\sqrt[3]{2}/11 \eta(\mathbf{T}), \quad i = 1, 2; \quad (4.4.2)$$

*and the lower bound is tight.*

**Proof.** Let  $\mathbf{T}$  be a tetrahedron of class DD, DSS2, or DSS3 as shown in Figure 4.1a, 4.1c, or 4.1d, respectively. Suppose  $\mathbf{t}_1\mathbf{t}_2$  is the bisected edge, which is the edge with maximum length. Label the two subtetrahedra by  $\mathbf{T}_1(\mathbf{t}_0, \mathbf{t}_1, \mathbf{t}_{12}, \mathbf{t}_3)$  and  $\mathbf{T}_2(\mathbf{t}_0, \mathbf{t}_{12}, \mathbf{t}_2, \mathbf{t}_3)$  after performing BISECT2 to  $\mathbf{T}$ , and let  $|\mathbf{t}_i\mathbf{t}_j| = l_{ij}$ ,  $i < j$ . By simple algebraic manipulation,  $|\mathbf{t}_0\mathbf{t}_{12}|^2 = (2l_{01}^2 + 2l_{02}^2 - l_{12}^2)/4$  and  $|\mathbf{t}_3\mathbf{t}_{12}|^2 = (2l_{13}^2 + 2l_{23}^2 - l_{12}^2)/4$ , so  $|\mathbf{t}_0\mathbf{t}_{12}|^2 + |\mathbf{t}_3\mathbf{t}_{12}|^2 = (l_{01}^2 + l_{02}^2 + l_{13}^2 + l_{23}^2 - l_{12}^2)/2$ . By (4.4.1) and the fact that the volume of  $\mathbf{T}_1$  is a half of the volume of  $\mathbf{T}$ , we obtain

$$\eta(\mathbf{T}_1)/\eta(\mathbf{T}) = (4/\sqrt[3]{4}) \times \frac{\sum_{0 \leq i < j \leq 3} l_{ij}^2}{6l_{01}^2 + 6l_{13}^2 + 4l_{03}^2 + 2l_{02}^2 + 2l_{23}^2 - l_{12}^2}.$$

Since  $l_{03}^2 \leq 2(l_{02}^2 + l_{23}^2)$  and  $l_{12}$  is the maximum edge length, it follows that

$$6l_{01}^2 + 6l_{13}^2 + 4l_{03}^2 + 2l_{02}^2 + 2l_{23}^2 - l_{12}^2 \leq 10(l_{03}^2 + l_{02}^2 + l_{23}^2)/3 + 5l_{01}^2 + 6l_{13}^2 \leq 11 \sum_{0 \leq i < j \leq 3} l_{ij}^2/3,$$

where the last inequality is due to  $5l_{01}^2 + 6l_{13}^2 \leq 11(l_{01}^2 + l_{12}^2 + l_{13}^2)/3$ . Thus  $\eta(\mathbf{T}_1)/\eta(\mathbf{T}) \geq 6\sqrt[3]{2}/11$ . Similarly, we have  $\eta(\mathbf{T}_2)/\eta(\mathbf{T}) \geq 6\sqrt[3]{2}/11$ .

The lower bound is tight for a tetrahedron of class DSS2. In Figure 4.1c, let  $|\mathbf{t}_0\mathbf{t}_2| = |\mathbf{t}_0\mathbf{t}_3| = |\mathbf{t}_2\mathbf{t}_3| \rightarrow 0$ , and  $|\mathbf{t}_0\mathbf{t}_1| = |\mathbf{t}_1\mathbf{t}_2| = |\mathbf{t}_1\mathbf{t}_3|$ . Then  $\eta(\mathbf{T}_1)/\eta(\mathbf{T}) \rightarrow 6\sqrt[3]{2}/11$ .  $\square$

**Theorem 4.4** *If  $\mathbf{T}_i^n$  is a refined tetrahedron of a tetrahedron  $\mathbf{T}$  of class DD, DSS1, DSS2, or DSS3, generated by QL RB, then*

$$\eta(\mathbf{T}_i^n) \geq c \eta(\mathbf{T}), \quad (4.4.3)$$

where  $c = 3(9 - \sqrt{17})(2 - \sqrt{2})/88 \approx 0.0974$ .

**Proof.** From Theorem 4.1 and the initial set-up for any tetrahedron  $\hat{\mathbf{T}}$  which is type similar to a tetrahedron of class DSS1, iteratively performing BISECT2 to  $\hat{\mathbf{T}}$  and TRANBIS to  $\hat{\mathbf{T}}$  produce the same set of subtetrahedra. Section 3.4 shows that for any refined subtetrahedron  $\hat{\mathbf{T}}_i^n$  of  $\hat{\mathbf{T}}$ , produced by TRANBIS,

$$\eta(\hat{\mathbf{T}}_i^n) \geq \sqrt[3]{4}(9 - \sqrt{17})(2 - \sqrt{2})/32 \eta(\hat{\mathbf{T}}). \quad (4.4.4)$$

If  $\mathbf{T}$  is a tetrahedron of class DSS1, then (4.4.4) holds with  $\hat{\mathbf{T}} = \mathbf{T}$  and  $\hat{\mathbf{T}}_i^n = \mathbf{T}_i^n$ . Suppose  $\mathbf{T}$  is a tetrahedron of class DD, DSS2, or DSS3, and  $\mathbf{T}_1$  is any subtetrahedron produced by performing BISECT2 to  $\mathbf{T}$ . Then from inequality (4.4.2), it follows that

$$\eta(\mathbf{T}_1) \geq 6\sqrt[3]{2}/11\eta(\mathbf{T}). \quad (4.4.5)$$

By Lemma 4.2,  $\mathbf{T}_1$  is type similar to a tetrahedron of class DSS1. Hence, combining (4.4.4), with  $\hat{\mathbf{T}} = \mathbf{T}_1$  and  $\hat{\mathbf{T}}_i^n = \mathbf{T}_i^n$ , and (4.4.5) yields

$$\eta(\mathbf{T}_i^n) \geq \sqrt[3]{4}(9 - \sqrt{17})(2 - \sqrt{2})/32 \eta(\mathbf{T}_1) \geq 3(9 - \sqrt{17})(2 - \sqrt{2})/88 \eta(\mathbf{T}). \quad (4.4.6)$$

Combining (4.4.4), with  $\hat{\mathbf{T}} = \mathbf{T}$  and  $\hat{\mathbf{T}}_i^n = \mathbf{T}_i^n$ , and (4.4.6), the theorem is established.  $\square$

For any interior face  $F$ , let  $\delta(F)$  denote the absolute value of the difference of the bisection levels of the two adjacent tetrahedra incident on  $F$ .

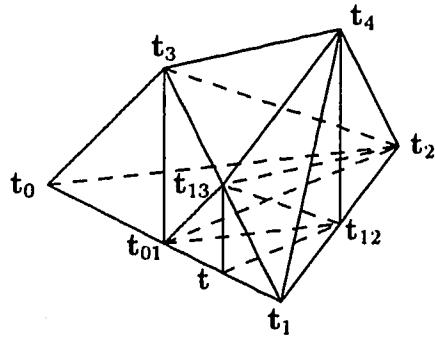


Figure 4.3: Illustration for the proof of Theorem 4.5;  $t_{ij} = (t_i + t_j)/2$ ,  $i < j$ ;  $t = (t_{01} + t_1)/2$ .

**Theorem 4.5** *For any interior face  $F$  in  $\mathcal{T}^m$ ,  $m > 0$ , generated by QLRB,  $\delta(F) \leq 2$ , and the upper bound is tight.*

**Proof.** Note that any face of a tetrahedron will be bisected after two levels of bisection on this tetrahedron (this observation will be used below). Suppose  $F$  is an interior face in a

conforming mesh  $\mathcal{T}^m$ ,  $m \geq 0$ . Let  $\mathbf{T}_1^p$  and  $\mathbf{T}_2^q$  be two adjacent tetrahedra sharing face  $F$  with bisection levels  $p$  and  $q$ ,  $p \geq q \geq 0$ , respectively. We shall prove by contradiction that  $\delta(F) = p - q \leq 2$ .

Suppose there exists an interior face  $F$  such that  $\delta(F) = r = p - q \geq 3$ . We have the following three cases.

Case 1:  $p = q + r = 3k$  for some integer  $k \geq 1$ . Suppose  $r \geq 3$  levels of bisection are performed on  $\mathbf{T}_2^q$ , which has bisection level  $q = 3k - r$ . Then  $F$  is bisected as a face of  $\mathbf{T}_2^q$ . But  $F$  is a face of  $\mathbf{T}_1^p$  with bisection level  $p = 3k$ . So,  $F$  is not a conforming face at level  $3k$  (all other tetrahedra not sharing  $F$  can be further bisected to level  $3k$  or have bisections “undone” to level  $3k$  without changing the non-conformity of  $F$ ), a contradiction of Lemma 4.3.

Case 2:  $p = q + r = 3k + 1$  for some integer  $k \geq 1$ . Let  $\mathbf{T}^{p-1}$  be the direct parent of  $\mathbf{T}_1^p$ . Then  $F$  is either a face or part of a face of  $\mathbf{T}^{p-1}$  with bisection level  $p - 1 = 3k$ . Suppose  $r - 1 \geq 2$  levels of bisection are performed on  $\mathbf{T}_2^q$ , which has bisection level  $q = 3k - (r - 1)$ . Then  $F$  is bisected as a face of  $\mathbf{T}_2^q$ . Again, this is a contradiction of Lemma 4.3.

Case 3:  $p = q + r = 3k + 2$  for some integer  $k \geq 1$ . Let  $\mathbf{T}^{p+1}$  be a subtetrahedron obtained by one level of bisection on  $\mathbf{T}_1^p$  such that either  $F$  or a direct subface of  $F$  is a face of  $\mathbf{T}^{p+1}$ . Then  $\mathbf{T}^{p+1}$  has bisection level  $p + 1 = 3(k + 1)$ . Suppose  $r + 1 \geq 4$  levels of bisection are performed on  $\mathbf{T}_2^q$ , which has bisection level  $q = 3(k + 1) - (r + 1)$ . Then  $F$  is bisected more than once as a face of  $\mathbf{T}_2^q$ . So, either  $F$  or a subface of  $F$  is not conforming at level  $3(k + 1)$ , a contradiction of Lemma 4.3.

Now we prove that the upper bound is tight. Suppose two tetrahedra  $\mathbf{T}(t_0, t_1, t_2, t_3)$  and  $\hat{\mathbf{T}}(t_1, t_2, t_3, t_4)$  share a common face  $t_1 t_2 t_3$  shown in Figure 4.3, and both are tetrahedra of class DSS1. In  $\mathbf{T}(t_0, t_1, t_2, t_3)$ , suppose  $e_B = t_0 t_1$ ,  $\tau(t_0 t_1) = 1$ ,  $\tau(t_0 t_3) = 2$ ,  $\tau(t_1 t_3) = 2$ , and the types of remaining edges are 3. In  $\hat{\mathbf{T}}(t_1, t_2, t_3, t_4)$ , suppose  $e_B = t_1 t_3$ ,  $\tau(t_1 t_3) = 1$ ,  $\tau(t_1 t_2) = 2$ ,  $\tau(t_2 t_3) = 2$ , and the types of remaining edges are 3. Tetrahedron  $\mathbf{T}_1^1(t, t_1, t_{12}, t_{13})$  is produced by bisections of  $\mathbf{T}(t_0, t_1, t_2, t_3)$ ,  $\mathbf{T}_1^1(t_{01}, t_1, t_2, t_3)$ ,  $\mathbf{T}_1^2(t_{01}, t_1, t_2, t_{13})$ , and  $\mathbf{T}_1^3(t_{01}, t_1, t_{12}, t_{13})$ , respectively. Tetrahedron  $\hat{\mathbf{T}}_1^1(t_1, t_{12}, t_{13}, t_4)$  is produced by bisections of  $\hat{\mathbf{T}}(t_1, t_2, t_3, t_4)$  and  $\hat{\mathbf{T}}_1^1(t_1, t_2, t_{13}, t_4)$ , respectively. Therefore, for face  $F = t_1 t_{12} t_{13}$ ,  $\delta(F) = 4 - 2 = 2$ .  $\square$

It is worth mentioning that Theorem 4.5 may not hold for longest edge bisection. In our experiments, only a few faces generated by QLRB achieve the upper bound of 2.

Using a similar technique and the fact that any edge of a tetrahedron will be bisected after 4 levels of bisection on this tetrahedron, we can prove the following theorem, where  $\delta(e)$  denotes the absolute value of the difference of the maximum and minimum bisection levels of all tetrahedra incident on edge  $e$ .

**Theorem 4.6** *For any edge  $e$  in  $T^m$ ,  $m > 0$ , generated by QLRB,  $\delta(e) \leq 4$ , and the upper bound is tight.*

## 4.5 Data structure and algorithmic details

Generally, refined tetrahedra are only a small part of an existing mesh. An ideal local refinement algorithm should have a time complexity that is linearly related to the number of refined tetrahedra in a refined mesh. To reach this goal, the implementation of step (3) in QLRB is essential. We detail data structures, algorithm, and implementation in this section.

Let  $T^0, T^1, \dots, T^k$  be a sequence of conforming tetrahedral meshes produced by QLRB, where  $T^0$  is an initial mesh, and  $T^i$  is produced by refining a set of tetrahedra  $S_{i-1}$  in  $T^{i-1}$ ,  $1 \leq i \leq k$ . We first describe some data structures for QLRB.

The vertex coordinates are stored in an array  $VC$  where  $VC[i].x$ ,  $VC[i].y$ , and  $VC[i].z$  are the coordinates of the  $i$ th vertex. An array  $TM$  is used to store a tetrahedral mesh, where  $TM[i]$  records information about the  $i$ th tetrahedron. The fields of  $TM[i]$  are  $v_1, v_2, v_3, v_4, t_1, t_2, t_3, t_4, bi, flag$ , where  $0 < v_1 < v_2 < v_3 < v_4$  are the four vertex indices of the  $i$ th tetrahedron;  $t_1, t_2, t_3, t_4$  are the indices of the four adjacent tetrahedra in  $TM$  if the mesh is conforming (some  $t_i$  may be zero for boundary faces);  $bi$  is zero if the tetrahedron is not bisected, otherwise it is an index of another array  $BI$  (bisection information) which contains all necessary information for the bisection of this tetrahedron; and  $flag$  is a boolean variable, which is initialized to *false*, for temporary use. If the  $i$ th tetrahedron is bisected, the fields of  $BI[TM[i].bi]$  are  $et_1, et_2, et_3, et_4, et_5, et_6, e_b, nref, p, t_1, t_2, t_3, t_4$ , where  $et_1, et_2, et_3, et_4, et_5, et_6$  are the types of the six edges of the tetrahedron;  $e_b$  points to the bisected edge;  $nref$  is an integer indicating the refinement step in which the  $i$ th tetrahe-

dron is refined;  $p$  stores the index of the parent tetrahedron of the  $i$ th tetrahedron. Since a non-conforming mesh may be temporarily produced, whenever  $TM[i].t_k, 1 \leq k \leq 4$ , is negative, it indicates that the corresponding face of the  $i$ th tetrahedron has two neighbor tetrahedra (our algorithm below produces at most two neighbors for each face of a tetrahedron); one has index  $-TM[i].t_k$ , and the other  $BI[TM[i].bi].t_k$ . A new tetrahedron or vertex is added at the end of  $TM$  or  $VC$ . Two integer arrays  $XTM$  and  $XVC$  are used to store the first indices of new tetrahedra and vertices created during the stage of refinement to get mesh  $T^i$ . That is, original or new tetrahedra are stored in  $TM$  from index  $XTM[i]$  to  $XTM[i+1]-1$ ; original or new vertices are stored in  $VC$  from index  $XVC[i]$  to  $XVC[i+1]-1$ .  $TM$ ,  $VC$ ,  $BI$ ,  $XTM$ , and  $XVC$  are the basic data structures for refinement/derefinement algorithms, where derefinement is an inverse process of refinement. Our data structure keeps all necessary information for derefinement, which will be briefly discussed in Chapter 7.

To implement the refinement algorithm, we need some temporary data structures. New vertices will be added at the midpoints of all bisected edges at each step of refinement, and may be used by several tetrahedra. We use a hash table  $EHT$  to store all bisected edges. Suppose a new vertex  $v_m$ , the midpoint of  $v_a$  and  $v_b$  where  $a$  and  $b$  are the vertex indices in  $VC$ , is added. Then  $v_m$  is stored in  $VC$ , and at the same time  $a, b, m$  are stored in  $EHT$  with direct chaining, where  $EHT[i]$  is the head pointer of the linked list of edges with hashing function value  $i$ . A satisfactory hashing function is  $h(a, b) = (an + b) \bmod M$  ( $a < b$ ) where the hash table size,  $M$ , is a prime number, and  $n$  is the number of vertices in the last conforming mesh. The linked lists are organized in an increasing order according to tuples  $(a, b)$ .

Two temporary stacks  $S_e$  and  $S_t$  are used to store non-conforming edges and bisected tetrahedra, respectively. Whenever a tetrahedron is bisected, one non-conforming edge  $e_B$  is produced. Therefore all tetrahedra incident on  $e_B$  have to be bisected. Since the bisected edges of these tetrahedra may not be  $e_B$ , more non-conforming edges may be introduced.  $S_e$  is used to store these non-conforming edges (each non-conforming edge  $e$  in  $S_e$  is associated with a tetrahedron incident on  $e$ ). A duplicate element is avoided by checking if the element is in  $EHT$ . Stack  $S_t$  is used to store tetrahedra to be bisected in this step of refinement. A duplicate element is avoided by checking field *flag* of  $TM[i]$ . If *flag* is *false*, which means that the tetrahedron is not in  $S_t$ , then the tetrahedron is added to  $S_t$ , and *flag* is set *true*.



To set fields  $t_1, t_2, t_3, t_4$  of  $TM[i]$  or  $BI[TM[i].bi]$  after the bisection of tetrahedra in  $S_t$ , we use a temporary hash table  $FHT$  with direct chaining to store the faces of the new tetrahedra produced, where  $FHT[i]$  is the head pointer of a linked list of faces with hashing function value  $i$ . The neighbor information is set up by scanning the faces of new tetrahedra. Let  $v_a v_b v_c$  be a face,  $a < b < c$ , where  $a, b, c$  are the indices of  $v_a, v_b$ , and  $v_c$ . A satisfactory hashing function is  $h_1(a, b, c) = (an^2 + bn + c) \bmod M_1$ , where  $M_1$  is a prime number, and  $n$  is the number of vertices in the last conforming mesh. We say the label of face  $v_a v_b v_c$ ,  $a < b < c$ , is greater than the label of face  $v_d v_e v_f$ ,  $d < e < f$ , if  $c > f$ , or  $c = f, b > e$ , or  $c = f, b = e, a > d$ . The fields of an element of the linked list are  $a, b, c, t, flink$ , where  $a, b, c$  are three vertex indices of a face;  $t$  is an index of a tetrahedron sharing the face;  $flink$  is used to link to the next element. The linked lists are organized in an increasing order in terms of the labels of faces.

With the above data structures, we implement steps (2) and (3) of QLRB by a more sophisticated means. Instead of bisecting  $T$  whenever we find that  $T$  has a non-conforming edge, we first determine the possible configuration of  $T$  resulting from step (3), and then perform actual bisection to  $T$  or its subtetrahedra. The following procedure PREBISECT is used to determine the configurations of tetrahedra bisected. We use negative values in the fields  $et_1, et_2, et_3, et_4, et_5, et_6$  of  $BI[TM[i].bi]$  of the  $i$ th tetrahedron to indicate that the corresponding edges need bisection.

```

Procedure PREBISECT(conform,  $L$ ,  $S_t$ )
#Input: Boolean variable conform indicating whether PREBISECT is
#       performed on a conforming or non-conforming mesh (see procedure
#       REFIN below); list  $L$  of records ( $e, T$ ),
#       where  $e$  is an edge of  $T$  and needs to be bisected
#Output: stack  $S_t$  of tetrahedra to be bisected
  Set stacks  $S_e, S_t$  to be empty
  for each record ( $e, T$ ) of  $L$  do
    if conform then
      if  $e$  is not in  $EHT$  then
        Insert  $e$  into  $EHT$  and push ( $e, T$ ) onto  $S_e$ 
      endif
    else
      Push ( $e, T$ ) onto  $S_e$ 
    endif
     $i := \text{index of } T \text{ in } TM$ 
    if not  $TM[i].flag$  then

```

```

    Push  $\mathbf{T}$  onto  $S_i$  and set  $TM[i].flag$  to true
  endif
endfor
while  $S_e$  is not empty do
  Pop  $(e, \mathbf{T})$  from the top of  $S_e$ 
  for each tetrahedron  $\bar{\mathbf{T}}$  incident on  $e$  do
     $i := \text{index of } \bar{\mathbf{T}} \text{ in } TM$ 
    if not  $TM[i].flag$  then
      Push  $\bar{\mathbf{T}}$  onto  $S_i$  and set  $TM[i].flag$  to true
      Set the bisection information of  $\bar{\mathbf{T}}$  in a  $BI$  record if  $TM[i].bi = 0$ 
    endif
    Negate the type of  $e$  in its  $BI[TM[i].bi]$  field
    if  $e$  is not the bisected edge of  $\bar{\mathbf{T}}$  then
      for any edge  $e_1$ , which has positive type in corresponding  $BI[TM[i].bi]$ 
        and needs to be bisected before  $e$  is bisected, do
          if  $e_1$  is not in  $EHT$  then
            Insert  $e_1$  into  $EHT$  and push  $(e_1, \bar{\mathbf{T}})$  onto  $S_e$ 
          endif
        endfor
      endif
    endfor
  endfor
endwhile

```

Note that procedure PREBISECT only negates some fields of a  $BI$  record to indicate that the corresponding edges need to be bisected. It is worth mentioning that bisecting each tetrahedron in  $S_i$  until all its edges with negative values in  $BI$  are bisected does not necessarily produce a conforming mesh. That is because some new edges, produced during the bisection of a tetrahedron, have to be bisected in order to bisect some original edges of the tetrahedron. For instance, suppose  $\mathbf{T}$ , shown in Figure 4.4a, is a tetrahedron, obtained by bisection of a tetrahedron of class DSS1, in a conforming mesh before a refinement step, where the numbers stand for types of edges, and a star superscript denotes an edge marked *new* in BISECT2. The bisected edge of  $\mathbf{T}$  is  $t_1t_3$ . If  $t_0t_{12}$  needs to be bisected for conformity (e.g., one of the tetrahedra, not  $\mathbf{T}$ , incident on  $t_0t_{12}$  is bisected using  $t_0t_{12}$  as the bisected edge), then  $\mathbf{T}$  is bisected as the following sequence subject to rule NEWTYPE for the types of edges. First,  $\mathbf{T}$  is bisected by edge  $t_1t_3$ ; one of the resulting subtetrahedra is  $\mathbf{T}_1(t_0, t_1, t_{12}, t_{13})$  shown in Figure 4.4b. Next,  $\mathbf{T}_1$  is bisected by edge  $t_0t_1$ ; one of the resulting subtetrahedra is  $\mathbf{T}_2(t_0, t_{01}, t_{12}, t_{13})$  shown in Figure 4.4c. In order to bisect  $t_0t_{12}$ , edge  $t_0t_{13}$ , which is a new edge produced when  $\mathbf{T}$  is bisected, must be bisected first; then

$t_0t_{12}$  can be bisected. Therefore, to bisect all edges with negative type, a tetrahedron in  $S_t$  may be bisected up to four levels (by analyzing all cases, it is easily seen that five levels are never needed, and the number of subtetrahedra produced by 1 to 4 levels of bisection of a tetrahedron in  $S_t$  is 2 to 10), and one new edge, e.g.,  $t_0t_{13}$ , may be a new non-conforming edge after the bisection.

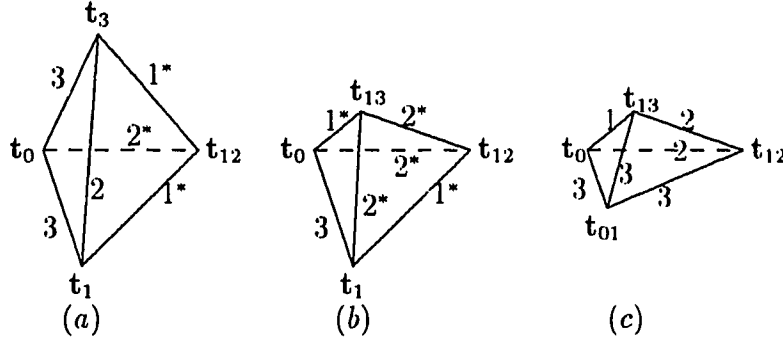


Figure 4.4: Tetrahedra produced by 1 to 3 levels of bisection of a tetrahedron of class DSS1. (a) After 1 level. (b) After 2 levels. (c) After 3 levels; the tetrahedron is type similar to a tetrahedron of class DSS1.

Tetrahedra needing further bisection (because of the bisection of some new edges) can be found when we fill in the neighbor information. By scanning faces of new tetrahedra (all subtetrahedra of tetrahedra in  $S_t$ ), if a face is not in  $FHT$ , insert the face into  $FHT$ ; otherwise, fill in its neighbor information, and delete the face from  $FHT$ . After the above process, all remaining faces in  $FHT$  are either boundary faces (in terms of new tetrahedra) or non-conforming faces (either being a part of another face or including another face). By checking whether a face includes a non-conforming edge (the non-conforming edge must be in  $EHT$ , since every edge bisected is inserted into  $EHT$ ), we can fill in the neighbor information for non-conforming faces, and find the set of non-conforming edges, which have been bisected in some but not all of its incident tetrahedra, as well as a tetrahedron associated with and incident on each non-conforming edge.

We now give the following pseudocode for QLRB.

**Algorithm QLRB**

```
# Input: initial conforming mesh  $\mathcal{T}$ 
# Output: refined conforming mesh  $\mathcal{T}$ 
 $m := 1$ 
repeat
```

```

Choose a set  $S_m$  of tetrahedra from  $\mathcal{T}$ 
Set list  $L$  to be empty
for each  $\mathbf{T}$  in  $S_m$  do
    Set the bisection information of  $\mathbf{T}$  in a  $BI$  record
    Add  $(e_B, \mathbf{T})$  to  $L$  where  $e_B$  is the bisected edge of  $\mathbf{T}$ 
endfor
REFINE( $\mathcal{T}, L, m$ )
 $m := m + 1$ 
until no more tetrahedra needed to be refined

Procedure REFINE( $\mathcal{T}, L, m$ )
# Input: conforming mesh  $\mathcal{T}$ ; list  $L$  of edges, which need to be bisected,
#       and tetrahedra associated with these edges;  $m$ , the refinement level
# Output: refined conforming mesh  $\mathcal{T}$ 
conform := true
while  $L$  is not empty do
    PREBISECT(conform,  $L, S_t$ )
    for each tetrahedron  $\mathbf{T}$  in  $S_t$  do
         $j :=$  index of  $\mathbf{T}$  in  $TM$ 
        Bisect  $\mathbf{T}$  and its subtetrahedra using BISECT2
        until all edges with negative values in  $BI[TM[j].bi]$  are bisected
        Add subtetrahedra of  $\mathbf{T}$  to the end of  $TM$ ,
        and the new vertices to  $VC$ 
        Update corresponding information in  $XTM$ ,  $XVC$ , and  $BI$ 
        if any face of  $\mathbf{T}$  is not bisected and its other incident
            tetrahedron  $\mathbf{T}_1$  (not  $\mathbf{T}$ ) is not in  $S_t$  then
            Fill in the neighbor information of  $\mathbf{T}_1$ 
            and a subtetrahedron of  $\mathbf{T}$ 
        endif
    endfor
    Set  $L$  to be empty
    (A) Scan new tetrahedra to fill out neighbor information using
        hash table  $FHT$ ; and add  $(e, \mathbf{T})$  to  $L$  for each
        non-conforming edge  $e$  and its associated  $\mathbf{T}$ 
    conform := false
endwhile

```

Note that REFINE may make several passes through the *while* loop, and the meshes in the intermediate passes are not conforming. The *while* loop will terminate in a finite number of passes by Theorem 4.2. To ensure that our data structure works validly for a non-conforming mesh, i.e., all tetrahedra incident on an edge can be traced correctly in

PREBISECT, we need to prove that each face of a tetrahedron is shared by at most two other adjacent tetrahedra, which is given in the following theorem. In the proof of this theorem, we can further see how the algorithm QLRB works. In particular, we see what kinds of configurations of tetrahedra may be produced in QLRB, and how the non-conformity is dealt with.

**Theorem 4.7** *In procedure REFINE, each face of a tetrahedron is shared by at most 2 other adjacent tetrahedra.*

**Proof.** Note that Figures 4.2 and 4.4 include all configurations (up to type similar) deduced from repeated bisection of tetrahedra of classes DSS2 and DSS1, respectively, and one level of bisection on a tetrahedron of class DD or DSS3 produces subtetrahedra with the configuration in Figure 4.2a by the proof of Lemma 4.3. Therefore, the configurations of tetrahedra of classes DD and DSS3 plus those in Figures 4.2 and 4.4 are all the possible configurations of tetrahedra in a mesh resulting from QLRB. From the proof of Lemma 4.3, after three levels of bisection on a tetrahedron which is type similar to a tetrahedron of class DSS1, DSS2, DSS3, or DD, all its edges are bisected, and no new edges produced in the three levels of bisection are bisected. Among the configurations in Figures 4.2a, 4.2b, 4.4a, and 4.4b, we can verify that there are exactly two configurations, Figures 4.2b and 4.4a, in which a new edge added in the interior of a face may be bisected in order to bisect all original edges of the tetrahedron. Thus, in one pass of the *while* loop of REFINE, each edge can be bisected at most once, and some new edges may be bisected. Furthermore, if a new edge added in the interior of a face  $F$  is bisected after one pass of the *while* loop,  $F$  must be a face with configuration  $[3^*, 3^*, 2]$  or  $[3, 3, 2]$  (see Figures 4.2b and 4.4a) at the start of the pass of the *while* loop.

Now we prove that all non-conforming faces produced in REFINE have the patterns shown in Figure 4.5. That is,  $s_0s_2s_{01}$  and  $s_1s_2s_{01}$  are faces of some tetrahedra, respectively, but  $s_0s_1s_2$  is a face of another tetrahedron (this implies that each face of a tetrahedron is shared by at most 2 other adjacent tetrahedra). The numbers in Figures 4.5 to 4.7 denote the types of edges.

Suppose  $F$  is a conforming interior face  $u_0u_1u_2$  (shared by exactly two tetrahedra) at the start of a pass of the *while* loop of REFINE. If  $F$  includes some non-conforming subfaces after one pass of the *while* loop, by the above discussion, the new edge added in the interior of  $F$  must be bisected. So  $F$  must be a face with configuration  $[3^*, 3^*, 2]$  or  $[3, 3, 2]$  at the



a tetrahedron in the configuration of Figure 4.5a or 4.5b may be subdivided into either the pattern shown in Figure 4.7c (the worst case), or a pattern with edges  $s_0s_2$  and/or  $s_0s_1$  missing in Figure 4.7c. There are up to three cases where a non-conforming face may occur. First, if  $s_0s_0s_2$  and  $s_0s_0s_1$  in Figure 4.7a or 4.7b are faces of some tetrahedra, respectively, and  $s_0s_0s_1s_2$  in Figure 4.7c is a face of another tetrahedron, this non-conformance has the pattern shown in Figure 4.5a or 4.5b, respectively. Next, if  $s_2s_0s_2$  and  $s_0s_0s_2$  in Figure 4.7a or 4.7b are faces of some tetrahedra, respectively, and  $s_2s_0s_1s_2$  in Figure 4.7c is a face of another tetrahedron, this non-conformance has the pattern shown in Figure 4.5b or 4.5a, respectively. Finally, if  $s_2s_0s_2$  and  $s_0s_0s_2$  in Figure 4.7c are faces of some tetrahedra, and  $s_2s_0s_1s_2$  in Figure 4.7a or 4.7b is a face of another tetrahedron, this non-conformance has the pattern of Figure 4.5a, since the interior edge  $s_2s_0$  of face  $s_0s_1s_2$  is bisected in the same pass in which it is created (cf. Figure 4.6).

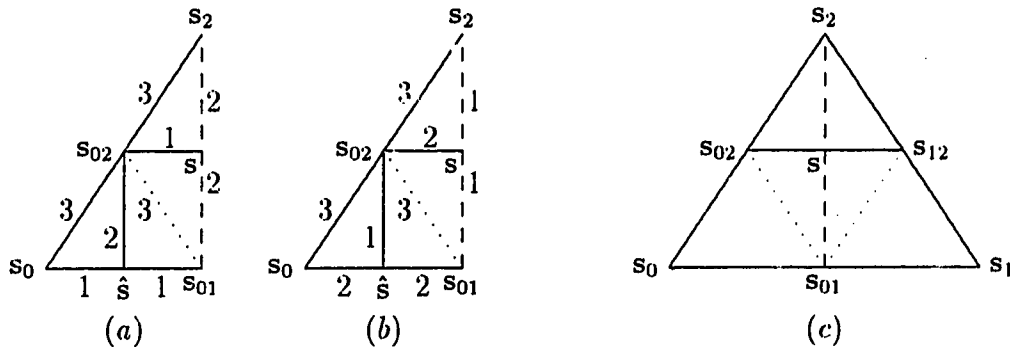


Figure 4.7: Illustration of the non-conforming patterns produced from a non-conforming face. (a) The configuration is produced by bisection of face  $s_0s_0s_2$  in Figure 4.5a; the sequence of bisected edges is  $s_0s_2$ ,  $s_0s_0s_1$ , or/and  $s_2s_0s_1$ . (b) The configuration is produced by bisection of face  $s_0s_0s_2$  in Figure 4.5b; the sequence of bisected edges is the same as in (a). (c) The configuration is produced by bisection of face  $s_0s_1s_2$  in Figures 4.5a and 4.5b; the sequence of bisected edges is  $s_0s_1$ ,  $s_0s_2$ ,  $s_1s_2$ , or/and  $s_2s_0s_1$ .

Note that after the first pass of the *while* loop in REFINE, the non-conforming faces occur only if some new edges added in the interior of some faces are bisected, and these non-conforming faces have the pattern of Figure 4.5a. By the induction argument of the previous paragraph, the theorem is established.  $\square$

## 4.6 Time complexity

We analyze the time complexity for one step of refinement, i.e., for procedure REFINE. Suppose  $k$  is the number of times through the *while* loop. Let  $N_j, 1 \leq j \leq k$ , be the number of new tetrahedra produced by bisecting tetrahedra in  $S_t$  at the  $j$ th pass. We assume that the table sizes of  $EHT$  and  $FHT$  are sufficiently large, and good hashing functions are used, so the expected time complexity of insertion and deletion of an element to  $EHT$  and  $FHT$  is  $O(1)$  (otherwise a balanced tree data structure with a logarithmic time complexity can be used to get a better worst case time complexity) [AHU74]. Note that in procedure PREBISECT, we only deal with non-conforming edges, i.e., all tetrahedra incident on a non-conforming edge are pushed onto  $S_t$ , and for any non-conforming edge  $e$  and tetrahedron  $T$  incident on  $e$ , the neighbors of  $T$  incident on  $e$  can be found in constant time. So, the time complexity for PREBISECT is  $O(|S_t|) = O(N_j)$ , where  $|S_t|$  is the number of tetrahedra in  $S_t$ , since there are at most 6 non-conforming edges for each tetrahedron. As the time used for bisection of each tetrahedron in  $S_t$  is constant, and the time spent on line (A) of REFINE is  $O(N_j)$ , the expected time complexity of REFINE is  $\sum_{j=1}^k O(N_j)$ . Suppose  $N$  is the number of refined new tetrahedra resulting from REFINE. We now prove that  $\sum_{j=1}^k O(N_j) = O(N)$ .

Suppose  $\mathcal{T}^m$  is the mesh before REFINE is called for the  $m$ th time. Let  $T_i^m, 1 \leq i \leq r$ , denote the tetrahedra of  $\mathcal{T}^m$  bisected in the  $m$ th call of REFINE. Consider the tree associated with  $T_i^m$ , where the root is tetrahedron  $T_i^m$ , the leaf nodes are subtetrahedra of  $T_i^m$ , produced by repeated bisection of  $T_i^m$ , in the mesh  $\mathcal{T}^{m+1}$ , and the interior nodes are subtetrahedra of  $T_i^m$  (not in the mesh  $\mathcal{T}^{m+1}$ ) in  $S_t$  for some passes of the *while* loop of REFINE. Suppose  $l_i$  is the number of leaf nodes and  $r_i$  is the number of non-leaf nodes in the tree for  $T_i^m$ . Note that the root node and each interior node is bisected into 2 to 10 subtetrahedra. It is straightforward to prove by induction that  $r_i \leq l_i$ , since bisecting a tetrahedron increases the number of interior nodes by one and the number of leaf nodes by at least one. Therefore,

$$\sum_{j=1}^k O(N_j) = \sum_{i=1}^r O(l_i + r_i) = \sum_{i=1}^r O(l_i) = O(N).$$



## 4.7 Summary

We have presented an algorithm for local refinement of a tetrahedral mesh, and have shown that the quality of tetrahedra in the refined mesh is guaranteed. As far as we know, this is the first theoretically guaranteed quality local refinement algorithm for a tetrahedral mesh based on bisection, although various local refinement algorithms are used in practice. We have also shown that the expected time complexity of this algorithm is  $O(N)$ , where  $N$  is the number of refined tetrahedra in the refined mesh, and  $N$  is bounded by a constant times the number of tetrahedra in the initial mesh by Theorem 4.2 (assuming the number of refinement levels is fixed), which may not be true using longest edge bisection. Experimental results (see Sections 6.1 and 6.2) on the quality of the refined tetrahedra show a very consistent performance for numerous test examples, and are much better than the theoretical estimate of the constant  $c$  in Theorem 4.4.

## Chapter 5

# Quality Local Refinement of Tetrahedral Meshes Based on 8-Subtetrahedron Subdivision

In this chapter, we present a 3-D local refinement algorithm for tetrahedral meshes, which is based mainly on a regular refinement procedure, and discuss the quality of meshes generated by the algorithm.

### 5.1 Introduction

In the previous chapter, we presented a local refinement algorithm for tetrahedral meshes based on a bisection procedure, which is the first theoretically guaranteed-quality mesh refinement algorithm for tetrahedral meshes based on bisection. In this chapter, we present a quality mesh refinement algorithm based on an *8-subtetrahedron subdivision* procedure, which is an extension of the 2-D mesh refinement technique in [BaS81, Ban90, LMZ85]. The 8-subtetrahedron subdivision may be preferable to bisection if the initial mesh is relatively coarse and needs to be refined quickly, because the volume of subtetrahedra in 8-subtetrahedron subdivision decreases faster than in bisection. Also, the 8-subtetrahedron subdivision is useful in the multigrid method, in which the solution of a problem is obtained by alternatively solving the problem on several levels of coarse to fine grids, since the grids at two consecutive levels should in general be significantly different.

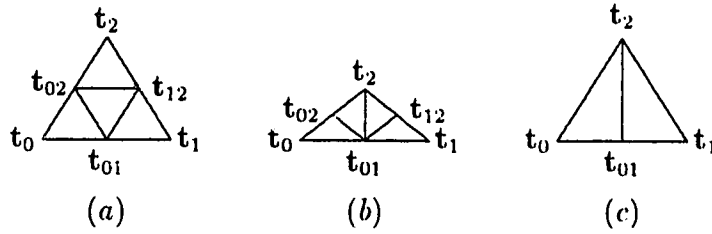


Figure 5.1: Illustration for 2-D local refinement in PLTMG;  $t_{ij} = (t_i + t_j)/2$ ,  $i < j$ . (a) Regular refinement; no interior angle is greater than  $\pi/2$ . (b) Regular refinement; one interior angle is greater than  $\pi/2$ . (c) Irregular refinement.

The basic idea in [Ban90] is as follows. Normally, a triangle is regularly refined by dividing it into 4 similar triangles, as illustrated in Figure 5.1a. If the triangle has an interior angle greater than  $\pi/2$ , then it is regularly refined into two similar triangles, and two geometrically better triangles, as illustrated in Figure 5.1b. At the boundary of a refined region, it is necessary to divide a triangle into only 2 “green” triangles by inserting a “green” edge, as illustrated in Figure 5.1c. Refinement into green triangles is done only as a temporary measure; at each step of the adaptive process, if the green triangles need to be further refined, then the green edges of these triangles are removed and the parent elements are regularly refined. Obviously, the degradation of geometry in this approach is bounded, since the green triangles are never further refined.

Likewise, in 3-D, we want to use a regular refinement called *8-subtetrahedron subdivision*, which is defined as follows. Suppose each triangular face of a tetrahedron  $T$  is refined into four similar subtriangles by connecting the midpoints of the edges (see Figure 5.1a) as shown in Figure 5.2. Then we obtain four similar subtetrahedra at the four corners and an octahedron in the interior. By adding an interior edge, called the *centre edge*,  $t_{02}t_{13}$  say, in the middle of the octahedron,  $T$  is subdivided into eight subtetrahedra. We use  $SUB_8$  to denote the 8-subtetrahedron subdivision described here.

Given a tetrahedron  $T$ ,  $SUB_8$  can be performed to  $T$  and its subtetrahedra repeatedly to produce a sequence of meshes. Note that the centre edge in  $SUB_8$  can be any one of the three choices (e.g.,  $t_{01}t_{23}$ ,  $t_{02}t_{13}$ , or  $t_{03}t_{12}$ ). Different strategies for choosing centre edges will produce substantially different meshes in terms of the quality of refined meshes. In Section 5.2, we design a refinement procedure, i.e., a way of selecting the centre edges,

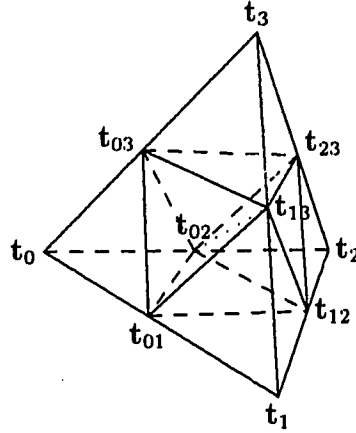


Figure 5.2: Illustration for the regular refinement (8-subtetrahedron subdivision)  $\text{SUB}_8$ ;  $t_{ij} = (t_i + t_j)/2$ ,  $i < j$ ; eight subtetrahedra are  $T_1^1(t_0, t_{01}, t_{02}, t_{03})$ ,  $T_2^1(t_{01}, t_1, t_{12}, t_{13})$ ,  $T_3^1(t_{02}, t_{12}, t_2, t_{23})$ ,  $T_4^1(t_{03}, t_{13}, t_{23}, t_3)$ ,  $T_5^1(t_{01}, t_{13}, t_{03}, t_{02})$ ,  $T_6^1(t_{01}, t_{12}, t_{13}, t_{02})$ ,  $T_7^1(t_{23}, t_{02}, t_{13}, t_{12})$ , and  $T_8^1(t_{23}, t_{02}, t_{13}, t_{03})$ .

such that (a) iteratively applying  $\text{SUB}_8$  to any tetrahedron  $T$  produces at most 24 classes of similar tetrahedra, and (b)  $\eta(T_i^n) \geq 0.5\eta(T)$ , where  $T_i^n$  is any refined tetrahedron of  $T$  and  $\eta$  is the mean ratio defined in Section 2.4. In light of property (b), it can be shown that there exists another means of selecting the centre edges, such that the shape of some subtetrahedra can be arbitrarily poor; in particular,  $\eta(T_i^n) \leq (6/7)^n\eta(T)$  for some refined tetrahedron  $T_i^n$ . In Section 5.3, we present a local refinement algorithm which is extensively based on  $\text{SUB}_8$ , and some properties of the algorithm are established. Data structure and implementation details are described in Section 5.4. The time complexity analysis is given in Section 5.5. A brief summary is provided in Section 5.6.

## 5.2 Subdivision of a single tetrahedron

In this section, we are mainly concerned about the quality of meshes produced by repeatedly performing  $\text{SUB}_8$  to a single tetrahedron  $T$  without considering the conformity of the refined meshes (which will be discussed in the next section). We first recall some notation used in previous chapters. For any (nondegenerate) tetrahedron  $T(t_0, t_1, t_2, t_3)$  with  $t_0, t_1, t_2, t_3$  as the coordinates of the four vertices in the form of column vectors in  $E^3$ ,  $T = [t_1 - t_0, t_2 - t_0, t_3 - t_0]$ . For any two tetrahedra  $S(s_0, s_1, s_2, s_3)$  and  $T(t_0, t_1, t_2, t_3)$ ,  $M(S, T) = TS^{-1}$  and  $A(S, T) = M^T(S, T)M(S, T)$ . Again, mean ratio  $\eta$  is used in analyzing the quality of meshes generated by our algorithm. We recall the following two formulae, which are often

used in the remainder of this chapter, for computing  $\eta$ .

$$\eta(\mathbf{T}) = 3\sqrt[3]{\lambda_1\lambda_2\lambda_3}/(\lambda_1 + \lambda_2 + \lambda_3) = 3\sqrt[3]{\det(A(\mathbf{R}, \mathbf{T}))/\text{trac}(A(\mathbf{R}, \mathbf{T}))}, \quad (5.2.1)$$

where  $\lambda_1$ ,  $\lambda_2$ , and  $\lambda_3$  are the eigenvalues of matrix  $A(\mathbf{R}, \mathbf{T})$ ,  $\mathbf{R}$  is a regular tetrahedron with the same volume as  $\mathbf{T}$ , and  $\eta$  is independent of the ordering of tetrahedron vertices and of the vertex coordinates of  $\mathbf{R}$ .

$$\eta(\mathbf{T}) = 12(3v)^{2/3} / \sum_{0 \leq i < j \leq 3} l_{ij}^2, \quad (5.2.2)$$

where  $v$  is the volume of  $\mathbf{T}$  and the  $l_{ij}$  are the lengths of the edges of  $\mathbf{T}$ .

As mentioned in the previous section, the centre edge in  $\text{SUB}_8$  is the edge connecting a pair of opposite edges, called the *base edges*. That is, the centre edge is the edge joining the midpoints of a pair of base edges. We say that a subtetrahedron has the same *subdivision pattern* as its direct parent if its base edges include either the centre edge or a half of a base edge of its parent, e.g., in Figure 5.2, if the base edges of  $\mathbf{T}_1^1(\mathbf{t}_0, \mathbf{t}_{01}, \mathbf{t}_{02}, \mathbf{t}_{03})$  are  $\mathbf{t}_0\mathbf{t}_{02}$  and  $\mathbf{t}_{01}\mathbf{t}_{03}$ , then  $\mathbf{T}_1^1(\mathbf{t}_0, \mathbf{t}_{01}, \mathbf{t}_{02}, \mathbf{t}_{03})$  has the same subdivision pattern as  $\mathbf{T}(\mathbf{t}_0, \mathbf{t}_1, \mathbf{t}_2, \mathbf{t}_3)$ , since  $\mathbf{t}_0\mathbf{t}_{02}$  is a half of the base edge  $\mathbf{t}_0\mathbf{t}_2$  of  $\mathbf{T}$ . It can be easily verified that if a subtetrahedron has the same subdivision pattern as its parent, then its two base edges and centre edge are uniquely determined. Now we describe a procedure SUBDIV for iteratively applying  $\text{SUB}_8$  to  $\mathbf{T}$ .

#### Algorithm SUBDIV

- (1) Subdivide  $\mathbf{T} = \mathbf{T}_i^0$  into eight subtetrahedra using  $\text{SUB}_8$  (see Figure 5.2); the centre edge can be any of the three choices, i.e.,  $\mathbf{t}_{01}\mathbf{t}_{23}$ ,  $\mathbf{t}_{02}\mathbf{t}_{13}$ , or  $\mathbf{t}_{03}\mathbf{t}_{12}$ ; label the eight subtetrahedra by  $\mathbf{T}_i^1$ ,  $1 \leq i \leq 8$ , and let  $\mathbf{T}_i^1$  have the same subdivision pattern as  $\mathbf{T}$ ;  $n := 1$ .
- (2) Subdivide  $\mathbf{T}_i^n$ ,  $1 \leq i \leq 8^n$ , using  $\text{SUB}_8$ , and let its subtetrahedra have the same subdivision pattern as  $\mathbf{T}_i^n$ ; label the resulting subtetrahedra by  $\mathbf{T}_i^{n+1}$ ,  $1 \leq i \leq 8^{n+1}$ .
- (3)  $n := n + 1$ ; repeat (2) or terminate the subdivision.

The superscript  $n$  in  $\mathbf{T}_i^n$  denotes the level of subdivision. We assume that each subtetrahedron is subdivided to the same level (this constraint will be removed in the next section). In order to study the quality of the mesh produced by SUBDIV (which is a main

procedure in our local refinement algorithm in the next section), we first describe SUBDIV by another equivalent procedure, which is relatively easy to use in analyzing the shape of the refined meshes. To this end, we introduce a canonical tetrahedron  $\mathbf{P}$  called a *rhombic tetrahedron* [MoW90], shown in Figure 5.3, which is used in an alternative description of SUBDIV.  $\mathbf{P}$  has two longer edges of the same length and four shorter edges of the same length. The most important property of  $\mathbf{P}$  is given in the following lemma, which is proved in [MoW90].

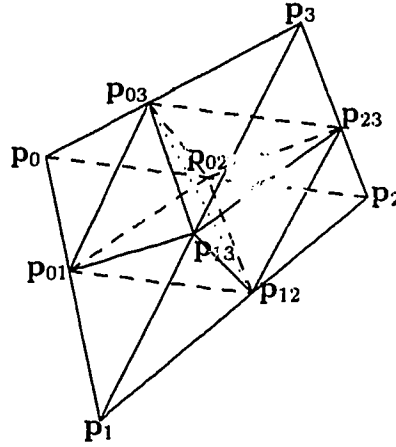


Figure 5.3: Rhombic tetrahedron  $\mathbf{P}(t_0, t_1, t_2, t_3)$  with  $|p_0p_1| = |p_2p_3| = |p_1p_3| = |p_0p_2| = m$ ,  $|p_0p_3| = |p_1p_2| = 2m/\sqrt{3}$ ;  $p_{ij} = (p_i + p_j)/2$ . The coordinates are  $p_0(-\sqrt{2}m/\sqrt{3}, 0, 0)$ ,  $p_1(0, -m/\sqrt{3}, 0)$ ,  $p_2(0, m/\sqrt{3}, 0)$ ,  $p_3(0, 0, \sqrt{2}m/\sqrt{3})$ ,  $p_{01}(-\sqrt{6}m/6, -\sqrt{3}m/6, 0)$ ,  $p_{02}(-\sqrt{6}m/6, \sqrt{3}m/6, 0)$ ,  $p_{03}(-\sqrt{6}m/6, 0, \sqrt{6}m/6)$ ,  $p_{12}(0, 0, 0)$ ,  $p_{13}(0, -\sqrt{3}m/6, \sqrt{6}m/6)$ , and  $p_{23}(0, \sqrt{3}m/6, \sqrt{6}m/6)$ .

**Lemma 5.1** *If  $\text{SUB}_8$  is applied to  $\mathbf{P}$  with the centre edge connecting its longest edges  $p_0p_3$  and  $p_1p_2$ , then the eight subtetrahedra  $\mathbf{P}_1^1(p_0, p_{01}, p_{02}, p_{03})$ ,  $\mathbf{P}_2^1(p_{01}, p_1, p_{12}, p_{13})$ ,  $\mathbf{P}_3^1(p_{02}, p_{12}, p_2, p_{23})$ ,  $\mathbf{P}_4^1(p_{03}, p_{13}, p_{23}, p_3)$ ,  $\mathbf{P}_5^1(p_{01}, p_{12}, p_{03}, p_{13})$ ,  $\mathbf{P}_6^1(p_{23}, p_{03}, p_{12}, p_{13})$ ,  $\mathbf{P}_7^1(p_{01}, p_{03}, p_{12}, p_{02})$ , and  $\mathbf{P}_8^1(p_{23}, p_{12}, p_{03}, p_{02})$  are all similar to the original tetrahedron  $\mathbf{P}(p_0, p_1, p_2, p_3)$  (see Figure 5.3).*

When  $\text{SUB}_8$  is applied to  $\mathbf{P}$ , the base edges of  $\mathbf{P}$  are its longest edges ( $p_0p_3, p_1p_2$ ). With each subtetrahedron having the same subdivision pattern as its parent, it is obvious that the base edges of  $\mathbf{P}_i^1$ ,  $1 \leq i \leq 4$ , are its longest edges. Since  $|p_{03}p_{12}| = |p_0p_3|/2 = |p_1p_2|/2$ , the base edges of  $\mathbf{P}_i^1$ ,  $5 \leq i \leq 8$ , are also its longest edges. Therefore, by Lemma 5.1 and induction, the base edges of any refined subtetrahedron of  $\mathbf{P}$  produced by  $\text{SUB}_8$  are always its two longest edges.

Let  $\mathbf{P}$  be the canonical tetrahedron in Figure 5.3 such that  $\mathbf{T}$  and  $\mathbf{P}$  have the same volume. We describe another procedure TRANSUB which uses an affine transformation, and prove that SUBDIV and TRANSUB are equivalent.

**Algorithm TRANSUB**

- (1) Transform  $\mathbf{T}$  to  $\mathbf{P}$  by an affine transformation  $\mathbf{y} = M^{-1}(\mathbf{P}, \mathbf{T})\mathbf{x} + \mathbf{b}_0$ , with the constraint that the two base edges of  $\mathbf{T}$  in step (1) of SUBDIV are transformed into the pair of edges with the longest length in  $\mathbf{P}$ , i.e.  $\mathbf{p}_0\mathbf{p}_3$  and  $\mathbf{p}_1\mathbf{p}_2$  in Figure 5.3.
- (2) Iteratively subdivide  $\mathbf{P}$  to some level, with each subtetrahedron having the same subdivision pattern as its parent (i.e. the two base edges are the two longest edges).
- (3) Transform all subtetrahedra in  $\mathbf{P}$  back to subtetrahedra in  $\mathbf{T}$  using the inverse affine transformation  $\mathbf{y} = M(\mathbf{P}, \mathbf{T})\mathbf{x} + \mathbf{b}_1$ .

**Theorem 5.1** *For any tetrahedron  $\mathbf{T}$ , if each subtetrahedron is refined to the same level, SUBDIV and TRANSUB produce the same set of refined tetrahedra.*

**Proof.** The theorem can be established by using the fact that the midpoint of a line segment is transformed into the midpoint of the corresponding line segment under an affine transformation.  $\square$

We now use TRANSUB to establish the main properties of meshes produced by SUBDIV.

**Theorem 5.2** *There are at most 24 classes of similar tetrahedra produced by SUBDIV in all the refined subtetrahedra of  $\mathbf{T}$ .*

**Proof.** We define two tetrahedra to be in the same equivalence class if one can be transformed into the other by translation and uniform scaling (i.e., the scale factors for the three coordinate axes are the same). So any two tetrahedra in the same equivalence class are similar to each other after any affine transformation. Let  $\mathbf{P}_i^n$  be any subtetrahedron of  $\mathbf{P}$  at level  $n$ ,  $n \geq 0$ . In order to prove the theorem, it suffices to prove that all subtetrahedra  $\mathbf{P}_i^n$  generated by TRANSUB are in at most 24 different equivalence classes.

After one level of subdivision, by Lemma 5.1, all the 8 subtetrahedra, denoted by  $\mathbf{P}_i^1$ ,  $1 \leq i \leq 8$ , are similar to  $\mathbf{P}$ . Let these tetrahedra be labeled as in Lemma 5.1. Let

$M_i = M(\mathbf{P}, \mathbf{P}_i^1)$ . From the coordinates shown in Figure 5.3, we obtain  $M_1 = M_2 = M_3 = M_4 = 1/2 I$ , where  $I$  is the identity matrix, and

$$M_5 = \frac{1}{4} \begin{bmatrix} 1 & -\sqrt{2} & 1 \\ \sqrt{2} & 0 & -\sqrt{2} \\ 1 & \sqrt{2} & 1 \end{bmatrix}, \quad M_6 = \frac{1}{4} \begin{bmatrix} -1 & \sqrt{2} & 1 \\ -\sqrt{2} & 0 & -\sqrt{2} \\ -1 & -\sqrt{2} & 1 \end{bmatrix},$$

$$M_7 = \frac{1}{4} \begin{bmatrix} 1 & \sqrt{2} & -1 \\ \sqrt{2} & 0 & \sqrt{2} \\ 1 & -\sqrt{2} & -1 \end{bmatrix}, \quad M_8 = \frac{1}{4} \begin{bmatrix} -1 & -\sqrt{2} & -1 \\ -\sqrt{2} & 0 & \sqrt{2} \\ -1 & \sqrt{2} & -1 \end{bmatrix}.$$

Let

$$\text{diag}(a_1, a_2, a_3) = \begin{bmatrix} a_1 & 0 & 0 \\ 0 & a_2 & 0 \\ 0 & 0 & a_3 \end{bmatrix}, \quad \text{skew}(a_1, a_2, a_3) = \begin{bmatrix} 0 & 0 & a_1 \\ 0 & a_2 & 0 \\ a_3 & 0 & 0 \end{bmatrix}.$$

The following equations are derived by straightforward computation.

$$\begin{aligned} M_7 &= \text{skew}(-1, -1, -1)M_6, \quad M_8 = \text{skew}(-1, -1, -1)M_5, \\ M_5M_6 &= 1/4\text{skew}(1, 1, -1)I, \quad M_6M_5 = 1/2\text{skew}(-1, 1, 1)M_6, \\ M_5M_7 &= 1/4\text{skew}(-1, 1, 1)I, \quad M_7M_5 = 1/2\text{diag}(-1, -1, 1)M_6, \\ M_5M_8 &= -1/4\text{skew}(1, 1, 1)I, \quad M_8M_5 = 1/4\text{diag}(-1, 1, -1)I, \\ M_6M_7 &= 1/2\text{diag}(1, -1, -1)M_5, \quad M_7M_6 = 1/2\text{diag}(-1, -1, 1)M_5, \\ M_6M_8 &= 1/2\text{diag}(1, -1, -1)M_6, \quad M_8M_6 = 1/4\text{diag}(1, -1, -1)I, \\ M_7M_8 &= 1/2\text{skew}(1, 1, -1)M_6, \quad M_8M_7 = 1/4\text{diag}(-1, -1, 1)I, \\ M_5^2 &= 1/4\text{skew}(1, -1, 1)I, \quad M_6^2 = 1/2\text{skew}(-1, 1, 1)M_5, \\ M_7^2 &= 1/2\text{skew}(1, 1, -1)M_5, \quad M_8^2 = 1/4I. \end{aligned}$$

After 2 levels of subdivision,  $M(\mathbf{P}, \mathbf{P}_i^2) = M(\mathbf{P}_j^1, \mathbf{P}_i^2)M(\mathbf{P}, \mathbf{P}_j^1)$  where  $\mathbf{P}_i^2$  is a subtetrahedron of  $\mathbf{P}_j^1$ . With a suitable ordering of vertices of  $\mathbf{P}_i^2$ , it follows that  $P_i^2 = M_j P_l^1$  for some  $l$ . So

$$M(\mathbf{P}, \mathbf{P}_i^2) = P_i^2 P^{-1} = M_j P_l^1 P^{-1} = M_j M_l,$$

since  $P_l^1 = M_l P$ . By induction, after  $k$  levels of subdivision, for each subtetrahedron  $\mathbf{P}_i^k$  with a suitable ordering of vertices  $\mathbf{p}_{ir}^k$ , we have

$$\mathbf{p}_{ir}^k = M_{l1} M_{l2} \cdots M_{lk} \mathbf{p}_r + \mathbf{b}_i^k, \quad 0 \leq r \leq 3,$$



where each  $M_{lm}$ ,  $1 \leq m \leq k$ , is one of the  $M_i$ ,  $1 \leq i \leq 8$ . Let  $\mathcal{S}$  be the set of all diagonal and skew diagonal 3 by 3 matrices with elements 1 or  $-1$ . Obviously,  $\mathcal{S}$  is closed under matrix multiplication and  $|\mathcal{S}| = 2^3 + 2^3 = 16$ . By the above equations,  $M_{l_1} M_{l_2} \cdots M_{l_k} = f D M$ , where  $f$  is a scale factor,  $D$  is an element of  $\mathcal{S}$ , and  $M$  is  $I$ ,  $M_5$ , or  $M_6$ . Note that  $D$  and  $-D$  can be considered to be the same matrix of  $\mathcal{S}$  due to the factor  $f$ . Therefore the number of different equivalence classes is  $\leq 3 \times 8 = 24$ . Hence the total number of classes similar tetrahedra in all refined subtetrahedra of  $\mathbf{T}$  is finite and bounded above by 24.  $\square$

Theorem 5.2 implies that the shape of subtetrahedra does not deteriorate arbitrarily. Moreover, the following theorem shows that the shape of the subtetrahedra are at least half as good as the shape of the very first tetrahedron  $\mathbf{T}$  in terms of the shape measure  $\eta$ .

**Theorem 5.3** *For any refined subtetrahedron  $\mathbf{T}_i^n$  of  $\mathbf{T}$ , produced by SUBDIV,*

$$\eta(\mathbf{T}_i^n) \geq 0.5\eta(\mathbf{T}), \quad (5.2.3)$$

*and the lower bound is tight.*

**Proof.** Let  $M(\mathbf{P}, \mathbf{T})$  and  $M(\mathbf{R}, \mathbf{P})$  be the two matrices involved in the affine transformations from  $\mathbf{P}$  to  $\mathbf{T}$  and  $\mathbf{R}$  to  $\mathbf{P}$ , respectively. Using the notation given at the beginning of this section,

$$T = M(\mathbf{P}, \mathbf{T})P = M(\mathbf{P}, \mathbf{T})M(\mathbf{R}, \mathbf{P})R,$$

where  $T$ ,  $P$  and  $R$  are the matrices derived from  $\mathbf{T}$ ,  $\mathbf{P}$  and  $\mathbf{R}$ . From step (3) of TRANSUB, the tetrahedron  $\mathbf{T}_i^n$  is transformed from  $\mathbf{P}_i^n$  using  $M(\mathbf{P}, \mathbf{T})$ , so

$$T_i^n = M(\mathbf{P}, \mathbf{T})P_i^n.$$

With a suitable ordering of vertices of  $\mathbf{P}_i^n$ ,  $P_i^n = \alpha Q P$  where  $\alpha$  is a positive constant and  $Q$  is an orthogonal matrix, since  $\mathbf{P}_i^n$  is similar to  $\mathbf{P}$  by Lemma 5.1. So

$$T_i^n = \alpha M(\mathbf{P}, \mathbf{T})Q P = \alpha M(\mathbf{P}, \mathbf{T})Q M(\mathbf{R}, \mathbf{P})R = M(\mathbf{P}, \mathbf{T})Q M(\mathbf{R}, \mathbf{P})R^n = M(\mathbf{R}^n, \mathbf{T}_i^n)R^n,$$

where  $\mathbf{R}^n$  is a regular tetrahedron having the same volume as  $\mathbf{T}_i^n$ .

From  $\det(A(\mathbf{R}, \mathbf{T})) = \det(A(\mathbf{R}^n, \mathbf{T}_i^n)) = 1$  and (5.2.1), we have

$$\eta(\mathbf{T}) = \frac{3 \sqrt[3]{\det(A(\mathbf{R}, \mathbf{T}))}}{\text{trace}(A(\mathbf{R}, \mathbf{T}))} = \frac{3}{\text{trace}((M(\mathbf{P}, \mathbf{T})M(\mathbf{R}, \mathbf{P}))^T M(\mathbf{P}, \mathbf{T}) M(\mathbf{R}, \mathbf{P}))}, \quad (5.2.4)$$

$$\eta(\mathbf{T}_i^n) = \frac{3\sqrt{\det(A(\mathbf{R}^n, \mathbf{T}_i^n))}}{\text{trace}(A(\mathbf{R}^n, \mathbf{T}_i^n))} = \frac{3}{\text{trace}((M(\mathbf{P}, \mathbf{T})Q M(\mathbf{R}, \mathbf{P}))^T M(\mathbf{P}, \mathbf{T})Q M(\mathbf{R}, \mathbf{P}))}. \quad (5.2.5)$$

Let  $\|B\|_F$  denote the Frobenius norm of matrix  $B$  [GoV89], i.e.,  $\|B\|_F = (\text{trace}(B^T B))^{1/2}$ .

By (5.2.4) and (5.2.5), it follows that

$$\frac{\eta(\mathbf{T}_i^n)}{\eta(\mathbf{T})} = \frac{\|M(\mathbf{P}, \mathbf{T})M(\mathbf{R}, \mathbf{P})\|_F^2}{\|M(\mathbf{P}, \mathbf{T})Q M(\mathbf{R}, \mathbf{P})\|_F^2}. \quad (5.2.6)$$

By the singular value decomposition [GoV89],  $M(\mathbf{P}, \mathbf{T}) = Q_1 \text{diag}(\sqrt{\lambda_1}, \sqrt{\lambda_2}, \sqrt{\lambda_3}) Q_2$  where  $Q_1, Q_2$  are orthogonal matrices and  $\lambda_1, \lambda_2, \lambda_3$  are the eigenvalues of  $A(\mathbf{P}, \mathbf{T})$  ( $\sqrt{\lambda_1}, \sqrt{\lambda_2}, \sqrt{\lambda_3}$  are the singular values of  $M(\mathbf{P}, \mathbf{T})$ ). It follows that

$$\|M(\mathbf{P}, \mathbf{T})M(\mathbf{R}, \mathbf{P})\|_F^2 = \|\text{diag}(\sqrt{\lambda_1}, \sqrt{\lambda_2}, \sqrt{\lambda_3}) Q_2 M(\mathbf{R}, \mathbf{P})\|_F^2, \quad (5.2.7)$$

$$\|M(\mathbf{P}, \mathbf{T})Q M(\mathbf{R}, \mathbf{P})\|_F^2 = \|\text{diag}(\sqrt{\lambda_1}, \sqrt{\lambda_2}, \sqrt{\lambda_3}) Q_2 Q M(\mathbf{R}, \mathbf{P})\|_F^2. \quad (5.2.8)$$

Let  $\mathbf{R}(\mathbf{r}_0, \mathbf{r}_1, \mathbf{r}_2, \mathbf{r}_3)$  be a regular tetrahedron having the same volume as  $\mathbf{P}$  with coordinates  $\mathbf{r}_0 = (-\sqrt{3}a/2, 0, 0)^T$ ,  $\mathbf{r}_1 = (0, -a/2, 0)^T$ ,  $\mathbf{r}_2 = (0, a/2, 0)^T$ , and  $\mathbf{r}_3 = (-\sqrt{3}a/6, 0, \sqrt{6}a/3)^T$ . From the coordinates shown in Figure 5.3, with  $\mathbf{r}_i$  being transformed to  $\mathbf{p}_i$ , we have

$$M(\mathbf{R}, \mathbf{P}) = k \begin{bmatrix} 2\sqrt{2} & 0 & 1 \\ 0 & 2\sqrt{3} & 0 \\ 0 & 0 & 3 \end{bmatrix},$$

where  $k^3 = \sqrt{6}/72$ . If  $U$  is an orthogonal matrix with elements  $u_{ij}$ ,  $1 \leq i, j \leq 3$ , we have

$$\|\text{diag}(\sqrt{\lambda_1}, \sqrt{\lambda_2}, \sqrt{\lambda_3}) U M(\mathbf{R}, \mathbf{P})\|_F^2 =$$

$$k^2(\lambda_1[9 + 3(1 - (u_{11} - u_{13})^2)] + \lambda_2[9 + 3(1 - (u_{21} - u_{23})^2)] + \lambda_3[9 + 3(1 - (u_{31} - u_{33})^2)]).$$

Since  $0 \leq (x + y)^2 \leq 2$  for any  $x, y$  satisfying  $x^2 + y^2 \leq 1$ ,

$$6k^2(\lambda_1 + \lambda_2 + \lambda_3) \leq \|\text{diag}(\sqrt{\lambda_1}, \sqrt{\lambda_2}, \sqrt{\lambda_3}) U M(\mathbf{R}, \mathbf{P})\|_F^2 \leq 12k^2(\lambda_1 + \lambda_2 + \lambda_3).$$

Then combining (5.2.6), (5.2.7), and (5.2.8) yields

$$0.5 \leq \frac{\eta(\mathbf{T}_i^n)}{\eta(\mathbf{T})} \leq 2.$$

We now prove that the lower bound cannot be improved. For any  $\epsilon > 0$ , we define a tetrahedron  $\mathbf{T}$  with vertices  $\mathbf{t}_0 = (0, \frac{\sqrt{11(0.5-\epsilon)}}{\sqrt{8\epsilon}}, 0)$ ,  $\mathbf{t}_1 = (-1, 0, 0)$ ,  $\mathbf{t}_2 = (1, 0, 0)$ , and

$\mathbf{t}_3 = (0, \frac{\sqrt{11(0.5-\epsilon)}}{\sqrt{8\epsilon}}, 1)$ . Consider subtetrahedron  $\mathbf{T}_1^1 = (\mathbf{t}_{03}, \mathbf{t}_{13}, \mathbf{t}_{12}, \mathbf{t}_{23})$  produced by using centre edge  $\mathbf{t}_{12}\mathbf{t}_{03}$ , where  $\mathbf{t}_{ij}$  is the midpoint of  $\mathbf{t}_i$  and  $\mathbf{t}_j$ . By straightforward computation using (5.2.2),  $\eta(\mathbf{T}_1^1)/\eta(\mathbf{T}) = 0.5 + \epsilon$ . Hence the lower bound is tight.  $\square$

In the subdivision procedure SUBDIV, the centre edge added in the interior of a tetrahedron is selected by a specific rule. Otherwise, refined subtetrahedra with good shape may not be guaranteed. In fact, there is a means of selecting centre edges such that the shape of some subtetrahedra become arbitrarily poor, as described by the following lemma and theorem.

**Lemma 5.2** *Suppose SUB<sub>8</sub> is applied to any tetrahedron  $\mathbf{T}(\mathbf{t}_0, \mathbf{t}_1, \mathbf{t}_2, \mathbf{t}_3)$ . If the centre edge of  $\mathbf{T}$  is chosen such that the minimum  $\eta$  value of the four interior subtetrahedra achieves a minimum value among the three possible choices of centre edges, then there exists a subtetrahedron  $\mathbf{T}_1^1$  of  $\mathbf{T}$ , such that  $\eta(\mathbf{T}_1^1) \leq 6/7\eta(\mathbf{T})$ , and the upper bound is tight.*

**Proof.** For any edge  $e$ , let  $|e|$  denote the length of  $e$ . Let  $e_1 = \mathbf{t}_1\mathbf{t}_2$ ,  $e_2 = \mathbf{t}_0\mathbf{t}_3$ ,  $e_3 = \mathbf{t}_0\mathbf{t}_1$ ,  $e_4 = \mathbf{t}_2\mathbf{t}_3$ ,  $e_5 = \mathbf{t}_1\mathbf{t}_3$ , and  $e_6 = \mathbf{t}_0\mathbf{t}_2$ . Let  $e(i)$  stand for a centre edge connecting the midpoint of  $e_{2i-1}$  and  $e_{2i}$ ,  $i = 1, 2, 3$ . For any centre edge  $e(j)$ , by formula (5.2.2) and the fact that the volume of any subtetrahedron is  $1/8$  times the volume of  $\mathbf{T}$ , the  $\eta$  measures of the four interior subtetrahedra are either

$$\frac{3(3v)^{2/3}}{\sum_{i=1}^6 |e_i|^2/4 + |e(j)|^2 - |e_{2j-1}|^2/4} \text{ or } \frac{3(3v)^{2/3}}{\sum_{i=1}^6 |e_i|^2/4 + |e(j)|^2 - |e_{2j}|^2/4},$$

where  $v$  is the volume of  $\mathbf{T}$ . Let  $\hat{e}(j) = |e(j)|^2 - \min^2(|e_{2j-1}|, |e_{2j}|)/4$ . Then for centre edge  $e(j)$ , the minimum  $\eta$  value of the four interior subtetrahedra is

$$\frac{3(3v)^{2/3}}{\sum_{i=1}^6 |e_i|^2/4 + \hat{e}(j)}.$$

Suppose  $\mathbf{T}_1^1$  is a subtetrahedron such that

$$\eta(\mathbf{T}_1^1) = \frac{3(3v)^{2/3}}{\sum_{i=1}^6 |e_i|^2/4 + \max_{1 \leq j \leq 3} \hat{e}(j)}. \quad (5.2.9)$$

That is,  $\mathbf{T}_1^1$  is a subtetrahedron of  $\mathbf{T}$  when the centre edge of  $\mathbf{T}$  is chosen such that the minimum  $\eta$  value of the four interior subtetrahedra achieves a minimum value. Since  $|e(1)| = |\mathbf{t}_{03}\mathbf{t}_{12}| = |\mathbf{t}_0 + \mathbf{t}_3 - \mathbf{t}_1 - \mathbf{t}_2|/2$ ,

$$|e(1)|^2 = \frac{1}{4}(\mathbf{t}_0 - \mathbf{t}_1 + \mathbf{t}_3 - \mathbf{t}_2)^T(\mathbf{t}_0 - \mathbf{t}_1 + \mathbf{t}_3 - \mathbf{t}_2) = \frac{1}{4}(|e_3|^2 + |e_4|^2 + 2(\mathbf{t}_0 - \mathbf{t}_1)^T(\mathbf{t}_3 - \mathbf{t}_2))$$

$$= \frac{1}{4}(|e_3|^2 + |e_4|^2 + |e_5|^2 + |e_6|^2 - |e_1|^2 - |e_2|^2). \quad (5.2.10)$$

Similarly, we obtain

$$|e(2)|^2 = \frac{1}{4}(|e_1|^2 + |e_2|^2 + |e_5|^2 + |e_6|^2 - |e_3|^2 - |e_4|^2),$$

and

$$|e(3)|^2 = \frac{1}{4}(|e_1|^2 + |e_2|^2 + |e_3|^2 + |e_4|^2 - |e_5|^2 - |e_6|^2).$$

So,

$$\sum_{i=1}^3 \hat{e}(i) = 1/4 \sum_{i=1}^6 |e_i|^2 - 1/4 \min(|e_1|^2, |e_2|^2) - 1/4 \min(|e_3|^2, |e_4|^2) - 1/4 \min(|e_5|^2, |e_6|^2).$$

Combining the above equation with  $\min(|e_i|^2, |e_{i+1}|^2) \leq (|e_i|^2 + |e_{i+1}|^2)/2$ ,  $i = 1, 2, 3$ , yields

$$\max_{1 \leq i \leq 3} \hat{e}(i) \geq \frac{1}{3} \sum_{i=1}^3 \hat{e}(i) \geq \frac{1}{24} \sum_{i=1}^6 |e_i|^2.$$

Combining (5.2.9), (5.2.2), and the above inequality yields  $\eta(\mathbf{T}_1^1) \leq 6/7\eta(\mathbf{T})$ .

The upper bound  $6/7$  is tight because no mean ratios of subtetrahedra generated in the regular tetrahedron  $\mathbf{T}$  can be worse than  $6/7$ .  $\square$

**Theorem 5.4** *There exists a means of selecting the centre edges, such that after  $n$  levels of refinement by applying SUB<sub>8</sub> to  $\mathbf{T}$ ,*

$$\eta(\mathbf{T}_i^n) \leq (6/7)^n \eta(\mathbf{T}),$$

*for some refined subtetrahedron  $\mathbf{T}_i^n$ .*

**Proof.** At each step of refinement, if the centre edge is chosen as described in Lemma 5.2, the theorem can be established by repeatedly using Lemma 5.2.  $\square$

In light of the scheme of selecting the centre edge in Lemma 5.2, we can always choose the centre edge such that the minimum shape measure of the four interior subtetrahedra achieves a maximum value, but it seems hard to obtain the nice properties in Theorems 5.2 and 5.3.

In addition, for any tetrahedron  $\mathbf{T}$ , we prove in Appendix B that there exists a centre edge of  $\mathbf{T}$  such that any refined mesh produced by SUBDIV is a Delaunay triangulation when all face angles of the tetrahedron  $\mathbf{T}$  are  $\leq 90^\circ$ . That is, a guaranteed-quality Delaunay triangulation is produced by SUBDIV under the face angle condition, while a Delaunay triangulation may in general contain some poorly-shaped tetrahedra.

### 5.3 Local refinement of a conforming mesh

Similar to the 2-D approach in [Ban90, p. 26], we design a 3-D mesh refinement algorithm mainly depending on the regular subdivision  $\text{SUB}_8$  illustrated in Figure 5.2, since the shape of refined tetrahedra produced by repeatedly performing  $\text{SUB}_8$  to a tetrahedron are bounded below if each subtetrahedron has the same subdivision pattern as its parent by the discussion in the previous section. Simply applying  $\text{SUB}_8$  to a set of subtetrahedra of a conforming mesh may produce non-conformity between tetrahedra. Therefore, at the boundary of a refined region, other non-regular refinements may be needed to ensure a conforming mesh.

A *split point* is defined to be the midpoint of an edge whenever the edge needs subdivision. In an initial mesh  $\mathcal{T}$ , suppose a set  $S$  of tetrahedra are chosen for refinement. A split point is added to each edge of each tetrahedron in  $S$ . Also, for any face of a tetrahedron not in  $S$  that contains two split points, a split point is added to the edge that does not have a split point so that there are either one or three split points on each face. A face with 3 or 1 split point(s) is subdivided like Figure 5.1a or 5.1c, respectively; we don't use the subdivision of Figure 5.1b, since this will significantly increase the difficulty of keeping a conforming mesh. Under the above assumptions, the number of split points for a tetrahedron in the initial mesh can be 1, 2 (on a pair of opposite edges), 3 (on the same face), or 6. According to the number of split points, the subdivision of a tetrahedron is illustrated in Figures 5.4a, 5.4b, 5.4c, and Figure 5.2. respectively. The three non-regular refinements in Figures 5.4a, 5.4b, and 5.4c are denoted by  $\text{SUB}_2$ ,  $\text{SUB}_4^1$ , and  $\text{SUB}_4^2$ , respectively, and are applied to the boundary of a refined region. In the next refinement, if any tetrahedron, produced by  $\text{SUB}_2$ ,  $\text{SUB}_4^1$ , or  $\text{SUB}_4^2$ , is chosen for refinement, its parent is always refined by  $\text{SUB}_8$  first. Thus we never need to add a split point on an edge, called an *irregular edge*, which is generated by connecting a vertex to the midpoint of an edge of a face in  $\text{SUB}_2$ ,  $\text{SUB}_4^1$ , or  $\text{SUB}_4^2$ , e.g.  $t_3t_{12}$  in Figure 5.4a and  $t_{03}t_{12}$  in Figure 5.4b. An *irregular face* is defined to be one containing an irregular edge, e.g. face  $t_1t_3t_{12}$  in Figure 5.4a, and may have 0, 1, or 2 split points (for the next refinement). A face that is not irregular is called a *regular face*, and may have 0, 1, or 3 split points.

We now give a local refinement procedure, QLRs (quality local refinement based on subdivision), based on  $\text{SUB}_8$ ,  $\text{SUB}_2$ ,  $\text{SUB}_4^1$ , and  $\text{SUB}_4^2$ . A more detailed pseudocode is provided after we discuss data structures in the next section. A tetrahedron  $T$  is called a

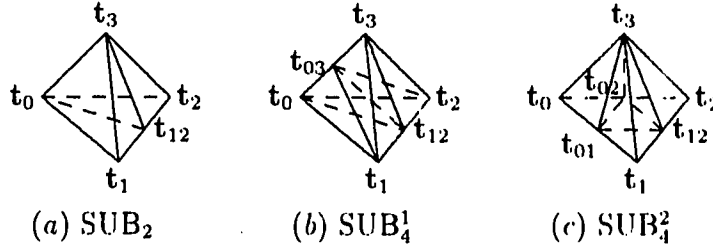


Figure 5.4: Illustration for non-regular refinements;  $t_{ij} = (t_i + t_j)/2$ ,  $i < j$ . (a) Subdivision of a tetrahedron with one split point ( $t_{12}$ ). (b) Subdivision of a tetrahedron with two split points ( $t_{12}$ ,  $t_{03}$ ) on a pair of opposite edges. (c) Subdivision of a tetrahedron with three split points ( $t_{01}$ ,  $t_{02}$ ,  $t_{12}$ ) on the same face.

tetrahedron of type  $S_8$  if  $\mathbf{T}$  is either a tetrahedron in the original mesh, or produced by SUB<sub>8</sub>. Similarly, a tetrahedron of type  $S_2$ ,  $S_4^1$ , or  $S_4^2$  means that the tetrahedron is produced by SUB<sub>2</sub>, SUB<sub>4</sub><sup>1</sup>, or SUB<sub>4</sub><sup>2</sup>, respectively. In the following, we assume that whenever SUB<sub>8</sub> is applied to a tetrahedron  $\mathbf{T}$  of the original mesh  $\mathcal{T}$ , the centre edge of  $\mathbf{T}$  is chosen such that the minimum shape value of the four interior subtetrahedra (i.e.,  $\mathbf{T}_5^1$ ,  $\mathbf{T}_6^1$ ,  $\mathbf{T}_7^1$ ,  $\mathbf{T}_8^1$  in Figure 5.2) of  $\mathbf{T}$  achieves a maximum value in terms of the tetrahedron shape measure  $\eta$ . Also, for any tetrahedron  $\mathbf{T}$ , an *unsplit edge* of  $\mathbf{T}$  is an edge that does not have a split point.

#### Algorithm QLRS

- (1) Set  $\mathcal{T}^0 := \mathcal{T}$ ;  $m := 0$ .
- (2) Select a set  $S_m$  of tetrahedra needing refinement from  $\mathcal{T}^m$ ; for each tetrahedron  $\mathbf{T}$  in  $S_m$ , if  $\mathbf{T}$  is a tetrahedron of type  $S_8$ , mark a split point on each unsplit edge of  $\mathbf{T}$ ; otherwise, mark a split point on each unsplit edge of  $\mathbf{T}$ 's parent.
- (3) For each tetrahedron  $\mathbf{T}$  of type  $S_2$  in  $\mathcal{T}^m$  (see Figure 5.4a), whenever one of edges  $t_3t_1$ ,  $t_3t_2$  (or  $t_0t_1$ ,  $t_0t_2$ ) has a split point, mark a split point on the other if it does not have a split point; whenever  $t_1t_{12}$  (or  $t_2t_{12}$ ) has a split point, mark a split point on each unsplit edge of  $\mathbf{T}$ 's parent. For each tetrahedron of type  $S_4^1$  or  $S_4^2$  in  $\mathcal{T}^m$ , whenever one of its edges has a split point, mark a split point on each unsplit edge of  $\mathbf{T}$ 's parent. In addition, whenever a regular face in  $\mathcal{T}^m$  has two split points, mark a split point on the unsplit edge of the face; repeat the above process until no more split points are needed.
- (4) For any  $\mathbf{T}$  in  $\mathcal{T}^m$  with a non-zero number of split points, if  $\mathbf{T}$  is a tetrahedron of

type  $S_8$ , subdivide  $\mathbf{T}$  using  $\text{SUB}_8$ ,  $\text{SUB}_2$ ,  $\text{SUB}_4^1$ , or  $\text{SUB}_4^2$  according to the number of split points on  $\mathbf{T}$ , and let the subtetrahedra have the same subdivision pattern as  $\mathbf{T}$ ; otherwise, remove  $\mathbf{T}$ 's sibling( $\cdot$ ), subdivide  $\mathbf{T}$ 's parent  $\mathbf{T}_p$  using  $\text{SUB}_8$ ,  $\text{SUB}_4^1$ , or  $\text{SUB}_4^2$  according to the number of split points on  $\mathbf{T}_p$ , and subdivide each subtetrahedron of  $\mathbf{T}_p$  if necessary using  $\text{SUB}_2$  or  $\text{SUB}_4^2$  according to the number of split points on the subtetrahedron; label the conforming mesh by  $\mathcal{T}^{m+1}$ .

(5)  $m := m + 1$ ; go to (2) if necessary or terminate.

Note that superscript  $m$  of  $\mathcal{T}^m$  indicates that mesh  $\mathcal{T}^m$  is created after  $m$  levels of refinement on  $\mathcal{T}^0$ . In step (3) of QLRs, whenever a split point is added to an edge of a tetrahedron  $\mathbf{T}$  of type  $S_4^1$  or  $S_4^2$ , the split points are also added to the edges of  $\mathbf{T}$ 's parent  $\mathbf{T}_p$ . This guarantees that a tetrahedron of type  $S_4^1$  or  $S_4^2$  will never be further refined, i.e., whenever a tetrahedron  $\mathbf{T}$  of type  $S_4^1$  or  $S_4^2$  needs to be refined,  $\mathbf{T}_p$  is always first refined by the regular refinement. For a tetrahedron  $\mathbf{T}$  of type  $S_2$ , its parent  $\mathbf{T}_p$  may be subdivided by  $\text{SUB}_4^1$ ,  $\text{SUB}_4^2$ , or  $\text{SUB}_8$ , and no subdivision is needed for subtetrahedra of  $\mathbf{T}_p$  if  $\mathbf{T}_p$  is subdivided by  $\text{SUB}_4^1$  or  $\text{SUB}_4^2$ . Figure 5.5 illustrates possible split points on subtetrahedra of  $\mathbf{T}_p$  after  $\text{SUB}_8$  is applied to  $\mathbf{T}_p$  in step (4) of QLRs.

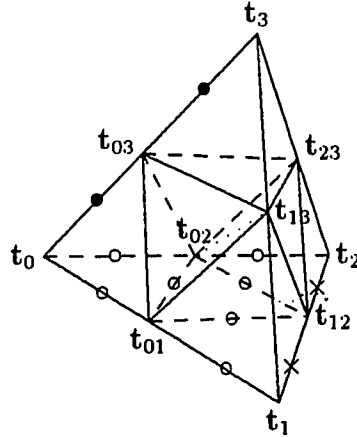


Figure 5.5: Illustration for possible split points after  $\text{SUB}_8$  is applied to  $\mathbf{T}$ 's parent  $\mathbf{T}_p(t_0, t_1, t_2, t_3)$ . Case 1:  $\mathbf{T}$  is a tetrahedron of type  $S_2$  (see Figure 5.4a); possible split points are on edges with  $\times$ . Case 2:  $\mathbf{T}$  is a tetrahedron of type  $S_4^1$  (see Figure 5.4b); possible split points are on edges with  $\times$  or  $\bullet$ . Case 3:  $\mathbf{T}$  is a tetrahedron of type  $S_4^2$  (see Figure 5.4c); possible split points are on edges with  $\times$  or  $\circ$ .

It is obvious that step (3) of QLRs will terminate in a finite number of steps, since in the worst case each regular edge, which is not an irregular edge, of  $\mathcal{T}^m$  has a split point.

To guarantee the validity of QLRS, we need to prove that step (4) of QLRS produces a conforming mesh.

**Theorem 5.5** *If  $\mathcal{T}^m$  is a conforming mesh, then step (4) of Algorithm QLRS produces a conforming mesh  $\mathcal{T}^{m+1}$ .*

**Proof.** Let  $\mathbf{T}$  be a tetrahedron of type  $S_2$ ,  $S_4^1$ , or  $S_4^2$  in  $\mathcal{T}^m$ , i.e.,  $\mathbf{T}$ 's parent  $\mathbf{T}_p$  has the configuration of Figure 5.4a, 5.4b, or 5.4c (we assume that  $\mathbf{T}_p$  has tetrahedron vertices  $\mathbf{t}_0$ ,  $\mathbf{t}_1$ ,  $\mathbf{t}_2$ , and  $\mathbf{t}_3$ ). We first prove that if  $\text{SUB}_8$  is applied to  $\mathbf{T}_p$  in step (4) of QLRS, each face of a subtetrahedron of  $\mathbf{T}_p$  has 0, 1, or 3 split points. Note that among edges of  $\mathbf{T}$  or  $\mathbf{T}$ 's sibling(s), only edges  $\mathbf{t}_1\mathbf{t}_{12}$ ,  $\mathbf{t}_2\mathbf{t}_{12}$  of Figure 5.4a (see Case 1 in Figure 5.5);  $\mathbf{t}_0\mathbf{t}_{03}$ ,  $\mathbf{t}_3\mathbf{t}_{03}$ ,  $\mathbf{t}_1\mathbf{t}_{12}$ ,  $\mathbf{t}_2\mathbf{t}_{12}$  of Figure 5.4b (see Case 2 in Figure 5.5); and all 9 edges on face  $\mathbf{t}_0\mathbf{t}_1\mathbf{t}_2$  of Figure 5.4c (see Case 3 in Figure 5.5) exist in subtetrahedra produced by applying  $\text{SUB}_8$  to  $\mathbf{T}_p$ . It can be easily verified that each face of a subtetrahedron of  $\mathbf{T}_p$  has 0, 1, or 3 edges of  $\mathcal{T}^m$ , and no pair of opposite edges in a subtetrahedron of  $\mathbf{T}_p$  are both in  $\mathcal{T}^m$ . This guarantees that no extra split point is needed for subtetrahedra of  $\mathbf{T}_p$  in order to satisfy that each face of a subtetrahedron does not have 2 split points, since only edges of  $\mathcal{T}^m$  may have split points. Therefore, it suffices to apply  $\text{SUB}_2$  or  $\text{SUB}_4^2$  to subtetrahedra of  $\mathbf{T}_p$  in step (4) of QLRS.

Now we prove that step (4) of QLRS produces a conforming mesh. It is obvious that any two tetrahedra cannot intersect in their interior. Therefore it suffices to prove that the resulting mesh is conforming on any face. Suppose  $F$  is an interior face in a conforming mesh  $\mathcal{T}^m$ ,  $m \geq 0$ . If  $F$  is a regular face, it will have the configuration of Figure 5.1a, 5.1c, or  $F$  itself at the end of step (4) of QLRS depending on the number of split points on the face, independent of the use of  $\text{SUB}_2$ ,  $\text{SUB}_4^1$ ,  $\text{SUB}_4^2$ , or  $\text{SUB}_8$  on the tetrahedra sharing  $F$ . If  $F$  is an irregular face, by step (4) of QLRS, either  $F$  does not change (in this case, the conformity is obvious) or the parents of the tetrahedra sharing  $F$  are first subdivided by  $\text{SUB}_8$  or  $\text{SUB}_4^2$  without producing non-conformity on  $F$ 's direct parent  $F'$ , i.e.  $F'$  is subdivided into the configuration of Figure 5.1a. Further possible subdivisions on the subfaces of  $F'$  can be treated just like the case for regular face, since the subfaces of  $F'$  are regular. Thus  $\mathcal{T}^{m+1}$  is conforming.  $\square$

Since we mainly use  $\text{SUB}_8$  in QLRS, Theorem 5.6 below gives a property similar to that in Theorem 5.2. A numerical bound on the shape of subtetrahedra produced by QLRS in terms of tetrahedron shape measure  $\eta$  is given in Theorem 5.7, which needs Lemma 5.3.



**Theorem 5.6** *For any initial mesh  $\mathcal{T}$ , there are only a finite number, which depends on the number of tetrahedra in  $\mathcal{T}$ , of classes of similar tetrahedra in all the refined tetrahedra generated by QLRS.*

**Proof.** Note that in QLRS, if a tetrahedron is subdivided to  $n \geq 1$  levels, SUB<sub>8</sub> is applied in the first  $n - 1$  levels of refinement, and each subtetrahedron is set to have the same subdivision pattern as its parent. At the  $n$ th level of refinement, SUB<sub>8</sub>, SUB<sub>2</sub>, SUB<sub>4</sub><sup>1</sup>, or SUB<sub>4</sub><sup>2</sup> is used. The theorem is established by Theorem 5.2, since each class of similar tetrahedra in the first  $n - 1$  levels of refinement produces at most 4 new classes of similar tetrahedra at the last step of refinement.  $\square$

**Lemma 5.3** *Let  $\mathbf{T}_k^1$  be any subtetrahedron generated by SUB<sub>2</sub>, SUB<sub>4</sub><sup>1</sup>, or SUB<sub>4</sub><sup>2</sup> applied to  $\mathbf{T}$ . Then*

$$\eta(\mathbf{T}_k^1) \geq 2\sqrt[3]{4}/11\eta(\mathbf{T}). \quad (5.3.1)$$

**Proof.** Let  $\mathbf{t}_{ij}$  denote the midpoint of  $\mathbf{t}_i\mathbf{t}_j$  and  $l_{ij} = |\mathbf{t}_i\mathbf{t}_j|$ . For a triangle  $\mathbf{t}_A\mathbf{t}_B\mathbf{t}_C$ ,

$$|\mathbf{t}_C\mathbf{t}_{AB}|^2 = (2l_{AC}^2 + 2l_{BC}^2 - l_{AB}^2)/4, \quad (5.3.2)$$

and for a tetrahedron with vertices  $\mathbf{t}_0, \mathbf{t}_1, \mathbf{t}_2, \mathbf{t}_3$ , by (5.2.10),

$$|\mathbf{t}_{03}\mathbf{t}_{12}|^2 = (l_{01}^2 + l_{23}^2 + l_{02}^2 + l_{13}^2 - l_{03}^2 - l_{12}^2)/4. \quad (5.3.3)$$

Case 1:  $\mathbf{T}_k^1$  is a subtetrahedron generated by SUB<sub>2</sub> (see Figure 5.4a). By simple algebraic manipulation using (5.3.2), (5.2.2), and the fact that the volume of  $\mathbf{T}_k^1$  is half the volume of  $\mathbf{T}$ , it follows that

$$\frac{\eta(\mathbf{T}_1^1(\mathbf{t}_0, \mathbf{t}_1, \mathbf{t}_{12}, \mathbf{t}_3))}{\eta(\mathbf{T})} = 2\sqrt[3]{2} \times \frac{\sum_{0 \leq i < j \leq 3} l_{ij}^2}{6l_{01}^2 + 6l_{13}^2 + 4l_{03}^2 + 2l_{23}^2 + 2l_{02}^2 - l_{12}^2} \geq \sqrt[3]{2}/3. \quad (5.3.4)$$

Similarly, we obtain

$$\eta(\mathbf{T}_2^1(\mathbf{t}_0, \mathbf{t}_2, \mathbf{t}_{12}, \mathbf{t}_3)) \geq \sqrt[3]{2}/3\eta(\mathbf{T}). \quad (5.3.5)$$

Case 2:  $\mathbf{T}_k^1$  is a subtetrahedron generated by SUB<sub>4</sub><sup>1</sup> (see Figure 5.4b). Using (5.3.2), (5.3.3), and (5.2.2), it follows that

$$\frac{\eta(\mathbf{T}_1^1(\mathbf{t}_0, \mathbf{t}_1, \mathbf{t}_{12}, \mathbf{t}_{03}))}{\eta(\mathbf{T})} = \sqrt[3]{4} \times \frac{\sum_{0 \leq i < j \leq 3} l_{ij}^2}{9l_{01}^2 + 3l_{13}^2 + 3l_{02}^2 + l_{23}^2 - l_{03}^2 - l_{12}^2}. \quad (5.3.6)$$

By the triangle inequality,

$$l_{01}^2 \leq 2(l_{03}^2 + l_{13}^2) \leq 2(l_{03}^2 + 2l_{12}^2 + 2l_{23}^2), \quad (5.3.7)$$

$$l_{01}^2 \leq l_{02}^2 + l_{03}^2 + l_{12}^2 + l_{13}^2. \quad (5.3.8)$$

Note that  $9l_{01}^2 = l_{01}^2 + 5l_{01}^2/2 + 11l_{01}^2/2$ ; if the first two items on the right side of this equality are replaced by (5.3.7) and (5.3.8), respectively, it follows that the denominator of the right side of (5.3.6) is  $\leq 11l_{01}^2/2 + 11l_{13}^2/2 + 11l_{02}^2/2 + 11l_{12}^2/2 + 5l_{23}^2 + 7l_{03}^2/2$ . Hence

$$\frac{\eta(\mathbf{T}_1^1(\mathbf{t}_0, \mathbf{t}_1, \mathbf{t}_{12}, \mathbf{t}_{03}))}{\eta(\mathbf{T})} \geq \frac{2\sqrt[3]{4}}{11}. \quad (5.3.9)$$

Similarly, for the other three subtetrahedra, we obtain the same bound as in (5.3.9).

Case 3:  $\mathbf{T}_k^1$  is a subtetrahedron generated by  $\text{SUB}_4^2$  (see Figure 5.4c). Using similar techniques as above, we obtain

$$\frac{\eta(\mathbf{T}_1^1(\mathbf{t}_0, \mathbf{t}_{01}, \mathbf{t}_{02}, \mathbf{t}_3))}{\eta(\mathbf{T})} = \sqrt[3]{4} \times \frac{\sum_{0 \leq i < j \leq 3} l_{ij}^2}{8l_{03}^2 + 2l_{13}^2 + 2l_{23}^2 + l_{12}^2} \geq \frac{\sqrt[3]{4}}{5}, \quad (5.3.10)$$

since  $3l_{03}^2 \leq 3l_{01}^2 + 3l_{02}^2 + 3l_{13}^2 + 3l_{23}^2$ . For the other two subtetrahedra in the corners, we obtain the same bound as in (5.3.10). For the subtetrahedron in the middle, we have

$$\frac{\eta(\mathbf{T}_4^1(\mathbf{t}_{01}, \mathbf{t}_{12}, \mathbf{t}_{02}, \mathbf{t}_3))}{\eta(\mathbf{T})} = \sqrt[3]{4} \times \frac{\sum_{0 \leq i < j \leq 3} l_{ij}^2}{4l_{03}^2 + 4l_{13}^2 + 4l_{23}^2} \geq \frac{\sqrt[3]{4}}{4}. \quad (5.3.11)$$

Combining (5.3.4), (5.3.5), (5.3.9), (5.3.10), and (5.3.11) yields (5.3.1).  $\square$

**Theorem 5.7** *If  $\mathbf{T}_i^n$  is a refined tetrahedron of any tetrahedron  $\mathbf{T}$  in  $\mathcal{T}$ , produced by QLRS, then*

$$\eta(\mathbf{T}_i^n) \geq c \eta(\mathbf{T}), \quad (5.3.12)$$

where  $c = \sqrt[3]{4}/11 \approx 0.1443$ .

**Proof.** If  $\mathbf{T}_i^n$  is of type  $S_8$ , then (5.3.12) follows from (5.2.3). Suppose  $\mathbf{T}_i^n$  is of type  $S_2, S_4^1$ , or  $S_4^2$ , and  $\mathbf{T}_j^{n-1}$  is the direct parent of  $\mathbf{T}_i^n$ ,  $n \geq 1$ . According to QLRS,  $\mathbf{T}_j^{n-1}$  is produced by repeatedly applying  $\text{SUB}_8$  to  $\mathbf{T}$ . By Theorem 5.3,

$$\eta(\mathbf{T}_j^{n-1}) \geq 0.5\eta(\mathbf{T}). \quad (5.3.13)$$

By Lemma 5.3,

$$\eta(\mathbf{T}_i^n) \geq 2\sqrt[3]{4}/11 \eta(\mathbf{T}_j^{n-1}). \quad (5.3.14)$$

Combining (5.3.13) and (5.3.14) yields (5.3.12).  $\square$

For any tetrahedron  $\mathbf{T}$  in  $\mathcal{T}^m$ ,  $m \geq 0$ , we recursively define the *subdivision level* of  $\mathbf{T}$ , denoted by  $\ell(\mathbf{T})$ , as follows. If  $\mathbf{T}$  is a tetrahedron of the initial mesh  $\mathcal{T}$ ,  $\ell(\mathbf{T}) = 0$ ; otherwise,  $\ell(\mathbf{T}) = \ell(\mathbf{T}_p) + 3$ ,  $\ell(\mathbf{T}_p) + 2$ , or  $\ell(\mathbf{T}_p) + 1$  if  $\mathbf{T}$  is a subtetrahedron produced by applying  $\text{SUB}_8$ ,  $\text{SUB}_4^1$  or  $\text{SUB}_4^2$ , or  $\text{SUB}_2$  to  $\mathbf{T}_p$ , respectively.

**Theorem 5.8** *For any interior face shared by two adjacent tetrahedra  $\mathbf{T}_L$  and  $\mathbf{T}_R$  in  $\mathcal{T}^m$ ,  $m \geq 0$ , generated by QLRs,  $|\ell(\mathbf{T}_L) - \ell(\mathbf{T}_R)| \leq 2$ , and the upper bound is tight.*

**Proof.** Let  $F$  be an interior face shared by two adjacent tetrahedra  $\mathbf{T}_L$  and  $\mathbf{T}_R$  in  $\mathcal{T}^m$ ,  $m \geq 0$ . We first prove by contradiction that if  $\mathbf{T}_L$  and  $\mathbf{T}_R$  are tetrahedra of type  $S_8$ ,  $\ell(\mathbf{T}_L) = \ell(\mathbf{T}_R)$ . Let  $\ell(\mathbf{T}_L) = 3p$ ,  $\ell(\mathbf{T}_R) = 3q < 3p$ , and  $0 < r \leq q$ . Note that when  $\text{SUB}_8$  is applied to a tetrahedron, each face of the tetrahedron is subdivided. Therefore, for any  $r$ , the ancestor  $\hat{\mathbf{T}}_L$  of  $\mathbf{T}_L$  at level  $3p - 3r$  must have a common face with the ancestor  $\hat{\mathbf{T}}_R$  of  $\mathbf{T}_R$  at level  $3q - 3r$ . Let  $r = q$ . Then  $\hat{\mathbf{T}}_R$  is a tetrahedron in the initial mesh, but  $\hat{\mathbf{T}}_L$  is a tetrahedron at level  $3(p - q)$ . These two tetrahedra cannot share a common face, a contradiction.

Suppose one of the two tetrahedra,  $\mathbf{T}_L$  say, is not a tetrahedron of type  $S_8$ . If  $\mathbf{T}_R$  is a tetrahedron of type  $S_8$ , then  $F$  must be like face  $t_0t_1t_3$  (or  $t_0t_2t_3$ ) in Figure 5.4a, or a subface of  $t_0t_1t_2$  in Figure 5.4c. In the former case,  $\ell(\mathbf{T}_R) = \ell(\mathbf{T}_L) - 1$ . In the latter case,  $\ell(\mathbf{T}_R) = \ell(\mathbf{T}_L) + 1$ .

Now suppose  $\mathbf{T}_R$  is also not a tetrahedron of type  $S_8$ . First, if  $F$  is an irregular face,  $\ell(\mathbf{T}_L) = \ell(\hat{\mathbf{T}}_L) + 1$  or  $\ell(\hat{\mathbf{T}}_L) + 2$ , and  $\ell(\mathbf{T}_R) = \ell(\hat{\mathbf{T}}_R) + 1$  or  $\ell(\hat{\mathbf{T}}_R) + 2$ , where  $\hat{\mathbf{T}}_L$  and  $\hat{\mathbf{T}}_R$  are  $\mathbf{T}_L$  and  $\mathbf{T}_R$ 's parents, respectively. So,  $|\ell(\mathbf{T}_L) - \ell(\mathbf{T}_R)| \leq 1$ , since  $\ell(\hat{\mathbf{T}}_R) = \ell(\hat{\mathbf{T}}_L)$  by the discussion in the first paragraph. Next, if  $F$  is a regular face, the types of  $\mathbf{T}_L$  and  $\mathbf{T}_R$  can be one of the following pairs  $(S_2, S_2)$ ,  $(S_4^2, S_4^2)$ , and  $(S_2, S_4^2)$ . For the first two pairs,  $\ell(\mathbf{T}_L) = \ell(\mathbf{T}_R)$ . For the final pair, suppose  $\mathbf{T}_L$  is a tetrahedron of type  $S_2$ , and  $\mathbf{T}_R$  is a tetrahedron of type  $S_4^2$ . Then the only possible situation is that the parent  $\hat{\mathbf{T}}_R$  of  $\mathbf{T}_R$  has a common face with the direct grandparent  $\hat{\mathbf{T}}_L$  of  $\mathbf{T}_L$ . Since  $\ell(\mathbf{T}_R) = \ell(\hat{\mathbf{T}}_R) + 2$ ,  $\ell(\mathbf{T}_L) = \ell(\hat{\mathbf{T}}_L) + 3 + 1$ , and  $\ell(\hat{\mathbf{T}}_R) = \ell(\hat{\mathbf{T}}_L)$ , it follows that  $\ell(\mathbf{T}_L) = \ell(\mathbf{T}_R) + 2$ .  $\square$

Note that if the maximum subdivision level of a tetrahedron in  $\mathcal{T}^k$  is  $\leq 3k$ , then the maximum subdivision level of a tetrahedron in  $\mathcal{T}^{k+1}$  is  $\leq 3(k+1)$ , since each subtetrahedron of a tetrahedron of type  $S_8$  in  $\mathcal{T}^k$  has subdivision level at most  $3k + 3$  in  $\mathcal{T}^{k+1}$ , and each

subtetrahedron of the parent of a tetrahedron of type  $S_2$ ,  $S_4^1$ , or  $S_4^2$  in  $\mathcal{T}^k$  has subdivision level at most  $3(k-1) + 3 + 2$  in  $\mathcal{T}^{k+1}$ . So, by induction on  $k$ , the maximum subdivision level of a tetrahedron in any  $\mathcal{T}^m$  is  $\leq 3m$ ,  $m \geq 0$ .

## 5.4 Data structure and algorithmic details

We use data structures similar to those described in Section 4.5. There are no changes for arrays  $VC$ ,  $XTM$ , and  $XVC$ . The  $BI$  array in QLRB is not needed. The only change to the fields of  $TM[i]$  (where  $TM[i]$  records information about the  $i$ th tetrahedron) is that the name of field  $bi$  is replaced by  $si$ , where  $si$  is zero if the tetrahedron belongs to the original mesh  $\mathcal{T}$  and is not subdivided; otherwise, it is an index of another array  $SI$  (subdivision information) which contains some necessary information for the subdivision of this tetrahedron. The fields of  $SI[TM[i].si]$  are  $nrcf, p, type, cf$ , where  $nrcf$  is an integer indicating the refinement step in which the  $i$ th tetrahedron is refined;  $p$  stores the index of the parent tetrahedron of the  $i$ th tetrahedron;  $type$  denotes the type (i.e.,  $S_8$ ,  $S_2$ ,  $S_4^1$ , or  $S_4^2$ ) of the  $i$ th tetrahedron;  $cf$  is an integer indicating either an edge or a face, depending on the type of the  $i$ th tetrahedron. That is, for a tetrahedron of type  $S_8$ ,  $cf$  indicates one of its base edges for choosing the centre edge of the  $i$ th tetrahedron; for a tetrahedron of type  $S_2$  or  $S_4^2$ ,  $cf$  indicates a regular face of the  $i$ th tetrahedron ( $t_0t_1t_3$  or  $t_0t_2t_3$  in Figure 5.4a, or a subface of face  $t_0t_1t_2$  in Figure 5.4c), and is used to determine the split edge  $t_1t_{12}$  or  $t_2t_{12}$  in the case of type  $S_2$  when combined with the record of the sibling of the  $i$ th tetrahedron;  $cf$  is not used for a tetrahedron of type  $S_4^1$ .  $TM$ ,  $VC$ ,  $SI$ ,  $XTM$ , and  $XVC$  are the basic data structures for our local refinement algorithm.

We still use the temporary hash table  $EHT$  to store all edges needing subdivision, i.e., an edge with a split point will be inserted into  $EHT$ . The two temporary stacks  $S_r$  and  $S_t$  are used to store subdivided edges and tetrahedra, respectively. Each edge  $e$  in  $S_r$  is associated with a tetrahedron incident on  $e$ . Stack  $S_t$  is used to store tetrahedra needing subdivision in this step of refinement. Also, the temporary hash table  $FHT$  is used to set fields  $t_1, t_2, t_3, t_4$  of  $TM[i]$  after the subdivision of tetrahedra in  $S_t$ .

With the above data structures, we describe an implementation of QLRS. We first determine the possible configuration of each tetrahedron  $\mathbf{T}$ , which needs refinement, according to step (3) of QLRS, and then perform the actual subdivision of  $\mathbf{T}$ ,  $\mathbf{T}$ 's parent, or  $\mathbf{T}$ 's sub-

tetrahedra. The following procedure PRESUBDIV is used to determine the configurations of tetrahedra needing refinement. When we say that an edge has a split point, it means that the edge is in  $EHT$ . To determine whether an edge has a split point,  $EHT$  must be searched.

```

Procedure PRESUBDIV( $S_e, S_t$ )
# Input: stack  $S_e$  of regular edges, which need to be subdivided,
#       and tetrahedra associated with these edges.
#Output: stack  $S_t$  of tetrahedra needing refinement
Set stack  $S_t$  to be empty
while  $S_e$  is not empty do
  Pop ( $e, \mathbf{T}$ ) from the top of  $S_e$ 
  for each tetrahedron  $\bar{\mathbf{T}}$  incident on  $e$  do
     $i :=$  index of  $\bar{\mathbf{T}}$  in  $TM$ 
    if not  $TM[i].flag$  then
      Push  $\bar{\mathbf{T}}$  onto  $S_t$  and set  $TM[i].flag$  to true
    endif
    for each regular face  $F$  of  $\bar{\mathbf{T}}$  with  $e$  as an edge of  $F$  do
      if  $F$  has two split points then
        Insert the edge  $e_1$  that does not have a split point into  $EHT$ 
        and push  $(e_1, \bar{\mathbf{T}})$  onto  $S_e$ 
      endif
    endfor
    if  $\bar{\mathbf{T}}$  is of type  $S_2$  (with  $e = t_1t_{12}$  or  $t_2t_{12}$ ),  $S_4^1$ , or  $S_4^2$  then
      for each unsplit edge  $c_1$  of  $\bar{\mathbf{T}}$ 's parent do
        Insert  $c_1$  into  $EHT$  and push  $(c_1, \bar{\mathbf{T}})$  onto  $S_e$ 
      endfor
    else if  $\bar{\mathbf{T}}$  is of type  $S_2$  with  $e = t_1t_3, t_2t_3, t_0t_1$ , or  $t_0t_2$  then
       $c_1 := t_2t_3, t_1t_3, t_0t_2$ , or  $t_0t_1$ , respectively
      Insert  $c_1$  into  $EHT$  and push  $(c_1, \bar{\mathbf{T}})$ 
      onto  $S_e$  if  $c_1$  is an unsplit edge
    endif
  endfor
endwhile

```

We now give the following pseudocode for QLRS.

#### Algorithm QLRS

```

# Input: initial conforming mesh  $\mathcal{T}$ 
# Output: refined conforming mesh  $\mathcal{T}$ 
 $m := 1$ 

```

```

repeat
  Choose a set  $S_m$  of tetrahedra from  $\mathcal{T}$ 
  Set stack  $S_e$  and  $EHT$  to be empty
  for each  $\mathbf{T}$  in  $S_m$  do
    if  $\mathbf{T}$  is a tetrahedron of type  $S_8$  then
      Set the subdivision information of  $\mathbf{T}$  in an  $SI$  record
      for each unsplit edge  $e$  of  $\mathbf{T}$  do
        Insert  $e$  into  $EHT$  and push  $(e, \mathbf{T})$  onto  $S_e$ 
      endfor
    else
      for each unsplit edge  $e$  of  $\mathbf{T}$ 's parent that is an
        edge of a tetrahedron  $\mathbf{T}_1$  in  $\mathcal{T}$  do
          Insert  $e$  into  $EHT$  and push  $(e, \mathbf{T}_1)$  onto  $S_e$ 
        endfor
      endif
    endfor
  endfor
  REFINEL( $\mathcal{T}, S_e, m$ )
   $m := m + 1$ 
until no more tetrahedra needed to be refined

```

Procedure REFINEL( $\mathcal{T}, S_e, m$ )

```

# Input: conforming mesh  $\mathcal{T}$ ; stack  $S_e$  of regular edges needing subdivision,
#       and tetrahedra associated with these edges;  $m$ , the refinement level
# Output: refined conforming mesh  $\mathcal{T}$ 
if  $S_e$  is not empty do
  PRESUBDIV( $S_e, S_t$ )
  for each tetrahedron  $\mathbf{T}$  in  $S_t$  do
    if  $\mathbf{T}$  is a tetrahedron of type  $S_8$  then
      Subdivide  $\mathbf{T}$  using  $SUB_8, SUB_2, SUB_4^1$ , or  $SUB_4^2$  according to
      the number of split points on  $\mathbf{T}$  and set each subtetrahedron
      of  $\mathbf{T}$  to have the same subdivision pattern as  $\mathbf{T}$ 
      if  $\mathbf{T}$  has one split point then
        Fill in the neighbor information of any subtetrahedron  $\mathbf{T}_1$  of  $\mathbf{T}$ 
        and a tetrahedron  $\mathbf{T}_2$  that shares a face with  $\mathbf{T}_1$  but is not in  $S_t$ 
      endif
    else
      Remove  $\mathbf{T}$ 's sibling(s); subdivide  $\mathbf{T}$ 's parent  $\mathbf{T}_p$ 
      using  $SUB_8, SUB_4^1$ , or  $SUB_4^2$ 
      if  $\mathbf{T}$  is of type  $S_2$  (with  $SUB_4^1$  or  $SUB_4^2$  is applied to  $\mathbf{T}_p$ ) or  $S_4^2$  then
        Fill in the neighbor information of any subtetrahedron  $\mathbf{T}_1$  of  $\mathbf{T}_p$ 
        and a tetrahedron  $\mathbf{T}_2$  that shares a face with  $\mathbf{T}_1$  but is not in  $S_t$ 
      endif
    endfor
  endfor
endif

```

```

endif
  Subdivide subtetrahedra of  $T_p$  using  $SUB_2$  or  $SUB_4^2$ 
  if there are a non-zero number of split points in the subtetrahedra
endif
  Add new subtetrahedra to the end of  $TM$ , update the  $SI$  records of
  these new tetrahedra, and add the new vertices to  $VC$ 
endfor
  Update corresponding information in  $XTM$ ,  $XVC$ 
  Set hash table  $FHT$  to be empty
(A) Scan new tetrahedra to fill out neighbor information using hash table  $FHT$ 
endif

```

## 5.5 Time complexity

Now we analyze the time complexity for one step of refinement, i.e., for procedure REFINE1. We assume that the table sizes of  $EHT$  and  $FHT$  are sufficiently large, and good hashing functions are used (the same hashing functions as in QLRB are used), so the expected time complexity of insertion and deletion of an element to  $EHT$  and  $FHT$  is  $O(1)$  (otherwise a balanced tree data structure with a logarithmic time complexity can be used to get a better worst case time complexity) [AHU74]. Note that in procedure PRESUBDIV, we only deal with edges needing subdivision, i.e., all tetrahedra incident on a subdivided edge are pushed onto  $S_t$ , and for any subdivided edge  $e$  and tetrahedron  $T$  incident on  $e$ , the neighbors of  $T$  incident on  $e$  can be found in a constant time. So, the time complexity for PRESUBDIV is  $O(|S_t|)$ , where  $|S_t|$  is the number of tetrahedra in  $S_t$ , since there are at most 6 subdivided edges for each tetrahedron. Suppose  $N$  is the number of new refined tetrahedra in this step of refinement. As the time used for subdivision of each tetrahedron in  $S_t$  is constant (any tetrahedron of  $S_t$  or its parent is subdivided into 2 to 20 subtetrahedra), and the time spent on line (A) of REFINE1 is  $O(N)$ , the expected time complexity of REFINE1 is  $O(|S_t|) + O(N) = O(N)$ .

## 5.6 Summary

We have presented a local refinement algorithm based mainly on an 8-subtetrahedron subdivision, and have shown that the algorithm produces guaranteed-quality meshes in an expected time complexity that is linearly related to the number of refined tetrahedra in a refined mesh. The theoretical estimate of the constant  $c$  in Theorem 5.7 is better than the constant in Theorem 4.4 for QLRB. If the degeneration on the shape of tetrahedra produced by irregular refinement is ignored, QLRS produces meshes with very good quality by Theorem 5.3. Further comparisons between QLRB and QLRS are given in Section 6.4.

The algorithm presented here is preferable if the mesh in a refined region is relatively coarse; otherwise, the one described in the previous chapter may be better. It is worth considering the situation that QLRS is applied to some parts of a refined region while QLRB is used in other parts. A critical problem is to ensure a conforming mesh with guaranteed-quality when the expansion of refinement from different parts meet each another.

After obtaining the results in this chapter, we discovered that a similar procedure to TRANSUB is presented in Ong's Ph.D. thesis [Ong89]. But instead of using one canonical tetrahedron as in TRANSUB, a tetrahedron  $T$  may be transformed to one of four canonical tetrahedra in Ong's procedure, and the centre edges of  $T$  and subtetrahedra of  $T$  are controlled by the types of the canonical tetrahedra. No discussion is provided for choosing centre edges on  $T$  and subtetrahedra of  $T$  directly without involving affine transformations as in SUBDIV. The quality of refined tetrahedra is given in terms of  $\zeta = 2r_{in}/d$ , where  $d$  is the diameter and  $r_{in}$  is the inradius of a tetrahedron. It is proved in [Ong89] that  $\zeta(T_i^n) \geq 0.043 \zeta(T)$ , where  $T_i^n$  is any tetrahedron at level  $n$ , which means that the shape of any refined tetrahedron is at least 0.043 times as good as the shape of the original tetrahedron in terms of  $\zeta$ . However, we get a much better bound in Theorem 5.3, which states that the shape of any refined tetrahedron is at least 0.5 times as good as the shape of the original tetrahedron in terms of  $\eta$ . Note that Ong's method is used in [BEK93], combined with four types of irregular refinement (i.e., the configurations in Figure 5.4 plus a case in which a tetrahedron has 2 split points on a single face) at the boundary of a refined region. But no theoretical and experimental results on the quality of refined meshes are provided in [BEK93]. Also, implementation details (e.g. algorithmic procedures, data structures, etc.) and the time complexity are not discussed.



## Chapter 6

### Performance of the Algorithms

We have implemented algorithms QLRB and QLRS in the C programming language, and here we report on the quality of tetrahedra in terms of tetrahedron shape measure  $\eta$ . The reason for using  $\eta$  is because our theoretical results are based on it, and we don't know whether Theorems 4.4 and 5.7 hold for other (valid) tetrahedron shape measures. By the “equivalence” of tetrahedron shape measures as described in Chapter 2, we can expect similar statistical results based on other tetrahedron shape measures, e.g., radius ratio  $\rho$ , minimum solid angle  $\theta_{min}$ , etc. In fact, we did obtain similar results based on  $\rho$  and  $\theta_{min}$ .

The quantities used to measure the quality at each level of refinement are the number of tetrahedra NTET in current mesh, the minimum mean ratio  $\eta_{min}$  (over all tetrahedra), the average mean ratio  $\eta_{ave}$ , and the percentage of tetrahedra whose  $\eta$  value is less/greater than a certain number. The mean ratio  $\eta$  ( $0 < \eta \leq 1$ ) approaches zero or the maximum value for a poorly-shaped or well-shaped tetrahedron, respectively. In our experiments, a tetrahedron with  $\eta < 0.3$  (or  $\eta \geq 0.7$ ) is considered poorly-shaped (or well-shaped).

Let NREF denote the number of refinement levels, NTC and NTR denote the number of tetrahedra chosen for refinement and the number of tetrahedra actually refined at each step of refinement, respectively. Let CPUT denote the CPU time spent at each step of refinement in seconds (not including the time in choosing a set of tetrahedra for refinement), and NNT denote the number of new tetrahedra produced at each step of refinement. Then the ratio NTR/NTC reflects the expansion of refinement at a refined region, and CPUT/NNT reflects an empirical time complexity of the algorithms.

## 6.1 Test examples

In [RiL92], a local refinement algorithm based on longest edge bisection is presented, and experimental results are given for five single tetrahedra. We use the first four tetrahedra, listed in Table 6.1, as our test examples. P1 and P2 are well-shaped tetrahedra; P3 is a poorly-shaped tetrahedron; P4 is the regular tetrahedron, where  $\sqrt{3}$  and  $\sqrt{2}$  are rounded to 16 decimal places. We omit the last example in [RiL92], since it is the same as P4 except that the number of digits after the decimal point in the coordinate is different.

P1 $\eta = 0.8846$			P2 $\eta = 0.8399$			P3 $\eta = 0.2835$			P4 $\eta = 1.0000$		
0.0	0.0	0.0	0.0	0.0	0.0	0.0	0.0	0.0	0.0	0.0	0.0
4.0	2.0	2.0	4.0	0.0	0.0	0.5	0.0	0.0	$2\sqrt{3}$	0.0	0.0
1.0	5.0	0.0	0.0	4.0	0.0	1.5	5.0	2.0	$\sqrt{3}$	3.0	0.0
0.5	0.5	5.0	0.0	0.0	4.0	0.5	0.5	5.0	$\sqrt{3}$	1.0	$2\sqrt{2}$

Table 6.1: Problems 1 to 4

We also provide experimental results for tetrahedral meshes in two polyhedral regions (one is a convex polyhedron, Figure 1a in [Joe91a], see Figure 6.1; the other is a U-shaped region, Figure 10 in [Joe94], see Figure 6.2). The initial tetrahedral meshes of the two polyhedral regions are generated by the methods described in [Joe91a, Joe94]. The convex polyhedron is subdivided into 273 tetrahedra, and has minimum mean ratio 0.6230 after local transformations [Joe89], which are based on two different triangulations of certain configurations of five distinct non-coplanar 3-D points, are applied to obtain an improved-quality mesh with respect to radius ratio  $\rho$ . Similarly, the U-shaped object is subdivided into 466 tetrahedra with minimum mean ratio 0.5580 after local transformations are performed.

For a single tetrahedron, we refine all tetrahedra in a mesh at each step of refinement as in [RiL92]. For the two tetrahedral meshes, a fixed point on each object is chosen as the center of a sphere; at each step of refinement, we refine any tetrahedron that has at least one vertex in the sphere, and reduce the radius of the sphere by a factor in the next refinement. The tests were done on a Sun 4/25 (ELC) workstation running the Sun O/S 4.1.3.

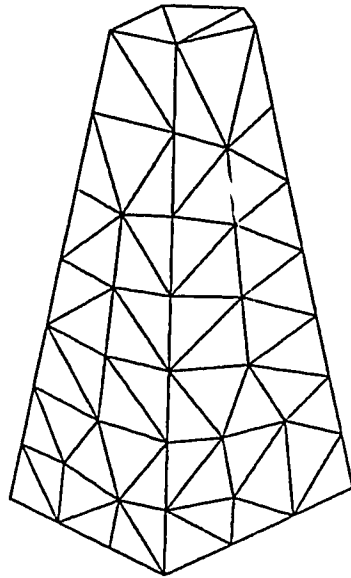


Figure 6.1: An original mesh of the convex polyhedron.

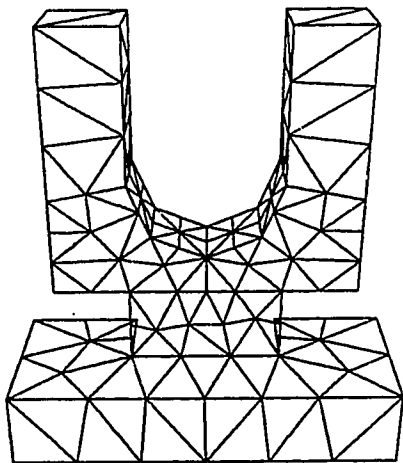


Figure 6.2: An original mesh of the U-shaped object.

## 6.2 Experimental results for QLRB

We first compare experimental results based on QLRB with those from longest edge bisection. The left parts of Tables 6.2 to 6.5 show the results reproduced based on longest edge bisection with respect to the shape measure  $\eta$ . The number of tetrahedra at each level are quite different from those reported in [RiL92], except in Table 6.2, which is exactly the same as in [RiL92]. The reason for this is because the algorithm based on longest edge bisection is extremely unstable in terms of the number of tetrahedra produced. Since there are many tie cases (more than one edge with longest length in subtetrahedra) in the given examples, different tie-breaking strategies will produce significantly different results. This phenomenon was also reported in [RiL92], where the number of tetrahedra at level 10 for Problem 4 is 17478, but if  $\sqrt{3}$  and  $\sqrt{2}$  in Table 6.1 are rounded to 2 decimal places (Table V in [RiL92]), the number of tetrahedra at level 10 is only 3966. Experimental results based on QLRB for the four problems are given in the right parts of Tables 6.2 to 6.5.

NREF	Longest edge bisection					QLRB				
	NTET	$\eta_{min}$	$\eta_{ave}$	$\eta$		NTET	$\eta_{min}$	$\eta_{ave}$	$\eta$	
0	1	0.8846	0.8846	0.00	100.00	1	0.8846	0.8846	0.00	100.00
1	2	0.8425	0.8464	0.00	100.00	2	0.8425	0.8464	0.00	100.00
2	4	0.7306	0.7555	0.00	100.00	4	0.7306	0.7555	0.00	100.00
3	8	0.6819	0.7714	0.00	62.50	8	0.6819	0.7714	0.00	62.50
4	16	0.6669	0.7900	0.00	75.00	16	0.6669	0.7900	0.00	75.00
5	38	0.5709	0.7359	0.00	76.32	32	0.6558	0.7326	0.00	75.00
6	86	0.4792	0.7611	2.33	60.47	64	0.6634	0.7451	0.00	46.88

Table 6.2: Bisection results for Problem 1

NREF	Longest edge bisection					QLRB				
	NTET	$\eta_{min}$	$\eta_{ave}$	$\eta$		NTET	$\eta_{min}$	$\eta_{ave}$	$\eta$	
0	1	0.8399	0.8399	0.00	100.00	1	0.8399	0.8399	0.00	100.00
1	2	0.7326	0.7326	0.00	100.00	2	0.7326	0.7326	0.00	100.00
2	4	0.6667	0.7619	0.00	50.00	4	0.6667	0.7619	0.00	50.00
3	8	0.6574	0.7832	0.00	75.00	8	0.5040	0.7178	0.00	50.00
4	16	0.6350	0.7204	0.00	87.50	16	0.5603	0.6680	0.00	62.50
5	32	0.5455	0.7472	0.00	43.75	32	0.4000	0.6762	18.75	31.25
6	102	0.4582	0.7399	3.92	66.67	64	0.5040	0.6548	0.00	31.25

Table 6.3: Bisection results for Problem 2

By comparing Tables 6.2 to 6.5, some remarks are in order. First, the number of subtetrahedra generated in QLRB is much fewer than from longest edge bisection when

NREF	Longest edge bisection					QLRB				
	NTET	$\eta_{min}$	$\eta_{ave}$	$\eta$		NTET	$\eta_{min}$	$\eta_{ave}$	$\eta$	
0	1	0.2835	0.2835	0.00	0.00	1	0.2835	0.2835	0.00	0.00
1	2	0.2102	0.2506	0.00	0.00	2	0.2102	0.2506	0.00	0.00
2	4	0.1826	0.2623	25.00	25.00	4	0.1826	0.2623	25.00	25.00
3	8	0.1811	0.2674	25.00	12.50	8	0.1811	0.2400	25.00	0.00
4	19	0.2026	0.2961	0.00	15.79	16	0.2087	0.2443	0.00	0.00
5	61	0.1382	0.3052	16.40	22.95	32	0.1689	0.2582	37.50	25.00
6	192	0.1648	0.3164	16.15	22.40	64	0.1695	0.2372	31.25	0.00

Table 6.4: Bisection results for Problem 3

NREF	Longest edge bisection					QLRB				
	NTET	$\eta_{min}$	$\eta_{ave}$	$\eta$		NTET	$\eta_{min}$	$\eta_{ave}$	$\eta$	
0	1	1.0000	1.0000	0.00	100.00	1	1.0000	1.0000	0.00	100.00
1	2	0.7957	0.7957	0.00	100.00	2	0.7957	0.7957	0.00	100.00
2	4	0.6350	0.6838	0.00	50.00	4	0.6350	0.6838	0.00	50.00
3	8	0.5455	0.7030	0.00	25.00	8	0.5455	0.7030	0.00	25.00
4	32	0.4615	0.6791	9.38	50.00	16	0.4877	0.6667	12.50	50.00
5	85	0.4535	0.6858	5.88	40.00	32	0.5603	0.6529	0.00	37.50
6	306	0.4582	0.6850	4.90	45.43	64	0.4286	0.6564	18.75	25.00

Table 6.5: Bisection results for Problem 4

$NREF \geq 6$ . This indicates in general that the conforming procedure in QLRB converges much faster than in longest edge bisection. For these specific examples, the number of tetrahedra is exactly doubled with the increase of bisection levels in QLRB, but is about tripled in longest edge bisection. The number of tetrahedra produced by longest edge bisection is  $> 10,000$  by level 10 or 11, but only about 2000 by QLRB for these examples. We feel that introducing too many tetrahedra is a main disadvantage of longest edge bisection, since this increases not only the time spent on refinement, but also the finite element analysis. Next, the quality of meshes generated by both algorithms is comparable. Observing the minimum shape measure  $\eta_{min}$  at different bisection levels, QLRB obtains better results for more cases, especially for Problems 1 and 3. However, longest edge bisection produces better  $\eta_{ave}$  values. It seems that performing longest edge bisection on a poor tetrahedron tends to improve the shapes of some subtetrahedra (see Problem 3), but at the same time the shapes of a small portion of subtetrahedra become worse. Third, QLRB in general creates much fewer number of classes of similar tetrahedra than longest edge bisection from our experiments. Finally, the constant  $c$  in Theorem 4.4 is pessimistic, compared with the experimental results. It seems that  $c$  is at least 0.4, although it is hard to obtain a tight bound.

Since the class of a tetrahedron uniquely determines the bisection of the tetrahedron, the bisection at each step may not be optimal with respect to the tetrahedron shape measure. Therefore, local transformations can be applied with respect to some criteria, such as locally improving the minimum tetrahedron shape measure value. The algorithms in [Joe89, Joe93] can be used to substantially improve the quality of tetrahedra towards an optimal mesh with respect to  $\eta$ . To keep the properties in Theorems 4.3 and 4.4, we only apply local transformations to the final refined mesh, i.e., no refinement is applied to meshes improved by local transformations. The improvements are significant, especially at some levels  $3k, k > 0$ . The results are provided in Tables 6.6 and 6.7.

NREF	Problem 1					Problem 2				
	NTET	$\eta_{min}$	$\eta_{ave}$	$\eta$ < 0.5	$\eta$ ≥ 0.7	NTET	$\eta_{min}$	$\eta_{ave}$	$\eta$ < 0.5	$\eta$ ≥ 0.7
0	1	0.8846	0.8846	0.00	100.00	1	0.8399	0.8399	0.00	100.00
1	2	0.8425	0.8464	0.00	100.00	2	0.7326	0.7326	0.00	100.00
2	4	0.7306	0.7555	0.00	100.00	4	0.8571	0.8929	0.00	100.00
3	8	0.8664	0.9068	0.00	100.00	8	0.6872	0.7789	0.00	87.50
4	16	0.6669	0.7900	0.00	75.00	16	0.5603	0.6680	0.00	62.50
5	32	0.6558	0.7326	0.00	75.00	32	0.4000	0.7253	18.75	50.00
6	64	0.8664	0.9124	0.00	100.00	64	0.6872	0.7626	0.00	90.62

Table 6.6: Improved-quality meshes from QLRB results for Problems 1 and 2

NREF	Problem 3					Problem 4				
	NTET	$\eta_{min}$	$\eta_{ave}$	$\eta$ < 0.2	$\eta$ ≥ 0.4	NTET	$\eta_{min}$	$\eta_{ave}$	$\eta$ < 0.5	$\eta$ ≥ 0.7
0	1	0.2835	0.2835	0.00	0.00	1	1.0000	1.0000	0.00	100.00
1	2	0.2102	0.2506	0.00	0.00	2	0.7957	0.7957	0.00	100.00
2	4	0.2026	0.2884	0.00	25.00	4	0.6350	0.6838	0.00	50.00
3	7	0.2088	0.2632	0.00	0.00	8	0.8571	0.9286	0.00	100.00
4	16	0.2087	0.2443	0.00	0.00	16	0.7200	0.7664	0.00	100.00
5	32	0.2026	0.3669	0.00	62.50	32	0.5603	0.6529	0.00	37.50
6	61	0.2088	0.2760	0.00	0.00	64	0.8571	0.9107	0.00	100.00

Table 6.7: Improved-quality meshes from QLRB results for Problems 3 and 4

We now give experimental results based on two tetrahedral meshes. Let IMPR be the algorithm which applies local transformations to obtain an improved-quality mesh with respect to mean ratio  $\eta$ . Tables 6.8 and 6.9 give the performance of QLRB and IMPR. The results seem to confirm that  $\eta_{min}$  and  $\eta_{ave}$  converge asymptotically to a fixed value for both QLRB and IMPR. Note that, with the increase of bisection level, local transformations increase the number of tetrahedra. That is because there are many “flat” tetrahedra (one of vertices of a tetrahedron is near the centroid of its opposite face) after QLRB. This does not

contradict previous results reported in [Joe93], where the number of tetrahedra in general decreases after local transformations, since the starting triangulation there is Delaunay or nearly Delaunay, and may include many “sliver” tetrahedra.

NREF	QLRB					IMPR				
	NTET	$\eta_{min}$	$\eta_{ave}$	$\eta$		NTET	$\eta_{min}$	$\eta_{ave}$	$\eta$	
				< 0.5	$\geq 0.7$				< 0.5	$\geq 0.7$
0	273	0.6230	0.8185	0.00	92.67	271	0.6230	0.8203	0.00	92.62
1	303	0.4671	0.8058	0.33	86.14	304	0.5313	0.8115	0.00	89.47
2	403	0.5064	0.7850	0.00	80.15	399	0.5610	0.8036	0.00	88.72
3	995	0.3185	0.7396	2.31	67.64	1005	0.5231	0.7794	0.00	81.39
4	1082	0.3185	0.7403	2.22	67.19	1095	0.5231	0.7792	0.00	80.37
5	1208	0.2918	0.7331	2.57	64.49	1225	0.5231	0.7745	0.00	77.88
6	1266	0.2918	0.7342	2.45	64.53	1285	0.5231	0.7730	0.00	77.28

Table 6.8: QLRB and IMPR results for a convex polyhedron

NREF	QLRB					IMPR				
	NTET	$\eta_{min}$	$\eta_{ave}$	$\eta$		NTET	$\eta_{min}$	$\eta_{ave}$	$\eta$	
				< 0.5	$\geq 0.7$				< 0.5	$\geq 0.7$
0	466	0.5580	0.7651	0.00	80.47	464	0.5825	0.7664	0.00	80.17
1	499	0.5198	0.7617	0.00	79.36	498	0.5825	0.7637	0.00	79.12
2	601	0.4059	0.7524	0.83	74.71	597	0.5540	0.7662	0.00	78.73
3	784	0.4321	0.7407	1.15	71.17	781	0.5644	0.7705	0.00	78.23
4	1158	0.3568	0.7252	3.02	63.30	1158	0.4956	0.7656	0.09	76.51
5	1375	0.3568	0.7231	3.42	62.47	1381	0.4956	0.7715	0.07	77.26
6	1435	0.3568	0.7239	3.34	62.58	1443	0.4956	0.7707	0.07	77.41

Table 6.9: QLRB and IMPR results for a U-shaped object

Finally, we discuss the “locality” of algorithm QLRB and the CPU times spent at each step of refinement. Tables 6.10 and 6.11 list NTC, NTR, NTR/NTC, CPUT, NNT, CPUT/NNT, and NTET for the two polyhedral regions. At each step of refinement, we choose either a small number of tetrahedra around a fixed point (Table 6.10) or a relatively large number of tetrahedra around a line segment (Table 6.11) for refinement. The experimental results show that the ratio NTR/NTC is bounded above by a small positive constant (i.e., NTR does not expand rapidly against NTC), which is what we expect for “local” refinement. Tables 6.10 and 6.11 also show an approximately linear time complexity of QLRB with respect to NNT.

Graphical illustrations for the refined meshes of two polyhedral regions based on QLRB are given in Figures 6.3 to 6.8 at the end of this chapter. For each object, we choose a point or line segment on the object as a reference for refinement, i.e. a tetrahedron is chosen for refinement if it has at least one vertex that is within a certain distance from the selected

point or line segment. Figures 6.3 and 6.4 correspond to the refined meshes in the right parts of Tables 6.8 and 6.9 with  $NREF = 4$ . All refined meshes in the figures are the results after local transformations are applied, and only boundary triangulations (with backfacing triangles removed) are shown.

	NREF	NTC	NTR	NTR/NTC	CPUT	NNT	CPUT/NNT	NTET
Convex Polyhedron	1	8	22	2.75	0.03	52	0.00058	273
	2	31	62	2.00	0.10	162	0.00062	303
	3	52	262	5.04	0.48	854	0.00056	403
	4	45	63	1.40	0.08	150	0.00053	995
	5	31	88	2.75	0.13	214	0.00061	1082
U-shaped Object	1	17	22	1.29	0.05	55	0.00091	466
	2	40	56	1.40	0.10	158	0.00063	499
	3	75	106	1.41	0.18	289	0.00062	601
	4	120	185	1.54	0.33	559	0.00059	784
	5	104	128	1.23	0.23	345	0.00067	1158

Table 6.10: Expansion of refinement and CPU times around a fixed point for QLRB

	NREF	NTC	NTR	NTR/NTC	CPUT	NNT	CPUT/NNT	NTET
Convex Polyhedron	1	45	81	1.80	0.15	214	0.00070	273
	2	94	125	1.33	0.18	309	0.00058	406
	3	146	262	1.79	0.48	801	0.00060	590
	4	306	1085	3.55	2.55	4023	0.00063	1129
	5	623	1020	1.64	1.78	2697	0.00066	4067
U-shaped Object	1	38	73	1.29	0.15	205	0.00073	466
	2	143	287	2.01	0.63	995	0.00063	598
	3	415	821	1.98	1.97	3027	0.00065	1306
	4	1503	2477	1.65	5.57	7918	0.00070	3512
	5	3680	5462	1.48	12.05	16230	0.00074	8953

Table 6.11: Expansion of refinement and CPU times around a line segment for QLRB

### 6.3 Experimental results for QLRS

Similar tests were done for QLRS on the four single tetrahedra in Table 6.1 and two tetrahedral meshes in Figures 6.1 and 6.2. Tables 6.12 to 6.14 show experimental results based on QLRS. Again, these results confirm that  $\eta_{min}$  and  $\eta_{ave}$  converge asymptotically to a fixed value for QLRS, and the experimental results indicate that the theoretical estimate of the constant  $c$  in Theorem 5.7 is pessimistic (since we do not have a tight bound). Improved-quality meshes after application of local transformations are given in Tables 6.15 to 6.17. Note that there are no changes for Problem 4 and very few changes for Problem 1 after



local transformations are applied. Overall, the improvements on the quality are not very significant in terms of  $\eta_{min}$ , compared with the improved results for QLRB. This may imply that QLRS produces tetrahedra of relatively good shape.

Tables 6.18 and 6.19 show the locality of the algorithm and corresponding CPU times for each refinement. Again, NTR/NTC is bounded above by a small positive constant, and CPUT and NNT show a roughly linear relationship. Graphical illustrations for the refined meshes of two polyhedral regions based on QLRS are given in Figures 6.9 to 6.14 at the end of this chapter. Figures 6.9 and 6.10 correspond to the refined meshes in Table 6.17 with NREF = 2.

NREF	Problem 1					Problem 2				
	NTET	$\eta_{min}$	$\eta_{ave}$	$\eta$		NTET	$\eta_{min}$	$\eta_{ave}$	$\eta$	
0	1	0.8846	0.8846	0.00	100.00	1	0.8399	0.8399	0.00	100.00
1	8	0.8664	0.9069	0.00	100.00	8	0.6872	0.7808	0.00	75.00
2	64	0.8664	0.9124	0.00	100.00	64	0.6872	0.7660	0.00	68.75
3	512	0.8664	0.9138	0.00	100.00	512	0.6872	0.7623	0.00	67.19

Table 6.12: QLRS results for Problems 1 and 2

NREF	Problem 3					Problem 4				
	NTET	$\eta_{min}$	$\eta_{ave}$	$\eta$		NTET	$\eta_{min}$	$\eta_{ave}$	$\eta$	
0	1	0.2835	0.2835	0.00	0.00	1	1.0000	1.0000	0.00	100.00
1	8	0.2756	0.2819	0.00	0.00	8	0.8571	0.9286	0.00	100.00
2	64	0.2756	0.2815	0.00	0.00	64	0.8571	0.9107	0.00	100.00
3	512	0.2756	0.2814	0.00	0.00	512	0.8571	0.9062	0.00	100.00

Table 6.13: QLRS results for Problems 3 and 4

NREF	Convex Polyhedron					U-shaped Object				
	NTET	$\eta_{min}$	$\eta_{ave}$	$\eta$		NTET	$\eta_{min}$	$\eta_{ave}$	$\eta$	
0	273	0.6230	0.8185	0.00	92.67	466	0.5580	0.7651	0.00	80.47
1	419	0.4265	0.7790	2.63	80.91	588	0.4373	0.7628	1.19	79.25
2	843	0.3729	0.7611	5.10	79.12	931	0.3957	0.7514	3.33	74.33
3	1392	0.3729	0.7616	4.24	78.38	1494	0.3877	0.7430	4.95	73.09
4	1830	0.3729	0.7611	3.88	77.54	2020	0.3877	0.7378	5.74	72.13

Table 6.14: QLRS results for two polyhedral regions

NREF	Problem 1					Problem 2				
	NTET	$\eta_{min}$	$\eta_{ave}$	$\eta$		NTET	$\eta_{min}$	$\eta_{ave}$	$\eta$	
				< 0.5	$\geq 0.7$				< 0.5	$\geq 0.7$
0	1	0.8846	0.8846	0.00	100.00	1	0.8399	0.8399	0.00	100.00
1	8	0.8664	0.9068	0.00	100.00	8	0.6872	0.7789	0.00	87.50
2	64	0.8664	0.9124	0.00	100.00	64	0.6872	0.7626	0.00	90.62
3	512	0.8664	0.9138	0.00	100.00	512	0.6872	0.7581	0.00	94.53

Table 6.15: Improved-quality meshes from QLRS results for Problems 1 and 2

NREF	Problem 3					Problem 4				
	NTET	$\eta_{min}$	$\eta_{ave}$	$\eta$		NTET	$\eta_{min}$	$\eta_{ave}$	$\eta$	
				< 0.2	$\geq 0.4$				< 0.5	$\geq 0.7$
0	1	0.2835	0.2835	0.00	0.00	1	1.0000	1.0000	0.00	100.00
1	8	0.2756	0.2826	0.00	0.00	8	0.8571	0.9286	0.00	100.00
2	64	0.2756	0.2826	0.00	0.00	64	0.8571	0.9107	0.00	100.00
3	512	0.2756	0.2828	0.00	0.00	512	0.8571	0.9062	0.00	100.00

Table 6.16: Improved-quality meshes from QLRS results for Problems 3 and 4

NREF	Convex Polyhedron					U-shaped Object				
	NTET	$\eta_{min}$	$\eta_{ave}$	$\eta$		NTET	$\eta_{min}$	$\eta_{ave}$	$\eta$	
				< 0.5	$\geq 0.7$				< 0.5	$\geq 0.7$
0	271	0.6230	0.8203	0.00	92.62	464	0.5825	0.7664	0.00	80.17
1	415	0.4297	0.7804	2.41	82.41	586	0.5554	0.7688	0.00	79.86
2	838	0.4297	0.7735	2.15	81.62	929	0.4458	0.7611	0.75	76.21
3	1388	0.4297	0.7710	1.51	80.04	1491	0.4348	0.7536	1.27	73.91
4	1825	0.4297	0.7700	1.15	79.01	2014	0.4159	0.7478	1.84	72.44

Table 6.17: Improved-quality meshes from QLRS results for two polyhedral regions

	NREF	NTC	NTR	NTR/NTC	CPUT	NNT	CPUT/NNT	NTET
Convex Polyhedron	1	15	38	2.53	0.08	184	0.00043	273
	2	38	116	3.05	0.27	540	0.00050	419
	3	62	121	1.95	0.30	670	0.00045	843
	4	47	100	2.13	0.28	538	0.00052	1392
	5	24	54	2.25	0.15	276	0.00054	1830
U-shaped Object	1	14	26	1.86	0.08	148	0.00054	466
	2	39	76	1.95	0.20	419	0.00048	588
	3	64	123	1.92	0.33	686	0.00048	931
	4	57	116	2.04	0.33	642	0.00051	1494
	5	41	87	2.12	0.25	464	0.00054	2020

Table 6.18: Expansion of refinement and CPU times around a fixed point for QLRS

	NREF	NTC	NTR	NTR/NTC	CPUT	NNT	CPUT/NNT	NTET
Convex Polyhedron	1	45	114	2.53	0.25	568	0.00044	273
	2	92	247	2.68	0.58	1182	0.00049	727
	3	182	517	2.84	1.23	2406	0.00051	1662
	4	350	936	2.67	2.55	4446	0.00057	3551
	5	686	1832	2.67	5.17	8702	0.00059	7061
U-shaped Object	1	38	107	2.82	0.23	498	0.00046	466
	2	146	407	2.79	1.10	2069	0.00053	857
	3	348	1039	2.99	2.72	4884	0.00056	2519
	4	508	1334	2.63	3.67	6624	0.00055	6364
	5	810	2209	2.73	6.40	10893	0.00059	11654

Table 6.19: Expansion of refinement and CPU times around a line segment for QLRS

## 6.4 Summary

Experimental results in Sections 6.2 and 6.3 demonstrate a very high quality performance of our local refinement algorithms for the test examples, i.e. good quality of refined meshes, locality of the algorithms, and empirical linear time complexity. The graphical illustrations for two tetrahedral meshes further show the locality of the algorithms. The degeneration of  $\eta_{min}$  in any refined mesh is never greater than 0.4 for all the test examples. Possible improvements on the constants of Theorems 4.4 and 5.7 may help us to explain the high quality of refined meshes produced by our algorithms.

Comparing the results produced by QLRS at NREF = 6 and QLRS at NREF = 2, we have following comments. First, QLRS produces refined meshes with better quality than QLRS in terms of  $\eta_{min}$  and  $\eta_{ave}$  for all the test examples. However, QLRS has the advantage of providing more flexibility for choosing the levels of refinement, which is useful for adaptive finite element analysis. Secondly, after local transformations are applied to meshes produced by QLRS and QLRS for Problems 1 to 4, the resulting meshes have very similar quality in terms of  $\eta_{min}$  and  $\eta_{ave}$ , e.g. the corresponding meshes for Problems 1, 2, and 4 have the exactly same  $\eta_{min}$  and  $\eta_{ave}$  values (see Tables 6.6, 6.7, 6.15, and 6.16). This observation further confirms that the use of “local transformations” is a successful tool in improving the quality of tetrahedra in a mesh.

In both algorithms, operations on hash tables *EHT* and *FHT* take a large part of computation times. Experimental results show that the hash functions used in our algorithms are satisfactory. That is, the time spent on insertion and deletion of an element to these hash tables are a small constant when the sizes of tables are sufficiently large. Table 6.20

reports a practical example for QLRB and QLRs, where ESIZE, TNE (FSIZE, TNF) are the size of the edge (face) hash table and the total number of edges (faces) in the hash table, respectively, i.e., TNE (TNF) edges (faces) are stored in ESIZE (FSIZE) buckets of the edge (face) hash table; NB denotes the number of buckets in which the number of edges (faces) is NEF, and the corresponding percentage of these buckets is denoted by FRE. For this test example, when NEF is about TNE/ESIZE (TNF/FSIZE), NB and FRE achieve the maximum values. The average number of edge (face) records compared when an edge (a face) is searched in the hash table is 1.99 (1.88) for QLRB, and 2.56 (3.32) for QLRs, respectively. Note that when  $EHT$  ( $FHT$ ) is organized as a balanced tree data structure, the average search length for each element is about  $(\log_2 TNE)/2 = 5.51$  ( $(\log_2 TNF)/2 = 5.37$ ) for QLRB, and 5.37 (7.25) for QLRs. Therefore, the hash functions used in our algorithms provide a very satisfactory performance.

Number of edges or faces	QLRB				QLRS			
	$EHT$		$FHT$		$EHT$		$FHT$	
	ESIZE = 1009 TNE = 2074		FSIZE = 1009 TNF = 1733		ESIZE = 521 TNE = 1703		FSIZE = 4993 TNF = 23110	
NEF	NB	FRE	NB	FRE	NB	FRE	NB	FRE
0	123	12.19	200	19.82	15	2.88	49	0.98
1	251	24.88	280	27.75	55	10.56	260	5.21
2	303	30.03	279	27.65	114	21.88	499	9.99
3	178	17.64	148	14.67	120	23.03	765	15.32
4	111	11.00	69	6.84	101	19.39	953	19.09
5	25	2.48	25	2.48	64	12.28	881	17.64
6	14	1.39	6	0.59	37	7.10	680	13.62
7	3	0.30	2	0.20	9	1.73	412	8.25
8	0	0.00			4	0.77	251	5.03
9	1	0.10			1	0.19	132	2.64
10					1	0.19	65	1.30
11							30	0.60
12							11	0.22
13							3	0.06
14							1	0.02
15							1	0.02

Table 6.20: Statistical results for hash tables

Finally, we point out that if local transformations are performed at each step of refinement, there is no significant improvement on the quality of tetrahedra in the final mesh, compared with the method described in this chapter (i.e., perform local refinements to some levels, then use local transformations on the final mesh only once), and at the same time the number of tetrahedra in the final mesh increases substantially. This may be because applying local transformations at each step of refinement destroys the property stated in

Theorems 4.3 and 5.6, and in general introduces more classes of similar tetrahedra than in QLRB and QLRS.

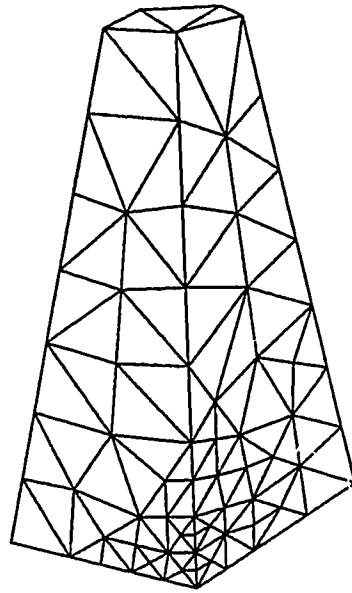


Figure 6.3: A refined mesh produced by QLRB and IMPR for 4 levels of bisection around a corner of the convex polyhedron.

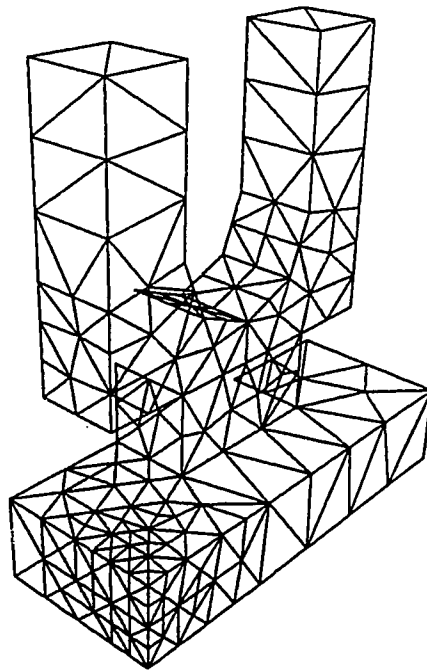


Figure 6.4: A refined mesh produced by QLRB and IMPR for 4 levels of bisection around a corner of the U-shaped object.

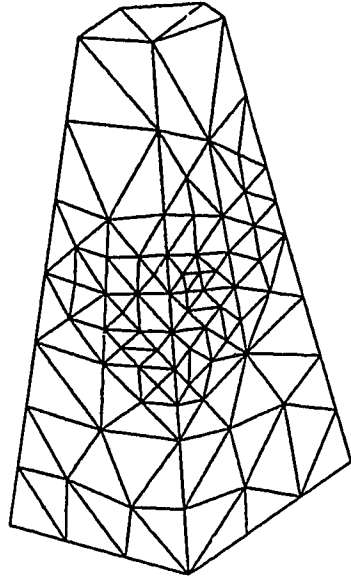


Figure 6.5: A refined mesh produced by QLRB and IMPR for 4 levels of bisection around the midpoint of an edge of the convex polyhedron.

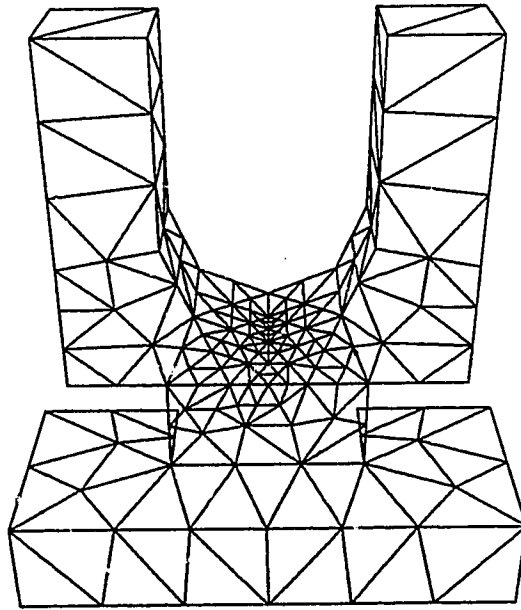


Figure 6.6: A refined mesh produced by QLRB and IMPR for 4 levels of bisection around a point of the U-shaped object.

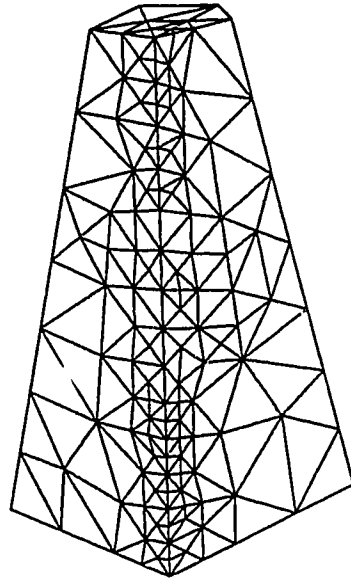


Figure 6.7: A refined mesh produced by QLRB and IMPR for 4 levels of bisection around a line segment of the convex polyhedron.

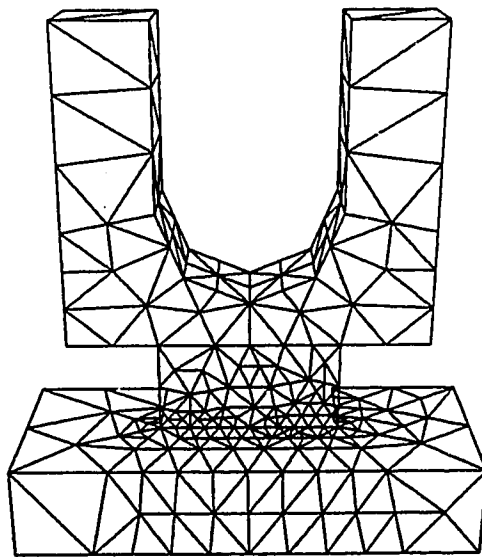


Figure 6.8: A refined mesh produced by QLRB and IMPR for 4 levels of bisection around a line segment of the U-shaped object.



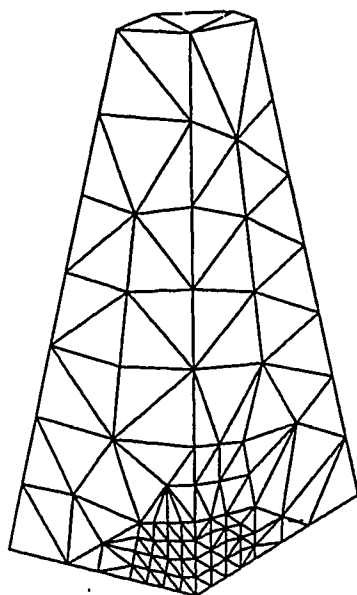


Figure 6.9: A refined mesh produced by QLRs and IMPR for 2 levels of subdivision around a corner of the convex polyhedron.

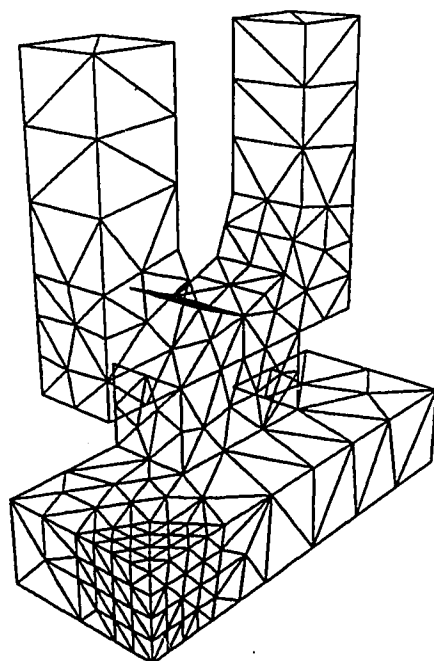


Figure 6.10: A refined mesh produced by QLRs and IMPR for 2 levels of subdivision around a corner of the U-shaped object.

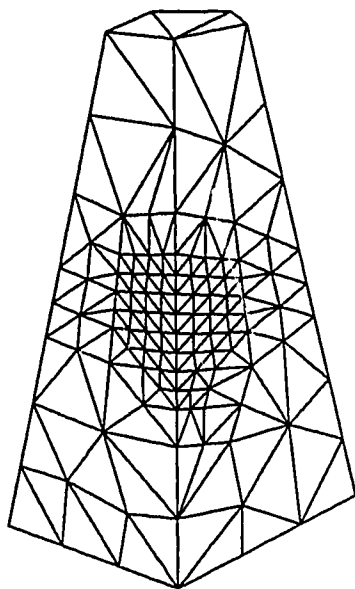


Figure 6.11: A refined mesh produced by QLRS and IMPR for 2 levels of subdivision around the midpoint of an edge of the convex polyhedron.

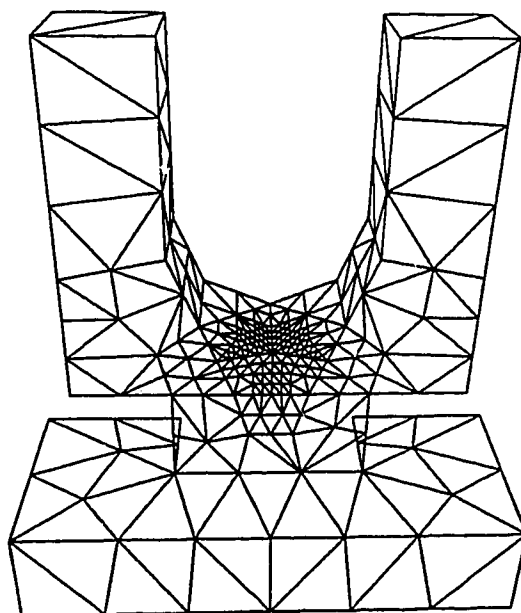


Figure 6.12: A refined mesh produced by QLRS and IMPR for 2 levels of subdivision around a point of the U-shaped object.

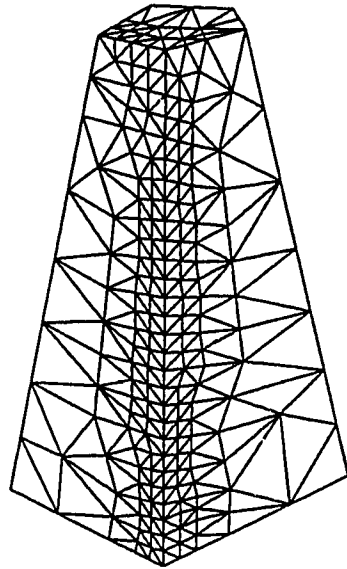


Figure 6.13: A refined mesh produced by QLRS and IMPR for 2 levels of subdivision around a line segment of the convex polyhedron.

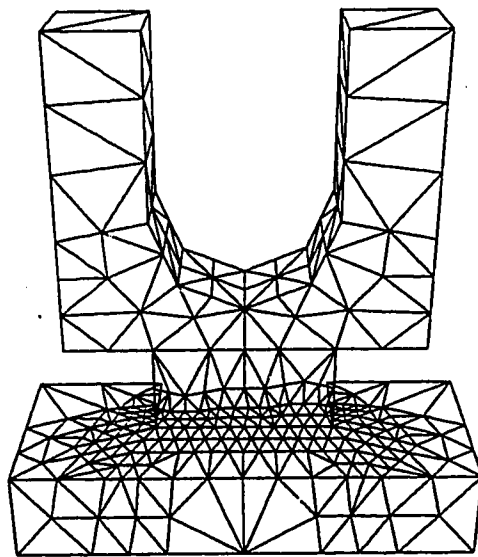


Figure 6.14: A refined mesh produced by QLRS and IMPR for 2 levels of subdivision around a line segment of the U-shaped object.

# Chapter 7

## Concluding Remarks

### 7.1 Summary

The main contributions of the thesis are as follows.

1. A novel tetrahedron shape measure, the mean ratio  $\eta$ , based on an affine transformation from the regular tetrahedron, is introduced, and used in analyzing the quality of meshes produced by our local mesh refinement algorithms. The formulae for computing three tetrahedron shape measures (radius ratio, minimum solid angle, and mean ratio) are derived, and the relationships among the measures have been studied. We conclude that the three shape measures are “equivalent” in the sense that they attain a maximum value only for the regular tetrahedron, and approach zero for a poorly-shaped tetrahedron. Consequently, any of the three measures can be used for evaluating the quality of tetrahedra in a finite element mesh. However, one must be aware of the different distributions of their values when reporting and interpreting statistics using different shape measures.
2. A bisection procedure for repeated refinement of a single tetrahedron has been presented, in which the quality of refined tetrahedra is ensured. Then a 3-D mesh refinement algorithm based mainly on the bisection procedure is designed, with emphasis on a fast algorithm for producing a guaranteed-quality conforming mesh. In particular, we have shown that there are no arbitrarily poorly-shaped tetrahedra generated by the algorithm in terms of the shape measure  $\eta$ . As far as we know, this is the

first theoretically guaranteed-quality local refinement algorithm based on bisection for a tetrahedral mesh. With properly designed data structures, an implementation of the algorithm is provided with an expected time complexity that is linearly related to the number of refined tetrahedra in a refined mesh. We have also proved that the refinement on a refined region can be smoothly extended to their adjacent sub-regions. Numerical results combined with graphical illustrations have demonstrated a very good “locality” of the algorithm (i.e. the ratio of the number of tetrahedra actually refined to the number of tetrahedra chosen for refinement is bounded above by a small positive constant).

3. Given a coarse mesh to start with, we have successfully extended a 2-D regular refinement technique to 3-D. With the help of mean ratio  $\eta$ , we have been able to prove that the 3-D regular refinement produces guaranteed-quality meshes. In particular, repeated refinement on a tetrahedron by the regular refinement produces refined tetrahedra with the shape no worse than a half of the shape of the original tetrahedron in terms of the mean ratio  $\eta$ . Accordingly, a 3-D local refinement algorithm based mainly on regular refinement has been developed and implemented. The algorithm has very similar properties to the one based on bisection, such as guaranteed-quality meshes, expected linear time complexity, mesh smoothness, and the locality of the algorithm.

## 7.2 Further research problems

Several problems need to be further studied.

1. We have reported the quality of meshes generated by our local refinement algorithms in terms of the shape of refined tetrahedra. One research topic is to integrate our mesh refinement techniques into adaptive finite element analysis, like in [Mit89], to verify how efficient and satisfactory the algorithms are. Hopefully, the conclusion made in [Mit89] for the 2-D case can be extended to 3-D.
2. As mentioned in Section 1.2.1, mesh refinement based on local refinement approaches does not take into consideration the boundary information of the original region. Research is needed to extend our mesh refinement techniques for curved surface boundaries. A possible method is to pull some points on a planar boundary face of an

existing mesh to a corresponding curved surface boundary of the original region after some levels of refinement.

3. Derefinement, an inverse process of refinement, may be needed in the adaptive mesh refinement and the multigrid method [Riv89]. Since our data structures record the whole process of refinement, derefinement can be done as follows. In algorithm QLRB or QLRS, suppose a set of elements in  $\mathcal{T}^m$  needs derefinement. Let  $1 \leq r \leq m$  be the minimum integer such that no derefined element belongs to meshes prior to  $\mathcal{T}^{m-r}$ . We first recover mesh  $\mathcal{T}^{m-r}$ , and then rechoose sets  $S_{m-r}, S_{m-r+1}, \dots, S_{m-1}$  (where  $S_i$  is a set of tetrahedra chosen in  $\mathcal{T}^i$  for refinement) such that derefined elements (or most of them) do not exist in the new refined mesh  $\mathcal{T}^m$  when QLRB or QLRS is reapplied with the new  $S_i$ ,  $m-r \leq i \leq m-1$ . Another possible method for derefinement is to recursively replace each element that is either a derefined element or causes non-conformity with its neighbors by its parent until a conforming mesh is obtained.
4. The possibility of developing a mesh generator based on our mesh refinement techniques would be an interesting research topic. A possible approach would be to first construct an initial coarse mesh that covers the region of interest such that the boundary of the mesh is not necessary the same as the boundary of the original region. If the initial coarse mesh can somehow be constructed such that it extracts most geometric information on the shape of the original region and contains relatively well-shaped elements (e.g. using a triangulation of the convex hull of the original region in some cases), then we may expect to produce a satisfactory mesh by combining our mesh refinement techniques with the solution of dealing with boundary problems.

# Appendix A

## Mean Ratio in $n$ -Dimensional Space

In this appendix, we generalize the mean ratio and its formula to arbitrary dimensions. Let  $\mathbf{T}$  be any  $n$ -dimensional simplex, and  $\mathbf{R}$  be a regular  $n$ -dimensional simplex. The mean ratio  $\eta(\mathbf{T})$  is defined as

$$\eta(\mathbf{T}) = \frac{n \sqrt[n]{\prod_{i=1}^n \lambda_i}}{\sum_{i=1}^n \lambda_i}, \quad (\text{A.1})$$

where  $\lambda_i$ ,  $1 \leq i \leq n$ , are the eigenvalues of  $A(\mathbf{R}, \mathbf{T}) = M^T(\mathbf{R}, \mathbf{T})M(\mathbf{R}, \mathbf{T})$ , and  $M(\mathbf{R}, \mathbf{T})$  is a matrix involved in an affine transformation from  $\mathbf{R}$  to  $\mathbf{T}$ .

**Theorem A.1** *For any  $n$ -dimensional simplex  $\mathbf{T}$ ,*

$$\eta(\mathbf{T}) = \frac{n(n+1)^{(n-1)/n} (vn!)^{2/n}}{\sum_{0 \leq i < j \leq n} l_{ij}^2},$$

where  $v$  is the volume of  $\mathbf{T}$  and the  $l_{ij}$  are the lengths of the edges of  $\mathbf{T}$ . Furthermore  $\eta(\mathbf{T})$  is independent of the ordering of vertices of  $\mathbf{T}$ ,  $\mathbf{R}$  and of the vertex coordinates of  $\mathbf{R}$ .

**Proof.** Suppose the vertex coordinates of  $\mathbf{R}$  are  $\mathbf{r}_0 = (a/\sqrt{2}, 0, \dots, 0)^T$ ,  $\mathbf{r}_1 = (0, a/\sqrt{2}, \dots, 0)^T$ ,  $\dots$ ,  $\mathbf{r}_{n-1} = (0, 0, \dots, 0, a/\sqrt{2})^T$ ,  $\mathbf{r}_n = (am/\sqrt{2}, am/\sqrt{2}, \dots, am/\sqrt{2})^T$ , where  $a$  is the length of any edge of  $\mathbf{R}$  and  $m = (1 + \sqrt{n+1})/n$ . Let  $\mathbf{T}$  be any  $n$ -dimensional simplex having the same volume as  $\mathbf{R}$ . Let  $T = (\mathbf{t}_1 - \mathbf{t}_0, \dots, \mathbf{t}_n - \mathbf{t}_0)$  and  $R = (\mathbf{r}_1 - \mathbf{r}_0, \dots, \mathbf{r}_n - \mathbf{r}_0)$ . Then

$$R = \frac{a}{\sqrt{2}} \begin{bmatrix} -\mathbf{e}^T & m-1 \\ I_{n-1} & m\mathbf{e} \end{bmatrix}, \quad (\text{A.2})$$

$$R^{-1} = \frac{\sqrt{2}}{a} \begin{bmatrix} -\frac{m}{\sqrt{n+1}}\mathbf{e} & I_{n-1} - \frac{m}{\sqrt{n+1}}\mathbf{e}\mathbf{e}^T \\ \frac{1}{\sqrt{n+1}} & \frac{1}{\sqrt{n+1}}\mathbf{e}^T \end{bmatrix}. \quad (\text{A.3})$$

where  $\mathbf{e} = (1, 1, \dots, 1)^T$  is an  $(n-1)$ -vector and  $I_{n-1}$  is the  $(n-1)$  by  $(n-1)$  identity matrix. Let  $d_{ij} = (\mathbf{t}_j - \mathbf{t}_i)^T(\mathbf{t}_j - \mathbf{t}_i)$ ,  $0 \leq i < j \leq n$ . Then

$$T^T T = \begin{bmatrix} d_{01} & (d_{01} + d_{02} - d_{12})/2 & \dots & (d_{01} + d_{0n} - d_{1n})/2 \\ (d_{01} + d_{02} - d_{12})/2 & d_{02} & \dots & (d_{02} + d_{0n} - d_{2n})/2 \\ \vdots & \vdots & \ddots & \vdots \\ (d_{01} + d_{0n} - d_{1n})/2 & (d_{02} + d_{0n} - d_{2n})/2 & \dots & d_{0n} \end{bmatrix}. \quad (\text{A.4})$$

Let

$$T^T T = \begin{bmatrix} T' & \mathbf{t} \\ \mathbf{t}^T & \tau \end{bmatrix},$$

where  $T'$  is an  $(n-1)$  by  $(n-1)$  submatrix,  $\mathbf{t}$  is an  $(n-1)$ -vector, and  $\tau$  is a scalar. Suppose  $\mathbf{r}_i$  is transformed to  $\mathbf{t}_i$  by  $M(\mathbf{R}, \mathbf{T})$ . Then  $M(\mathbf{R}, \mathbf{T}) = T R^{-1}$ . From (A.2), (A.3), and  $A(\mathbf{R}, \mathbf{T}) = M^T(\mathbf{R}, \mathbf{T})M(\mathbf{R}, \mathbf{T}) = (R^{-1})^T T^T T R^{-1}$ , we obtain

$$A(\mathbf{R}, \mathbf{T}) = \frac{2}{a^2} \begin{bmatrix} \alpha & \# \\ \# & A' \end{bmatrix}, \quad (\text{A.5})$$

where

$$\alpha = \frac{m}{\sqrt{n+1}} \mathbf{e}^T \left( \frac{m}{\sqrt{n+1}} T' \mathbf{e} - \frac{1}{\sqrt{n+1}} \mathbf{t} \right) - \frac{m}{n+1} \mathbf{t}^T \mathbf{e} + \frac{1}{n+1} \tau, \quad (\text{A.6})$$

$$\begin{aligned} A' &= (I_{n-1} - \frac{m}{\sqrt{n+1}} \mathbf{e} \mathbf{e}^T) [T' (I_{n-1} - \frac{m}{\sqrt{n+1}} \mathbf{e} \mathbf{e}^T) + \frac{1}{\sqrt{n+1}} \mathbf{t} \mathbf{e}^T] \\ &\quad + \frac{1}{\sqrt{n+1}} \mathbf{e} [\mathbf{t}^T (I_{n-1} - \frac{m}{\sqrt{n+1}} \mathbf{e} \mathbf{e}^T) + \frac{1}{\sqrt{n+1}} \tau \mathbf{e}^T], \end{aligned} \quad (\text{A.7})$$

and  $\#$  denotes a vector which is irrelevant.

Let  $x_{ij}$ ,  $1 \leq i, j \leq n$ , denote the elements of  $T^T T$ . Then  $x_{ij} = x_{ji}$  since  $T^T T$  is a symmetric matrix. Note that the trace of the sum of two matrices is equal to the sum of the trace of each matrix and the trace of a matrix is equal to the trace of the transpose of



the matrix. By (A.6), (A.7), and simple algebraic manipulation,

$$\begin{aligned}\alpha &= \frac{n^2}{n+1} \sum_{i=1}^{n-1} \sum_{j=1}^{n-1} x_{ij} - \frac{2m}{n+1} \sum_{i=1}^{n-1} x_{in} + \frac{x_{nn}}{n+1}, \\ \text{trace}(A') &= \frac{n-1}{n+1} x_{nn} + \sum_{i=1}^{n-1} x_{ii} + \left( \frac{2}{\sqrt{n+1}} - \frac{2m(n-1)}{n+1} \right) \sum_{i=1}^{n-1} x_{in} \\ &\quad + \left( \frac{m^2(n-1)}{n+1} - \frac{2m}{\sqrt{n+1}} \right) \sum_{i=1}^{n-1} x_{ij}.\end{aligned}$$

Thus,

$$\alpha + \text{trace}(A') = \frac{1}{(n+1)} \left[ (n+1) \sum_{i=1}^n x_{ii} - \sum_{1 \leq i, j \leq n} x_{ij} \right]. \quad (\text{A.8})$$

From (A.4),

$$\sum_{1 \leq i, j \leq n} x_{ij} = n \sum_{i=1}^n d_{0i} - \sum_{1 \leq i < j \leq n} d_{ij}, \quad (\text{A.9})$$

and

$$\sum_{i=1}^n x_{ii} = \sum_{i=1}^n d_{0i}. \quad (\text{A.10})$$

Combining (A.5), (A.8), (A.9), and (A.10) yields

$$\sum_{1 \leq i \leq n} \lambda_i = \text{trace}(A(\mathbf{R}, \mathbf{T})) = \frac{2}{a^2} (\alpha + \text{trace}(A')) = \frac{2}{a^2(n+1)} \sum_{0 \leq i < j \leq n} d_{ij}. \quad (\text{A.11})$$

Let  $v$  be the volume of  $\mathbf{T}$ . Since  $\mathbf{R}$  and  $\mathbf{T}$  have the same volume,

$$v = \frac{\sqrt{n+1}}{n!} \left( \frac{a}{\sqrt{2}} \right)^n, \quad (\text{A.12})$$

and  $\det(M(\mathbf{R}, \mathbf{T})) = \pm 1$ . So

$$\prod_{1 \leq i \leq n} \lambda_i = \det(A(\mathbf{R}, \mathbf{T})) = 1. \quad (\text{A.13})$$

Combining (A.1), (A.11), (A.12), (A.13) yields

$$\eta(\mathbf{T}) = \frac{n \sqrt[n]{\det(A(\mathbf{R}, \mathbf{T}))}}{\text{trace}(A(\mathbf{R}, \mathbf{T}))} = \frac{n(n+1)^{(n-1)/n} (vn!)^{2/n}}{\sum_{0 \leq i < j \leq n} l_{ij}^2},$$

where the  $l_{ij}$  are the lengths of edges of  $\mathbf{T}$ .

Using an argument similar to the proof of Theorem 2.4, it can be shown that  $\eta(\mathbf{T})$  is independent of the ordering of vertices of  $\mathbf{T}$ ,  $\mathbf{R}$  and of the vertex coordinates of  $\mathbf{R}$ .  $\square$

# Appendix B

## Delaunay Property in SUBDIV

Let  $\mathbf{T}$  be any tetrahedron. An infinite sequence of tetrahedral meshes produced by SUBDIV is denoted by  $\mathcal{T}^0 = \mathbf{T}, \mathcal{T}^1, \mathcal{T}^2, \dots$ , where  $\mathcal{T}^n = \{\mathbf{T}_i^n, 1 \leq i \leq 8^n\}$  and the centre edge of  $\mathbf{T}$  can be any of the three choices as in step (1) of SUBDIV. The main purpose of this appendix is to prove that there exists a centre edge of  $\mathbf{T}$  such that  $\mathcal{T}^n, n > 0$ , is a Delaunay triangulation when all face angles of  $\mathbf{T}$  are  $\leq 90^\circ$ , where a *face angle* of a tetrahedron refers to an interior angle of a triangular face of the tetrahedron. This property indicates that a guaranteed-quality Delaunay triangulation is produced by SUBDIV under the face angle condition of the initial tetrahedron, while a Delaunay triangulation may in general contain some poorly-shaped tetrahedra.

We first state some well known properties of a Delaunay triangulation in 2-D and 3-D.

- P1. A triangulation  $\mathcal{T}$  of a set  $\mathcal{V}$  of points in 2-D (3-D) is a Delaunay triangulation iff the interior of the circumcircle (circumsphere) of every triangle (tetrahedron) of  $\mathcal{T}$  does not contain any point of  $\mathcal{V}$ .
- P2. A 2-D (3-D) triangulation  $\mathcal{T}$  is a Delaunay triangulation iff every interior edge (face) of  $\mathcal{T}$  is *locally optimal*, where an interior edge (face) shared by two adjacent triangles (tetrahedra)  $\mathbf{T}_1$  and  $\mathbf{T}_2$  is called locally optimal if the interior of the circumcircle (circumsphere) of  $\mathbf{T}_1$  does not contain any vertex of  $\mathbf{T}_2$  [Law86, Joe91b].
- P3. Given a set  $\mathcal{V} = \{v_1, v_2, \dots, v_N\}$  of points in 2-D, an edge  $v_i v_j$  exists in a Delaunay triangulation of  $\mathcal{V}$  iff there exists a point  $v$  such that the interior of the circle centered at  $v$  and passing through  $v_i$  and  $v_j$  does not contain any point of  $\mathcal{V}$  [LeS81].

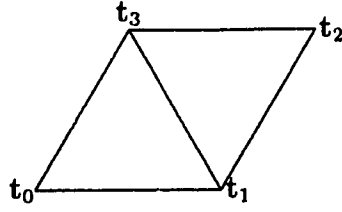


Figure B.1: Illustration for the proof of Lemma B.1;  $t_0t_1t_2t_3$  is a parallelogram.

The following lemmas are needed in Theorem B.1.

**Lemma B.1** *A triangulation produced by connecting two non-adjacent points  $t_0, t_3$  of a parallelogram  $t_0t_1t_2t_3$  is a Delaunay triangulation iff  $\angle t_3t_0t_1$  or  $\angle t_1t_2t_3$  is  $\leq 90^\circ$  (see Figure B.1).*

**Proof.** Note that the interior of the circle with diameter  $t_1t_3$  does not contain  $t_0$  and  $t_2$  iff  $\angle t_3t_0t_1$  and  $\angle t_1t_2t_3$  are  $\leq 90^\circ$ . Combined with Property P3, it follows that the configuration of Figure B.1 is a Delaunay triangulation iff  $\angle t_3t_0t_1$  or  $\angle t_1t_2t_3$  is  $\leq 90^\circ$ .  $\square$

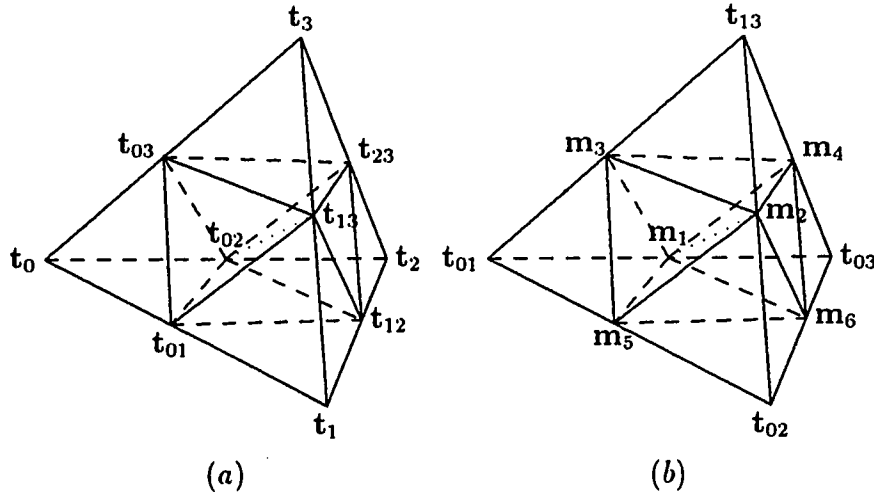


Figure B.2: (a) Illustration for the proof of Lemmas B.2, B.3, B.4, and B.5.

(b) A rotated and enlarged version of  $T_5^1(t_{01}, t_{13}, t_{03}, t_{02})$  for the proof of Lemma B.3.

**Lemma B.2**  $T^1$  is a 3-D Delaunay triangulation iff every planar triangulation of  $T^1$  formed by the union of triangles lying on a plane is a 2-D Delaunay triangulation.

**Proof.** Suppose  $T^1$  is a Delaunay triangulation, i.e. the interior of the circumsphere of any tetrahedron in  $T^1$  does not contain any point of  $T^1$ . If a 2-D triangulation  $S$  on a plane

is not a Delaunay triangulation, then there exists a triangle  $\Delta$  of  $\mathcal{S}$  such that the interior of the circumcircle of  $\Delta$  contains a vertex  $\mathbf{p}$  of  $\mathcal{S}$ . It follows that the circumsphere  $O$  of a tetrahedron incident on  $\Delta$  must contain  $\mathbf{p}$  (since the circumcircle of  $\Delta$  is the intersection of plane containing  $\mathcal{S}$  and sphere  $O$ ), a contradiction of Property P1.

Now we suppose each planar triangulation in  $\mathcal{T}^1$  is a 2-D Delaunay triangulation and the centre edge of  $\mathbf{T}$  is  $\mathbf{t}_{02}\mathbf{t}_{13}$  (see Figure B.2a). Since  $\mathbf{t}_{02}\mathbf{t}_{12} \parallel \mathbf{t}_0\mathbf{t}_1 \parallel \mathbf{t}_{03}\mathbf{t}_{13}$ ,  $\mathbf{t}_{02}\mathbf{t}_{03} \parallel \mathbf{t}_2\mathbf{t}_3 \parallel \mathbf{t}_{12}\mathbf{t}_{13}$ ,  $\mathbf{t}_{01}\mathbf{t}_{13} \parallel \mathbf{t}_0\mathbf{t}_3 \parallel \mathbf{t}_{02}\mathbf{t}_{23}$ , and  $\mathbf{t}_{01}\mathbf{t}_{02} \parallel \mathbf{t}_1\mathbf{t}_2 \parallel \mathbf{t}_{13}\mathbf{t}_{23}$ , quadrilaterals  $\mathbf{t}_{02}\mathbf{t}_{12}\mathbf{t}_{13}\mathbf{t}_{03}$  and  $\mathbf{t}_{01}\mathbf{t}_{13}\mathbf{t}_{23}\mathbf{t}_{02}$  are parallelograms. Table B.1 lists every interior face of  $\mathcal{T}^1$ , the two adjacent tetrahedra incident on each interior face, and the four vertices of a planar triangulation. Note that the four vertices associated with each interior face in the last column of Table B.1 form a parallelogram in order. It is straightforward to verify that each interior face in  $\mathcal{T}^1$  is locally optimal due to the corresponding 2-D Delaunay triangulation formed by the parallelogram in the last column of Table B.1. By Property P2, the lemma is established.  $\square$

Interior face	Two adjacent tetrahedra	Vertices on a plane
$\mathbf{t}_{01}\mathbf{t}_{02}\mathbf{t}_{03}$	$\mathbf{T}_1^1(\mathbf{t}_0, \mathbf{t}_{01}, \mathbf{t}_{02}, \mathbf{t}_{03}), \mathbf{T}_5^1(\mathbf{t}_{01}, \mathbf{t}_{13}, \mathbf{t}_{03}, \mathbf{t}_{02})$	$\mathbf{t}_{01}, \mathbf{t}_{13}, \mathbf{t}_{03}, \mathbf{t}_0$
$\mathbf{t}_{01}\mathbf{t}_{12}\mathbf{t}_{13}$	$\mathbf{T}_2^1(\mathbf{t}_{01}, \mathbf{t}_1, \mathbf{t}_{12}, \mathbf{t}_{13}), \mathbf{T}_6^1(\mathbf{t}_{01}, \mathbf{t}_{12}, \mathbf{t}_{13}, \mathbf{t}_{02})$	$\mathbf{t}_{01}, \mathbf{t}_1, \mathbf{t}_{12}, \mathbf{t}_{02}$
$\mathbf{t}_{02}\mathbf{t}_{12}\mathbf{t}_{23}$	$\mathbf{T}_3^1(\mathbf{t}_{02}, \mathbf{t}_{12}, \mathbf{t}_2, \mathbf{t}_{23}), \mathbf{T}_7^1(\mathbf{t}_{23}, \mathbf{t}_{02}, \mathbf{t}_{13}, \mathbf{t}_{12})$	$\mathbf{t}_{12}, \mathbf{t}_2, \mathbf{t}_{23}, \mathbf{t}_{13}$
$\mathbf{t}_{03}\mathbf{t}_{13}\mathbf{t}_{23}$	$\mathbf{T}_4^1(\mathbf{t}_{03}, \mathbf{t}_{13}, \mathbf{t}_{23}, \mathbf{t}_3), \mathbf{T}_8^1(\mathbf{t}_{23}, \mathbf{t}_{02}, \mathbf{t}_{13}, \mathbf{t}_{03})$	$\mathbf{t}_{03}, \mathbf{t}_{02}, \mathbf{t}_{23}, \mathbf{t}_3$
$\mathbf{t}_{02}\mathbf{t}_{13}\mathbf{t}_{12}$	$\mathbf{T}_6^1(\mathbf{t}_{01}, \mathbf{t}_{12}, \mathbf{t}_{13}, \mathbf{t}_{02}), \mathbf{T}_7^1(\mathbf{t}_{23}, \mathbf{t}_{02}, \mathbf{t}_{13}, \mathbf{t}_{12})$	$\mathbf{t}_{02}, \mathbf{t}_{01}, \mathbf{t}_{13}, \mathbf{t}_{23}$
$\mathbf{t}_{03}\mathbf{t}_{02}\mathbf{t}_{13}$	$\mathbf{T}_5^1(\mathbf{t}_{01}, \mathbf{t}_{13}, \mathbf{t}_{03}, \mathbf{t}_{02}), \mathbf{T}_8^1(\mathbf{t}_{23}, \mathbf{t}_{02}, \mathbf{t}_{13}, \mathbf{t}_{03})$	$\mathbf{t}_{02}, \mathbf{t}_{01}, \mathbf{t}_{13}, \mathbf{t}_{23}$
$\mathbf{t}_{01}\mathbf{t}_{13}\mathbf{t}_{02}$	$\mathbf{T}_5^1(\mathbf{t}_{01}, \mathbf{t}_{13}, \mathbf{t}_{03}, \mathbf{t}_{02}), \mathbf{T}_6^1(\mathbf{t}_{01}, \mathbf{t}_{12}, \mathbf{t}_{13}, \mathbf{t}_{02})$	$\mathbf{t}_0, \mathbf{t}_{12}, \mathbf{t}_{13}, \mathbf{t}_{03}$
$\mathbf{t}_{02}\mathbf{t}_{13}\mathbf{t}_{23}$	$\mathbf{T}_7^1(\mathbf{t}_{23}, \mathbf{t}_{02}, \mathbf{t}_{13}, \mathbf{t}_{12}), \mathbf{T}_8^1(\mathbf{t}_{23}, \mathbf{t}_{02}, \mathbf{t}_{13}, \mathbf{t}_{03})$	$\mathbf{t}_{02}, \mathbf{t}_{12}, \mathbf{t}_{13}, \mathbf{t}_{03}$

Table B.1: Information associated with each interior face of  $\mathcal{T}^1$

**Lemma B.3** *If  $\mathcal{T}^1$  is a Delaunay triangulation, so is  $\mathcal{S}_j$ , where  $\mathcal{S}_j$  is a mesh produced by applying  $\text{SUB}_8$  to any  $\mathbf{T}_j^1$ ,  $1 \leq j \leq 8$ .*

**Proof.** Suppose  $\mathbf{T}_j^1$ ,  $1 \leq j \leq 4$ , is a tetrahedron at one of the four corners in  $\mathcal{T}^1$ . It is obvious that  $\mathcal{S}_j$ ,  $1 \leq j \leq 4$ , is a Delaunay triangulation since  $\mathbf{T}_j^1$  is similar to  $\mathbf{T}$ , the centre edge of  $\mathbf{T}_j^1$  has the same subdivision pattern as  $\mathbf{T}$ , and  $\mathcal{T}^1$  is a Delaunay triangulation. Suppose the centre edge of  $\mathbf{T}$  is  $\mathbf{t}_{02}\mathbf{t}_{13}$  (see Figure B.2a). We prove that mesh  $\mathcal{S}_5$  produced from  $\mathbf{T}_5^1(\mathbf{t}_{01}, \mathbf{t}_{13}, \mathbf{t}_{03}, \mathbf{t}_{02})$  is a Delaunay triangulation (see Figure B.2b). By Lemmas B.1 and B.2, it suffices to prove that every face angle in  $\mathcal{S}_5$ , which is opposite a diagonal edge of a parallelogram formed from two adjacent triangles, is  $\leq 90^\circ$ . Since  $\mathcal{T}^1$  is a Delaunay triangulation, all face angles of  $\mathbf{T}$ ,  $\angle \mathbf{t}_{02}\mathbf{t}_{01}\mathbf{t}_{13}$ , and  $\angle \mathbf{t}_{02}\mathbf{t}_{03}\mathbf{t}_{13}$  are  $\leq 90^\circ$  by Lemmas B.1 and

B.2. Note that  $\Delta t_{01}t_{03}t_{13}$  and  $\Delta t_{01}t_{02}t_{03}$  are similar to  $\Delta t_0t_1t_3$  and  $\Delta t_1t_2t_3$ , respectively. We only need to prove that  $\angle t_{01}t_{02}t_{13}$ ,  $\angle t_{02}t_{13}t_{01}$ ,  $\angle t_{03}t_{02}t_{13}$ ,  $\angle t_{03}t_{13}t_{02}$ ,  $\angle m_1m_3m_2$ , and  $\angle m_1m_4m_2$  are  $\leq 90^\circ$ , where  $m_1$ ,  $m_2$ ,  $m_3$ , and  $m_4$  are the midpoints of  $t_{01}t_{03}$ ,  $t_{02}t_{13}$ ,  $t_{01}t_{13}$ , and  $t_{03}t_{13}$ , respectively. Let  $l_{ij} = |t_i - t_j|$ ,  $i < j$ . By the fact that the angle between two vectors is  $\leq 90^\circ$  iff the inner product of the two vectors is  $\geq 0$ , we have

$$\begin{aligned}
 (t_{01} - t_{02}) \cdot (t_{13} - t_{02}) &= l_{12}^2/4 + (t_1 - t_2) \cdot (t_3 - t_0)/4 \\
 &= l_{12}^2/4 + (t_1 - t_2) \cdot (t_3 - t_2)/4 - (t_1 - t_2) \cdot (t_0 - t_2)/4 \\
 &\geq l_{12}^2/4 - (t_1 - t_2) \cdot (t_0 - t_2)/4 \\
 &= l_{12}^2/4 - (l_{12}^2 + l_{02}^2 - l_{01}^2)/8 \\
 &= (l_{12}^2 + l_{01}^2 - l_{02}^2)/8 \geq 0,
 \end{aligned}$$

since  $l_{12}^2 + l_{02}^2 - l_{01}^2 = 2(t_1 - t_2) \cdot (t_0 - t_2)$  and  $l_{12}^2 + l_{01}^2 - l_{02}^2 = 2(t_2 - t_1) \cdot (t_0 - t_1) \geq 0$ . Thus  $\angle t_{01}t_{02}t_{13} \leq 90^\circ$ . Similarly  $\angle t_{02}t_{13}t_{01}$ ,  $\angle t_{03}t_{02}t_{13}$ , and  $\angle t_{03}t_{13}t_{02}$  are each  $\leq 90^\circ$ . Note that  $(m_1 - m_3) \cdot (m_2 - m_3) = (t_{03} - t_{13}) \cdot (t_{02} - t_{01})/4 = (t_0 - t_{01}) \cdot (t_{02} - t_{01})/4 \geq 0$ , since  $\angle t_0t_{01}t_{02} = \angle t_0t_1t_2 \leq 90^\circ$ . Thus  $\angle m_1m_3m_2 \leq 90^\circ$ , and similarly  $\angle m_1m_4m_2 \leq 90^\circ$ . So,  $S_5$  is a Delaunay triangulation.

Similarly, it can be proved that  $S_j$ ,  $6 \leq j \leq 8$ , is a Delaunay triangulation.  $\square$

**Lemma B.4** *If all face angles of  $T$  are  $\leq 90^\circ$ , there exists a centre edge of  $T$  such that  $T^1$  is a Delaunay triangulation.*

**Proof.** We choose the centre edge of  $T$  to be the shortest edge among  $t_{01}t_{23}$ ,  $t_{02}t_{13}$ , and  $t_{03}t_{12}$ , say  $t_{02}t_{13}$  (see Figure B.2a). Then  $\angle t_{02}t_{01}t_{13}$  and  $\angle t_{02}t_{03}t_{13}$  are  $\leq 90^\circ$ , since quadrilaterals  $t_{02}t_{12}t_{13}t_{03}$  and  $t_{01}t_{13}t_{23}t_{02}$  are parallelograms, and  $|t_{02}t_{13}| \leq |t_{01}t_{23}|$ ,  $|t_{02}t_{13}| \leq |t_{03}t_{12}|$ . By Lemmas B.1 and B.2,  $T^1$  is a Delaunay triangulation.  $\square$

**Lemma B.5** *Let  $T_1^n(s_0, s_1, s_2, s_3)$  and  $T_2^n(s_0, s_1, s_2, s_4)$  be two adjacent tetrahedra in  $T^n$ ,  $n \geq 1$ . Then  $T_1^n$  and  $T_2^n$  share one of their base edges, say  $s_1s_2$ , on their common face, and quadrilateral  $s_1s_3s_2s_4$  forms a parallelogram (see Figure B.3a).*

**Proof.** Suppose the centre edge of  $T$  is  $t_{02}t_{13}$ . Note that an edge connecting the first and third vertices in the last column of Table B.1 is one common base edge of two adjacent tetrahedra incident on the corresponding interior face in the first column, and the four vertices in the last column form a parallelogram in order. It can be easily verified that the

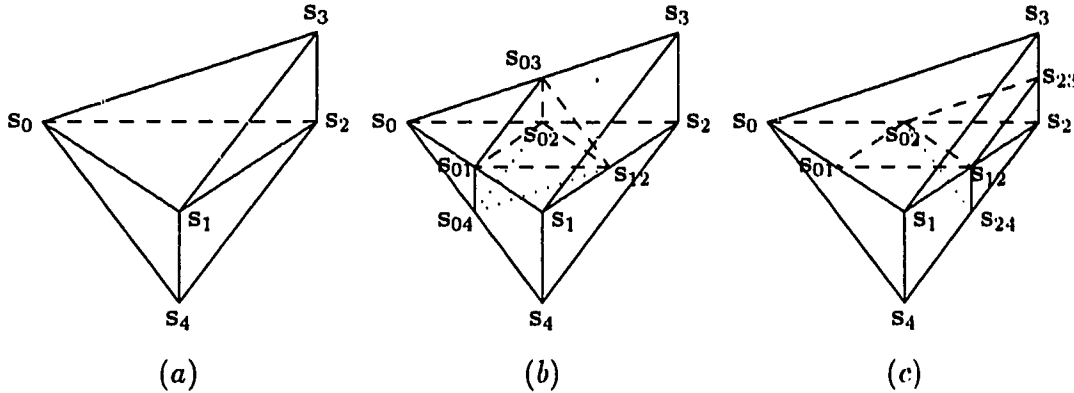


Figure B.3: Illustration for the proof of Lemma B.5;  $s_1s_4s_2s_3$  is a parallelogram, and  $s_{ij} = (s_i + s_j)/2$ ,  $i < j$ .

lemma holds for  $\mathcal{T}^1$  by Table B.1 (see Figure B.2a). Now we suppose two adjacent tetrahedra  $\mathbf{T}_1(s_0, s_1, s_2, s_3)$  and  $\mathbf{T}_2(s_0, s_1, s_2, s_4)$  have the configuration of Figure B.3a, where  $s_1s_2$  is their common base edge and  $s_1s_4s_2s_3$  is a parallelogram. To prove the lemma, it suffices to prove that, after  $\text{SUB}_8$  is applied to  $\mathbf{T}_1$  and  $\mathbf{T}_2$ , any two adjacent tetrahedra incident on a subface of face  $s_0s_1s_2$  have the configuration as stated in the lemma. Note that  $s_{12}s_{03}$  and  $s_{12}s_{04}$  are the centre edges of  $\mathbf{T}_1$  and  $\mathbf{T}_2$  in procedure  $\text{SUBDIV}$  (see Figure B.3b and Section 5.2), since  $s_1s_2$  is one of their base edges. Thus,  $s_0s_1s_2$  is a base edge of  $\mathbf{T}_1^1(s_0, s_{01}, s_{02}, s_{03})$ ,  $\mathbf{S}_1^1(s_0, s_{01}, s_{02}, s_{04})$ ,  $\mathbf{T}_2^1(s_{01}, s_{12}, s_{02}, s_{03})$ , and  $\mathbf{S}_2^1(s_{01}, s_{12}, s_{02}, s_{04})$ . Since  $s_{03}s_{02} \parallel s_2s_3$ ,  $s_{01}s_{04} \parallel s_1s_4$ ,  $s_{01}s_{03} \parallel s_1s_3$ , and  $s_{02}s_{04} \parallel s_2s_4$ , quadrilateral  $s_{01}s_{03}s_{02}s_{04}$  is a parallelogram. Thus, tetrahedron pairs  $(\mathbf{T}_1^1, \mathbf{S}_1^1)$  and  $(\mathbf{T}_2^1, \mathbf{S}_2^1)$  have the configuration of Figure B.3a. It can be easily verified that the lemma holds for the two adjacent tetrahedra  $\mathbf{T}_3^1(s_{02}, s_{12}, s_2, s_{23})$  and  $\mathbf{S}_3^1(s_{02}, s_{12}, s_2, s_{24})$  from Figure B.3c where quadrilateral  $s_2s_{23}s_{12}s_{24}$  is a parallelogram; the final case of face  $s_0s_1s_{12}$  is similar.  $\square$

Now we give the main result of this appendix.

**Theorem B.1** *If all face angles of  $\mathbf{T}$  are  $\leq 90^\circ$ , there exists a centre edge of  $\mathbf{T}$  such that all the  $\mathcal{T}^n$ ,  $n \geq 1$ , are Delaunay triangulations.*

**Proof.** By Lemma B.4, we can choose a centre edge of  $\mathbf{T}$  such that  $\mathcal{T}^1$  is a Delaunay triangulation. Repeatedly using Lemmas B.3, B.2, and B.1, it follows that any face angle of a tetrahedron in  $\mathcal{T}^n$ ,  $n \geq 0$ , is  $\leq 90^\circ$ .

Suppose  $F$  is an interior face shared by  $\mathbf{T}_1^n(s_0, s_1, s_2, s_3)$  and  $\mathbf{T}_2^n(s_0, s_1, s_2, s_4)$  in  $\mathcal{T}^n$ .

By Lemma B.5,  $T_1^n$  and  $T_2^n$  must have the configuration of Figure B.3a. Note that the triangulation of parallelogram  $s_1s_3s_2s_4$  is a 2-D Delaunay triangulation due to  $\angle s_1s_3s_2 \leq 90^\circ$ . Thus,  $F$  is locally optimal by an argument similar to the proof of Lemma B.2. So,  $T^n$  is a Delaunay triangulation by Property P2, since every interior face in  $T^n$  is locally optimal.  $\square$

## Bibliography

- [Adl83] A. Adler (1983), On the bisection method for triangles, *Math. Comp.*, 40, pp. 571-574.
- [AHU74] A. V. Aho, J. E. Hopcroft, and J. D. Ullman (1974), *The Design and Analysis of Computer Algorithms*, Addison-Wesley Publishing Company.
- [Atk78] K. E. Atkinson (1978), *An Introduction to Numerical Analysis*, Wiley, New York.
- [BaS89] P. L. Baehmann and M. S. Shephard (1989), Adaptive multiple-level h-refinement in automated finite element analysis, *Engineering with Computers*, 5, pp. 235-247.
- [Bak89] T. J. Baker (1989), Automatic mesh generation for complex three-dimensional regions using a constrained Delaunay triangulations, *Engineering with Computers*, 5, pp. 161-175.
- [Ban90] R. E. Bank (1990), *PLTMG: A Software Package for Solving Elliptic Partial Differential Equations: Users' Guide 6.0*, SIAM, Philadelphia.
- [BaS81] R. E. Bank and A. H. Sherman (1981), An adaptive multilevel method for elliptic boundary value problems, *Computing*, 29, pp. 91-105.
- [BeE92] M. Bern and D. Eppstein (1992), Mesh generation and optimal triangulations, in *Computing in Euclidean Geometry*, ed. D. E. Du and F. K. Hwang, World Scientific Publishing Company.
- [BEG90] M. Bern, D. Eppstein, and J. Gilbert (1990), Provably good mesh generation, *Proc. IEEE 31st Annual Symposium on Foundations of Computer Science*, pp. 231-241.



- [Bey81] W. H. Beyer (1981), *CRC Standard Mathematical Tables*, 26th edition, CRC Press, Boca Raton, Florida.
- [BEK93] F. Bornemann, B. Erdmann, and R. Kornhuber (1993), Adaptive multivlevel methods in three space dimensions, *Intern. J. Num. Meth. Eng.*, 36, pp. 3187-3203.
- [Bur90] E. K. Buratynski (1990), A fully automatic three-dimensional mesh generator for complex geometries, *Intern. J. Num. Meth. Eng.*, 30, pp. 931-952.
- [CSW88] G. F. Carey, M. Sharma, and K. C. Wang (1988), A class of data structures for 2-D and 3-D adaptive mesh refinement, *Intern. J. Num. Meth. Eng.*, 26, pp. 2607-2622.
- [CFF85] J. C. Cavendish, D. A. Field, and W. H. Frey (1985), An approach to automatic three-dimensional finite element mesh generation, *Intern. J. Num. Meth. Eng.*, 21, pp. 329-347.
- [CSS83] Z. J. Cendes, D. Shenton, and H. Shahnasser (1983), Magnetic field computing using Delaunay triangulation and complementary finite element methods, *IEEE Trans. on Magnetism*, 19, pp. 2551-2554.
- [Cha84] B. Chazelle (1984), Convex partitions of polyhedra: a lower bound and worst-case optimal algorithm, *SIAM J. Comput.*, 13, pp. 448-507.
- [ChP89] B. Chazelle and L. Palios (1989), Triangulation a non-convex polytope, *Proc. 5th ACM Symp. on Computational Geometry*, pp. 393-400.
- [Dey91] T. K. Dey (1991), Triangulation and CSG representation of polyhedra with arbitrary genus, *Proc. 7th ACM Symp. on Computational Geometry*, pp. 364-372.
- [DBS91] T. K. Dey, C. L. Bajaj, and K. Sugihara (1991), On good triangulations in three dimensions, *Proc. ACM Symp. on Solid Modeling Foundations and CAD/CAM Applications*, pp. 431-441.
- [Eri90] F. Eriksson (1990), On the measure of solid angles, *Math. Magazine*, 63, pp. 184-187.

- [Fie86] D. A. Field (1986), Implementing Watson's algorithm in three dimensions, *Proc. 2nd ACM Symposium on Computational Geometry*, pp. 246-259.
- [FiS91] D. A. Field and W. D. Smith (1991), Graded tetrahedral finite element meshes, *Intern. J. Num. Meth. Eng.*, 31, pp. 413-425.
- [Fre87] W. H. Frey (1987), Selective refinement: a new strategy for automatic node placement in graded triangular meshes, *Intern. J. Num. Meth. Eng.*, 24, pp. 2183-2200.
- [Gad52] J. W. Gaddum (1952), The sums of the dihedral and trihedral angles in a tetrahedron, *Amer. Math. Monthly*, 59, pp. 370-371.
- [GoV89] G. H. Golub and C. F. Van Loan (1989), *Matrix Computations*, 2nd edition, Johns Hopkins University Press, Baltimore.
- [JaB87] A. Jameson and T. J. Baker (1987), Improvements to the aircraft Euler method, *Proceedings AIAA 25th Aerospace Sciences Meeting*, Reno, Nevada, Paper 87-0452, 18 pages.
- [Joe89] B. Joe (1989), Three-dimensional triangulations from local transformations, *SIAM J. Sci. Stat. Comput.*, 10, pp. 718-741.
- [Joe91a] B. Joe (1991), Delaunay versus max-min solid angle triangulations for three-dimensional mesh generation, *Intern. J. Num. Meth. Eng.*, 31, pp. 987-997.
- [Joe91b] B. Joe (1991), Construction of three-dimensional Delaunay triangulations using local transformations, *Computer Aided Geometric Design*, 8, pp. 123-142.
- [Joe93] B. Joe (1993), Construction of three-dimensional improved-quality triangulations using local transformations, submitted for publication.
- [Joe94] B. Joe (1994), Tetrahedral mesh generation in polyhedral regions based on convex polyhedron decompositions, *Intern. J. Num. Meth. Eng.*, 37, pp. 693-713.
- [JoS86] B. Joe and R. B. Simpson (1986), Triangulation meshes for regions of complicated shape, *Intern. J. Num. Meth. Eng.*, 23, pp. 751-778.
- [JuL93] Y. H. Jung and K. Lee (1993), Tetrahedron-based octree encoding for automatic mesh generation, *Computer-Aided Design*, 25, pp. 141-153.

- [Kaz61] N. D. Kazarinoff (1961), *Geometric Inequalities*, Random House, New York.
- [Kea78] B. Kearfott (1978), A proof of convergence and an error bound for the method of bisection in  $\mathbf{R}^n$ , *Math. Comp.*, 32, pp. 1147-1153.
- [Law77] C. L. Lawson (1977), Software for  $C^1$  surface interpolation, in *Mathematical Software III*, ed. J. R. Rice, Academic Press, New York, pp. 161-194.
- [Law86] C. L. Lawson (1986), Properties of  $n$ -dimensional triangulations, *Computer Aided Geometric Design*, 3, pp. 231-246.
- [Le88] K. H.-Le (1988), Finite element mesh generation methods: a review and classification, *Computer-Aided Design*, 1, pp. 27-38.
- [LeS80] D. T. Lee and B. J. Schachter (1980), Two algorithms for constructing a Delaunay triangulation, *Intern. J. Computer Info. Sciences*, 9, pp. 219-242.
- [LiJ94a] A. Liu and B. Joe (1994), On the shape of tetrahedra from bisection, to appear in *Mathematics of Computation*.
- [LiJ94b] A. Liu and B. Joe (1994), Relationship between tetrahedron shape measures, to appear in *BIT*.
- [LiJ94c] A. Liu and B. Joe (1994), Quality local refinement of tetrahedral meshes based on bisection, submitted for publication.
- [LiJ94d] A. Liu and B. Joe (1994), Quality local refinement of tetrahedral meshes based on 8-subtetrahedron subdivision, submitted for publication.
- [Lo85] S. H. Lo (1985), A new mesh generation scheme for arbitrary planar domains, *Intern. J. Num. Meth. Eng.*, 21, pp. 1403-1426.
- [Lo91a] S. H. Lo (1991), Volume discretization into tetrahedra – I. verification and orientation of boundary surfaces, *Computer & Structures*, 39, pp. 493-500.
- [Lo91b] S. H. Lo (1991), Volume discretization into tetrahedra – II. 3D triangulation by advancing front approach, *Computer & Structures*, 39, pp. 501-511.
- [LMZ85] R. Löhner, K. Morgan, and O. C. Zienkiewicz (1985), Adaptive grid refinement for the compressible Euler equations, in I. Babuska et al. *Accuracy Estimates and Adaptive Refinements in Finite Element Computations*, Wiley, New York.

- [LoP88] R. Löhner and P. Parikh (1988), Generation of three-dimensional unstructured grids by the advancing front method, *Proceedings AIAA 26th Acrospacc Sciences Meeting*, Reno, Nevada, Paper 88-0515, 12 pages.
- [Mit89] W. F. Mitchell (1989), A comparison of adaptive refinement techniques for elliptic problems, *ACM Trans. on Mathematical Software*, 15, pp. 326-347.
- [MiV92] S. Mitchell and S. Vavasis (1992), Quality mesh generation in three dimensions, *Proc. 8th ACM Symp. on Computational Geometry*, pp. 212-221.
- [MPV89] D. S. Mitrinovic, J. E. Pecaric, and V. Volenec (1989), *Recent Advances in Geometric Inequalities*, Kluwer Academic Publishers, Dordrecht, Netherlands.
- [MoW90] D. Moore and J. Warren (1990), Adaptive mesh generation I: packing space, *Technical Report, Department of Computer Science, Rice University*
- [NeF91] T. W. Nehl and D. A. Field (1991), Adaptive refinement of first order tetrahedral meshes for magnetostatics using local Delaunay subdivisions, *IEEE Trans. on Magnetics*, 27, pp. 4193-4196.
- [Ong89] M. E. Go Ong (1989), Hierarchical basis preconditioners for second order elliptic problems in three dimensions, *Ph.D. Thesis, University of California, Los Angeles*.
- [PPF88] J. Peraire, J. Peiro, L. Formaggia, K. Morgan, and O. C. Zenkiewicz (1988), Finite element Euler computation in three dimensions, *Intern. J. Num. Meth. Eng.*, 26, pp. 2135-2159.
- [PSK89] R. Perucchio, M. Saxena, and A. Kela (1989), Automatic mesh generation from solid models based on recursive spatial decompositions, *Intern. J. Num. Meth. Eng.*, 28, pp. 2469-2501.
- [Raj91] V. T. Rajan (1991), Optimality of the Delaunay triangulation in  $R^d$ , *Proc. 7th ACM Symp. on Computational Geometry*, pp. 357-363.
- [Riv84] M.-C. Rivara (1984), Algorithms for refining triangular grids suitable for adaptive and multigrid techniques, *Intern. J. Num. Meth. Eng.*, 20, pp. 745-756.
- [Riv87] M.-C. Rivara (1987), A grid generator based on 4-triangles conforming mesh-refinement algorithms, *Intern. J. Num. Meth. Eng.*, 24, pp. 1343-1354.

- [Riv89] M.-C. Rivara (1989), Selective refinement/derefinement algorithms for sequences of nested triangulations, *Intern. J. Num. Meth. Eng.*, 28, pp. 2889-2906.
- [RiL92] M.-C. Rivara and C. Levin (1992), A 3-D refinement algorithm suitable for adaptive and multi-grid techniques, *Comm. Appl. Num. Meth.*, 8, pp. 281-290.
- [RoS75] I. G. Rosenberg and F. Stenger (1975), A lower bound on the angles of triangles constructed by bisecting the longest side, *Math. Comp.*, 29, pp. 390-395.
- [Sab91] M. Sabin (1991), Criteria for comparison of automatic mesh generation methods, *Adv. Eng. Software*, 13, pp. 221-225.
- [ScS90] W. J. Schroeder and M. S. Shephard (1990), A combined octree/Delaunay method for fully automatic 3-D mesh generation, *Intern. J. Num. Meth. Eng.*, 29, pp. 37-55.
- [Sen81] M. Senechal (1981), Which tetrahedra fill space?, *Math. Magazine*, 54, pp. 227-243.
- [She88] M. S. Shephard (1988), Approaches to the automatic generation and control of finite element meshes, *Appl. Mech. Rev.*, 41, pp. 169-185.
- [ShG91] M. S. Shephard and M. K. Georges (1991), Automatic three-dimensional mesh generation by finite octree techniques, *Intern. J. Num. Meth. Eng.*, 32, pp. 709-749.
- [SYB86] M. S. Shephard, M. A. Yerry, and P. L. Baehmann (1986), Automatic mesh generation allowing for efficient a priori and a posteriori mesh refinement, *Comp. Meth. Appl. Mech. Eng.*, 55, pp. 161-180.
- [Sty80] M. Stynes (1980), On faster convergence of the bisection method for all triangles, *Math. Comp.*, 35, pp. 1195-1201.
- [ToL49] I. Todhunter and J. G. Leathem (1949), *Spherical Trigonometry*, Macmillan, London.
- [Wat81] D. F. Watson (1981), Computing the  $n$ -dimensional Delaunay tessellation with application to Voronoi polytopes, *Comput. J.*, 24, pp. 167-172.

- [YeS83] M. A. Yerry and M. S. Shephard (1983), Finite element mesh generation based on a modified-quadtree approach, *IEEE Comput. Graphics Appl.*, 3, pp. 36-46.
- [YeS84] M. A. Yerry and M. S. Shephard (1984), Automatic three dimensional mesh generation by the modified-octree technique, *Intern. J. Num. Meth. Eng.*, 20, pp. 1965-1990.
- [YTH91] M. M. F. Yuen, S. T. Tan, and K. Y. Hung (1991), A hierarchical approach to automatic finite element mesh generation, *Intern. J. Num. Meth. Eng.*, 32, pp. 501-525.